


December 2016

# Characterization and Use of Folate Receptor Isoforms for Targeting of Epithelial and Myeloid Cells

Sreya Biswas

*University of Wisconsin-Milwaukee*

Follow this and additional works at: <https://dc.uwm.edu/etd>

 Part of the [Biology Commons](#), and the [Molecular Biology Commons](#)

---

## Recommended Citation

Biswas, Sreya, "Characterization and Use of Folate Receptor Isoforms for Targeting of Epithelial and Myeloid Cells" (2016). *Theses and Dissertations*. 1352.

<https://dc.uwm.edu/etd/1352>

This Dissertation is brought to you for free and open access by UWM Digital Commons. It has been accepted for inclusion in Theses and Dissertations by an authorized administrator of UWM Digital Commons. For more information, please contact [open-access@uwm.edu](mailto:open-access@uwm.edu).

CHARACTERIZATION AND USE OF FOLATE RECEPTOR ISOFORMS FOR  
TARGETING OF EPITHELIAL AND MYELOID CELLS

by

Sreya Biswas

A Dissertation Submitted in  
Partial Fulfillment of the  
Requirements for the Degree of

Doctor of Philosophy

in Biological Sciences

at

The University of Wisconsin-Milwaukee

December 2016

## ABSTRACT

# CHARACTERIZATION AND USE OF FOLATE RECEPTOR ISOFORMS FOR TARGETING OF EPITHELIAL AND MYELOID CELLS

by

Sreya Biswas

The University of Wisconsin-Milwaukee, 2016  
Under the Supervision of Professor Douglas A. Steeber

Folate receptor (FR) is a GPI-anchored glycoprotein with high binding affinity for folic acid. FR has two membrane-associated isoforms,  $\alpha$  and  $\beta$ , that are overexpressed on epithelial and myeloid tumors, respectively. Normal cells may also exhibit FR expression at very low levels but interestingly, FR- $\alpha$  on normal cells is restricted to the apical surface i.e., away from the blood stream. This differential expression and orientation of the FR- $\alpha$  isoform on tumor cells has been exploited to selectively target and deliver conjugates (e.g., drugs, nanoparticles, liposomes) to tumor cells without harming neighboring healthy cells. However, the functions and use of FR- $\beta$  as a potential target have not been explored, and its functions on myeloid cells remain largely unknown. Therefore, we investigated the functions of FR- $\beta$  to determine its potential as a target in myeloid malignancies using a human myelomonocytic leukemia cell line, U937. FR- $\alpha$  studies were conducted using a murine epithelial breast carcinoma cell line, 4T1, and tumors harvested from 4T1 tumor-bearing mice. The isoforms were found overexpressed on tumor cells and tissues, both *in vitro* and *in vivo*, with no expression observed on corresponding normal cells. Studies conducted using folic acid-fluorochrome conjugates to determine intracellular receptor fate indicated that FR- $\beta$  was not internalized into cells unlike FR- $\alpha$ . However, both isoforms

exhibited strong binding to folic acid conjugates (e.g., fluorochromes, nanoparticles) thus indicating that they could be selectively targeted using folic acid-dependent methods.

We also determined the potential of a novel histone deacetylase (HDAC) inhibitor (HDACi) as an anti-cancer agent that could be used along with folic acid for achieving better selectivity in targeting tumor cells. Preliminary studies showed that Compound 5 (Cpd5) is stable with strong anti-proliferative activities against human tumor cells. Cpd5 was also able to reduce the rate of 4T1 tumor growth in mice without inducing systemic toxicity in the animals. In addition, Cpd5 exhibited desirable pharmacokinetic properties and showed direct effects on acetylation levels of histone proteins. These studies not only provide insights into the functional differences associated with FR- $\alpha$  and FR- $\beta$  isoforms, but also highlight the potential of future targeting strategies utilizing these to target both epithelial and myeloid malignancies with improved selectivity.

© Copyright by Sreya Biswas, 2016  
All Rights Reserved

## TABLE OF CONTENTS

<b>ACKNOWLEDGEMENTS</b> .....	viii
<b>LIST OF FIGURES</b> .....	ix
<b>LIST OF TABLES</b> .....	xi
<b>LIST OF ABBREVIATIONS</b> .....	xii
<b>CHAPTER 1--- GENERAL INTRODUCTION</b> .....	1
Figures and Figure Legends .....	36
<b>CHAPTER 2--- FOLATE RECEPTOR ISOFORMS <math>\alpha</math> AND <math>\beta</math> HAVE DISTINCT EXPRESSION PROFILES AND EXHIBIT DIFFERENTIAL ACTIVITY</b>	
Abstract .....	39
Introduction .....	41
Materials and Methods .....	45
Results .....	51
Discussions .....	56
Figures and Figure Legends .....	59
<b>CHAPTER 3 --- FR-<math>\alpha</math> and FR-<math>\beta</math> ISOFORMS EXHIBIT DIFFERENT INTRACELLULAR FATE</b>	
Abstract .....	71
Introduction .....	73
Materials and Methods .....	76
Results .....	85
Discussions .....	97
Figures and Figure Legends .....	103
<b>CHAPTER 4--- DETERMINING THE POTENTIAL OF A NOVEL HISTONE DEACETYLASE INHIBITOR (HDACi) AS AN ANTI-CANCER AGENT</b>	
Abstract .....	131
Introduction .....	133
Materials and Methods .....	136
Results .....	143
Discussions .....	147
Figures and Figure Legends .....	150
<b>CHAPTER 5--- CONCLUSIONS</b> .....	158
Figures and Figure Legends .....	165

<b>REFERENCES</b> .....	167
<b>CURRICULUM VITAE</b> .....	195

To  
my parents  
and my husband



## **ACKNOWLEDGEMENTS**

I would sincerely like to express my heartfelt gratitude to Dr. Douglas Steeber for providing me with such a wonderful opportunity to work on this project. His guidance, persistence, and words of encouragement have been a constant source of inspiration for me, throughout my research. I have always tried to imbibe maximal knowledge on this subject through our scientific research discussions.

I would also like to thank other members of my supervisory committee, Dr. Julie Oliver, Dr. Heather Owen, Dr. Mahmum Hossain and Dr. Reinhold Hutz for their valuable input. I thank Dr. Julie Oliver and her lab for sharing the tissue culture equipment, as well as Dr. Heather Owen for her help with the electron microscope. I would like to thank my lab members and the entire faculty, and staff in the department for their help and support in some way or the other during my doctoral research. Last but not the least, I would like to express my love and appreciation towards my parents, in-laws, and my husband for believing in my abilities, and for the endless support I received from them throughout my research work.

## LIST OF FIGURES

<b>Figure 1.</b> Differential expression of FR- $\alpha$ in normal and cancer cells facilitates selective targeting.....	36
<b>Figure 2.</b> Receptor-mediated endocytosis of folic acid-conjugates .....	37
<b>Figure 3.</b> FR- $\alpha$ expression on murine epithelial breast carcinoma cell line 4T1 .....	59
<b>Figure 4.</b> <i>In vivo</i> expression of FR- $\alpha$ on 4T1 tumor cells .....	60
<b>Figure 5.</b> Comparing FR- $\alpha$ expression in normal and tumor epithelial cells .....	62
<b>Figure 6.</b> FR- $\beta$ expression on U937 myeloid leukemia cell line .....	63
<b>Figure 7.</b> FR- $\beta$ expression on the Jurkat T-cell leukemia cell line.....	64
<b>Figure 8.</b> Comparing FR- $\beta$ expression on normal peripheral blood monocytes to that of the U937 myelomonocytic leukemia cell line .....	65
<b>Figure 9.</b> FR- $\alpha$ and FR- $\beta$ expression patterns on 4T1 and U937 cells .....	67
<b>Figure 10.</b> High-resolution imaging by confocal microscopy comparing FR- $\alpha$ and FR- $\beta$ staining patterns .....	67
<b>Figure 11.</b> Effect of exogenous folate on FR expression .....	68
<b>Figure 12.</b> Comparing FR- $\alpha$ and FR- $\beta$ activity in 4T1 and U937 cells .....	69
<b>Figure 13.</b> Synthesis of folic acid-conjugated fluorescent probes .....	103
<b>Figure 14.</b> UV-Vis analysis of the BSA-FITC, BSA-TRITC, FA-BSA-FITC and FA-BSA-TRITC probes .....	104
<b>Figure 15.</b> FA-BSA-FITC probe showed specific binding to FR- $\alpha$ in 4T1 cells .....	105
<b>Figure 16.</b> FA-BSA-FITC probe showed specific binding to FR- $\beta$ in U937 cells .....	107
<b>Figure 17.</b> Comparing FR- $\alpha$ and FR- $\beta$ internalization by high-resolution confocal microscopy .....	110
<b>Figure 18.</b> The FA-BSA-TRITC probe showed strong staining on tumor sections harvested from 4-week 4T1 tumor-bearing mice .....	111
<b>Figure 19.</b> Free folic acid did not compete with the FA-BSA-FITC probe for binding to the FR- $\alpha$ isoform.....	112

<b>Figure 20.</b> The FA-BSA-TRITC probe showed specific binding to the FR- $\beta$ receptors on myeloid-derived suppressor cells (MDSCs) .....	113
<b>Figure 21.</b> The FA-BSA-Au <sub>18</sub> conjugates showed specific binding to FR- $\alpha$ receptors on 4T1 cells .....	117
<b>Figure 22.</b> The FA-BSA-Au <sub>18</sub> conjugates were localized to spread areas of U937 cells ...	118
<b>Figure 23.</b> Comparing FR- $\alpha$ and transferrin internalization pathways .....	120
<b>Figure 24.</b> Comparing FR- $\alpha$ internalization with dextran pinocytosis .....	121
<b>Figure 25.</b> FR- $\alpha$ binding activity was inhibited by cholesterol depletion .....	122
<b>Figure 26.</b> Transferrin-mediated endocytosis was largely unaffected by cholesterol depletion in both 4T1 and U937 cells .....	124
<b>Figure 27.</b> Pinocytosis in 4T1 and U937 cells was unaffected by cholesterol depletion ...	126
<b>Figure 28.</b> Cholesterol depletion inhibited FA-BSA-TRITC probe binding and internalization without affecting transferrin receptor activity in 4T1 and U937 cells .....	128
<b>Figure 29.</b> Cholesterol depletion inhibited FA-BSA-TRITC probe binding and internalization but pinocytosis activity remained unaffected in 4T1 and U937 cells .....	129
<b>Figure 30.</b> In vitro anti-proliferative effects of Cpd5, SAHA and FK228 against a panel of human tumor cell lines .....	150
<b>Figure 31.</b> Immunofluorescence staining of acetylated histones in DU-145 cells .....	152
<b>Figure 32.</b> Human and murine microsomal analysis depicting Cpd5 stability over time ..	154
<b>Figure 33.</b> Pharmacokinetic study depicting availability of Cpd5 in normal mouse blood	155
<b>Figure 34.</b> Cpd5-mediated tumor growth inhibition in 4T1 tumor-bearing mice .....	157
<b>Figure 35.</b> FR- $\alpha$ (and to a lesser extent FR- $\beta$ ) exhibited sensitivity to membrane cholesterol depletion and is internalized via non-clathrin coated pathways.....	165
<b>Figure 36.</b> Cpd5 conjugation to folic acid to induce selective targeting in tumor cells.....	166

## LIST OF TABLES

<b>Table I.</b> Growth inhibitory concentration (IC <sub>50</sub> ) of Cpd5, SAHA and FK228 against human tumor cell lines .....	151
<b>Table II.</b> Metabolic activity of Cpd5 determined by human and murine microsomal assays .....	153
<b>Table III.</b> Comparing systemic toxicity levels of Cpd5, FK228 and SAHA <i>in vivo</i> .....	156

## LIST OF ABBREVIATIONS

5-mTHF	5-methyltetrahydrofolate
AML	Acute myeloid leukemia
ARG1	Arginase 1
Au <sub>18</sub>	18 nm colloidal gold
BCL	B-cell lymphoma
CAR	Chimeric antigen receptor
CDK4	Cyclin dependent kinase 4
CLL	Chronic lymphocytic leukemia
CML	Chronic myeloid leukemia
CNT	Carbon nanotubes
Co-REST	Co-repressor to RE1 silencing factor
CTCL	Cutaneous T-cell lymphoma
DNA	Deoxyribonucleic acid
EPR	Enhanced permeability and retention effect
FA	Folic acid
FDA	Food and Drug Administration
FITC	Fluorescein isothiocyanate
FR	Folate receptor
G-CSF	Granulocyte colony stimulating factor
GEEC	Glycophosphatidylinositol enriched early endosomal compartment
GM-CSF	Granulocyte monocyte colony stimulating factor
GPI	Glycophosphatidylinositol

HAT	Histone acetylase transferase
HBSS	Hank's balanced salt solution
HDAC	Histone deacetylase
HDACi	Histone deacetylase inhibitor
HIF-1	Hypoxia inducible factor 1
IC <sub>50</sub>	Inhibitory concentration
IFN	Interferon
IL	Interleukin
iNOS	Inducible nitric oxide synthase
Jak	Janus kinase
K <sub>D</sub>	Dissociation constant
MDSC	Myeloid-derived suppressor cells
MEF2	Monocyte enhancer factor 2
MHC	Major histocompatibility complex
MMP	Metalloproteinase
MO	Monocytic
N-CoR	Nuclear receptor co-repressor
NES	Nuclear export signal
NF-κB	Nuclear factor-kappa B
NK	Natural killer cell
NLS	Nuclear localization signal
NO	Nitric oxide
NOX	NADPH oxidase

NuRD	Nucleosome remodeling histone deacetylase
OMF	Oscillating magnetic field
PBMC	Peripheral blood mononuclear cells
PCR	Polymerase chain reaction
PGE2	Prostaglandin E2
PLZF	Promyelocytic leukemia zinc finger
PMN	Polymorphonuclear
RA	Rheumatoid arthritis
RFC	Reduced folate carrier
ROS	Reactive oxygen species
SAHA	Suberoylanilide hydroxamic acid
SCF	Stem cell factor
Sin3	Switch independent 3
SMRT	Silencing mediator for retinoic acid and thyroid hormone receptor
STAT	Signal transducer and activator of transcription
TAA	Tumor-associated antigen
TCR	T-cell receptor
TGF- $\beta$	Transforming growth factor- $\beta$
TLR	Toll-like receptor
TNF	Tumor necrosis factor
Treg	Regulatory T-cell
TRITC	Tetramethylrhodamine
TSA	Trichostatin A

VEGF      Vascular endothelial growth factor



**CHAPTER 1**

**GENERAL INTRODUCTION**

## **I. Introduction**

Immunotherapy is mainly of two kinds, active and passive with both having a potential role in cancer therapy. Passive immunotherapy involves passive diffusion-based or -derived therapies while active therapy is dependent on targeting tumor-associated antigens (TAA) with specific characteristics<sup>1</sup>. The effectiveness of active therapeutic strategies is highly dependent on the efficiency of TAAs to stimulate the effector arm of the immune response that can overcome the immunosuppression generated during cancer progression, but without generating toxicity<sup>1</sup>. There has been a great deal of research oriented to determining such effective therapies with a focus on identifying the most suitable TAAs to target. In order to be a suitable TAA, the molecule needs to have a relatively high specificity and distinct overexpression or hyperactivity in the targeted cancer cells. Proteins, gene-therapy vectors and liposome-encapsulated drugs have shown promising effects in cancer therapy as compared to traditional chemotherapeutic agents due to their high specificity and prolonged delivery<sup>2-5</sup>. On the contrary, high molecular weight agents such as macromolecular drugs encounter significant permeability barriers that limit potential therapies. Hence, use of ligand-specific therapies can be a potential alternative to overcome such limitations. This approach however, has been applied mostly to epithelial tumors and has not been examined for its effectiveness for myeloid tumors. Therefore, there remains a significant need to investigate the prospects of using a ligand-specific approach in targeting epithelial and myeloid cells.

## **II. Folate receptor (FR)**

The folate receptor (FR) is also known as the folate binding protein. It is a single-chain cell surface glycoprotein having a high affinity for folic acid (FA) with a dissociation constant ( $K_D$ )  $< 10^{-9}$ M and its circulating form, 5-methyltetrahydrofolate (5-mTHF). FR is a glycosylphosphatidylinositol (GPI)-anchored glycopolyptide with a  $K_D$  in the subnanomolar range<sup>6</sup>. The folate receptor is expressed in a limited number of normal tissues but overexpressed in several malignancies<sup>7-10</sup>. The FR transports FA as well as the derivatives of folate by a non-classical endocytic mechanism<sup>11</sup>. For most normal cells that lack FR expression, other folate carriers mediate folate uptake<sup>12</sup>. Among them, the reduced folate carrier (RFC), usually expressed ubiquitously in normal adult tissues, is unable to bind to folic acid but can efficiently bind to folate derivatives such 5-mTHF and transport them efficiently into cells. The transport process is quite rapid and sufficient to fulfill the cellular stores of the co-enzyme<sup>13</sup>. FR is predominantly expressed on the apical surface of polarized epithelial cells where it never encounters circulating folate<sup>6,14</sup>. In addition, FR expressed in mature hematopoietic stem cells is unable to bind folate. Importantly, the FR is capable of transporting or binding to a wide variety of conjugates of FA, anti-folate drugs and other immunological agents<sup>1,2</sup>. All these factors have initiated intense interest in the field of therapeutics and tumor therapy to selectively target FR in cancer<sup>15</sup>. Human FR is encoded by a family of genes whose homologous products are FR- $\alpha$ , - $\beta$  and - $\gamma$ <sup>9,11-13,15,16</sup>. A fourth isoform named FR- $\delta$  has been recently identified, but neither its expression nor its function as a folate binder has been established<sup>17</sup>. Based on the structural similarity of the encoded proteins, FR genes appear to belong to a superfamily that includes the riboflavin protein<sup>18</sup> and a putative carotenoid

or flavonoid binding retinal protein called retbindin<sup>19</sup>. In addition, based on the National Center for Biotechnology Information genomic database, this family also appears to have accompanied the evolution of vertebrates with close homologs in fish, amphibians, birds and mammals.

### **A. FR- $\alpha$**

FR- $\alpha$  is the most widely expressed FR isoform in normal adult tissues, located at the apical surface of the epithelium where it does not come in contact with blood vessels and thus does not interact with circulating folate<sup>20,21,22</sup>. In contrast, tumor cells lose polarization of FR- $\alpha$  and thus are in contact with circulating folate. This is an advantage in the case of drug delivery with folate-conjugates, which can be selectively used to treat tumor cells, leaving the normal healthy cells unharmed<sup>23</sup> (Fig. 1). FR- $\alpha$  is a membrane-associated form of the FR and is capable of transporting folate into the cells<sup>24</sup>. FR- $\alpha$  is predominantly expressed on epithelial cells and many of their malignant derivatives<sup>14</sup> such as proximal tubules of kidney and renal cell carcinoma, choroid plexus and its carcinoma, ovarian carcinoma and breast carcinoma cells<sup>10,25,26</sup>. In general, FR-targeted therapeutics have been focused more on ovarian<sup>27</sup> and endometrial cancers<sup>28</sup> as these more frequently overexpress FR- $\alpha$  in a consistent manner. FR- $\alpha$  expression is reported to vary with the stage of malignancies, and is found to be down regulated in mucinous and cervical adenocarcinomas but expressed *de novo* in adenocarcinoma of the uterine endometrium<sup>28-30</sup>. FR- $\alpha$  is consistently expressed in non-mucinous adenocarcinomas of the ovary, uterine adenocarcinoma, testicular choriocarcinoma, ependymal brain tumors and non-functioning pituitary adenoma, frequently in malignant pleural mesothelioma and less frequently in breast, colon and renal carcinomas<sup>28-31</sup>. There is also variability in

the expression levels of this receptor sub-type among tumors obtained from different patients as well as within the same tumor<sup>30</sup>. It is evident from numerous reports that there is a quantitative increase in FR- $\alpha$  expression associated with foci of poor differentiation as well as the more poorly differentiated tumors<sup>32</sup>. This observation is in contrast to an increase in FR- $\alpha$  associated with differentiation in an epithelial squamous carcinoma cell line, which suggests there might be systemic as well as cellular effectors of FR regulation in cancers<sup>33</sup>.

FR- $\alpha$  has a globular structure with four long  $\alpha$ -helices ( $\alpha 1$ ,  $\alpha 2$ ,  $\alpha 3$ ,  $\alpha 6$ ), two short  $\alpha$ -helices ( $\alpha 4$ ,  $\alpha 5$ ), four short  $\beta$ -strands ( $\beta 1$ -  $\beta 4$ ) and many loop regions<sup>34</sup>. The presence of eight disulfide bonds (formed by 16 conserved cysteine residues) stabilizes the tertiary structure of this isoform<sup>13</sup>. FR- $\alpha$  also has three N-glycosylation sites<sup>12,18,35</sup>, which contribute to the receptor's ability to bind the oxidized form of folate, folic acid, with high affinity ( $K_D$  ranging from 0.1- 1 nM)<sup>35-37</sup>. On the contrary, FR- $\alpha$  exhibits  $\sim 10$  times lower affinity for the reduced forms of folate such as methotrexate ( $K_D$ : 1-10 nM) and 5-mTHF ( $K_D$ : 1-10  $\mu$ M)<sup>38-41</sup>. Thus, the high selectivity of these transport mechanisms is dependent on the low affinity of FA for RFC, and its high affinity for FR- $\alpha$ <sup>6,42</sup>.

## **B. FR- $\beta$**

FR- $\beta$  is mainly found in cells of myelomonocytic lineage with increased expression during the maturation of neutrophils<sup>43</sup>; however, in normal tissues it is restricted only to the placenta and hematopoietic stem cells<sup>7,15,44,45</sup>. FR- $\beta$  is co-expressed with the myeloid markers CD14, CD33 and CD11b markers but not with lymphocyte markers CD3 (T cells) and CD19 (B cells)<sup>46</sup>. FR- $\beta$  is also consistently expressed in chronic myeloid leukemia (CML), while in acute myeloid leukemia (AML) 70% of the AMLs are FR- $\beta$

positive and often co-express CD34<sup>10,47</sup>. FR- $\beta$  expression is also reported to be increased in activated monocytes and macrophages with a recent study showing its elevated expression on synovial macrophages in Rheumatoid Arthritis (RA) patients<sup>48</sup> and in a rat arthritic model<sup>49</sup>. Since macrophages are a major contributor to the pathogenesis in RA, FR- $\beta$  could be exploited to target the synovial macrophages in RA patients<sup>50</sup>. Interestingly, FR- $\beta$  expressed on normal CD34<sup>+</sup> progenitor cells in the bone marrow and on mature neutrophils and monocytes is unable to bind folate while FR- $\beta$  expressed on CML, AML and on synovial macrophages is capable of binding folate<sup>46,47,51</sup>. This difference in ligand binding between normal hematopoietic cells and pathogenic cells appears to be related to certain post-translational modifications of the receptor and could be beneficial by providing protection to normal cells from FR-targeted drugs and therapies<sup>2,10,25</sup>. Also, FR- $\beta$  has been reported to have much lower binding affinity ( $K_D$  ranging from 10-50 nM) to FA and other reduced forms of folate than FR- $\alpha$ <sup>38,52,53</sup>. Importantly, this functional difference between the two receptor isoforms is attributed to a few amino acid residue differences between the isoforms<sup>13,15,24,37,39</sup>. The functional differences between the FR isoforms might be advantageous for selective tissue-targeting and FR-mediated drug delivery.

### **C. FR- $\gamma$**

FR- $\gamma$  was detected by polymerase chain reaction analysis (PCR) and was found to be secreted constitutively in normal and leukemic (CML, AML, CLL) hematopoietic tissues, including bone marrow, spleen and thymus<sup>9,10,16,25</sup>. Since, FR- $\gamma$  is almost undetectable in serum and is not a membrane-bound receptor; few studies have been performed.

However, this protein might be useful as a serum marker for myeloid and lymphoid tumors<sup>9</sup>.

## **II. Transport of reduced folates**

### **A. Reduced folate carrier (RFC)**

The RFC is a cellular uptake system that transports folates to the cytoplasm of cells using a bidirectional anion exchange mechanism<sup>40,54</sup>. The transport kinetics and affinity for oxidized and reduced forms of folates differ significantly between the FR and the RFC systems<sup>48,53</sup>. The RFC is a 591 amino acid transporter with 12 transmembrane domains<sup>55</sup>. It is widely expressed on cells and mediates the uptake of reduced folates such as dihydrofolate, tetrahydrofolate and 5-mTHF with relatively high affinity at micromolar concentrations ( $K_M$ : 1-10  $\mu\text{M}$ )<sup>42</sup>. However, it has relatively poor affinity for the oxidized form of folate, folic acid ( $K_M$ : 200-400  $\mu\text{M}$ )<sup>24,40,41,56</sup>, and is unable to transport it across the membrane. The potential binding capacity of the RFC is about one hundred times greater than the amount of folate in serum<sup>57</sup>. Thus, the high selectivity of these mechanisms resides in the low affinity of folic acid for the RFC, and the high affinity of folic acid for the folate receptors<sup>58</sup>.

### **B. Regulation of FR expression**

FR- $\alpha$  regulation by folate has important implications in transport-related anti-folate drug resistance mechanisms and in developing strategies to increase FR- $\alpha$  expression in malignant tissues for targeting/therapeutic purpose. However, FR- $\alpha$  does not bind and carry reduced folates as efficiently as does the RFC<sup>53,59</sup>. Several studies have demonstrated that varying the concentration of either intracellular or extracellular folate

is able to modulate the expression of FR- $\alpha$  in a variety of cells<sup>58,60,61</sup>. For example, in cervical carcinoma cells, folate-dependent regulation of FR- $\alpha$  expression was found to occur at the transcriptional level while in other cases, expression was reported to be regulated by FR- $\alpha$  mRNA levels<sup>62</sup>. In cultured chinese hamster lung fibroblasts, FR- $\alpha$  gene amplification was observed in response to severe folate restriction<sup>61</sup>. Interestingly, some FR- $\alpha$  negative tumors have been found to start expressing FR- $\alpha$  following treatment with anti-folate chemotherapeutic drugs such as methotrexate, likely to facilitate folate uptake to support cell proliferation. These tumors would now be susceptible to FR-targeting strategies which is important since many tumors develop drug resistance due to defective transport of the drugs into the cell<sup>63</sup>. Hence, regulation of FR expression in response to folate or a combination of folates and anti-folates, is a potential avenue for developing novel FR-mediated therapies<sup>25,64-66</sup>.

### **III. Transport of oxidized folate**

FA is the oxidized form of folate that exhibits high affinity for FR and is required by cells in the biosynthesis of nucleotide bases. Hence, cell survival and proliferation are dependent on a cell's ability to acquire this vitamin<sup>67</sup>. As mentioned above, cellular uptake of folate is facilitated by either the RFC or the FR. The RFC is selective in facilitating transport of mainly reduced forms of folate while the FR has the ability to transport FA as well as folic acid-linked cargos of various kinds (e.g., chemotherapeutics, imaging agents, proteins, liposomes and nanoparticles)<sup>6,68-70</sup>. FA is also known as pteroylglutamate and is non-immunogenic in nature. It is small (441 Da) and stable over a broad range of temperatures and pH. It is also inexpensive and retains its ability to bind to the FR after conjugation with drugs or diagnostic markers<sup>71-74</sup>. Cells expressing FR- $\alpha$ ,



thus bind FA with high affinity and transport it by endocytosis. Although the literature suggests many possible mechanisms associated with FR- $\alpha$ -mediated endocytosis, the process has yet to be fully elucidated.

### **A. Receptor-mediated endocytosis**

Receptor-mediated endocytosis is also known as clathrin-dependent endocytosis and involves binding of a ligand and activation of a receptor-mediated internalization pathway (Fig 2). Initially, internalization of FA conjugates in tumor cells was considered to proceed in a similar manner through the binding of the folate-conjugate to the cell-surface FRs<sup>75,60,76</sup>. After binding, membrane invagination would occur followed by internalization of the conjugate to form an endocytic vesicle. Acidification of the endosomal compartment occurs at pH 5-6, which results in the release of some of the folate conjugates from the receptor<sup>77,78</sup>. The acidic endosome is then transported to a recycling center, which allows separation of the membrane-bound FR- $\alpha$  from the released conjugates<sup>74,79</sup>. Released folate conjugates are reported to escape the endosome through an unknown mechanism resulting in their release into the cytoplasm<sup>74</sup>. The dissociated receptors recycle back to the plasma membrane surface allowing for delivery of additional folate-conjugates into the cell<sup>75</sup>.

### **B. Internalization via non-clathrin coated pathways**

The exact mechanism by which FR- $\alpha$  transports FA into cells remains unresolved. There have been conflicting reports describing the internalization pathway and trafficking of FR- $\alpha$ <sup>2,60,80</sup> and some studies have suggested that receptor internalization is associated with non-clathrin-coated pathways<sup>81</sup>. This is a distinct phenomenon associated with most

GPI-anchored proteins where the GPI anchor likely plays a role in mediating receptor clustering in association with flask-shaped membrane structures, called caveolae<sup>82,83</sup>. It was proposed that FR was internalized by the pinching off of the membrane, forming small pockets of caveolae followed by formation of small vesicles called caveosomes that are distinct from endosomes<sup>84</sup>. Polymerization of a protein called caveolin is thought to trigger the formation of caveosomes; however, the mechanisms are still under investigation<sup>40,60,85</sup>. Recent studies have proposed that the receptors are organized by the GPI anchor into “lipid rafts” or receptor-rich complexes on the cell membrane<sup>60,86,87</sup>. These domains are rich in sphingolipids and cholesterol, and are anticipated to have a role in facilitating FR internalization after binding with FA<sup>88-90</sup>. It has been suggested that there are special protein kinase residues inside the rafts that generate signaling pathways which further directs the sorting of lipid raft-mediated vesicles<sup>91,92</sup>. It is further speculated that the receptors could internalize through their interactions with the lipid rafts and eventually form caveosomes inside the cell; however, the exact mechanism for this is still unknown. In parallel with lipid rafts, GPI-enriched early endosomal compartments (GEECs) have also been proposed as a potential mechanism involved with FR internalization<sup>93,94</sup>. According to this pathway, the receptors can also be endocytosed into cells via clathrin-coated pathways but specifically are sorted into specialized endosomal compartments that are different from those formed in receptor-mediated endocytosis<sup>95</sup>. Regardless of the route of entry, physiologic FA clearly moves across the plasma membrane into the cytoplasm via a specialized endocytic pathway mediated by the FR.

#### **IV. Folate-targeted therapeutics**

FR- $\alpha$  despite being expressed on a few normal cells and tissues, is mostly restricted to the apical side of polarized epithelia. Hence, they are inaccessible to blood-borne folate conjugates, which makes FR- $\alpha$  targeting a potential selective therapy<sup>96</sup>. Considering this, many FR- $\alpha$  targeting studies have been initiated in recent years utilizing the high affinity ligand, FA. A major application of folate targeting involves the specific delivery of drugs to abnormal or pathologic tissues, which in their non-targeted form would show systemic toxicity. Keeping this in mind, a variety of folate-linked molecules and complexes have been designed to achieve selective delivery of therapeutics to the target cell, including FR-positive cancer cells and activated macrophages<sup>25,74,79</sup>.

Delivery of therapeutic agents utilizing FA can occur via a ligand-activated endocytosis pathway where drugs requiring intracellular release to induce cytotoxicity are transported into the cytoplasm of targeted cancer cells by FR<sup>70,97,2</sup>. Some examples of molecules that fall into this category are protein toxins<sup>98-100</sup>, drug-encapsulating liposomes<sup>101-103</sup>, gene therapy vectors<sup>104,105</sup> and many colloidal drug carriers<sup>106-108</sup>.

On the contrary, there are also several drugs that do not require intracellular release to mediate their actions. Instead, they can induce cytotoxic effects at the surface of a target cell. FR then acts as a tumor marker that functions to concentrate the drug on that specific cell<sup>2</sup>. Examples of this class of molecules include pro-drug activating enzymes<sup>109</sup> and immunotherapeutic agents that can stimulate or redirect the immune system of the host to the cancer cell<sup>110,111</sup>. The most important part of such targeting is based on the fact that FR is continuously recycled back to the cell surface, thus enabling both types of targeting strategies to be exploited.

## **A. Protein toxins**

Folate-targeted protein toxins have been explored as a tumor-selective cytotoxic agent since the 1990s. *Pseudomonas* exotoxin and momordin are protein synthesis inhibitors<sup>98,99</sup> that were tested *in vitro* as protein toxins for targeting purposes. Folate-momordin (IC<sub>50</sub>~ 1 nM) was shown to selectively kill malignant cells when cocultured with nontransformed cells<sup>112</sup>. Although both nontargeted toxins inhibited protein synthesis in cell-free systems with equal potency, folate-*Pseudomonas* exotoxin was found to exhibit higher cytotoxicity (inhibitory concentration, IC<sub>50</sub> < 10 pM) than folate-momordin<sup>74</sup>. The difference was due to the fact that *Pseudomonas* exotoxin has a translocation domain that allows its escape from intracellular endosomal vesicles whereas momordin does not<sup>113</sup>. This led to an understanding that escape of folate conjugates from their endosomal compartments is an important factor that can affect therapeutic efficiency and thus needs to be taken into account when designing conjugates or drugs for delivery into cells<sup>74</sup>.

Another form of folate-mediated protein targeting is the delivery of enzymes to cancer cells for pro-drug therapy<sup>109</sup>. This is an enzyme-based method where an enzyme that converts an inactive prodrug to an active therapeutic agent is targeted to the cancer cell with folate<sup>114</sup>. When the prodrug is administered systemically, it will not have any activity until it encounters the enzyme. In this way the enzyme-containing cancer cells will be killed while the normal cells without the enzyme will be unaffected<sup>115</sup>. However, to date little has been reported on the efficacy of protein-folate conjugates in live animals. In addition, repeated administration of a foreign protein can elicit an immune response, thus inhibiting the therapy. The size of the protein also needs to be considered since large

proteins may penetrate solid tissues less efficiently than smaller ones. Therefore, size of the folate conjugate is a major obstacle in treating solid tumors.

### **B. Small molecular weight chemotherapeutics**

FA-conjugated therapeutic agents can serve as alternatives to FA-targeted protein toxins. Although they are less potent than protein toxins, their small size helps in better tissue penetration and their non-immunogenic nature enables multiple dosing regimens. So far, most folate-drug conjugates have been developed as anti-cancer agents<sup>116-119</sup>. For example, folate-maytansinoid and folate-mitomycin C (EC72) have shown high cytotoxicity and selectivity for FR-positive cells<sup>116,120,121</sup>. In addition, repeated administration of folate-mitomycin C in mice was successful without any signs of toxicity in the animals<sup>120</sup>. However, certain factors such as the hydrophobic nature of some therapeutic agents can limit these approaches as they show less tumor specificity than water-soluble ones<sup>122</sup>. Thus, it is necessary to build a water-soluble linker between folate and the therapeutic cargo. Second, it is important to ensure that the affinity of folate for its receptor is retained even after conjugating the therapeutic cargo<sup>74</sup>. This can be achieved by preventing intramolecular interactions between folate and the tethered drug. Third, it is important for drugs to be released into the cell in unmodified form to maintain their activity. This can be assured by inserting a cleavable bond between the drug and the molecule<sup>20</sup>. Several linkers such as disulfide bonds, acid-sensitive linkers and enzymatically cleavable bonds have been tested and approved<sup>123,124</sup>. Hence, there are many approaches that can be investigated to improve the potential of folate-conjugated chemotherapeutics including the novel use of nanoparticles.

### **C. Nanoparticles**

Targeted nanoparticle delivery of therapeutic molecules has the potential to provide safer and more effective therapies for cancer treatment<sup>125</sup>. Current research is focused towards understanding the parameters that influence targeted nanoparticle behavior for easy development of nanoparticle-based therapeutics and imaging agents. Nanoparticles have specific properties that enable their use in cancer treatment. Their high surface-to-volume ratio makes them perfect for functionalization and conjugation with therapeutic agents. Their size and malleable nature allows their use in both active and passive targeting systems with higher tumor specificity than other methods<sup>126,127</sup>.

Passive targeting takes advantage of two major differences between tumor tissue and healthy tissue, including a leaky vasculature and an acidic tumor microenvironment<sup>128</sup>. Rapid growth of tumor cells requires rapid vascularization, leading to an abnormal vasculature that is more permeable than that of normal tissues. This increase in permeability makes cancerous tissues easily accessible to therapeutic drugs. In combination with the lack of lymphatics in the tumor bed, this allows for increased accumulation of the drug within the tumor resulting in an enhanced permeability and retention (EPR) effect<sup>129</sup>. This is applicable to all nanoparticle-based therapies and enables them to penetrate into the tumor vasculature with much higher retention times than normal tissues<sup>130,131</sup>. In addition to a leaky vasculature and lack of lymphatics, the tumor microenvironment also aids passive targeting through an acidic cytosol within the tumors, which potentially can be exploited by the use of pH-sensitive drug conjugates<sup>132</sup>. These are designed to be broken down after entering the tumor cells resulting in the release of the drug into the cytoplasm<sup>133,134</sup>.

Similarly, nanoparticles can also be used in active targeting of cancer cells. In this case, a nanoparticle is directly conjugated with a targeting moiety, thus allowing selective accumulation of the drug into target cells and tissues that are associated with tumor-specific molecules<sup>128,134</sup>. Several classes of molecular targets for active targeting have been proposed including cell-surface carbohydrates (carbohydrate targeting), cellular antigens (antibody targeting) and cell-surface receptors (receptor targeting)<sup>100,135,136,126</sup>.

Carbohydrates are targeted by directing nanoparticle-mediated treatments to tumor cells by attaching lectins that bind to cell-surface carbohydrates<sup>137</sup>. Antibody targeting utilizes overexpressed antigens on the tumor cell surface<sup>138,139</sup>. Receptor targeting makes use of a ligand that can bind to specific receptors expressed on the tumor cell surface<sup>140,141</sup>. The ligand is often conjugated to drugs and then allowed to internalize via receptor-mediated endocytosis, resulting in the release of the drug into the cell<sup>97,107,142</sup>.

A variety of nanoparticle materials are currently being used and tested for use in drug targeting. Polymeric nanoparticles have drugs conjugated to the side-chain of the linear polymer through a linker that has a cleavable bond<sup>126,130</sup>. The drug is activated as soon as the linker is cleaved after entering the tumor tissue. Micelles have a nano-sized core shell structure with a hydrophobic core region that serves as a reservoir for drugs<sup>143,144</sup>. The outer hydrophilic shell helps stabilize the core and makes it amenable to intravenous administration. Dendrimers are synthetic polymeric macromolecules with multiple highly branched chains emerging from the core region with multiple sites for drug attachment<sup>145,146</sup>.

Other methods make use of liposomes, viral nanoparticles or carbon nanotubes (CNTs)<sup>74,101,147</sup>. Liposomes are spherical structures that are composed of an outer lipid

bilayer surrounding a central aqueous space<sup>148</sup>. Once a liposome enters a cell, it is important for it to unload its cargo into the cell. However, the stable nature of liposomes can prevent the encapsulated drug from being released efficiently<sup>149,150</sup>. Hence, studies are ongoing to synthesize liposomes with pH-sensitive lipids and peptides to accelerate drug release into cells<sup>80,151,152</sup>. These can help liposomes maintain stability in the circulation but enable them to release their cargo into the cytosol of cells.

Viral nanoparticles, derived from a variety of viruses including the cowpea mosaic virus, canine parvovirus and bacteriophages, have recently been shown to be useful for active targeting in combination with CNTs<sup>153,154</sup>. CNTs can also be conjugated to several active molecules such as nucleic acids, peptides, proteins and other therapeutic compounds, and functionalized for cancer treatment<sup>155-158</sup>. Recent studies have indicated that CNTs can also serve as ideal targeted imaging agents that can produce strong magnetic resonance imaging contrast, which can be beneficial in detecting circulating tumor cells in peripheral blood<sup>159-161</sup>.

Inorganic nanoparticles are primarily metal-based and have been extensively studied for imaging. They are easily functionalized, non-toxic and non-immunogenic<sup>162,163</sup>. Several types of nanoparticles can convert energy into heat at levels up to 70°C<sup>164-166</sup>. Iron oxide nanoparticles coated with aminosilane are in clinical phase II trials in Germany for brain and prostate cancer therapy using hyperthermia<sup>167,168</sup>. The phase I trial results indicated that tumor cells could be locally killed by magnetic oxide nanoparticles<sup>168,169</sup>. The small nanoparticles (20 nm) reportedly penetrated the tumor and generated heat when exposed to magnetic fields (50kZ and 100kZ). This allowed treatment within a circular area of 20 cm of diameter without any signs of toxicity in the



patients<sup>170</sup>. Several formulations are still in the discovery stage using drugs such as paclitaxel, doxorubicin or interleukin (IL)-12<sup>171-176</sup>.

Compared to polymeric micelles and liposomes, gold nanoparticles are much smaller making them more desirable for passive targeting via the EPR effect<sup>129,177</sup>. Gold nanoparticles have also been used for hyperthermia treatment of tumors. Gold nanoparticles absorb strongly in the near-infrared wavelengths, and release this energy in the form of heat, which has been shown to induce antitumor efficacy in tumor cells. In addition, this has also been combined with traditional chemotherapy to enhance its effects<sup>178</sup>. However, a major limitation associated with it is non-specific tissue damage<sup>179</sup>. Alternatively, the issue of nonspecific tissue damage could be addressed by an approach that could generate highly localized heating. This could be accomplished by the active targeting of nanoparticles composed of magnetic iron oxide, such as magnetite, and subsequent exposure to an oscillating magnetic field (OMF). Heating in the region of the membrane-bound nanoparticles would then cause cell damage and, potentially, cell death. Although light- and temperature-based targeting strategies like this may reduce toxicity, they can also cause damage to adjacent tissues due to non-specific accumulation<sup>178</sup>.

## **V. Immunosuppression in Cancer**

Preclinical studies of cancer immunotherapies have shown considerable promise; however, their potential is often not realized *in vivo*. This is mostly due to infiltration by immature population of myeloid cells that are associated with undesirable clinical outcomes<sup>180</sup>. Tumor-induced immunosuppression is a key factor that allows tumors to escape the immune-mediated destruction initiated in the host<sup>181</sup>. Despite a still incomplete

understanding of tumor immunology, current approaches to immunotherapy focus on enhancing the capability of surveillance by the host's immune system<sup>182-184</sup>. With this strategy, abnormal or cancerous cells can be eliminated and cancer progression can be inhibited. However, several cellular interactions and feedback loops within the immune system tend to limit clinical applications and immunotherapeutic approaches. Studies have demonstrated that the immune responses generated during malignant conditions are often inhibited by different subsets of tumor-infiltrating myeloid cells, among which myeloid-derived suppressor cells (MDSCs) have been of special interest<sup>185,186</sup>. Due to their critical role in cancer progression, MDSCs have been extensively studied in many human cancers and in experimental models with human xenografts<sup>187,188</sup>. MDSCs primarily inhibit T cell activity against tumor antigens, thereby reducing the effectiveness of therapeutic approaches<sup>188,189</sup>. For example, a patient's T cells can be modified to express novel receptors on their surface called chimeric antigen receptors (CARs) that recognize a specific protein or antigen on tumor cells<sup>190</sup>. These engineered CAR T cells are infused back into patients, where they multiply and then recognize and kill the tumor cells. CAR T cells have been successfully used for the treatment of hematologic malignancies<sup>191</sup>, but their use in solid tumors has been completely unsuccessful as MDSCs tend to inhibit these CAR T cells. Therefore, targeting and eliminating suppressor cells is expected to emerge as a successful immunotherapeutic strategy. A better understanding of the local tumor microenvironment and the mechanisms resulting in expansion of suppressor cells will provide more opportunities for novel treatments directed to target these undesirable populations of cells, thus improving the anti-tumor immune response in the host.

## **VI. Myeloid-derived suppressor cells (MDSCs)**

### **A. Generation and activation**

MDSCs are a heterogeneous population of immature myeloid cells that are expanded in various pathologic conditions including cancer<sup>192,193</sup>. MDSCs function to inhibit the immune response in the host, thus inhibiting immunotherapy<sup>188,194,180,195</sup>. MDSCs are characterized as a morphologic mixture of granulocytes and monocytes including myeloid progenitor cells, macrophages, and immature granulocytes and macrophages<sup>197,202</sup>, that lack the expression of cell-surface markers associated with the fully differentiated forms of such cells<sup>197</sup>. MDSCs are generated in the bone marrow in response to several cancer-derived factors, such as granulocyte colony stimulating factor (G-CSF)<sup>188,198</sup>, granulocyte-monocyte colony stimulating factor (GM-CSF)<sup>199</sup>, stem cell factor (SCF)<sup>200</sup>, IL-6<sup>201</sup>, IL-1 $\beta$ <sup>202</sup>, prostaglandin E2 (PGE2)<sup>203,204</sup>, vascular endothelial growth factor (VEGF), and tumor necrosis factor- $\alpha$  (TNF- $\alpha$ )<sup>199,205,206</sup>. Most of these factors affect myelopoiesis and tumor progression via the signal transducer and activator of transcription (STAT) 3 signaling pathway<sup>207-209</sup>. Activated STAT3 is suggested to increase the survival and proliferation of immature myeloid cells via upregulation of factors such as B-cell lymphoma (BCL)-XL, cyclin-D, c-Myc and survivin<sup>183,210,211</sup>. Further activation of MDSCs is reportedly driven by factors such as toll-like receptor (TLR) ligands, IL-4, IL-13 and transforming growth factor- $\beta$  (TGF- $\beta$ ), which trigger signaling via STAT1, STAT6 and nuclear factor-kappa B (NF-kB)<sup>212-214</sup>. This results in an increased expression of enzymes such as arginase-1 and inducible nitric oxide synthase (iNOS) that are involved in MDSC-mediated immunosuppression<sup>215-217</sup>.

## **B. Subsets of murine and human MDSCs**

In mice, MDSCs are characterized by the co-expression of the myeloid lineage differentiation antigens CD11b and Gr-1<sup>197,218,219</sup>. In healthy mice, cells with this phenotype constitute about 20-30% of cells in the bone marrow and 2-4 % in the spleen; however, in tumor-bearing mice these percentages increase significantly<sup>218</sup>. Anti-Gr-1 antibodies can bind to two distinct epitopes, Ly-6G and Ly-6C, thus making it possible to further discriminate subsets of MDSCs using antibodies that can specifically target these antigens. Specifically, Ly-6G is primarily expressed by granulocytes while Ly-6C is expressed by monocytes<sup>180,197</sup>. Therefore, polymorphonuclear (PMN)-MDSCs have a CD11b<sup>+</sup>Ly-6G<sup>+</sup>Ly-6C<sup>low</sup> phenotype while the monocytic (MO)-MDSCs have a CD11b<sup>+</sup>Ly-6G<sup>-</sup>Ly-6C<sup>+</sup> phenotype<sup>220,221</sup>.

In humans, MDSCs have a CD14<sup>-</sup>CD11b<sup>+</sup>CD33<sup>+</sup>CD15<sup>+</sup> phenotype<sup>187,213,222</sup>. They lack expression of markers of mature myeloid and lymphoid cells and also lack expression of the major histocompatibility complex (MHC) class II molecule HLA-DR<sup>220,223</sup>. About 0.5% of peripheral blood mononuclear cells (PBMC) are comprised of this population in healthy individuals, but in cancer patients this increases to about 10%<sup>224-226</sup>. Recent studies have also indicated that there is a significant diversity in the MDSC subsets in different human cancers<sup>218,221,227</sup>. However, it remains unknown if this diversity arises due to different mechanisms by which the MDSCs are expanded in different cancers.

### **C. Mechanisms of MDSC-mediated immunosuppression**

T-cell proliferation is affected by several factors that include cytokines, growth factors and amino acids<sup>228</sup>. These factors are altered under pathologic conditions often due to the increased expansion of suppressor cells. Specifically, MDSC-mediated immunosuppression is reported to be primarily regulated by two enzymes: Arginase-1 (ARG1) and iNOS<sup>194,229</sup>.

ARG1 metabolizes L-arginine to L-ornithine and urea, and is induced in myeloid cells by anti-inflammatory cytokines such as IL-10, IL-4, IL-13<sup>230,231</sup> as well as TGF- $\beta$ <sup>232,233</sup> and GM-CSF<sup>234</sup>, and its expression is largely regulated by STAT6 activity<sup>235</sup>. iNOS converts L-arginine to L-citrulline and nitric oxide (NO) and can be induced by pro-inflammatory cytokines such as interferon (IFN)- $\gamma$ , IL-1, IFN- $\alpha$ , IFN- $\beta$  and TNF- $\alpha$  via the STAT1 signaling pathway<sup>214,228,234,236,237</sup>. Hence, the expression of these two enzymes is differentially regulated. Furthermore, inhibition of ARG1 results in an increase in iNOS function, while upregulation of ARG1 depletes L-arginine, thus leading to a decrease in iNOS translation and NO production<sup>217,238</sup>.

L-arginine depletion is reported to suppress T cell function by two distinct mechanisms: first, by inducing loss of CD3 $\zeta$  chain expression<sup>239</sup>, which is an important co-factor associated with T cell receptor (TCR) function; and second by preventing up-regulation of cell cycle regulators such as cyclin D3 and cyclin-dependent kinase 4 (CDK4) which results in arrest of T cells in the G<sub>0</sub>/G<sub>1</sub> phase of the cell cycle<sup>240</sup>. Lack of L-arginine also interferes with IL-2 receptor signaling in T cells by inhibiting the upregulation of the tyrosine kinase Janus kinase (Jak)-3 necessary for STAT5-dependent

transcription in response to IL-2<sup>241-243</sup>. IL-2 signaling is also inhibited by exposure to NO, which induces T cell apoptosis<sup>244-247</sup>.

Reactive oxygen species (ROS) production has emerged as a key mechanism of MDSC-mediated immunosuppression<sup>248</sup>. Hyper-production of ROS is observed to be a key feature exhibited by MDSCs in both tumor models and cancer patients<sup>249-253</sup>. This elevated level of ROS is accounted for by an increase in NADPH oxidase 2 (NOX2) activity<sup>250</sup>. In addition, L-arginine depletion in the tumor environment triggers superoxide generation from iNOS, which then reacts with water to generate hydrogen peroxide<sup>254-257</sup>. ROS are implicated in the inhibition of specific CD8<sup>+</sup> T cell responses in tumor-bearing mice and are also suggested to have a direct role in inhibiting T cell responses by increasing the expression of the anti-apoptotic protein Bcl-2 expression<sup>250,252,254,258,259</sup>. In addition, peroxynitrite, a highly reactive cell-permeable molecule, inhibits T cell function by nitration and nitrosylation of cysteine, methionine, tryptophan and tyrosine in multiple protein targets<sup>260-264</sup>. MDSCs are efficient producers of peroxynitrite and their increased levels are associated with tumor progression<sup>189,264,265</sup>. Direct contact between T cells and MDSCs allows MDSCs to induce nitration of tyrosine residues in the TCR and CD8 co-receptors, thereby impairing T cell interactions with the MHC and inhibiting T cell cytotoxic responses<sup>260,266-268</sup>.

MDSCs also exert their suppressive functions through the immunoregulatory cytokine TGF- $\beta$ , which is regulated in MDSCs by IL-13 and CD4<sup>+</sup>CD1d<sup>-</sup> restricted T cells<sup>269,270</sup>. Blocking IL-13 or TGF- $\beta$  is shown to inhibit tumor progression in murine transplanted tumor models<sup>271-273</sup>. MDSCs can also systemically downregulate L-selectin (CD62L) on T cells in tumor-bearing mice, which eventually impairs naïve CD4<sup>+</sup> and CD8<sup>+</sup> T cell

homing to lymph nodes<sup>204,267,274</sup>. Thus, T cells lose their ability to become activated by tumor antigens<sup>275</sup>. In addition, MDSCs indirectly suppress anti-tumor responses by inducing differentiation of other immunosuppressive populations such as regulatory T cells (Treg)<sup>276-278</sup>. They can activate both clonal expansion of existing Treg cells and the conversion of naïve CD4<sup>+</sup> T cells into Treg cells via various mechanisms, including secretion of IL-10 and TGF- $\beta$  as well as ARG1 functions<sup>204,279,280</sup>. Furthermore, a recent study reported the importance of the CD40 co-stimulatory molecule on MDSCs to induce tumor-specific Treg expansion in a mouse colon cancer model<sup>281</sup>.

In addition to T cell suppression, MDSCs restrict innate immune responses via their interactions with macrophages and natural killer (NK) cells to impair anti-tumor immunity. MDSCs inhibit expression of the NKG2D receptor on NK cells, thus impairing NK cell activity<sup>282</sup>. They also downregulate IL-12 production by macrophages, thus skewing tumor immunity<sup>283</sup>. Apart from immunosuppression, MDSCs support tumor growth by augmenting blood vessel development and enhancing tumor cell invasion and metastasis, a process called angiogenesis<sup>284-286</sup>. Matrix metalloproteinase (MMP) 9 is considered to be a critical factor in angiogenesis as it promotes degradation of the extracellular matrix along with an increase in the pro-angiogenic signal, VEGF<sup>287</sup>. In addition to MMP9, various other MMPs such as MMP14, MMP13 and MMP2 that are reportedly present in high levels in the tumor microenvironment, are reported to facilitate tumor progression and metastasis and escalate MDSC-mediated immunosuppression<sup>287-289</sup>.

## **VII. Epigenetic regulation and cancer therapy**

Cancer is a complex process that is influenced by multiple factors and progresses in multiple steps. Progression of tumor growth is facilitated by tumor cells that manage to escape the host's immune surveillance thus restricting immunotherapy. As mentioned above, the presence of immunosuppressive factors such as MDSCs and Treg cells play a major role in inhibiting cancer treatments. In addition to tumor-suppressive factors, genetic abnormality of cancer-related genes and epigenetic regulation are major factors associated with cancer<sup>290,291</sup>. Epigenetic regulation involves modification of deoxyribonucleic acid (DNA) and/or histones that alters gene expression. Modifications such as DNA methylation, acetylation, deacetylation, and ubiquitination of specific amino acid residues of the histones can all affect transcriptional regulation of genes that are involved with cell cycle progression, proliferation and apoptosis<sup>292,293</sup>.

### **A. Histone-modifying enzymes as key regulators in gene expression**

Histones are one of the most evolutionary conserved and most abundant proteins found in the nucleosome of eukaryotic cells<sup>294</sup>. There are five classes of histones (H1, H2A, H2B, H3 and H4) organized into core histones (H2A, H2B, H3 and H4) and linker histones (H1) that are assembled in an octameric core with 146-147 bp of deoxyribonucleic acid (DNA) wrapped around it<sup>295,296</sup>. The core histone N-terminal domains are rich in positively charged amino acid residues that actively interact with the DNA. This interaction is largely regulated by the modification of lysine residues<sup>295</sup>. Among several modifications, histone acetylation is one of the most crucial events associated with the transcriptional response of the cell<sup>297-299</sup>. Acetylated histones are



reported to be associated with transcriptionally active chromatin while deacetylated histones are associated with inactive chromatin<sup>299–301</sup>.

Under normal conditions, chromatin acetylation is regulated by the balance between two key enzymes: the histone acetyltransferases (HATs) and histone deacetylases (HDACs)<sup>299,300</sup>. The HATs transfer acetyl groups from acetyl coenzyme A onto conserved lysine residues within the histones, neutralizing their positive charge and thereby inhibiting interactions with the negatively charged DNA backbone. This leads to an active chromatin structure that enables the binding of several transcription factors for active gene transcription<sup>298,302,303</sup>. On the contrary, the HDACs catalyze the establishment of positive charges in the amino terminal tails of the core histones by removing acetyl groups. This strengthens the interactions between the histones and the DNA backbone, blocking the binding sites on promoters, thus inhibiting transcription<sup>304,305</sup>. Hence, this subtle balance between the HATs and HDACs is required to maintain normal cellular functions<sup>306,307</sup>. Perturbation of this balance is considered to be a key factor in cancer development<sup>308–310</sup>.

## **B. Histone deacetylases (HDACs)**

In eukaryotes, HDACs are classified into four major classes based on their homology to yeast HDACs<sup>311,312</sup>. The class I family is comprised of HDAC1, 2, 3 and 8, and is related to the yeast HDAC reduced potassium dependency 3 protein that is ubiquitously expressed and characterized by a nuclear localization signal (NLS) that primarily confines them in the nucleus of the cell<sup>313</sup>. Class II HDACs are comprised of HDAC4, 5, 6, 7, 9 and 10, and are homologous to histone deacetylase Hos3 (also known as HDA1) in yeast<sup>314</sup>. They are primarily located in the cytoplasm but also have the ability to shuttle

between the nucleus and cytoplasm due to the presence of a NLS<sup>315,316</sup>. Class I and II HDACs are evolutionarily related and have a catalytic domain that assists in the removal of acetyl groups via a Zn<sup>+</sup> ion<sup>317</sup>.

HDAC1 and HDAC2 are reported to be inactive deacetylases that require the involvement of multi-protein complexes such as Sin3 (switch independent 3), NuRD (nucleosome remodeling histone deacetylase) and Co-REST (co-repressor to RE1 silencing transcription factor) to mediate deacetylase activity and DNA binding<sup>318,319</sup>. HDAC3 is slightly different from HDAC1 and 2 as it contains a nuclear export signal (NES) as well as a NLS, thus enabling it to shuttle between the nucleus and the cytoplasm. In addition, it is implicated in other multi-protein complexes with co-repressors N-CoR (nuclear receptor co-repressor) and SMRT (silencing mediator for retinoic acid and thyroid hormone receptor)<sup>320</sup>. HDAC8 is the newest member of the Class I family and is yet to be isolated as part of a multi-unit HDAC complex<sup>311</sup>.

Class II HDACs are classified into two subsets: Class IIa, which is composed of HDAC4, 5, 7 and 9; and Class IIb, made up of HDAC6 and 10<sup>321,322</sup>. These HDACs exhibit specific tissue expression patterns. Specifically, HDAC4, 5 and 9 are mainly expressed in the heart, skeletal muscles and brain tissues, while HDAC7 is expressed in the heart and lungs. HDAC6 is mostly found in the testis while HDAC10 is found in the liver, spleen and kidney. The Class IIb subset is characterized by the presence of a single C-terminal catalytic domain, an NES, an NLS and an N-terminal region comprising multi-protein binding domains<sup>314,315,323</sup>. Class IIa HDACs are reported to interact directly with transcription factors such as MEF2 (monocyte enhancer factor 2), BCL-6 and PLZF (promyelocytic leukemia zinc finger) and are also found to be associated with nuclear co-

repressors such as N-CoR and SMRT<sup>320,322,324</sup>. Class Iib HDACs are characterized by the presence of two HDAC domains. HDAC6 contains two functional catalytic domains while HDAC10 contains a single functional domain, the second one being a vestigial domain<sup>325,326</sup>. In addition to this, a major difference between HDAC6 and the rest of the Class I and II HDACs is that HDAC6 is primarily located in the cytoplasm with the microtubule network and is associated with the deacetylation of  $\alpha$ -tubulin<sup>326</sup>. On the contrary, HDAC10 mainly resides in the nucleus and interacts with HDAC3 and SMRT<sup>320</sup>.

The class III family of HDACs (Sirtuins) is homologous to SirT2 in yeast. This family has seven members and is reported to be conserved in organisms ranging from bacteria to humans<sup>327</sup>. However, they are different from the Class I and II family as they utilize NAD as a co-factor instead of a  $Zn^{+2}$  ion<sup>328</sup>.

A new member protein, HDAC11, was identified but remained unclassified for quite a long time. However, it is now suggested that HDAC11 is located in both the nucleus and cytoplasm and belongs to the Class IV family of HDACs. It has a conserved domain in the catalytic region and is reported to share features with both the class I and II family of HDACs<sup>329</sup>.

### **C. Role of HDACs in cancer**

It is well established that the acetylation state of histones has a significant impact on the biological activity of a cell. Any imbalance in the levels of acetylation can induce abnormal outgrowth and cell death, leading to neoplastic transformations<sup>309</sup>. HDACs are reported to be overexpressed in several tumor lines and tissues and can affect global

transcriptional profiles<sup>330</sup>. However, recent studies have reported that the primary substrates of HDACs do not just include histone proteins but also several non-histone proteins such as tumor suppressor genes that include p53, p21, NF- $\kappa$ B and RUNX3<sup>331,332</sup>. These tumor suppressor genes are reported to be repressed while the tumor activator genes, such as hypoxia-inducible factor-1 (HIF-1), VEGF and heat shock protein 90 are up-regulated<sup>333,334</sup>. In addition, these tumor activator genes are also overexpressed under conditions of hypoxia and hypoglycemia<sup>335</sup>. Hypoxia is one of the key factors that induces angiogenesis, which is the process of formation of new blood vessels by endothelial cells. This plays a major role in the spread of cancer cells in blood, and peripheral organs and tissues<sup>336</sup>. Hence, inhibition of HDAC activity has emerged as a potential strategy for cancer therapy. Inhibition of HDACs by HDAC-specific inhibitors has gained much attention in recent years, and studies have shown that these inhibitors induced changes at both the molecular and cellular level. Changes reported include acetylation levels of histones, gene expression, and morphology and proliferation of cells<sup>296</sup>.

#### **D. Histone deacetylase inhibitors (HDACi)**

Histone deacetylase inhibitors (HDACi) are small molecule inhibitors that block the activity of HDACs thus increasing acetylation levels in cancer cells<sup>337-339</sup>. They have the ability to affect epigenetic regulation of histones by shifting the balance between HAT and HDAC enzyme activity by inducing hyperacetylation of histones<sup>340,341</sup>. However, many of the mechanisms associated with HDAC-mediated activity are still unknown although there are reports of multiple pathways that could be involved in this process<sup>338,342-344</sup>.

Association of HDACs with carcinogenesis has increased interest in the use of these inhibitors as potential anti-tumor agents<sup>337,345-349</sup>. HDAC inhibitors are reported to mediate activity in tumor cells by triggering cell cycle arrest in the G<sub>1</sub> and/or G<sub>2</sub> phase, and by inducing apoptosis and differentiation in cultured cells<sup>343,350-352</sup>. HDACi have shown strong growth-inhibitory activities in almost all transformed cell lines arising from hematologic and epithelial tumors while normal cells remain relatively resistant to HDACi-induced cell death<sup>351,353-355</sup>. HDACi can lead to accumulation of acetylated histones and even non-histone proteins that are associated with cell proliferation, differentiation, cell migration and apoptosis<sup>331,356</sup>. HDACi can trigger these events by activating intrinsic apoptotic pathways, extrinsic apoptotic pathways<sup>357,358</sup>, mitotic failure<sup>359</sup>, autophagy<sup>360,361</sup> and ROS-facilitated death<sup>362,363</sup>. In addition, these inhibitors are also reported to induce anti-angiogenic effects by suppressing HIF-1 $\alpha$  and VEGF levels<sup>364-367</sup>. However, generation of these effects is reported to be dependent on the state of the cell such as the type of molecular changes the cell has or is likely to undergo<sup>345,368</sup>. In addition, the type of HDACi, the concentration used and even the time of exposure are also expected to have added effects on the fate of the cell<sup>369</sup>. The effectiveness of the HDACi in binding to the HDAC enzyme pocket can also play an important role in determining their activity<sup>370,371</sup>. Tighter binding would slow the release process of the inhibitor from the pocket, thus leading to a more lasting inhibition. This can also lead to higher toxicity and other adverse effects on the cells or tumor models.

HDAC inhibitors are usually classified on the basis of their chemical structure and include hydroxamates, cyclic peptides, aliphatic acids and benzamides<sup>290</sup>. In addition, they can also be classified based on their selectivity to HDACs. There are over 500

clinical trials ongoing with HDACi as monotherapy or in combination with other agents such as retinoids, paclitaxel (Taxol), radiation, etc., in patients with hematologic malignancies and solid tumors including breast, pancreas, leukemias, lymphoma and multiple lymphoma<sup>338,346,368</sup>. Although these inhibitors differ in structure, potency and HDAC enzyme selectivity, they are reported to primarily target Class I and II HDACs with almost no effect on Class III. However, most of the downstream effects associated with these inhibitors are still under investigation as it is suggested that those are highly dependent not only on the type of the inhibitor but also on the cells that are being targeted.

Trichostatin-A (TSA) is a natural hydroxamate and was one of the first discovered compounds to show HDAC inhibition<sup>372</sup>. Since then, several hydroxamic acids have been identified including suberoylanilide hydroxamic acid (SAHA), also commercially known as Vorinostat, which was the first one to be approved by the FDA for the treatment of cutaneous T-cell lymphoma (CTCL)<sup>373,374</sup>. Clinical trials using SAHA showed significant anti-cancer activity at all given doses and it was also well tolerated by patients. PCI-24781 is a phenyl hydroxamic acid that has been evaluated alone as well as with ionizing radiation and other DNA-damage agents in pre-clinical studies. A phase I clinical trial in advanced solid tumor patients indicated that intravenous or oral doses of PCI-24781 were well tolerated. ITF2357 is a synthetic HDACi containing a hydroxamic acid group linked to an aromatic ring. Reports indicated that this compound induced pro-inflammatory cytokines and cytotoxicity both *in vitro* and *in vivo* in patients with malignant tumors<sup>375,376</sup>. Panobinostat (LBH-589) is a novel hydroxamate analog HDACi that is reported to induce acetylation of H3 and H4. In addition, it also increases p21 levels,

disrupts chaperone functions, induces cell cycle arrest and triggers apoptosis in K562 cells and acute leukemia (MV4-11) cells<sup>377,378</sup>. The first clinical trial of Panobinostat was conducted in patients with hematologic malignancies, and preliminary data suggested it was well tolerated in the patients<sup>379</sup>. It is also reported to have a longer half-life than SAHA and is currently in clinical trials for CTCL<sup>380</sup>.

Romidepsin (FK228, FR901228) is a bicyclic peptide that was naturally isolated from *Chromobacterium violaceum*<sup>381,382</sup>. It has shown strong anti-proliferative activities against tumor cell lines and good efficacy against human tumor xenografts. Several clinical trials were conducted in patients with various malignant conditions including renal cancer, lung cancer, CLL and AML. FK228 received FDA approval in November 2009 for the treatment of CTCL<sup>383</sup>.

For further development of more potent and specific HDAC specific inhibitors, X-ray crystal structure analysis was performed to decode the molecular action of HDACs. Initial studies involved X-ray crystallography of the catalytic domain of an HDAC from a hyperthermophilic bacterium, *Aquifex aeolicus*, to determine structure-function relationship of the HDAC<sup>384</sup>. Results showed that the HDAC catalytic domain consisted of a tubular pocket, a zinc-binding site, and two asparagine-histidine charge-relay systems<sup>290,296</sup>. Structure-activity relationship determination showed that inhibitors such as TSA and SAHA were able to block the HDAC activity through chelation of the zinc ion using a polar moiety such as hydroxamic acid or benzamide groups<sup>385-388</sup>.

Results from preliminary studies have encouraged further development of more HDAC inhibitors for use in cancer therapy. However, the quest for class-specific inhibitors that would provide selective targeting is still ongoing. Many clinical trials for HDAC

inhibitors that can target both hematologic and solid malignancies are also in progress. Currently, HDAC inhibitors are considered to be one of the most promising targets for the development of anti-cancer drugs. However, the mechanism by which they are recruited to the HDAC pocket and mediate corresponding cellular activities is still unknown. A better understanding of the nature of the molecular basis of the selectivity of the HDAC inhibitors will enable the development of more effective and specific agents to treat cancer.

### **VIII. Study Rationale:**

Folate receptor is overexpressed in almost all cancers including epithelial (breast, lung, cervical, prostate, renal, colon) and myeloid (leukemias) malignancies<sup>25,26</sup>. However, only 4-6% of normal cells are reported to express FR, and those that do, express FR only on their apical surface and thus away from the bloodstream<sup>6,14</sup>. This distinct expression profile enables opportunities for selective targeting of FR in tumor cells using therapeutics such as drugs and nanoparticles. In addition, a major difference between FR isoforms is that FR- $\alpha$  is expressed only on epithelial cells while FR- $\beta$  has only been reported in myeloid cells<sup>7,17,46,390</sup>. However, a common feature applicable to both isoforms is that they both exhibit high affinity for FA<sup>35,75</sup>. Previous studies have focused on understanding and targeting the FR- $\alpha$  isoform while the functions and role of FR- $\beta$  remain unknown. Another important aspect of studying the FR- $\beta$  isoform is that it is reported to be expressed on some immunosuppressive cell populations such as MDSCs. These cells dramatically expand in number during pathogenesis and cancer where they inhibit T cell activity thereby suppressing the immune responses in the host<sup>180,195</sup>. Hence, targeting FR- $\beta$  to selectively eliminate MDSCs could be a potential immunotherapeutic



strategy for cancer patients. Therefore, the overall goal of the first part of this study was to compare FR- $\alpha$  and FR- $\beta$  activity and determine the potential of FA-mediated therapeutic approaches to target these receptors in malignant epithelial and myeloid cells.

FR- $\alpha$  studies were performed on a murine epithelial breast cancer line, 4T1, which serves as a model of stage IV human breast cancer. The FR- $\beta$  studies were conducted on U937 cells, which is a human myelo-monocytic leukemia cell line. FR- $\alpha$  is reported to be internalized by tumor cells while FR- $\beta$  is considered partially inactive<sup>44,45</sup>. However, this can vary across tumor lines. Hence, it was important to determine the receptor expression and localization on the model cell lines, 4T1 and U937. It was also necessary to track both receptors intracellularly, compare their activities and define their functions. This was achieved by utilizing the high-affinity ligand, FA. Folic acid was conjugated to fluorochromes (fluorescein isothiocyanate, FITC; and tetramethylrhodamine, TRITC) to enable tracking of receptors using flow cytometry and fluorescence microscopy. Previous reports suggest that FRs can be internalized by receptor-mediated endocytosis<sup>60,76</sup>; however, more recent studies have proposed that special lipid-rich membrane deposits, also known as “lipid rafts”, are associated with the internalization of most GPI-linked proteins including FRs. Lipid rafts are small microdomains on the membrane that are formed from deposits of cholesterol and sphingolipids<sup>87,90</sup>. Therefore, the role of cholesterol on FR- $\alpha$  and FR- $\beta$  receptor activity was investigated. In addition, comparisons were made with well-established markers of internalization, transferrin and dextran. Transferrin receptor is internalized via receptor-mediated endocytosis to transport iron into the cells while dextran is commonly used to define the process of pinocytosis or “cell-drinking”<sup>69,105</sup>.

With the help of the above experiments, we can gain a better understanding of the activity of FR- $\beta$  and accordingly develop therapeutics to target both isoforms. For example, if FR- $\beta$  did not show internalization, therapeutic strategies to deliver cargo (e.g., drugs) into the cells will not work. This would require developing a method that can mediate cell-surface selective killing of the FR- $\beta$ -expressing cells. Therefore, a preliminary study was initiated to determine if gold nanoparticles could be selectively targeted to FR-expressing cells. If successful, this would serve as a model system to develop FA-conjugated gold-coated magnetite nanoparticles that can be used to target and destroy FR-expressing cells following exposure to an oscillating magnetic field. Application of an oscillating magnetic field generates localized heat around the nanoparticles causing membrane damage and cell death without causing damage to the neighboring healthy cells.

Most anti-cancer therapy is dependent on the concepts of active and passive targeting. The active form of targeting utilizes a specific molecule or protein expressed by the tumor cells (e.g., folate receptor) as described above, which is then targeted via linking the appropriate ligand or antibody to drugs, nanoparticles or other therapeutic molecules<sup>2,136</sup>. On the other hand, passive targeting utilizes the leaky vasculature of blood vessels and tissue matrix in a tumor environment, also known as the EPR effect. This enables drugs or any carrier molecules to easily diffuse into the tissue<sup>71</sup>. Hence, exploring the prospects of passive targeting in parallel with actively targeting the folate receptor can help determine the effectiveness of both methods in the field of cancer therapy. The use of HDACi has gained intense interest in recent years as biologically active molecules that can target and manipulate cells at the gene level. These naturally derived or

synthesized compounds can inhibit HDAC hyperactivity in tumor cells<sup>368</sup>. It is already known that many epithelial tumors, as well as hematologic malignancies, overexpress HDACs that suppress transcription factors that are associated with normal cellular activity<sup>315,330</sup>. HDACis such as SAHA and FK228 have made it through clinical trials and are currently FDA approved for the treatment of cutaneous and cytotoxic T-cell lymphoma. Despite this limited success, there is still a major need for new HDAC class-specific inhibitors. Hence, the synthesis of novel compounds with potent anti-cancer activity as well as HDAC specificity, are required to address drug-associated toxicity and other side-effects in patients. Therefore, a collaborative study was undertaken to characterize a novel compound (Cpd5) having increased class I HDAC specificity. Initial studies of metabolism, pharmacokinetics, histone acetylation, cytotoxicity against tumor cell lines, *in vivo* tumor growth and systemic toxicity all showed promising results. It is tempting to speculate that the increased specificity of Cpd 5 for class I HDACs resulted in retaining the desirable HDACi effects while producing fewer side effects in the animals. This project hopes to contribute significantly to the understanding of functional differences in the folate receptor isoforms and provide insights into potential therapeutic strategies that can be used to target malignant epithelial and myeloid cells with improved selectivity.

## FIGURES AND LEGENDS

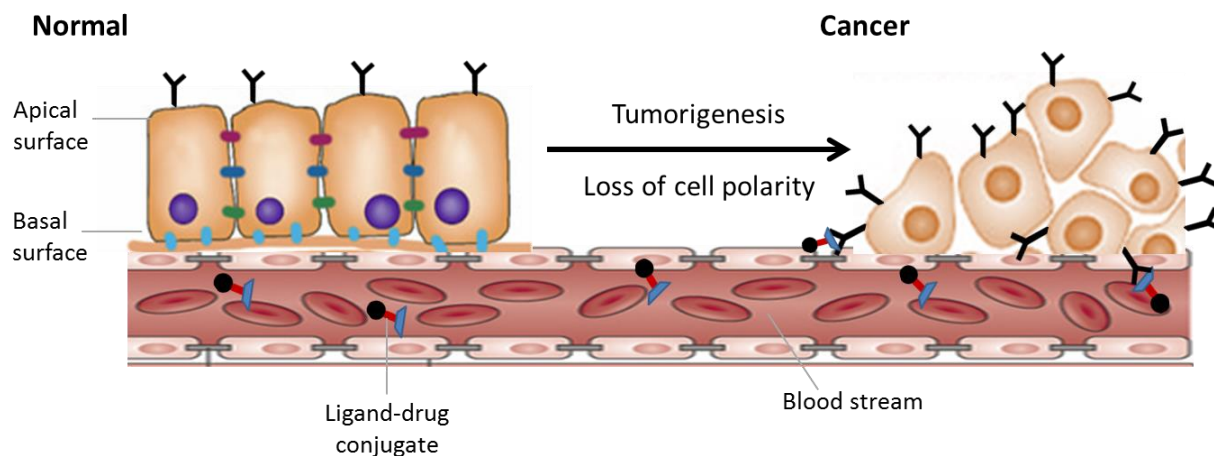


**Figure 1. Differential expression of FR- $\alpha$  in normal and cancer cells facilitates selective targeting.**

FR- $\alpha$  receptor expression is restricted to the apical surface of normal epithelial cells and tissues. This orientation keeps the receptors away from the basal surface and bloodstream thus making the receptors inaccessible to FA-conjugates that are administered intravenously. Tumor-transformed cells lose polarity and intercellular junctions resulting in expression of folate receptors across the cell surface. This enables FA-conjugated drug or therapeutic molecules to gain access to the receptors and selectively induce effects in these cells without harming the neighboring healthy cells (adapted from Madduri Srinivasarao *et al.*, Nature Reviews, Drug Discovery<sup>392</sup>).

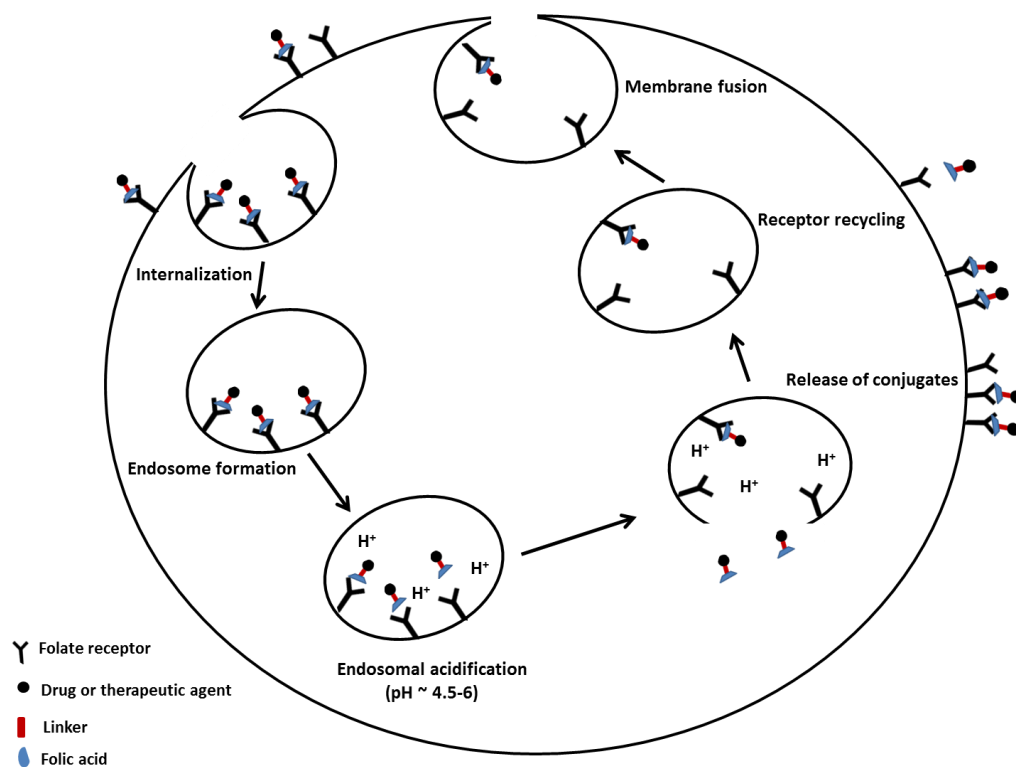


**Figure 2. Proposed receptor-mediated endocytosis of folic acid-conjugates in a tumor cell.**

The folate-conjugate binds to FR expressed on the surface of a cell. The membrane forms an invagination and internalizes the folate-conjugate via formation of an endocytic vesicle. As the pH reduces to 4.5 to 6, the conjugates dissociate from the receptors due to a process called endosomal acidification initiated by a proton gradient. The unbound receptors are then recycled back to the surface for delivery of additional folate-conjugates to the cell. It has been reported that only 15-25 % of the receptor-bound conjugates are actually released into the cell while the rest of the bound receptors get recycled back to the surface<sup>75</sup>.

## **CHAPTER 2**

FOLATE RECEPTOR ISOFORMS  $\alpha$  AND  $\beta$  HAVE DISTINCT EXPRESSION PROFILES  
AND EXHIBIT DIFFERENTIAL ACTIVITY

## ABSTRACT

The folate receptor- $\alpha$  (FR- $\alpha$ ) has been under extensive study for its potential use as a target in cancer therapy. FR- $\alpha$  is expressed on a wide range of epithelial tissues but found only on the apical surface of the polarized cells. However, during malignant transformation, the cell loses polarity, which results in FR- $\alpha$  expression across the cell surface. Expression of FR- $\alpha$  in cancer is well established and usually varies among tumors, showing high expression in serous ovarian cancer and renal carcinoma versus low-to-moderate expression in breast, colorectal and lung cancer. However, its high binding affinity for its physiologic ligand folic acid, has encouraged tumor-targeting studies utilizing folic acid conjugates. The FR- $\beta$  isoform is primarily found on cells of myelo-monocytic lineage. A significant amount of FR- $\beta$  is also expressed in normal tissues such as placenta and hematopoietic cells. In addition, FR- $\beta$  has been reported to be expressed on myeloid-derived suppressor cells (MDSCs). MDSCs are of myeloid lineage and are dramatically expanded during cancer where they act to inhibit T cell functions. Preliminary studies on FR- $\beta$  have indicated structural variability from FR- $\alpha$  suggesting possible functional differences. Therefore, the expression profile and activity of FR- $\beta$  were examined to determine its potential use as a therapeutic target in parallel to FR- $\alpha$ . In this part of the study the expression of FR- $\alpha$  and FR- $\beta$  in both normal and tumor cell lines of epithelial and myeloid origin, respectively were determined. Antibody-labeling studies using the 4T1 murine mammary carcinoma epithelial cell line and the human myeloid myelomonocytic leukemia cell line, U937, showed restricted expression of FR- $\alpha$  and the FR- $\beta$ , respectively. Thus, 4T1 and U937 cells were appropriate models to examine these receptors individually. Qualitative analyses showed that FR- $\alpha$  receptors exhibited a strong punctate staining pattern on the 4T1 cell membrane, while FR- $\beta$  on U937 cells was mostly polarized to one end of the cell membrane. Next, the effect of free

folic acid on FR internalization and recycling was investigated. Both isoforms showed strong binding to folic acid; however, FR- $\beta$  exhibited lower binding affinity than FR- $\alpha$ . FR- $\alpha$  receptors efficiently internalized into 4T1 cells after exposure to folic acid and showed evidence of recycling and/or re-expression. On the contrary, FR- $\beta$  on U937 cells lacked the ability to internalize. These findings suggest: 1) FR- $\alpha$  and FR- $\beta$  have distinct cell surface localization; 2) both receptors exhibit differential activity but strong binding to folic acid; and 3) both receptors can be potentially targeted by folic acid-dependent strategies.



## INTRODUCTION

The high-affinity folate receptor (FR) was originally reported in membrane fractions of placenta, choroid plexus, proximal kidney tubules, and KB epidermoid carcinoma cells<sup>7,8</sup>. The complete and partial amino acid sequences of FR- $\alpha$  were derived from bovine and human milk, respectively<sup>18</sup>. The cDNA of FR- $\alpha$  was isolated from KB cells, CaCo-2 cells, and the placenta,<sup>42,393</sup> while that of FR- $\beta$  was cloned from placenta<sup>9,46</sup>. Mouse homologues for FR- $\alpha$  and FR- $\beta$  have also been identified<sup>17</sup>. FR- $\alpha$  and FR- $\beta$  are reported to only share 71-73% amino acid sequence similarity<sup>37,39</sup>. The predicted amino acid sequences from the cDNAs contained amino terminal signal sequences of 25 residues for FR- $\alpha$  and 19 residues for FR- $\beta$  alongside 16 conserved cysteine residues. Mutagenesis studies have also indicated that the number of N-glycosylation sites for the two isoforms are different, with FR- $\alpha$  having three sites while FR- $\beta$  only has two. These N-glycosylation sites are thought to mainly contribute to cell surface expression of FR, without having any effect on the ligand-binding efficiencies of the receptors<sup>13,36</sup>. Membrane-bound FR- $\alpha$  and FR- $\beta$  are both able to bind folic acid with high affinity ( $K_D < 1$  nM), but bind reduced forms of folate such as 5-methyltetrahydrofolate (5-mTHF) with a much lower affinity. However, FR- $\beta$  still exhibits >50-fold lower affinity for folates than FR- $\alpha$ <sup>37</sup>. These ligand specificities were attributed to amino acid sequence divergence that involved Leu-49 in FR- $\beta$ , and Ala-49, Val-104 and Glu-166 in FR- $\alpha$ <sup>36,39</sup>. These structural differences showed direct correlation with binding affinity thus suggesting possible major functional differences, and hence required further investigation.

FR expression exhibits a distinct tissue and tumor specificity. mRNA and protein expression patterns of the respective FR isoforms have been well studied using non-quantitative immunohistochemical methods as well as quantitative methods including northern blots, radio-

immunoassays, flow cytometry and PCR<sup>7,29</sup>. Results from various studies have indicated that the functionality of FR in normal and malignant tissues correlates with their ability to bind either <sup>3</sup>H-labeled or fluorochrome-conjugated folate. Importantly, the mRNA results also showed that FR expression in cell lines did not reflect the expression profiles *in vivo*<sup>75</sup>.

Previous studies have shown that FR- $\alpha$  on normal cells is present on the germinal epithelium of the ovary, fallopian tubes, uterus and placenta<sup>7,14,42</sup>. These receptors are typically expressed on the apical surface of polarized epithelial cells which protects the normal tissues from FR-targeted agents that are administered through the blood. Various studies have utilized mRNA microarray techniques to test the expression of FR- $\alpha$  in malignant tissues; however, most of the attention in developing FR-targeted therapies has focused on ovarian and endometrial cancers<sup>30,394</sup>. These tumors have a consistent expression of FR- $\alpha$  throughout the stages of cancer progression, unlike the adenocarcinomas. FR- $\alpha$  was reportedly downregulated in mucinous and cervical adenocarcinoma and expressed *de novo* in uterine adenocarcinoma. Inconsistent FR- $\alpha$  expression was also observed in breast, colon and renal carcinomas<sup>395</sup>; however, the folate binding ability of the receptors was intact in both early and malignant stages of the cancer. Thus, the variable and limited expression of FR- $\alpha$  in epithelial tumors limits the prospects of folate-targeted therapy to only specific cancers. Expanding the targeting strategy to include the FR- $\beta$  isoform would increase the number of cancers that could be treated, such as leukemias.

The initial suggestion that FR- $\beta$  was a myeloid marker was based on an early study that showed elevated levels of membrane-bound FR- $\beta$  in splenic tissues of patients with myelogenous leukemia<sup>45</sup>. Flow cytometric data for peripheral blood leukocytes showed consistent results with the observation that FR- $\beta$  expression was mainly restricted to neutrophils. Hence, co-expression of FR- $\beta$  with CD19 and CD3 was not observed while FR- $\beta$  co-expression

with myeloid markers such as CD13 and CD11b was found<sup>46</sup>. In addition, lack of co-expression of FR- $\beta$  in CD34<sup>+</sup> cells from normal bone marrow indicated that FR- $\beta$  is not expressed during early stages of normal bone marrow hematopoiesis. Interestingly, FR- $\beta$  in normal cells are unable to bind folate whereas various leukemia cells such as AML and CML, have high folate binding ability<sup>36,47</sup>. This difference can offer a huge advantage in developing methods to selectively target cells overexpressing this isoform. Therefore, additional studies examining FR- $\beta$  expression and folic acid binding characteristics are required to determine the prospects of folate-conjugates to target leukemic cells.

To further characterize functional properties of FR- $\alpha$  and FR- $\beta$ , an epithelial murine breast carcinoma cell line, 4T1, and a human myelomonocytic leukemia cell line, U937, were chosen. FR- $\alpha$  and FR- $\beta$  expression patterns were analyzed for each cell line to determine distribution of the receptors. In addition, FR expression was quantified on normal epithelial and normal myeloid cells to determine whether FR expression was restricted to only carcinomas. Folic acid, the high affinity ligand, was utilized to determine receptor activity. Binding and internalization by the receptor isoforms were investigated and compared.

Consistent with previous studies, FR- $\alpha$  and FR- $\beta$  were found limited to epithelial and myeloid cell lines, respectively, and thus these two cell lines are appropriate models to further examine these receptors. However, the isoforms demonstrated very different staining patterns on the respective cells. Importantly, FR- $\alpha$  was found consistently overexpressed in tumors harvested from 4T1 tumor-bearing mice showing that expression was maintained *in vivo*. In contrast, normal epithelial cells isolated from the trachea of healthy mice did not exhibit FR- $\alpha$  expression. Similarly, FR- $\beta$  expression was significantly elevated on the U937 cell line while monocytes isolated from normal human blood lacked expression of the isoform. FR- $\alpha$  in the 4T1 cells not

only showed binding to folic acid, but also demonstrated rapid internalization within 5 minutes of exposure to free folic acid. Results also showed that receptor recycling and re-expression occurred 2 hours after folic acid binding. In contrast, the FR- $\beta$  receptors on U937 cells also showed binding to folic acid but did not show any signs of internalization. Taken together, these findings indicate that the FR isoforms are functionally distinct from one another. Therefore, despite the ability of both FR isoforms to bind folic acid, the differences observed in receptor activity following binding will have to be taken into account when designing FR-targeting strategies for epithelial and myeloid tumors.

## MATERIALS AND METHODS

### Cell lines and reagents

The 4T1 murine mammary carcinoma epithelial cell line (ATCC CRL-2539) was purchased from ATCC (Manassas, VA). The line was originally derived from a spontaneous mammary tumor from a BALB/cfC3H mouse<sup>396</sup>. When transplanted ectopically into syngeneic BALB/c mice, the 4T1 cell line generates a solid, highly metastatic tumor that spreads to nearby lymph nodes, lungs, bones, brain, and liver, thus resembling stage IV metastatic breast cancer in humans. The U937 human myelomonocytic leukemia (myeloid) cell line (ATCC CRL-1593.2) was also purchased from ATCC and was originally derived from malignant cells obtained from the pleural effusion of a patient with histiocytic lymphoma. The 4T1 cell line was cultured in RPMI 1640 medium (Life Technologies, Grand Island, NY), supplemented with 10% fetal bovine serum (Atlanta Biologicals, Flowery Branch, GA), 100 U/ml penicillin, 100 µg/ml streptomycin and 2mM L-Glutamine (all from ThermoFisher Scientific, Waltham, MA) and 55 µM 2-mercaptoethanol (Life Technologies, Grand Island, NY). The U937 cells were cultured similarly as above except without 2-mercaptoethanol. At a confluency of 70% or less, the 4T1 cells were lifted with Cellstripper<sup>TM</sup> (Mediatech Inc., Manassas, VA) according to the manufacturer's instructions. However, the U937 cell line, being non-adherent, was grown in suspension. Cell counts and viability were determined using a hemacytometer following appropriate dilution in trypan blue exclusion dye.

Antibodies used in flow cytometry, fluorescence and confocal microscopy, and immunohistochemistry experiments included polyclonal rabbit anti-FR-β antibody (Thermo Fisher Scientific, Waltham, MA); polyclonal rabbit anti-mouse/rat/human all isotype FR antibody (Santa Cruz Biotechnology, Santa Cruz, CA); and Alexa Fluor<sup>®</sup> 647 conjugated anti-

human CD14 antibody (BioLegend, San Diego, CA). The primary rabbit antibodies were detected with a secondary Alexa Fluor<sup>®</sup> 647- or Alexa Fluor<sup>®</sup> 488-conjugated goat anti-rabbit IgG antibody (Jackson ImmunoResearch, West Grove, PA). Leukocytes were identified using an allophycocyanin (APC)-conjugated anti-mouse CD45 antibody (eBioscience, San Diego, CA).

Folic acid (Thermo Fisher Scientific) was used to determine receptor binding kinetics in pulse chase experiments. Folic acid powder was weighed and dissolved in 100% DMSO (250 mM) and stored at 4°C for no longer than one month. Working concentrations were prepared by diluting in phosphate-buffered saline (PBS) immediately before performing experiments.

### **Animals and tumor induction**

BALB/c (wild type) mice were originally purchased from the Jackson Laboratories (Bar Harbor, ME) and further housed and bred in a specific pathogen-free barrier facility in the animal resource center at the University of Wisconsin-Milwaukee, and screened regularly for pathogens. All procedures were approved by the Animal Care and Use Committee of the University of Wisconsin-Milwaukee. For tumor induction,  $1 \times 10^4$  4T1 cells in 50  $\mu$ l supplement-free RPMI 1640 medium were injected subcutaneously into the mammary fat pad of 8-12 week old wild type BALB/c female mice. Tumors were monitored by caliper measurements of the major (L, length; mm) and minor (W, width; mm) axes and tumor volume (V, volume; mm<sup>3</sup>) was calculated by the formula:  $V = (L \times W^2) / 2$ .

### **FR- $\alpha$ and FR- $\beta$ labeling on tumor cell lines**

4T1 and U937 cells were cultured and suspended in RPMI 1640 medium at a concentration of  $0.5 \times 10^6$  cells per 50  $\mu$ l in 5 ml round-bottomed tubes. The cells were labeled with 50  $\mu$ l of anti-all isotype FR antibody that recognizes both FR- $\alpha$  and FR- $\beta$  isoforms or an antibody specific to FR- $\beta$ , diluted to 10  $\mu$ g/mL in culture medium. Negative controls received PBS containing 2%

normal horse serum (NHS, ThermoFisher Scientific) in PBS (PBS/NHS) and all samples were incubated on ice for 30 minutes. The cells were then washed with PBS/NHS followed by detection with an Alexa Fluor<sup>®</sup> 647-conjugated goat anti-rabbit IgG antibody diluted to 7.5 µg/mL in PBS/NHS for 30 minutes on ice. Following labeling, the cells were washed again in PBS/NHS, fixed in 1.5% formaldehyde in PBS, and analyzed with a FACSCalibur flow cytometer (BD Biosciences, San Jose, CA) using BD CellQuest<sup>™</sup> Pro software. 10,000 cells/sample were analyzed with fluorescence intensity displayed on a 4-decade log scale. Four to five experiments were analyzed per labeling combination.

### **FR- $\alpha$ and FR- $\beta$ labeling on blood and tissues**

To assess the cellular distribution of FR- $\alpha$ , control mice without tumors and 4T1-tumor-bearing mice at the 4-week stage were euthanized. Tumors were harvested and single-cell suspensions were prepared as follows: tumors were minced with scissors into ~1 mm pieces and incubated 30-60 minutes at 37°C and 5% CO<sub>2</sub> in digestion buffer, containing 562 U/ml collagenase, 20.6 U/ml deoxyribonuclease I (both from Sigma Aldrich, St. Louis MO), and 5 mg/ml bovine serum albumin (Fisher, Hampton, NH) in PBS. The red blood cells were then lysed in ACK buffer (0.15 M NH<sub>4</sub>Cl, 10 mM KHCO<sub>3</sub>, 0.1 mM NA<sub>2</sub>EDTA, pH 7.4), filtered through 70 µm mesh and washed three times in PBS. FR- $\alpha$  expression was also analyzed on normal murine epithelial cells by harvesting the trachea of mice followed by preparation of single-cell suspension as follows: trachea from 2-3 mice were harvested, placed in a 60 mm culture dish containing the same digestion buffer described above, and incubated for 30-60 minutes at 37°C in 5% CO<sub>2</sub>. The cells were then filtered through 70 µm mesh and washed three times in PBS.

For assessing the distribution of FR- $\beta$  in peripheral blood mononuclear cells (PBMCs), 5 ml blood was drawn from healthy human donors and collected into heparinized tubes. Blood was diluted in a 1:1 ratio with RPMI media and gently overlaid onto 4 ml of Ficoll (Sigma Aldrich, St. Louis, MO) in a 15 ml centrifuge tube followed by centrifugation at 550 x g for 30 minutes at room temperature. The PBMC layer was collected and washed two times with PBS. Human monocytes were identified with an Alexa Fluor<sup>®</sup> 647-conjugated mouse anti-human CD14 antibody as described above.

Cell counts and viability were determined using a hemacytometer following appropriate dilution in trypan blue exclusion dye. Cell concentrations were adjusted to  $10 \times 10^6$  cells/ml and  $0.5 \times 10^6$  cells were immunolabeled for FR- $\alpha$  and FR- $\beta$  receptors and analyzed by flow cytometry as described above.

#### **Immunofluorescence labeling to determine localization of FR- $\alpha$ and FR- $\beta$ receptors**

4T1 cells were seeded at a density of  $0.2 \times 10^6$  cells/ml on 10 mm round no. 1.5 glass coverslips (Ted Pella, Redding, CA) and cultured in supplemented RPMI 1640 medium for 18 hours. Cells were incubated as above with the primary antibodies to FR- $\alpha$  or FR- $\beta$  for 30 minutes on ice followed by detection with an Alexa Fluor<sup>®</sup> 647-conjugated goat anti-rabbit IgG antibody for 30 minutes on ice. Cells were washed with PBS/NHS and fixed in 1.5% formaldehyde in PBS. Coverslips with the adherent 4T1 cells were then mounted inverted on glass microscope slides in ProLong Gold<sup>®</sup> (Life Technologies). The U937 cells were cultured in suspension and were suspended in RPMI 1640 medium at a concentration of  $0.5 \times 10^6$  cells/50  $\mu$ l in 5 ml round-bottomed tubes. The cells were labeled with antibodies as described above and then cytopun for 10 minutes. Both 4T1 and U937 cells were then analyzed on a Nikon Eclipse TE2000-U inverted epifluorescence microscope (Nikon Instruments Inc., Melville, NY) and digital images were



acquired at a constant exposure setting through a Nikon Plan Apo 60x oil immersion objective using a Cool SNAP ES digital monochromatic camera (Photometrics, Tucson, AZ). Images were analyzed using MetaVue™ software (Universal Imaging Corporation, Downingtown, PA), pseudocolored and imported into Microsoft Powerpoint software. Confocal analyses were performed using a Leica Microsystems™ TCS SP2 laser-scanning microscope (Richmond, IL). Images were acquired using a 40x objective and pseudocolored using Leica confocal software. Images are representative of a minimum of 3-5 independent experiments.

### **Labeling of tumor cryosections for fluorescence microscopy**

4T1 tumors (~4-weeks) were harvested from BALB/c mice and then snap-frozen in tissue freezing medium (Triangle Biomedical Sciences, Inc, Durham, NC) in liquid nitrogen or on dry ice. Tissue sections with a thickness of 7 µm were cut on a cryostat and adhered onto poly-L-lysine-coated microscopic slides. The sections were fixed in -20°C acetone for 5 minutes and stored at -20°C until labeling. The sections were thawed for 5 minutes and rehydrated in PBS for 10 minutes. The sections were then incubated in 5% normal goat serum in PBS to block non-specific antibody binding. The sections were labeled for both FR- $\alpha$  and FR- $\beta$  as described above. Negative controls received PBS/NHS in place of the primary antibody. To visualize tumor-infiltrating leukocytes, the sections were blocked with 5% normal rabbit serum followed by also labeling with an Alexa Fluor® APC-conjugated mouse anti-CD45 antibody for 30 minutes at room temperature. Sections were washed with PBS for 5 minutes followed by incubation with 0.3 µM DAPI (Sigma Aldrich, St. Louis, MO) for 10 minutes. The slides were washed again with PBS for 5 minutes and mounted in ProLong Gold®. The tumor sections were imaged using epifluorescence microscopy as above using a 20x objective, pseudocolored and overlaid using MetaVue™ software. Images are representative of of 3-5 independent experiments.

### **Analysis of FR- $\alpha$ and FR- $\beta$ activity in the presence of free folic acid**

4T1 and U937 cells were used at a concentration of  $0.5 \times 10^6$  cells/50  $\mu$ l and pulsed with 2.2  $\mu$ M folic acid for 5 minutes at 37°C. Cells were washed with warm folate-free RPMI 1640 medium and then chased with folate-free medium for 5, 15, 30 or 120 minutes. Cells were labeled with anti-FR- $\alpha$  and anti-FR- $\beta$  antibodies and analyzed by flow cytometry as described above.

### **Statistical analysis**

Data are presented as mean  $\pm$  SEM. Significant differences between sample means were determined using a Student's *t* test with  $p < 0.05$  being considered significant. Data between various treatment groups were analyzed using one-way ANOVA with post-hoc comparison using Bonferroni multiple-comparison tests using Graph Pad Prism Software, Version 3.00 (San Diego, CA, USA).

## RESULTS

### **FR- $\alpha$ expression was restricted to cells of epithelial origin**

The FR isoform expressed on 4T1 cells was determined by flow cytometry and microscopy analyses using FR isoform-specific antibodies. 4T1 cells stained with the anti-FR all isotype antibody showed a significant increase in the mean fluorescence intensity as compared to the negative control (Fig. 3A,  $49\pm 7$  vs  $12\pm 1$ ;  $p<0.05$ ). The 4T1 cells were also stained with the anti-FR- $\beta$  antibody to determine FR- $\beta$  expression. The cells did not show any detectable FR- $\beta$  expression (Fig. 3B). These results demonstrate that 4T1 cells expressed only the FR- $\alpha$  isoform.

### **Tumors harvested from 4T1 tumor-bearing mice retained FR- $\alpha$ expression**

Although FR- $\alpha$  expression was found on the 4T1 cells in culture it was necessary to determine whether 4T1 tumors harvested from animals retained this expression. Therefore, 4T1 tumors were harvested from BALB/c mice at an advanced stage (~4-week) and labeled for FR- $\alpha$  expression. Single-cell suspensions from the tumors were also labeled with anti-CD45 antibody to identify and exclude infiltrating leukocytes and analyzed by flow cytometry. Gating on the CD45<sup>-</sup> population (Fig. 4A, left histogram) eliminated all leukocytes and thus enabled determination of FR- $\alpha$  expression only on the non-leukocyte population that primarily contained the 4T1 epithelial tumor cells (Fig. 4A, right histogram). The CD45<sup>-</sup> cell population showed uniform positive labeling for FR- $\alpha$  ( $12\pm 2$ ;  $p<0.05$ ); however, the expression levels were lower than that of the 4T1 cultured cells. (Fig. 5,  $p<0.05$ ).

Tumor sections were also labeled with either the anti-FR-all isotype or the FR- $\beta$ -specific antibody along with CD45 (Fig. 4B). With the FR all isotype antibody (left panel), large regions of the tumor sections showed strong staining indicating positive FR expression. However, no

positive staining was observed in these same regions in the FR- $\beta$  stained (right panel) tissue sections clearly indicating the absence of FR- $\beta$  receptors in the tissue. CD45-labeled cells indicated leukocyte infiltration in the tumors and some of these cells showed positive FR- $\beta$  staining. Taken together, these results demonstrate that the 4T1 epithelial tumor tissues retain expression of FR- $\alpha$ .

### **Tracheal epithelial cells from healthy mice did not express FR- $\alpha$**

Based on previous literature, normal epithelial tissues were expected to have negligible to no FR expression; however, no reports of FR- $\alpha$  expression on normal murine epithelial cells by flow cytometry could be found. Hence, the trachea of normal mice were harvested for isolating epithelial cells. FR- $\alpha$  labeling on the normal epithelial cells was quantified by flow cytometry and was compared to that of cultured 4T1 cells and 4T1 tumor cell suspensions (Fig. 5). Results showed that the normal tracheal epithelial cells did not show any FR- $\alpha$  expression. Compared to the control, significantly higher FR- $\alpha$  expression was observed in the cultured 4T1 tumor cells ( $p < 0.005$ ) as well as in the 4T1 tumors ( $p < 0.05$ ). These results taken together, confirmed the overexpression of FR- $\alpha$  on the 4T1 epithelial tumor cells (both *in vitro* and *in vivo*) but not on normal epithelial cells.

### **FR- $\beta$ expression was restricted to cells of myeloid lineage**

FR isotype expression on U937 cells was quantified by flow cytometry and microscopy analyses, using FR- $\beta$ -specific antibodies. U937 cells stained strongly with the anti-FR- $\beta$  antibody (Fig 6). Specifically, the FR- $\beta$  labeled cells had a mean fluorescence intensity of  $23.5 \pm 6.5$  compared to the negative control values of  $3.6 \pm 0.2$ . Therefore, the U937 cells can be used as a model myeloid cell line for functional studies of FR- $\beta$ . It was also of interest to determine if FR-

$\beta$  expression was restricted to myeloid leukemias. To address this, the Jurkat T-cell lymphoma cell line was used. Jurkat cells showed no positive staining with either the anti-FR all isotype or anti-FR- $\beta$  antibodies (Fig. 7). Therefore, FR- $\beta$  expression appears to be restricted to the myeloid leukemias.

### **Monocytes isolated from normal human blood did not express FR- $\beta$**

FR- $\beta$  receptors are reported to be overexpressed on myeloid malignancies including leukemia with very low to negligible expression on normal cells of myeloid lineage. After validating its expression on the U937 cell lines, it was now important to determine the expression of this receptor on normal myeloid cells. For this purpose, monocytes from normal human blood were isolated to serve as a relevant model for comparison to that of the U937 cells. Peripheral blood mononuclear cells (PBMC) isolated from whole blood were analyzed for FR- $\beta$  expression (Fig. 8A). The CD14<sup>+</sup> population, representing the monocytes, was gated (left histogram) and FR- $\beta$  staining on the gated cells was quantified by flow cytometry (right histogram). Results showed that the anti-FR- $\beta$  antibody stained cells had the same level of mean fluorescence intensity as that of the negative control, thus confirming that normal human monocytes do not express FR- $\beta$  receptors. Summary data are shown in Fig. 8B and demonstrate the overexpression of FR- $\beta$  on U937 tumor cells and the level of expression on normal monocytes.

### **The FR- $\alpha$ and FR- $\beta$ receptors exhibited distinct patterns of membrane localization**

4T1 and U937 cells stained with either anti-FR all isotype or anti-FR- $\beta$ -specific antibodies were analyzed by fluorescence microscopy to determine the patterns of receptor localization on the cell surface (Fig 9). The 4T1 cells showed distinct punctate receptor staining which was observed as clusters over the entire cell surface (left panel) while the U937 cells exhibited a more

polarized staining pattern, where the receptors were found localized towards one end of the cell (right panel). This distinct membrane localization pattern of the isoforms was further confirmed by confocal microscopy (Fig. 10). These results suggest that FR- $\alpha$  and FR- $\beta$  are oriented differently on the cell surface.

### **FR- $\alpha$ and FR- $\beta$ receptors exhibit differential activity in cells**

The effect of endogenous folate (present in culture media) was analyzed to determine any effects in regulating FR expression. 4T1 and U937 cells grown in folate-free RPMI supplemented media when stained with either anti-FR all isotype or anti-FR- $\beta$  antibodies exhibited similar levels of FR- $\alpha$  or FR- $\beta$  expression compared to cells that were grown in folate-supplemented regular media (Fig. 11). Thus, it was evident that the folate in culture medium did not affect receptor expression on the cells. Therefore, experiments associated with folic acid and receptor activity or targeting could be performed using regular folate-supplemented RPMI media.

To determine the activity of FR- $\alpha$  and FR- $\beta$  receptors, cells were pulsed with free folic acid (2.2  $\mu$ M) and chased with folate-free medium for varying time points to determine receptor activity in response to the high affinity ligand, folic acid. Receptor expression was quantified using flow cytometry. 4T1 cells showed a significant (1.5-fold,  $p < 0.05$ ) reduction in cell-surface FR- $\alpha$  expression within 5 minutes following addition of free folic acid when compared to non-pulsed control cells (Fig. 12). In addition, receptor expression did not begin to recover until 1 hour post-pulse, suggesting that there was no receptor recycling or re-expression during this time. After a 2-hour post-pulse, FR- $\alpha$  receptor expression was restored back to that of the positive control. To make sure folic acid was not interfering with antibody binding, cells were

treated with sodium azide to block cellular activity or treated at 4°C to inhibit membrane movement. In both cases anti-FR labeling remained unchanged (data not shown). These results demonstrate that FR- $\alpha$  is rapidly internalized by 4T1 cells following binding of folic acid. To determine if FR- $\beta$  expression was regulated similar to FR- $\alpha$ , U937 cells were subjected to the same pulse-chase experiments (Fig. 12). Interestingly, the U937 cells when exposed to folic acid did not show any change in receptor staining intensity over the 2-hour time period when compared to the non-pulsed positive control indicating that the FR- $\beta$  isoform was not internalized in response to folic acid treatment.

## DISCUSSION

The folate receptor is overexpressed in many carcinomas with very low or negligible expression on normal cells<sup>21,22</sup>. This restricted expression of the receptors has encouraged several studies utilizing the FR- $\alpha$  isoform for selective targeting of tumor cells<sup>79</sup>. FR has two membrane-associated isoforms,  $\alpha$  and  $\beta$ , that are reportedly restricted to epithelial and myeloid malignancies, respectively<sup>1,43</sup>. However, the  $\beta$  isoform is not well defined. Therefore, we sought to investigate the role of FR- $\beta$  as a potential target for the treatment of myeloid leukemias. It is already known that both isoforms exhibited high affinity for the ligand, folic acid, but most studies have only examined targeting of FR- $\alpha$  using folic acid-conjugated drug delivery systems with almost no information available about FR- $\beta$ -mediated targeting. Therefore, we also compared FR- $\alpha$  and FR- $\beta$  isoforms in epithelial and myeloid cells, respectively to determine differences in terms of cell-surface expression and activities in response to folic acid.

To study the FR- $\alpha$  and FR- $\beta$  individually, cell lines expressing only one of the isoforms were needed. Therefore, the 4T1 murine epithelial breast carcinoma and the U937 myelomonocytic leukemia cell lines were tested. Antibody labeling experiments showed that the FR- $\alpha$  and FR- $\beta$  isoforms were strictly restricted to the respective epithelial and myeloid cell lines (Figs. 3 and 6). Thus, these cell lines could serve as useful models to study FR- $\alpha$  and FR- $\beta$  activity. Importantly, FR- $\alpha$  expression was maintained in tumor cells harvested from 4T1 tumor-bearing mice indicating consistency between *in vivo* and *in vitro* conditions (Fig. 4). In addition, FR- $\alpha$  expression was significantly higher in 4T1 cells in culture or isolated from tumor tissue than in normal epithelial cells isolated from the trachea of healthy mice (Fig. 5). This was again consistent with previous reports indicating the selective expression of the FR- $\alpha$  isoform in tumor cells but not in healthy cells<sup>22</sup>. The FR- $\beta$  receptor is reported to be elevated on myeloid



leukemias; however, its expression on lymphoid leukemias had not been investigated. Hence, FR- $\beta$  expression was analyzed on the Jurkat lymphoid T-cell leukemia cell line. Flow cytometry analyses revealed that the cells did not express FR- $\beta$  (Fig. 7), thus confirming the myeloid-lineage-restricted expression of this isoform. Furthermore, while FR- $\beta$  was highly expressed in the U937 leukemia cell line, normal monocytes (CD14<sup>+</sup> cells) isolated from PBMCs of healthy human donors lacked FR- $\beta$  expression (Fig. 8).

Antibody staining of FR- $\alpha$  and FR- $\beta$  in the 4T1 and U937 tumor cell lines, respectively indicated distinct membrane staining patterns of the receptors. The 4T1 cells had FR- $\alpha$  receptors over the entire cell surface organized in clusters that looked like punctate while the U937 cells had the FR- $\beta$  receptors polarized to one end of the cell (Fig. 9). Confocal analyses confirmed these distinct staining patterns of the FR isoforms (Fig. 10), which could be attributed to possible differences associated with the orientation of the isoforms on the cell surface. However, at this time there is no substantial information regarding any mechanism or regulatory factors that could be associated with the orientation of the GPI-linked folate receptors on the cell membrane.

Based on past literature, both FR isoforms have high binding affinity to folic acid; however, FR- $\beta$  is reported to have ~50 times lower binding affinity than that of FR- $\alpha$ <sup>37</sup>. That FR- $\alpha$  can easily internalize into cells<sup>95</sup> is one of the most important characteristics of this isoform that has been utilized to deliver folic-acid drug conjugates into tumor cells<sup>74</sup>. However, internalization and/or recycling properties of FR- $\beta$  are not clearly defined. Hence, FR- $\beta$  activity in response to folic acid treatment was investigated and compared to that of FR- $\alpha$ . Results showed that FR- $\alpha$  and FR- $\beta$  exhibited differential response when exposed to free folic acid. Specifically, FR- $\alpha$  receptors showed internalization within 5 minutes of pulse-chase treatment with folic acid and media, respectively. Receptors remained internalized for at least 30 minutes after which there

was an increase in FR- $\alpha$  levels (Fig. 12). This could be attributed to either receptors recycling to the cell surface or new receptors being expressed. On the contrary, FR- $\beta$  showed no evidence of internalization over the 2-hour period. In addition, there were no signs of increased FR- $\beta$  levels even after 2 hours (Fig. 12). This suggests that FR- $\beta$  receptors are less active than the FR- $\alpha$  receptors and may not bind folic acid in U937 cells.

Thus, the results of these studies clearly demonstrate that FR- $\alpha$  and FR- $\beta$  isoforms are different from each other in terms of expression, localization and activity in the cells. Despite this, their high expression level on tumor cells, coupled with their lack of expression on normal cell lineages, supports further investigation of folic acid-dependent therapies targeting both isoforms in epithelial and myeloid tumors. However, given that FR- $\beta$  showed no effects of free folic acid treatment in U937 cells, it is important to directly test the binding ability of this receptor to folic acid before any folic acid-dependent therapy is attempted. Of equal importance, the lack of FR- $\beta$  internalization following folic acid treatment strongly suggests that any proposed folic acid-dependent therapies be efficacious at the cell surface level.

## FIGURES AND LEGENDS

### 4T1 cells

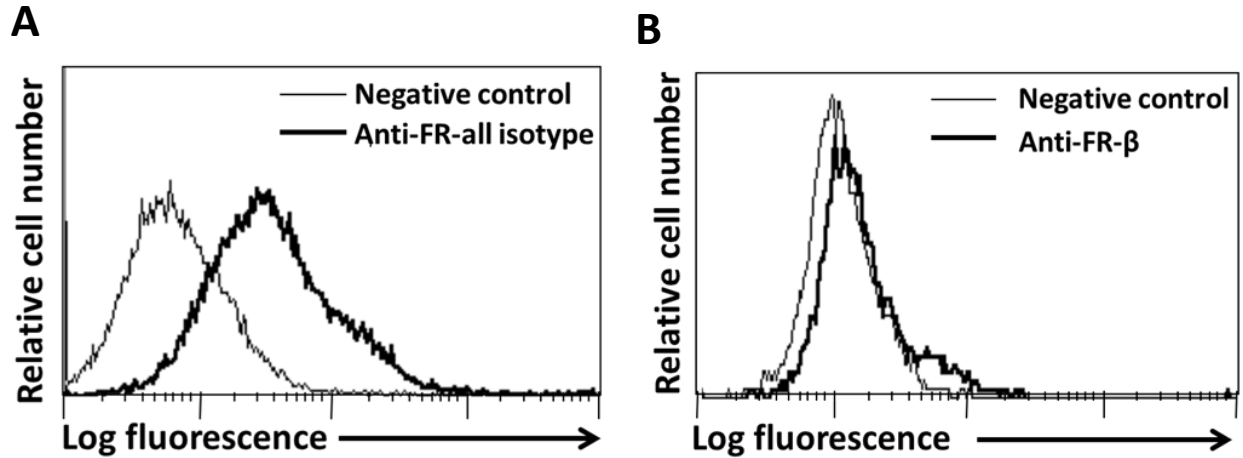


**Figure 3. FR expression on the 4T1 murine epithelial breast carcinoma cell line.**

4T1 cells were labeled with A) rabbit anti-FR all isotype or B) anti-FR- $\beta$  antibody followed by detection with Alexa Fluor<sup>®</sup> 647-conjugated goat anti-rabbit IgG antibody. The primary antibody was omitted from the negative control cells. Results represent 5-7 independent experiments.

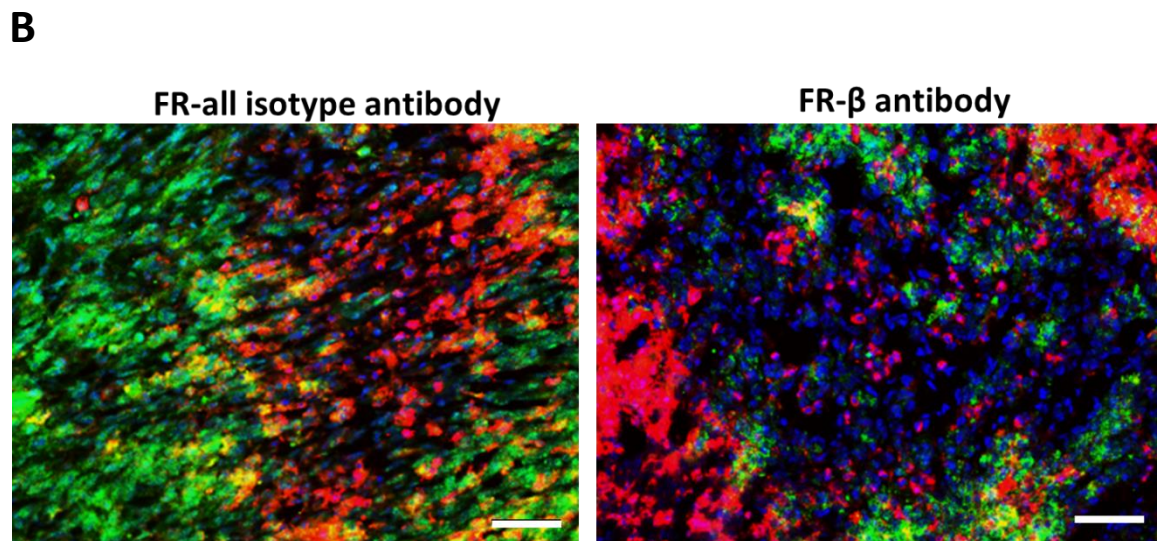
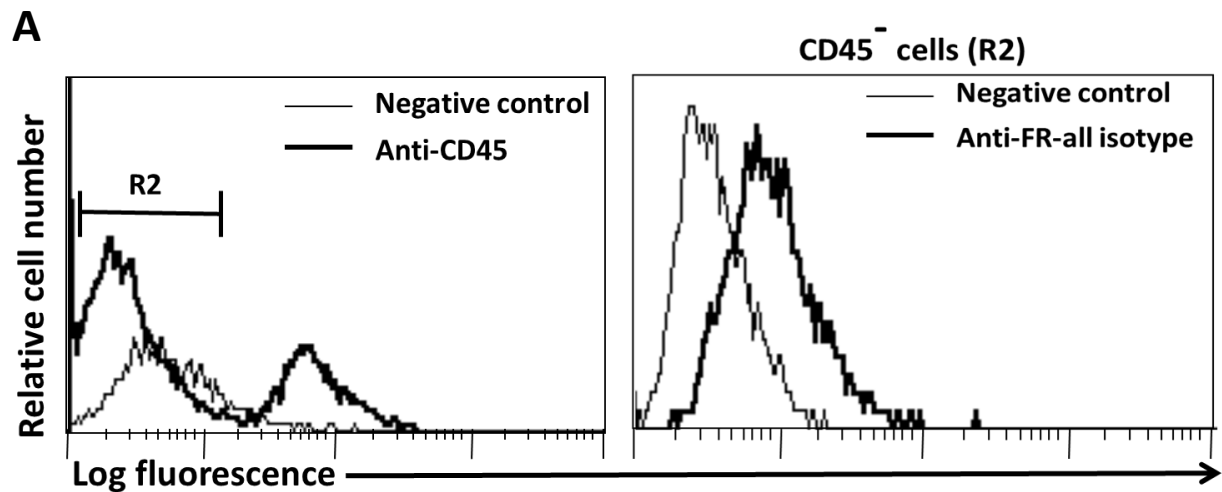


**Figure 4**

**Figure 4. *In vivo* FR- $\alpha$  expression on 4T1 tumor cells.**

Tumors were harvested from 4T1-tumor bearing mice at an advanced stage (4-week) and single-cell suspensions were prepared. Cell suspensions were labeled with rabbit anti-FR-all isotype antibody and were detected with Alexa Fluor<sup>®</sup> 488-conjugated goat anti-rabbit IgG antibody. The cell suspensions were also labeled with APC-conjugated anti-CD45 mouse antibody to identify infiltrating leukocytes present in the tumor. A) The CD45<sup>-</sup> cells from the tumor cell suspensions were gated (R2) (left histogram) and analyzed for FR- $\alpha$  expression (right histogram)

by flow cytometry. Results represent a minimum of three independent experiments. B) Tumors that were harvested from advanced stage (4-week) 4T1 tumor-bearing mice were frozen and cryosections were immunolabeled with anti-FR-all isotype (left panel) or anti-FR- $\beta$  (right panel) antibodies. Tissues were also labeled with APC-conjugated anti-CD45 antibody to identify infiltrating leukocytes and analyzed by epifluorescence microscopy. Digital monochromatic images were acquired at a constant exposure, and pseudocolored and overlaid using MetaVue™ software. Representative images showing FR expression in green. The CD45<sup>+</sup> cells were pseudocolored red. Nuclear staining was performed with DAPI (blue). Scale bar on all images = 100  $\mu$ m.

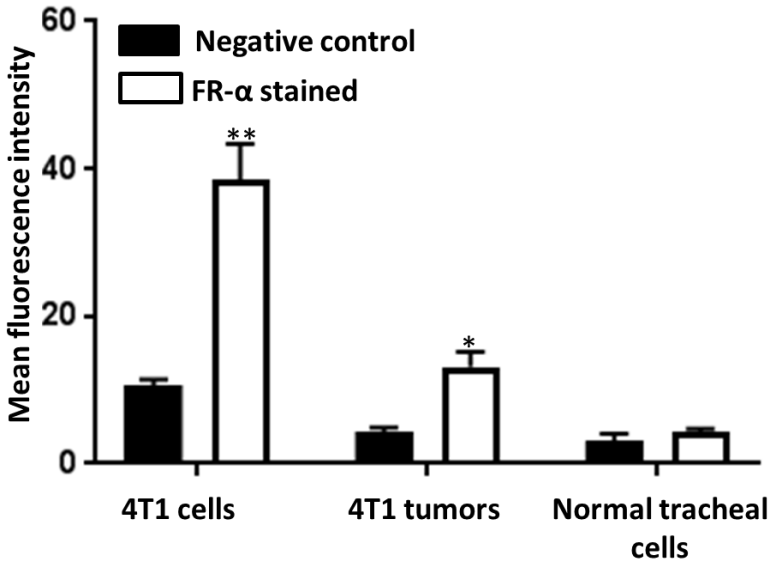


**Figure 5. Comparing FR- $\alpha$  expression in normal and tumor epithelial cells.**

Normal epithelial cells were isolated from the trachea of healthy mice and were compared to those of tumors harvested from 4T1 tumor-bearing mice, and cultured 4T1 tumor cells. The mean fluorescence intensity from flow cytometry experiments was quantified and represented as mean  $\pm$  SEM from 3-5 independent experiments. \*Differences between FR labeled normal tracheal cells and 4T1 cells and 4T1 tumors was significant.  $p < 0.05$ ; \*\* $p < 0.005$ .

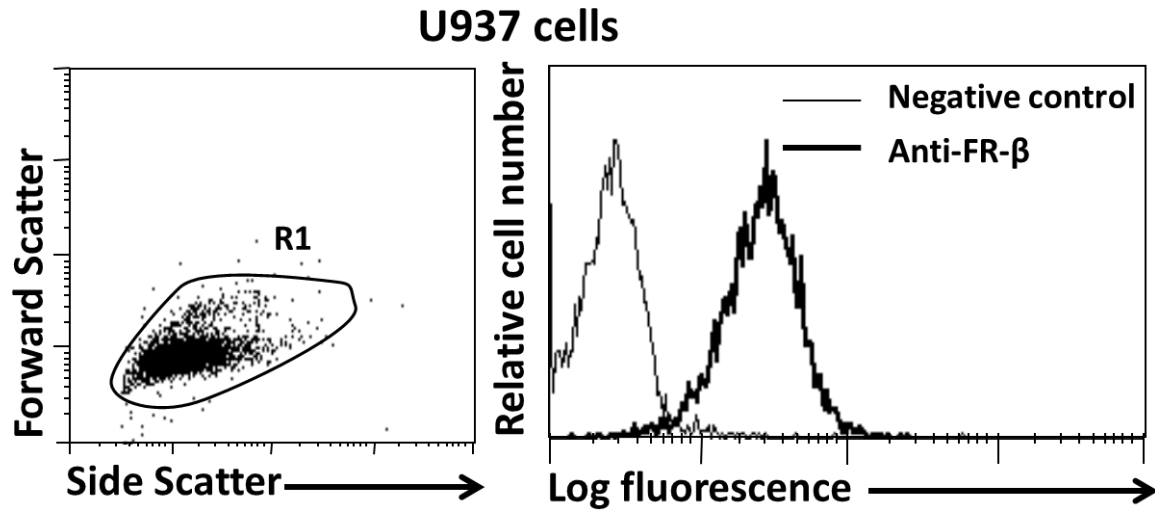


**Figure 6. FR expression on the U937 myeloid leukemia cell line.**

U937 cells were labeled with a rabbit anti-FR- $\beta$  antibody and detected using Alexa Fluor<sup>®</sup> 647-conjugated goat anti-rabbit IgG antibody. The U937 cell population was gated (left) and analyzed for FR- $\beta$  expression (right). Results are representative from 5-7 independent experiments.

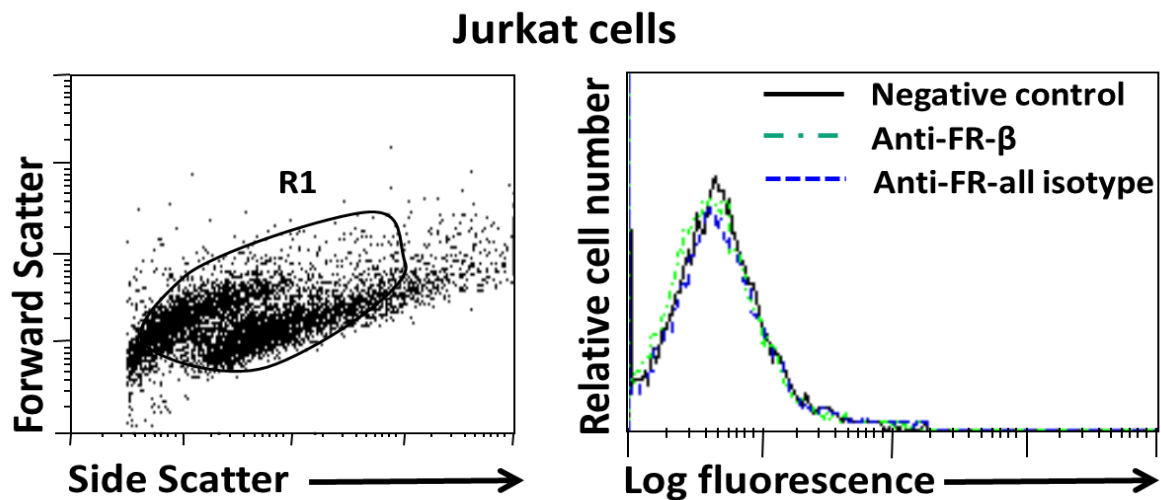


**Figure 7**

**Figure 7. FR expression on the Jurkat T-cell leukemia cell line.**

Jurkat cells were labeled with rabbit anti-FR-all isotype or anti-FR- $\beta$  antibody and detected using Alexa Fluor® 647-conjugated goat anti-rabbit IgG antibody. The cell population was gated (left) and analyzed for FR- $\alpha$  expression and FR- $\beta$  expression (right). Black line represents negative control; green dashed line represents labeling with FR- $\beta$  antibody and blue dashed line represents labeling with FR-all isotype antibody. Results are representative of three independent experiments.



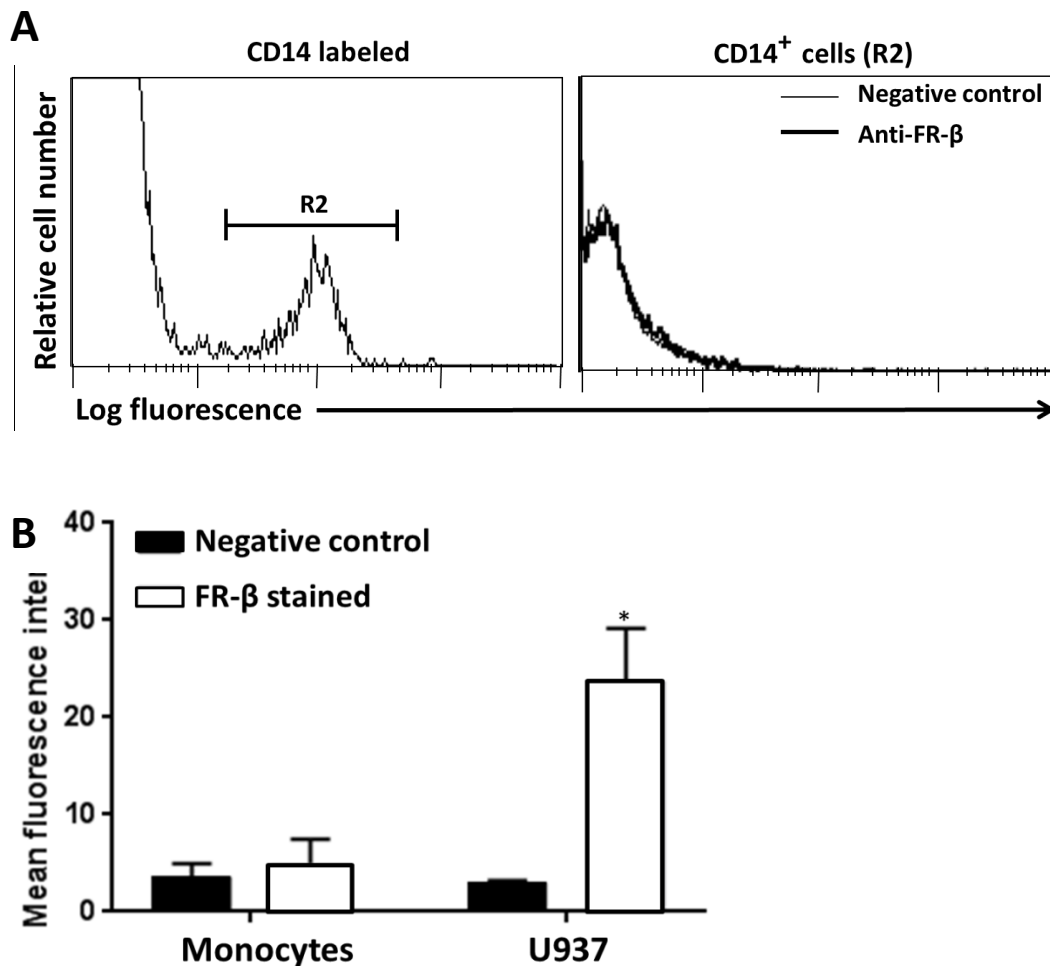


**Figure 8. Comparing FR-β expression on normal peripheral blood monocytes to that of the U937 myelomonocytic leukemia cell line.**

Human blood was drawn and collected over Ficoll followed by separation of the peripheral blood mononuclear cells (PBMCs). Cells were labeled with Alexa Fluor<sup>®</sup> 647-conjugated anti-CD14 antibody and anti-FR-β specific antibody followed by detection with Alexa Fluor<sup>®</sup> 488-conjugated goat anti-rabbit IgG antibody and analyzed by flow cytometry. A) The CD14<sup>+</sup> cells (or monocytes) were gated (R2, left histogram) and FR-β expression quantified (right histogram). B) The mean fluorescence intensity of the monocytes was compared with that of the U937 cells and presented as means ± SEM from three independent experiments. \*Differences between FR-β labeled monocytes and U937 cells was significant, p<0.05.

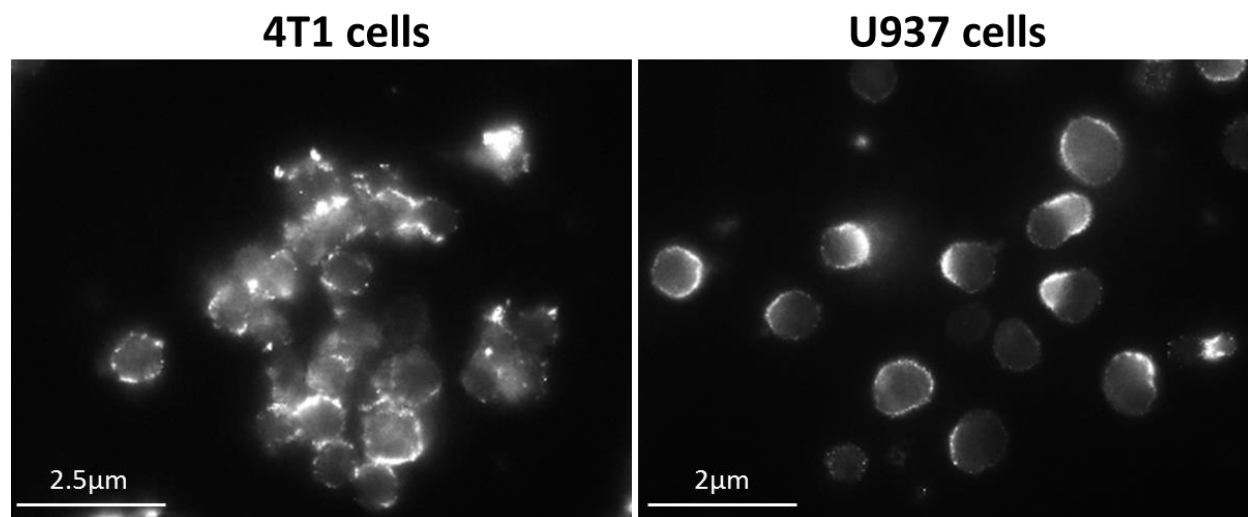


**Figure 9. FR- $\alpha$  and FR- $\beta$  expression on 4T1 and U937 cells.**

4T1 and U937 cell suspensions were labeled with anti-FR-all isotype and anti-FR- $\beta$  antibody, respectively, and collected onto Poly-L-lysine-coated slides. Cells were mounted and analyzed by epifluorescence microscopy. Digital monochromatic images were acquired at a constant exposure using a 60X objective and MetaVue™ software. Representative images are of 4T1 cells expressing FR- $\alpha$  (left) and U937 cells expressing FR- $\beta$  (right). Results are representative of 5-7 independent experiments.

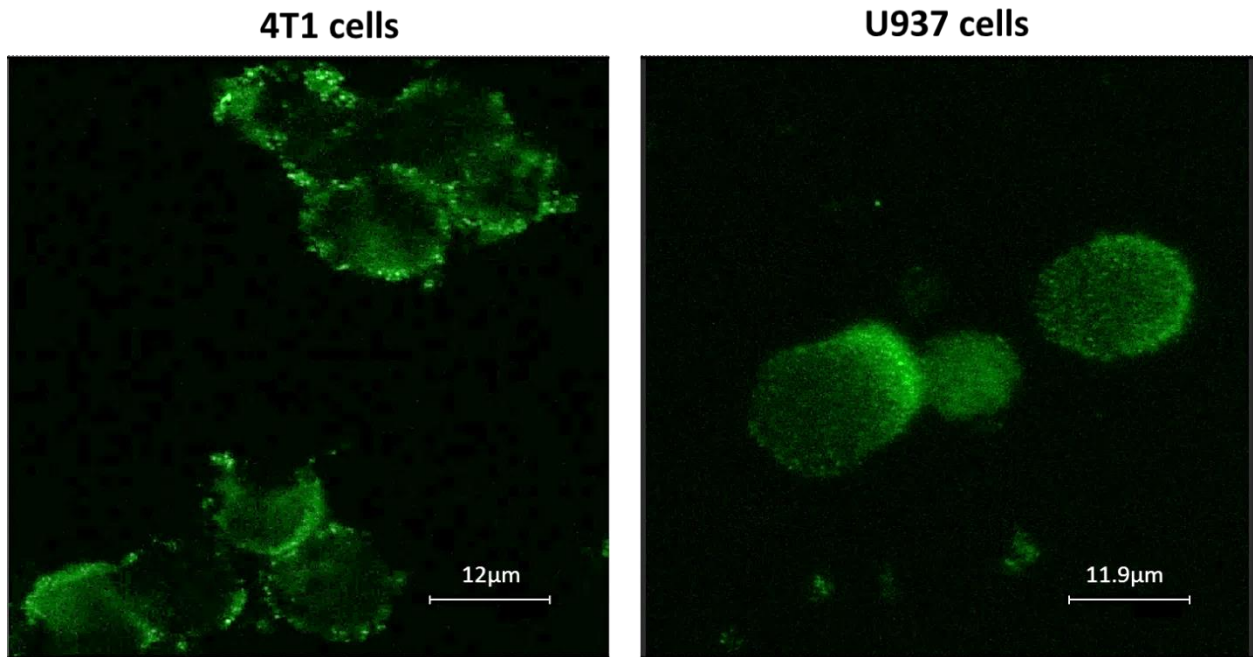


**Figure 10. High-resolution imaging by confocal microscopy comparing FR- $\alpha$  and FR- $\beta$  staining patterns.**

4T1 and U937 cells were labeled with anti-FR all isotype or anti-FR- $\beta$  antibodies and analyzed on a Leica Microsystems™ TCS SP2 confocal laser-scanning microscope. Images were acquired using the 40x objective and pseudocolored using the Leica confocal software. Representative images are of 4T1 cells expressing FR- $\alpha$  (left) and U937 cells expressing FR- $\beta$  (right). Results are representative of three independent experiments.

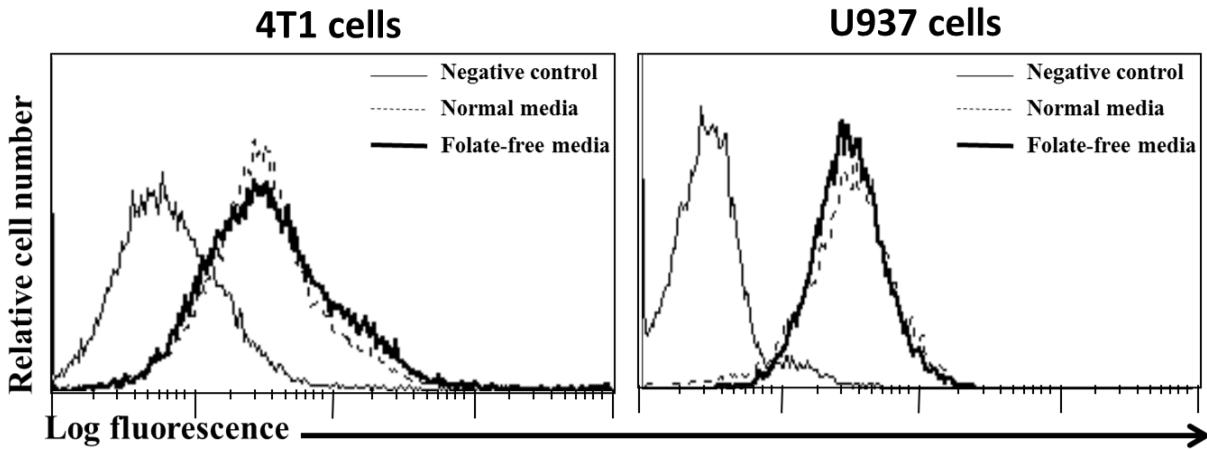


**Figure 11. Effect of endogenous folate on FR expression.**

4T1 and U937 cells were grown in normal or folate-free media and labeled with rabbit anti-FR all isotype or anti-FR- $\beta$  antibody and detected using Alexa Fluor<sup>®</sup> 647-conjugated goat anti-rabbit IgG antibody. 4T1 cells were analyzed for FR- $\alpha$  expression (left), and U937 cells were analyzed for FR- $\beta$  expression (right). Results are representative of a minimum of three independent experiments.

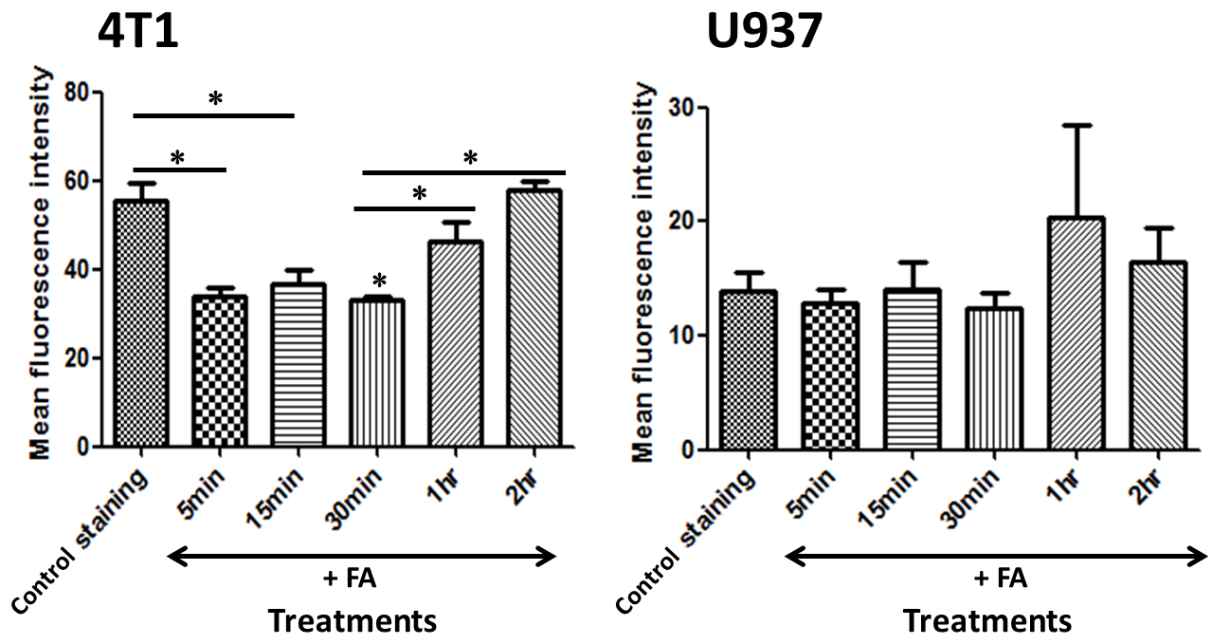


**Figure 12. Comparing FR- $\alpha$  and FR- $\beta$  activity in 4T1 and U937 cells.**

4T1 and U937 cells were cultured in suspension and pulsed with 2.2  $\mu$ M free folic acid for 5 minutes, washed and the cells harvested after 5, 15, 30, 60 or 120 minutes incubation in normal media. Cells were then labeled with primary rabbit antibodies recognizing FR- $\alpha$  (left) or FR- $\beta$  (right) receptors followed by detection with Alexa Fluor® 647-conjugated goat anti-rabbit IgG antibody. Cells were fixed and analyzed by flow cytometry. The mean fluorescence intensity of the cells was compared and analyzed over time. Values represent the mean  $\pm$  SEM results from 6-8 independent experiments. \*Differences in sample means were significant,  $p < 0.05$ .

### **CHAPTER 3**

FR- $\alpha$  and FR- $\beta$  ISOFORMS EXHIBIT DIFFERENT INTRACELLULAR FATE

## ABSTRACT

Knowledge of the overexpression of the FR- $\alpha$  isoform on epithelial cancers and its restricted expression on normal cells have initiated many targeting studies. In addition, its high binding affinity has led to the use of folic acid-mediated strategies for effective cancer therapy. In contrast, the FR- $\beta$  isoform that is elevated on myeloid leukemias remains undefined, hence its potential use as a therapeutic target has not been evaluated. In many cancer patients, the anti-tumor immune response is often inhibited by a population of suppressor cells known as myeloid-derived suppressor cells (MDSCs), which have been reported to express FR- $\beta$ . Therefore, FR- $\beta$  targeting could potentially be used to eliminate MDSCs in addition to myeloid leukemias. The goal of this study was to determine the potential of FR- $\beta$  in targeting myeloid cells. FR- $\beta$  studies were performed using the myelomonocytic leukemia cell line (U937) and MDSCs that were harvested from 4T1 tumor-bearing mice. FR- $\alpha$  studies were also performed using the 4T1 breast epithelial tumor cell line. Our previous findings suggested that the FR- $\beta$  isoform was comparatively less active than the FR- $\alpha$  and also did not internalize into U937 cells. Therefore, to further investigate the details of the intracellular fate of FR- $\alpha$  and FR- $\beta$ , studies were conducted using the physiologic ligand, folic acid. Folic acid (FA)-fluorochrome conjugates were synthesized using the fluorescent dyes fluorescein isothiocyanate (FITC) and tetramethylrhodamine isothiocyanate (TRITC) to track the receptors. Bovine serum albumin (BSA) was used as a linker to stabilize the conjugate. The resulting probes, FA-BSA-FITC and FA-BSA-TRITC, were used to examine FR- $\alpha$  and FR- $\beta$  binding activity and the fate of the bound receptors in tumor cells (4T1 and U937) and in MDSCs. Flow cytometry and light microscopy analyses demonstrated that the FA-BSA-FITC and FA-BSA-TRITC probes showed strong and specific binding to both tumor cell lines and MDSCs. However, one dramatic

difference was that while probe bound to FR- $\alpha$  was readily internalized, the FR- $\beta$  receptors did not internalize the bound probe.

To examine the differences more closely, mechanisms associated with FR trafficking were investigated. Comparisons with clathrin-mediated endocytosis using transferrin receptor as a model, and with pinocytosis using fluorescent dextran revealed that FR- $\alpha$  internalization was not associated with these pathways. The role of lipid rafts in FR trafficking was also investigated by determining the sensitivity of FR- $\alpha$  and FR- $\beta$  to membrane cholesterol depletion. Results showed that removal of membrane cholesterol dramatically reduced FR- $\alpha$  binding and internalization while uptake of transferrin and dextran remained mostly unaffected.

The above results suggested that the FR- $\beta$  isoform could be targeted using folic acid-dependent methods; however, only at the cell surface. Hence, we sought to determine the potential of a folic acid-based technique that could be potentially used to target both FR isoforms at the cell surface. Therefore, a folic acid-nanoparticle conjugate was synthesized using 18 nm gold nanoparticles (FA-BSA-Au<sub>18</sub>) to which both 4T1 and U937 cells showed specific nanoparticle binding compared to the control (BSA-Au<sub>18</sub>). This provided direct evidence that future nanoparticle-mediated targeting of FR- $\alpha$  and FR- $\beta$  at the cell surface could take advantage of magnetic nanoparticle technology to destroy target cells through localized hyperthermia. All these findings suggest: 1) both FR- $\alpha$  and FR- $\beta$  can be targeted using folic acid-dependent techniques; 2) FR- $\alpha$  binding and internalization was regulated by membrane cholesterol content, thus indicating possible association of FR- $\alpha$  with lipid rafts; and 3) colloidal nanoparticles can be specifically targeted to FR- $\alpha$  and FR- $\beta$ -expressing cells thereby increasing the number of potential therapeutic strategies.



## INTRODUCTION

Selective overexpression of FR isoforms on tumor cells identifies them as potential targets for effective cancer therapy. A variety of ligand- and antibody-conjugated cancer targeting strategies have gained prominence for their potential use as therapeutics<sup>2</sup>. The high binding affinity for folic acid (FA) exhibited by both the FR- $\alpha$  and FR- $\beta$  isoforms makes them ideal candidates for FA-dependent therapies. The importance of FA in such ligand-based therapies is further enhanced due to its low immunogenicity, small size, compatibility with a variety of organic and aqueous solvents, stability and low cost. In addition, conjugation of potential targeting molecules to FA generally does not affect their binding affinity for the receptor making it highly desirable for such a purpose<sup>106</sup>. There have been many studies that have shown successful delivery of FA-conjugated therapeutic agents to epithelial tumors *in vitro* and *in vivo*<sup>3,77</sup>; however, the prospects of using FA-dependent therapeutics to target FR- $\beta$  remains unknown. FR- $\beta$  is reportedly overexpressed on some myeloid leukemias<sup>45</sup> and some myeloid suppressor populations, namely myeloid-derived suppressor cells (MDSCs)<sup>399</sup>. MDSCs are of special interest because they are expanded significantly during pathological conditions such as inflammation and cancer and function to suppress T cell immune responses. In cancer patients, this results in inhibition of the anti-tumor immune response. Thus, characterizing the FR- $\beta$  isoform could provide insights into the role these receptors play in myeloid cell function and assess their potential as a therapeutic target.

Previous studies have indicated that folate-conjugates directed to target FR- $\alpha$  were internalized via receptor-mediated endocytosis<sup>136</sup>. However, later studies contradicted this idea and suggested that they were not associated with clathrin-coated pathways<sup>74,106</sup>. Instead, they proposed that FRs were arranged as clusters in association with flask-shaped structures called “caveolae” or into

cholesterol-rich domains, also known as lipid-rafts<sup>87,93</sup>. Thus, the actual mechanism(s) associated with FR internalization is yet to be elucidated. Interestingly, the FR- $\beta$  isoform has long been considered to be inactive despite being detected on cells of the myelomonocytic lineage<sup>50,51</sup>. However, its strong binding affinity for FA still makes it a potential candidate for targeting myeloid cells. Therefore, in the present studies, the function of FR- $\beta$  in myeloid cells and the potential of FA-conjugated therapeutics to target this isoform were investigated. The intracellular fates of both the FR- $\alpha$  and FR- $\beta$  isoforms were compared and potential approaches for targeting them are proposed.

In this study, we synthesized FA-fluorochrome conjugates, showed that they bound specifically to tumor cells and MDSCs, and determined that the FR- $\alpha$  isoform was internalized following binding while the FR- $\beta$  isoform was not. To further characterize the FR isoforms, potential pathways that could be associated with FR trafficking were investigated. Results demonstrated that the FA-conjugated probe was internalized into the 4T1 cells; however, there was no co-localization with either clathrin-mediated endocytosis or pinocytosis. Our findings also indicated that upon membrane cholesterol depletion, FR- $\alpha$  binding and internalization was significantly inhibited while clathrin-mediated endocytosis and pinocytosis remained mostly unaffected. This result, indicating sensitivity of FR- $\alpha$  to membrane cholesterol content, suggests their possible association with lipid rafts.

A common FA-based system that could target both FR isoforms and be used for cell depletion was prepared and tested. Specifically, a FA-colloidal gold conjugate (FA-BSA-Au<sub>18</sub>) was produced and tested for binding efficiency to the 4T1 and U937 cells. Compared to the BSA-Au<sub>18</sub> control, the FA-BSA-Au<sub>18</sub> exhibited strong binding to both cell lines indicating the conjugate could bind to both the FR- $\alpha$  and FR- $\beta$  isoforms. This result was important in validating

that future nanoparticle-mediated therapy using magnetic nanoparticles and hyperthermia to target receptors at the cell surface would be applicable to both FR isoforms.

## MATERIALS AND METHODS

### Animals and tumor induction

BALB/c (wild type) mice were originally purchased from the Jackson Laboratories (Bar Harbor, ME) and further housed and bred in a specific pathogen-free facility at the University of Wisconsin-Milwaukee and screened regularly for pathogens. All procedures were approved by the Animal Care and Use Committee of the University of Wisconsin-Milwaukee. For tumor induction,  $1 \times 10^4$  4T1 cells in 50  $\mu$ l of supplement-free RPMI 1640 medium were injected subcutaneously into the mammary fat pad of 8-12 week old wild type BALB/c female mice. Tumors were monitored by caliper measurements of the major (L, length; mm) and minor (W, width; mm) axes and tumor volume (V, volume;  $\text{mm}^3$ ) was calculated by the formula:  $V = (L \times W^2) / 2$ .

### Cell lines and reagents

The 4T1 murine mammary carcinoma epithelial cell line (ATCC CRL-2539) and the U937 human myelomonocytic leukemia (myeloid) cell line (ATCC CRL-1593.2) were both purchased from ATCC (Manassas, VA) and maintained as described in Chapter 2, "Materials and Methods". Cell counts and viability were determined using a hemacytometer following appropriate dilution in trypan blue exclusion dye.

Antibodies used in the flow cytometry and fluorescence microscopy experiments included: polyclonal rabbit anti-FR- $\beta$  antibody (Cat #PA5-24963, ThermoFisher Scientific, Waltham, MA); and polyclonal rabbit anti-mouse/rat/human FR-all isotypes antibody (FL-257, Santa Cruz Biotechnology, Santa Cruz, CA). The primary rabbit antibodies were detected with a secondary Alexa Fluor<sup>®</sup> 647- or Alexa Fluor<sup>®</sup> 488-conjugated goat anti-rabbit IgG antibody (Jackson

Immunoresearch, West Grove, PA). Other antibodies included fluorescein FITC-conjugated, allophycocyanin (APC)-conjugated, or biotinylated anti-CD11b (Clone M1/70 BD Biosciences, San Jose, CA); phycoerythrin (PE)-conjugated or FITC-conjugated anti-Ly-6G (Clone 1A8, BD Biosciences); and peridinin-chlorophyll protein-cyanine 5.5 (PerCP-Cy5.5)-conjugated anti-Ly-6C (Clone RM4-5, BD Biosciences). Biotinylated antibodies were detected with Alexa Fluor® 488-conjugated neutralite avidin (Life Technologies, Grand Island, NY).

For the synthesis of FA-conjugates, folic acid powder was purchased commercially (ThermoFisher). 1-ethyl-3-(3dimethylaminopropyl) carbodiimide (EDC, Pierce) was used as an activator of the carboxyl group on FA. Bovine serum albumin (BSA, ThermoFisher) was used as a linker, and the fluorescent dyes FITC and TRITC (ThermoFisher) were used for tracking receptors on the cell surface as well as intracellularly. Gold (Au) nanoparticles (18nm) were synthesized by standard methods and provided by Dr. Julie Oliver, Department of Biological Sciences, University of Wisconsin-Milwaukee. The colloidal Au<sub>18</sub> nanoparticles were conjugated to FA-BSA and BSA and analyzed by scanning electron microscopy (SEM) for determining receptor activity. Dimethylsulfoxide (DMSO) was used as a universal solvent to dissolve FA and EDC during synthesis of the conjugates.

Transferrin (Tfn)-FITC (Invitrogen, Carlsbad, CA) was used to track internalization of transferrin receptors and served as a marker for clathrin-mediated endocytosis. Dextran (Dxt)-FITC (Sigma Aldrich), which is a fluid-phase marker, was used to study macropinocytosis in cells. DAPI (4',6-diamidino-2-phenylindole, Sigma Aldrich) was used as a nuclear stain. Methyl- $\beta$ -cyclodextrin (M $\beta$ CD, Sigma Aldrich) was used to deplete plasma membrane cholesterol for the analysis of receptor activity.

## **MDSC isolation and labeling**

For labeling MDSCs, spleens were harvested from 4T1 tumor-bearing mice at an advanced stage (4-weeks) and a single-cell suspension of the spleen was performed as follows: the spleen was harvested and then teased apart in a 60 mm culture dish filled with PBS as previously described<sup>401</sup>. Briefly, the suspensions were filtered through 70  $\mu\text{m}$  mesh and centrifuged; red blood cells were lysed in ACK buffer (0.15 M  $\text{NH}_4\text{Cl}$ , 10 mM  $\text{KHCO}_3$ , 0.1  $\text{Na}_2\text{EDTA}$ , pH 7.4), and the cells were filtered again and then washed three times with PBS. Cell counts and viability were determined using a hemacytometer following appropriate dilution in trypan blue exclusion dye. A 2X optimal dilution of anti-CD11b, anti-Ly-6G, and anti-Ly-6C antibodies in PBS containing 2% normal horse serum (PBS/NHS), was added at a 1:1 ratio of  $1 \times 10^6$  per 50  $\mu\text{l}$  of spleen cells and incubated for 30 minutes on ice. Following labeling, the cells were washed in PBS/NHS, fixed in 1.5% paraformaldehyde in PBS and analyzed with a FACSCalibur flow cytometer (BD Biosciences, San Jose, CA) using BD CellQuest<sup>TM</sup> Pro software. 10,000 cells/sample were analyzed with the fluorescence intensity displayed on a 4-decade log scale.

## **Synthesis of FA-linked fluorescent probes (FA-BSA-FITC or FA-BSA-TRITC)**

Folic acid was conjugated to BSA and FITC as previously described<sup>402-404</sup>. Briefly, FA was dissolved in anhydrous DMSO and incubated with a 5-fold molar excess of EDC and stirred for 1 hour at 23°C in the dark to activate the carboxyl group of FA. BSA solution (4 mg/ml) was prepared by dissolving BSA in 0.1 M  $\text{KH}_2\text{PO}_4$  and 0.1 M  $\text{H}_3\text{BO}_3$  at pH 8.5, and then dialyzing (M.W. cut-off 12,000) against the same buffer overnight. Then the “activated” vitamin, FA-EDC, was added at a 10-fold molar excess to the BSA solution and stirred for 16 hours at 23°C in the dark followed by overnight dialysis against 0.1 M  $\text{KH}_2\text{PO}_4$  and 0.1 M  $\text{H}_3\text{BO}_3$  at pH 8.5. FITC (3 mg/ml in DMSO) or TRITC (3 mg/ml in DMSO) was then added to the FA-EDC-BSA

mixture at a ratio of 50  $\mu$ l per 1 mg BSA, incubated for 4 hours with stirring at 23°C in the dark and then dialyzed extensively against PBS. The control or untargeted probes (BSA-FITC or BSA-TRITC) were made by directly adding 50  $\mu$ l FITC or TRITC per 1 mg of BSA solution as described above. The mixture was incubated on a shaker for 4 hours in the dark at 23°C, followed by dialysis against three changes of PBS. The final concentration of the probe was determined using the absorbance of BSA (OD<sub>280</sub>), folic acid (OD<sub>368</sub>), FITC (OD<sub>494</sub>) and TRITC (OD<sub>545</sub>) using a Nanodrop<sup>®</sup> ND-1000 Spectrophotometer (ThermoFisher Scientific, Waltham, MA). The Beer-Lambert formula,  $A_{280} = \epsilon c l$  was used to determine the final protein concentration ( $A$  = absorbance,  $\epsilon$  = molar extinction co-efficient,  $c$  = concentration,  $l$  = path length of the nanodrop). A FITC or TRITC correction factor (CF) was also included before calculating the final protein concentration using the formula,  $A_{max} = A_{280} \times CF_{dye}$ . Degree of labeling of folate-BSA was calculated as follows: Moles of folate per moles of BSA = Number of moles of folate / Number of moles of BSA.

### **Analysis of FR- $\alpha$ and FR- $\beta$ receptor binding to FA-BSA-FITC probe**

4T1 and U937 cells were lifted and treated in suspension as described in Chapter 2, “Materials and Methods”. MDSCs were isolated from single-cell suspension of spleen that was harvested from 4T1 tumor-bearing mice as described above. Cell counts and viability were determined using a hemacytometer following appropriate dilution in trypan blue exclusion dye. Cell concentrations were adjusted to  $20 \times 10^6$  cells/ml. All cells were incubated for 30 or 120 minutes at 37°C and 5% CO<sub>2</sub> with either medium alone, BSA-FITC, or FA-BSA-FITC at concentrations of 10 and 100  $\mu$ g/ml. Probe binding by MDSCs was also determined by treating the cells with either the FA-BSA-FITC probe or the BSA-FITC control followed by labeling with antibodies for 30 minutes on ice, which would identify the granulocytic and monocytic subsets of MDSCs

as previously described. All cells were washed with cold PBS to prevent further membrane mobility and immediately fixed in 1.5% formaldehyde in PBS and analyzed by flow cytometry using a FACSCalibur flow cytometer (BD Biosciences, San Jose, CA) using BD CellQuest™ Pro software. 10,000 cells/sample were analyzed with fluorescence intensity displayed on a 4-decade log scale.

### **Visualization of FR- $\alpha$ and FR- $\beta$ binding and/or internalization**

Flow cytometry does not discriminate between FA-BSA-FITC on the cell surface or internalized conjugate. Therefore, to directly visualize internalized FA-BSA-FITC, analysis was performed using fluorescence microscopy. 4T1 cells were cultured on 10 mm round no. 1.5 glass coverslips (Ted Pella) for 18 hours and U937 cells were handled in suspension in 5 ml conical tubes (BD Biosciences) as described above. MDSCs were harvested from the spleen of 4-week tumor-bearing mice followed by preparation of single-cell suspensions as described above. 4T1 cells were labeled with 1  $\mu$ g/ml BSA-FITC or FA-BSA-FITC probe while U937 cells and MDSCs were labeled with 100  $\mu$ g/ml probe. All samples were incubated for 30 or 120 minutes at 37°C. Cells were washed with PBS, fixed in 1.5% formaldehyde and stained with 0.3  $\mu$ M DAPI (Sigma Aldrich). Following DAPI staining, 4T1 cells were mounted on glass slides in ProLong Gold®, anti-fade media. The U937 cells and MDSCs were cytospun at 16,000 x g for 10 minutes using a cytocentrifuge (Beckman Coulter, Inc., Brea, CA) followed by mounting under glass coverslips in ProLong Gold®. All samples were then analyzed on a Nikon Eclipse TE2000-U inverted epifluorescence microscope (Nikon Instruments Inc., Melville, NY) equipped with a CoolSNAP ES digital monochromatic camera (Photometrics, Tucson, AZ). Images were acquired using 40 and 60x Plan Apo objectives at a constant exposure setting, pseudocolored and overlaid using MetaVue™ software (Universal Imaging Corporation, Downingtown, PA).



Internalization of folate receptors was determined with a Leica Microsystems™ confocal laser-scanning upright microscope (Richmond, IL) using a 40x objective. Images were pseudocolored using the Leica confocal software. All experiments were performed a minimum of 5 times.

### **Immunohistochemistry of 4T1 tumors**

4T1 tumors (~4-week) were harvested from BALB/c mice and then snap-frozen in tissue freezing medium (Triangle Biomedical Sciences, Inc., Durham, NC) in liquid nitrogen or on dry ice. Tissue sections with a thickness of 7  $\mu\text{m}$  were cut on a cryostat and placed on poly-L-lysine-coated microscopic slides. The tumor sections were fixed in cold acetone for 5 minutes and stored at  $-20^{\circ}\text{C}$  until labeling. The sections were thawed for 5 minutes and rehydrated in PBS for 10 minutes. The sections were then incubated in 5% normal goat serum in PBS to block non-specific antibody binding. To visualize the location of the myeloid population, the sections were incubated with a fluorochrome-conjugated antibody against CD11b for 30 minutes at room temperature. Sections were washed with PBS for 5 minutes followed by incubation with the FA-BSA-TRITC or the BSA-TRITC probe (100  $\mu\text{g}/\text{ml}$ ) for 1 hour at room temperature. Sections were again washed and incubated with 0.3  $\mu\text{M}$  DAPI for 10 minutes. The slides were washed again with PBS for 5 minutes and mounted in ProLong Gold® anti-fade mounting medium. The tumor sections were imaged as described above. Images are representative of a minimum of 3 independent experiments.

### **Determining effect of free folic acid on FR binding activity**

4T1 cells and U937 cells were cultured in folate-free RPMI 1640 medium as described above. The cells were pre-incubated with 2.2  $\mu\text{M}$  FA acid for 30 minutes at  $37^{\circ}\text{C}$  followed by 30 minutes incubation with either BSA-FITC or FA-BSA-FITC at 100  $\mu\text{g}/\text{ml}$ . The cells were

washed with cold PBS to prevent further membrane mobility, immediately fixed in 1.5% formaldehyde in PBS and analyzed by flow cytometry.

### **Comparing FR internalization with receptor-mediated endocytosis and pinocytosis**

4T1 cells were cultured on coverslips as described above. Cells were treated with BSA-TRITC or FA-BSA-TRITC at 1  $\mu\text{g/ml}$ , FITC-conjugated transferrin (Tfn-FITC) at 20  $\mu\text{g/ml}$ , or FITC-conjugated dextran (Dxt-FITC) at 50  $\mu\text{g/ml}$  for 30 or 120 minutes at 37°C. Following treatment, cells were washed with PBS and fixed with 1.5% paraformaldehyde in PBS. 0.3  $\mu\text{M}$  DAPI was added to the cells for 15 minutes to stain the nucleus, followed by mounting in ProLong Gold<sup>®</sup> and analysis by epifluorescence microscopy as described above. Images were acquired at a constant exposure using an oil immersion 60X objective as described above.

### **Analyzing the role of membrane cholesterol in regulating FR activity**

For cholesterol removal, cell monolayers were washed with PBS and incubated for 1 hour at 37°C in the absence (control cells) or presence (treated cells) of 5 mM M $\beta$ CD). After 1 hour, the medium was removed and the cells were washed with PBS. Following cholesterol depletion, the cells were treated with the FA-BSA-FITC or BSA-FITC probes (100  $\mu\text{g/ml}$ ) and Tfn-FITC (20  $\mu\text{g/ml}$ ) or Dxt-FITC (50  $\mu\text{g/ml}$ ) conjugates for 30 or 120 minutes at 37°C. Cells were washed with PBS, fixed in 1.5% paraformaldehyde in PBS and analyzed by flow cytometry as described above.

For microscopy, the cells were treated with M $\beta$ CD as described above followed by treatment with the BSA-TRITC or the FA-BSA-TRITC probe at 1  $\mu\text{g/ml}$  (for 4T1 cells) and 100  $\mu\text{g/ml}$  (for U937 cells). Cells were also simultaneously labeled with either Tfn-FITC (20  $\mu\text{g/ml}$ ) or Dxt-

FITC (50  $\mu\text{g/ml}$ ) to determine and compare receptor internalization and/or co-localization with that of FR- $\alpha$  and FR- $\beta$ .

### **Synthesis of FA-BSA-Au<sub>18</sub> nanoparticle conjugates**

FA-BSA (or BSA as control) was conjugated to Au<sub>18</sub> nanoparticles that were provided by Dr. Julie Oliver<sup>178</sup>. Briefly, the optimal concentration of protein to stabilize the Au<sub>18</sub> nanoparticles was determined empirically through concentration isotherms and 200  $\mu\text{g}$  of FA-BSA was found to stabilize 1 ml of Au<sub>18</sub>. Once determined, the protein was conjugated to the Au<sub>18</sub> nanoparticles at pH 5.1 and the conjugates were stabilized by addition of polyethylene glycol (average MW 20,000, Sigma Aldrich). Free protein was removed by pelleting the Au<sub>18</sub> nanoparticles at 16,000 x g for 5 minutes. The nanoparticles were resuspended in 250  $\mu\text{l}$  of RPMI 1640 medium and used immediately.

### **Analyzing FA-BSA-Au<sub>18</sub> binding using scanning electron microscopy (SEM)**

4T1 cells were grown on coverslips and U937 cells were cultured in RPMI 1640 medium until they reached ~70% confluency as described above. All cells were washed in PBS and labeled with FA-targeted (FA-BSA-Au<sub>18</sub>) or control nanoparticles (BSA-Au<sub>18</sub>) in Hank's balanced salt solution (HBSS) for 1 hour at 37°C. After labeling, the cells were washed three times in HBSS. The cells were then fixed for 30 minutes in 1% glutaraldehyde and 0.4% osmium tetroxide (OsO<sub>4</sub>) in 0.1 M HEPES, (pH 7.3), followed by 3 washes in 0.1 M HEPES. The U937 cells were allowed to adhere to poly-L-lysine-coated Thermanox™ coverslips (Ted Pella) overnight at 37°C, while the 4T1 cells were kept in 0.1 M HEPES overnight. Both 4T1 and U937 cells were then dehydrated in a graded ethanol series, and dried by the critical-point method. The coverslips were mounted onto stubs, sputter-coated with 4 nm iridium, and visualized with a

Hitachi S-4800 scanning electron microscope using secondary and backscattered electron detection.

### **Statistical analysis**

Data are presented as mean  $\pm$  SEM. Significant differences between sample means were determined using a Student's *t* test with \* $p < 0.05$  considered significant. Data between various treatment groups were analyzed using one-way ANOVA and then compared by Bonferroni multiple comparison tests using GraphPad Prism Software, Version 3.00 (San Diego, CA, USA).

## RESULTS

### **Folic acid-conjugated fluorescent probes were successfully synthesized**

To specifically target folate receptors, FA-conjugated fluorescent probes were designed using BSA as a linker protein and FITC or TRITC as the fluorochrome to track receptor binding and/or internalization (Fig. 13). UV-Vis analysis confirmed the presence of FA in the FA-BSA-FITC and FA-BSA-TRITC probes (Fig. 14). On the contrary, the untargeted probes, BSA-FITC or BSA-TRITC showed no absorbance at OD<sub>368</sub> that corresponded to the wavelength of folic acid. The presence of FITC and TRITC in the probes was also confirmed at OD<sub>494</sub> and OD<sub>545</sub>, respectively. There were approximately 2-3 molecules of folic acid per molecule of BSA.

### **FR- $\alpha$ receptors showed strong binding to the FA-BSA-FITC probe**

The probe binding efficiency of the FR- $\alpha$  expressed on 4T1 cells was assessed by treating the cells with varying concentrations of the FA-BSA-FITC probe or control (BSA-FITC) for 30 and 120 minutes followed by analysis of their fluorescence intensity using flow cytometry. Results at the 30-minute time-point showed that the 4T1 cells bound the FA-BSA-FITC probe weakly at the 10  $\mu\text{g/ml}$  concentration but had higher binding at the 100  $\mu\text{g/ml}$  concentration (Fig. 15A). At the 120-minute time-point, both concentrations of FA-BSA-FITC probe showed increased binding over that of the 30-minute time-point, with the 100  $\mu\text{g/ml}$  concentration showing the highest level of binding overall. In all cases, the control BSA-FITC conjugate showed little-to-no binding to 4T1 cells. Summary data for the 100  $\mu\text{g/ml}$  concentration of FA-BSA-FITC showed that there was a significant 5-fold increase in binding over that of the BSA-FITC at 30 minutes that increased to 8-fold by 120 minutes (Fig. 15B). Comparison between FA-BSA-FITC binding at 30 minutes vs 120 minutes showed a significant ~2-fold increase. Therefore, FA-BSA-FITC

probe binding to FR- $\alpha$  on 4T1 cells demonstrated both concentration- and time-dependent effects. As a result of these experiments, 100  $\mu\text{g/ml}$  was considered to be an optimal concentration for studying FA-BSA-FITC probe binding in the 4T1 cells.

Immunofluorescence microscopy analysis confirmed the specific binding of FA-BSA-FITC probe to the 4T1 cells but not the BSA-FITC control. Interestingly, the probe concentrations of 10 and 100  $\mu\text{g/ml}$  (used for flow cytometry) were too high and gave poor resolution results with fluorescence microscopy. Therefore, lower concentrations were tested and 1  $\mu\text{g/ml}$  was found to be optimal for microscopy. Analysis showed that the 4T1 cells had significant binding of the FA-BSA-FITC probe at the 30 minute time point that was localized primarily to the cell surface (Fig. 15C). At this time point, the FA-BSA-FITC probe was mostly localized in larger aggregates or clusters which was different from the distinct punctate staining observed following anti-FR antibody labeling (Chapter 2, Figs. 9 & 10). After 120 minutes, the staining intensity was not only higher compared to the 30 minute time point, but a large amount of what appeared to be internalized probe had accumulated within the cell (as indicated by arrows). In contrast, the cells showed only minimal binding of the BSA-FITC control at either 30 or 120 minutes. Therefore, these results demonstrate that the FR- $\alpha$  receptors on the 4T1 cells not only showed specific dose- and time-dependent binding to the FA-BSA-FITC probe but also showed internalization.

### **FR- $\beta$ receptors showed strong binding to the FA-BSA-FITC probe**

The binding activity of FR- $\beta$  on U937 cells was assessed by treating the cells with varying concentrations of the FA-BSA-FITC probe or control BSA-FITC conjugates for 30 and 120 minutes followed by flow cytometric analysis. Initial labeling experiments showed that binding activity of FR- $\beta$  on the U937 cells was much lower than that of the FR- $\alpha$  on 4T1 cells. Specifically, at a concentration of 10  $\mu\text{g/ml}$  of the FA-BSA-FITC probe, the U937 cells did not

show any positive staining above the control BSA-FITC staining (data not shown). Subsequent experiments were next performed using concentrations of 100 and 200  $\mu\text{g/ml}$ . At the 100  $\mu\text{g/ml}$  concentration, the cells showed specific binding of the FA-BSA-FITC probe at 30 minutes that increased by 2-fold at 120 minutes (Fig. 16A). At 200  $\mu\text{g/ml}$ , the FA-BSA-FITC probe showed increased binding over that of the 100  $\mu\text{g/ml}$  concentration at the 120-minute time-point; however, this was not observed at the 30-minute time-point. Thus the probe binding efficiency of the U937 cells was lower compared to the 4T1 cells and therefore the 200  $\mu\text{g/ml}$  concentration was considered optimal for all U937 cell analysis.

The mean fluorescence intensity of probe (200  $\mu\text{g/ml}$ ) binding across experiments was analyzed and results showed a 3-fold difference between the BSA-FITC and the FA-BSA-FITC treated samples at both 30 and 120 minutes (Fig. 16B,  $p < 0.05$ ). Although there was no significant difference in probe binding at 30 and 120 minutes unlike what was observed in the 4T1 cells, increased binding approached significance at 120 minutes ( $p < 0.07$ ). Thus, overall the data demonstrate that the FR- $\beta$  receptors exhibited a lower binding activity than FR- $\alpha$  receptors.

In contrast to the 4T1 cells, initial experiments showed that a FA-BSA-FITC probe concentration of 100  $\mu\text{g/ml}$  gave optimal labeling for FR- $\beta$  for microscopic analysis. The U937 cells demonstrated markedly higher staining with the FA-BSA-FITC probe compared to the BSA-FITC control (Fig. 16C). However, there was no change in the staining intensity over time, unlike that observed in 4T1 cells. The FA-BSA-FITC probe staining on the U937 cells was found somewhat polarized on the surface of the cell membrane at 30 minutes (as indicated by arrows) while at 120 minutes the probe was located diffusely on the cell surface. Importantly, there was no evidence of internalization over the 120-minute time-period unlike that observed for 4T1 cells. Taken together, the flow cytometric data and microscopic analyses demonstrated

that the FR- $\beta$  isoform has strong specific binding to the FA-BSA-FITC probe, but is not internalized following binding.

Overall, in comparison to the FR- $\beta$  receptors on U937 cells, the FR- $\alpha$  receptors expressed on the 4T1 cells showed significantly higher binding of the FA-BSA-FITC probe at the 100  $\mu\text{g/ml}$  concentration at both 30 and 120 minutes (Fig. 16D;  $p < 0.05$ ). Thus, these results suggest that the FR- $\alpha$  receptors are more active relative to FR- $\beta$ .

### **Internalization of FR- $\alpha$ following binding**

Fluorescence microscopic analysis strongly suggested that the FA-BSA-FITC probe was internalized into 4T1 cells while it was not internalized following binding to U937 cells. To confirm internalization, confocal microscopy was performed on 4T1 and U937 cells that were treated with FA-BSA-FITC probe for 120 minutes as described above. Image analysis indicated that the FA-BSA-FITC probe was internalized in the 4T1 cells at this time. The axes on the images showed that the probe was localized directly beneath the membrane in the form of clusters (Fig. 17A). On the contrary, the FA-BSA-FITC probe bound on the U937 cells was found diffusely located over the cell surface, and did not demonstrate internalization even after 120 minutes (Fig. 17B).

### **4T1 tumors showed strong and specific binding to the FA-BSA-TRITC probe**

Previous studies showed that advanced stage (4-week) 4T1 tumor cells exhibited FR- $\alpha$  expression (Chap 2, Fig. 4). Therefore, the binding activity of the FA-BSA-TRITC probe to 4T1 tumor sections was analyzed. The tumor sections showed strong binding to the FA-BSA-TRITC probe but not to the BSA-TRITC control (Fig. 18, red). Specifically, the FA-BSA-TRITC probe bound throughout the tumor, with the tumor epithelial cells (CD11b<sup>-</sup>) staining the most intensely,



consistent with their expression of FR- $\alpha$  (Fig. 18 b, d) The myeloid cell population in the tumor sections was identified using an antibody against CD11b (green), and these cells demonstrated lower binding of the FA-BSA-TRITC probe. Therefore, these results indicate that FR- $\alpha$  present on the epithelial tumor tissue, and also to a lesser degree FR- $\beta$  on tumor myeloid cells, were able to specifically bind to the folic acid conjugate.

### **Free folic acid did not competitively inhibit FA-BSA-FITC binding to FR- $\alpha$**

In order to determine potential competition between the free FA and the FA-BSA-FITC probe for binding to the receptors, 4T1 and U937 cells were pre-treated with 2.2  $\mu$ M FA and then incubated with probe followed by analysis with flow cytometry. In the 4T1 cells, the mean fluorescence intensity of the FA-BSA-FITC probe-treated samples remained unchanged when pre-treated with free FA (Fig. 19). In contrast, the U937 cells that were pre-treated with free FA prior to FA-BSA-FITC probe treatment exhibited a significant reduction in fluorescence intensity compared to untreated cells. These results demonstrate that free FA does not block the binding or uptake of FA-targeted molecules to the high affinity FR- $\alpha$  isoform, but can block binding to the lower affinity FR- $\beta$  isoform.

### **Myeloid-derived suppressor cells (MDSCs) showed strong and specific binding to the FA-BSA-FITC probe**

Bulk MDSCs were harvested from the spleens of advanced stage (4-week) 4T1 tumor-bearing mice. Cells were treated with 100  $\mu$ g/ml of BSA-FITC or the FA-BSA-FITC probe for 30 and 120 minutes followed by flow cytometric analysis. Results showed that both the monocytic and granulocytic MDSC subsets had specific binding to the FA-BSA-FITC probe at both 30 and 120 minutes (Fig. 20A). Notably, the monocytic subset of MDSC had much higher binding to the

FA-BSA-FITC probe as compared to the granulocytic subset. In addition, while the monocytic MDSC subset showed increased binding to the FA-BSA-FITC probe with the longer incubation time, the granulocytic subset remained mostly unchanged.

Summary data for the flow cytometry results are shown in Fig. 20B. The granulocytic MDSC subset showed an ~7-fold increase ( $p < 0.05$ ) in the mean fluorescence intensity when treated with the FA-BSA-FITC probe for 30 minutes compared to the BSA-FITC control. After 120 minutes of treatment, these cells showed an ~2-fold increase in binding to the FA-BSA-FITC probe compared to the 30-minute time-point but this did not reach statistical significance ( $p = 0.08$ ). The monocytic MDSC subset also exhibited specific binding to the FA-BSA-FITC probe. Specifically, the cells showed a significant 12-fold increase ( $p < 0.005$ ) in binding to the FA-BSA-FITC probe at 30 minutes and a 15-fold increase ( $p < 0.005$ ) after 120 minutes compared to the control. Therefore, the overall FA-BSA-FITC probe binding intensity exhibited by the monocytic MDSC subset was significantly higher than that of the granulocytic MDSC subset at both 30 and 120 minutes.

For microscopic analysis, MDSCs were treated with 100  $\mu\text{g/ml}$  of the BSA-FITC or FA-BSA-FITC probe along with antibodies to identify the granulocytic and monocytic MDSCs as described above. Compared to the BSA-FITC control (Fig. 20, upper panel), both subsets of MDSCs showed significantly higher binding with the FA-BSA-FITC probe (Fig. 20, lower panels). MDSCs isolated from the spleen of advanced stage tumor mice were mostly of the granulocytic subset (~90%) or  $\text{CD11b}^+\text{Ly-6C}^{\text{low}}$  (red) and showed moderate binding to the FA-BSA-FITC probe (green). The monocytic subset or  $\text{CD11b}^+\text{Ly-6C}^{\text{high}}$  (blue) exhibited strong binding to the FA-BSA-FITC probe and could be identified by a pink hue on the cell membrane. In particular, the FA-BSA-FITC probe binding by the monocytic MDSCs was quite evident from

the high intensity of probe staining (green) that was visible on these cells. Therefore, consistent with the flow cytometric data, fluorescence microscopic analysis of bulk MDSCs not only showed specific binding to the FA-BSA-FITC probe but also confirmed higher probe binding activity in the monocytic MDSC subset.

To determine if MDSCs internalized the FA-BSA-TRITC probe following binding, confocal laser-scanning microscopy was used. MDSCs harvested from 4T1 tumor-bearing mice were isolated and treated with the FA-BSA-TRITC probe as described above. Interestingly, the probe was found localized at the surface of the cells after 30 minutes (left panel) while after 120 minutes (right panel), the probe was internalized (Fig. 20D). Thus, these results suggest that a more active version of FR- $\beta$  is expressed on MDSCs that behave differently from that found on the U937 tumor cells.

### **The FA-BSA-Au<sub>18</sub> conjugates exhibited specific binding to the 4T1 and U937 cells**

The previous studies showed that the FR- $\beta$  isoform expressed on U937 myeloid tumor cells did not internalize. Therefore, a successful targeting strategy using FR- $\beta$  to eliminate these cells could not depend on delivery of a drug or toxin into the cell. A previous study done in collaboration with Dr. Oliver's lab was able to successfully target the 4T1 cells using an anti-FR antibody-magnetite nanoparticle conjugate and then kill the cells by generating localized heating at the cell surface<sup>178</sup>. This technique utilizes an optimized oscillating magnetic field (OMF) that can generate localized heating around the Au-coated magnetite nanoparticles strong enough to kill the target cells without affecting the neighboring healthy cells. In the present study, we demonstrated the potential of FA-targeted nanoparticle conjugates to specifically bind to the 4T1 and U937 cells. Specifically, 4T1 cells were treated with either FA-BSA-Au<sub>18</sub> or BSA-Au<sub>18</sub> nanoparticle conjugates and then analyzed by SEM (Fig. 21). Results showed that the FA-BSA-

Au<sub>18</sub> conjugates showed significantly higher numbers of nanoparticles bound to the cell surface as compared to the BSA-Au<sub>18</sub> control. In addition, the FA-BSA-Au<sub>18</sub> nanoparticles were located in clusters bound to flattened regions of the membranes as well as on membrane protrusions and ruffles.

Similarly, U937 cells were treated with either FA-BSA-Au<sub>18</sub> or BSA-Au<sub>18</sub> nanoparticle conjugates and analyzed by SEM (Fig. 22). The U937 cells treated with the FA-BSA-Au<sub>18</sub> conjugates showed significantly higher numbers of nanoparticles bound to the cell surface as compared to the BSA-Au<sub>18</sub> control. In addition, the FA-BSA-Au<sub>18</sub> nanoparticles were found mostly as individual labels or in small clusters, but confined to a specific area of the cell membrane. This finding was similar to the polarized anti-FR- $\beta$  antibody-staining pattern observed on the U937 cells previously (Chapter 2, Figs. 9 & 10).

#### **FR- $\alpha$ receptors did not internalize via clathrin-mediated endocytosis in the 4T1 cells**

Previous reports have also demonstrated internalization of the FR- $\alpha$  into epithelial cells; however, the mechanisms associated with this process have not been completely elucidated. Therefore, we sought to investigate the FR- $\alpha$  internalization pathway in the 4T1 cells. Specifically, 4T1 cells were treated with the FA-BSA-TRITC probe to track the receptors intracellularly. The cells were also treated with a transferrin (Tfn)-FITC conjugate as a marker for clathrin-mediated endocytosis so direct comparisons could be made with that of FR- $\alpha$  internalization.

Analysis of 4T1 cells treated with the FA-BSA-TRITC probe along with Tfn-FITC for 30 minutes showed two distinct staining patterns. Specifically, the FA-BSA-TRITC probe was mostly localized to the cell surface (Fig. 23, red staining) while the transferrin receptors were

internalized in the form of clusters (green staining). After 120 minutes, the FA-BSA-TRITC probe showed internalization but there was no co-localization with the internalized transferrin receptors. These results clearly indicated that FR- $\alpha$  internalization was not associated with the clathrin-mediated endocytic pathway.

### **FR- $\alpha$ internalization in the 4T1 cells was not associated with pinocytosis**

A second major pathway of uptake by cells is pinocytosis which is also commonly known as “cell-drinking”<sup>97</sup>. Therefore, we sought to determine if there was any co-localization of the FR- $\alpha$  internalization pathway with that of pinocytosis. Dextran is a standard marker for studying pinocytosis in cells and hence was used to compare FA-BSA-TRITC probe internalization in the 4T1 cells.

Pinocytosis in tumor cells is reported to occur as early as 5 minutes thus we analyzed the cells treated with the FA-BSA-TRITC probe and dextran-FITC conjugate from 5-120 minutes. At the early time points of 5 and 15 minutes, both the dextran-FITC conjugate (Fig. 24, green staining) and the FA-BSA-TRITC probe (red staining) were found on the cell membrane. Interestingly, both the FA-BSA-TRITC and dextran-FITC conjugates exhibited punctate staining and some co-localization on the cell membrane (yellow color) at this time. After 30 minutes of treatment, the intensity of dextran-FITC staining as well as the FA-BSA-TRITC staining appeared much stronger and indicated some internalization had occurred in both cases. However, the internalized FA-BSA-TRITC probe at this time did not exhibit any co-localization with that of the dextran-FITC conjugate. After 120 minutes, the amount of internalized FA-BSA-TRITC probe and dextran-FITC were further enhanced, indicating increased uptake by the cells and both exhibited internalized clusters. However, the dextran-FITC uptake by the cells remained distinct from that

of the FA-BSA-TRITC probe, thus indicating that FR- $\alpha$  internalization is not mediated through pinocytosis.

### **FR-mediated binding activity was sensitive to cell membrane cholesterol depletion**

Previous reports have suggested a possible role of lipid rafts in FR binding activity. Specifically, it is proposed that the cholesterol deposits present within the lipid rafts on the cell membrane are responsible for mediating FR binding to ligands and facilitating FR internalization; however, this process remains obscure<sup>60</sup>. Therefore, the role of cholesterol in FR- $\alpha$  and FR- $\beta$  binding and internalization was investigated in 4T1 and U937 cells, respectively. For these studies, a cholesterol inhibitor, methyl- $\beta$ -cyclodextrin (M $\beta$ CD) was used to deplete free cholesterol from the cell surface membrane. 4T1 and U937 cells were pre-treated with M $\beta$ CD and then incubated with the FA-BSA-FITC probe or BSA-FITC for 30 and 120 minutes, and binding ability was quantified by flow cytometry. Initial analysis showed that FA-BSA-FITC probe binding to 4T1 cells was reduced in the presence of M $\beta$ CD (Fig. 25A). A similar albeit lesser effect was also observed in the M $\beta$ CD-treated U937 cells. Summary data showed that the 4T1 cells showed significant reduction ( $p < 0.05$ ) in FA-BSA-FITC probe binding after treatment with M $\beta$ CD at both 30 and 120 minutes (Fig. 25B). Specifically, pre-treatment of 4T1 cells with M $\beta$ CD followed by FA-BSA-FITC probe staining for 30 minutes resulted in a 2-fold reduction in the fluorescence intensity compared to untreated cells. After 120 minutes, this difference in mean fluorescence intensity was increased to ~2.5 –fold indicating that this inhibition of FR- $\alpha$  binding activity remained consistent over time. In fact, at both the 30 and 120 minute time points, the fluorescence intensity of the M $\beta$ CD-treated FA-BSA-FITC stained cells was equal to or lower than the equivalent BSA-FITC stained cells. Therefore, these results showed that the FR- $\alpha$

binding activity was completely inhibited by cholesterol depletion, thus suggesting a possible association of lipid rafts with FR- $\alpha$  binding activity.

The U937 cells pre-treated with M $\beta$ CD also showed a reduction (~1.5-fold) in FA-BSA-FITC staining; however, this change did not reach statistical significance ( $p = 0.08$ ) and was only observed after 120 minutes (Fig. 25B). To determine if the above observed inhibition in FR binding activity was due to receptor sensitivity to cholesterol depletion or due to cellular stress resulting from cell-surface cholesterol depletion, the effects of cholesterol depletion on clathrin-mediated endocytosis and pinocytosis were determined. In general, M $\beta$ CD-treated 4T1 cells showed a reduction in Tfn-FITC binding at later time points (Fig. 26A). Specifically, Tfn-FITC binding to M $\beta$ CD-treated 4T1 cells was reduced by 50% ( $p < 0.05$ ) compared to untreated cells at the 120-minute time-point (Fig. 26B). By contrast, the U937 cells did not exhibit any statistically significant change in transferrin binding activity with the M $\beta$ CD treatment, although labeling tended to be reduced. Similarly, the effect of cholesterol depletion on pinocytosis was also determined using flow cytometric analysis. After treatment with M $\beta$ CD, neither the 4T1 cells nor U937 cells exhibited a significant reduction in dextran-FITC binding (Fig. 27). While a reduction in dextran-FITC fluorescence was observed at the 120-minute time-point in both cell lines, this did not reach statistical significance ( $p = 0.08$ ). Fluorescence microscopy analysis showed that FA-BSA-TRITC probe binding in the 4T1 cells was significantly inhibited at both 30 and 120 minutes while the transferrin receptor activity and dextran-mediated pinocytosis remained unaffected in the cells (Fig. 28). Although the FA-BSA-TRITC probe binding in the U937 cells was not significantly affected by cholesterol depletion unlike the 4T1 cells (Fig. 25B), fluorescence microscopic analysis showed markedly reduced probe binding in the cells at the 120 minute time point while transferrin internalization and pinocytosis remained unaffected in

the U937 cells (Figs. 28 and 29). Importantly, cholesterol depletion did not affect FR- $\alpha$  and FR- $\beta$  expression in the 4T1 and U937 cells, respectively, as assessed by antibody labeling (data not shown). Thus, taken together, these studies revealed that cholesterol, possibly in the form of lipid rafts, may be a key factor in regulating FR binding activity in tumor cells without affecting receptor expression levels.



## DISCUSSION

FR- $\alpha$  and FR- $\beta$  isoforms are reported to not only be differentially expressed, but are also suggested to function differently in cells<sup>36</sup>. However, the differences associated with their intracellular trafficking are not completely understood. We have already shown their lineage-specific expression and their differential activity in response to folic acid (Chapter 2). Therefore, in these studies, FR- $\alpha$  and FR- $\beta$  isoforms were tracked to determine their intracellular fate following ligand binding. The goal of the study was to provide new information that would aid in designing folic acid-based methods to target these isoforms.

For tracking the receptors, FA-fluorochrome conjugates (FA-BSA-FITC or FA-BSA-TRITC) were synthesized (Fig. 13 and 14). BSA-FITC and BSA-TRITC were also synthesized as equivalent controls. The FA-BSA-FITC probe exhibited strong and significantly higher binding to the 4T1 cells than did the BSA-FITC control (Fig. 15A & B). In addition, there was a dose-dependent as well as time-dependent increase in FA-BSA-FITC probe binding in the cells. The specific binding ability of the FA-BSA-FITC probe alone to the 4T1 cells demonstrated the high affinity of the FR- $\alpha$  receptors for FA and confirmed the utility of FA for targeting. The FA-BSA-FITC probe was found localized to the 4T1 cell membrane surface 30 minutes after addition but began to internalize thereafter (Fig. 15C) which was consistent with previous reports<sup>75</sup>. However, the time taken by the receptors to internalize the probe (~120 minutes) was longer than that observed with addition of free folic acid (5-30 minutes), which could be attributed to the size of the probe molecule being internalized (Fig. 12, Chapter 2). The probe (FA-BSA-FITC) being a much larger molecule may require a longer time to be internalized as compared to the free folic acid. Alternatively, the FA-BSA-FITC probe may engage multiple FRs at once given that there are ~2 molecules of FA in each conjugate, and this could alter the internalization rate.

As in the 4T1 cells, the FA-BSA-FITC probe showed significantly higher binding to the U937 cells than the BSA-FITC control (Fig. 16). However, demonstration of specific binding to the FA-BSA-FITC probe required a higher concentration of probe (200  $\mu\text{g/ml}$ ) than for the 4T1 cells, thus indicating a lower binding affinity of the FR- $\beta$  isoform to the FA-BSA-FITC probe. In addition, the FA-BSA-FITC probe binding remained constant at both 30 and 120 minutes in U937 cells, suggesting saturation of the FR- $\beta$  receptor activity in these cells. Fluorescence microscopy studies also revealed that the FA-BSA-FITC probe was not internalized by the U937 cells. Instead, the probe remained localized on the cell surface up to 120 minutes (Fig. 17C). Taken together, these studies revealed that the FR- $\alpha$  isoform has a high binding activity for FA conjugates and has the ability to internalize into cells. On the contrary, the FR- $\beta$  isoform has lower binding activity than FR- $\alpha$  and lacks the ability to internalize into cells.

Previous studies showed that tumor sections harvested from 4T1 tumor-bearing mice exhibited high FR- $\alpha$  expression (Chapter 2, Fig. 4). The present studies determined whether the receptors exhibited correspondingly high FA binding activity in the tumors. For this, tumors from 4T1 tumor-bearing mice were harvested and tissue sections were treated with the FA-BSA-TRITC probe. Results showed that the FA-BSA-TRITC probe exhibited strong staining on the tumor sections (Fig. 18). Therefore, FR- $\alpha$  expressed in the tumors maintained its ability to specifically bind to the FA-conjugated probe. Interestingly, pretreatment of 4T1 cells with free FA had no effect on the subsequent binding of the FA-BSA-FITC probe (Fig. 19). In contrast, similar treatment in U937 cells reduced FA-BSA-FITC binding. This suggests that the affinity of the FA-BSA-FITC probe for the FR- $\alpha$  receptor is higher than that of free folate, while this is not the case for binding the lower affinity FR- $\beta$  isoform. This may also reflect the fact that FR- $\alpha$  is internalized and recycled following binding while FR- $\beta$  remains on the cell surface.

It has previously been reported that FR- $\beta$  is restricted to cells of the myeloid lineage. Apart from the *in vitro* model cell line, U937, it was also of interest to investigate the role of FR- $\beta$  in non-tumor cells isolated from *in vivo* conditions, which would add relevance in interpreting the functions of this isoform. For this, MDSCs were chosen to examine the expression and functional characteristics of FR- $\beta$ . These cells increase during chronic inflammatory responses and during cancer where they inhibit the immune response of the host<sup>229</sup>. Previously in our laboratory, MDSCs were shown to express the FR- $\beta$  receptor; hence, this was a relevant cell type to further study the functions of this isoform<sup>399</sup>. Understanding the role of FR- $\beta$  in this population of suppressor cells can provide valuable insights in determining its potential as a target to eliminate MDSCs. The FA-BSA-FITC probe showed significantly stronger binding to both the granulocytic and monocytic subsets of MDSCs than the BSA-FITC control (Fig. 20A and B). However, the monocytic subset demonstrated significantly higher binding activity than the granulocytic subset, which could be attributed to higher expression of FR- $\beta$  on their surface<sup>399</sup>. In addition, the FA-BSA-FITC probe showed increased binding over time to the monocytic subset while binding to the granulocytic subset remained unchanged. This also suggests that the monocytic MDSCs are the more active subset in the population, and in fact have been shown to be more immunosuppressive than the granulocytic subset<sup>405</sup>. Fluorescence microscopy analysis further confirmed the specific binding of the FA-BSA-TRITC probe to both subsets of MDSCs (Fig. 20C). Unexpectedly, confocal microscopy showed that the FA-BSA-TRITC probe was internalized by MDSCs at 120 minutes (Fig.20D), unlike in the U937 cells. However, cells isolated from *in vivo* inflammatory conditions or the tumor environment exhibit higher uptake rates or pinocytosis than cultured cell lines<sup>75</sup>. Hence, this ability of MDSCs to internalize the probe may be attributed to the more active nature of the cells being isolated from

4T1 tumor-bearing mice. Regardless, this difference in FR- $\beta$  function in MDSCs *vs* tumor cells following FA-conjugate binding should be considered when designing future targeting strategies.

The current studies demonstrate that both FR- $\alpha$  and FR- $\beta$  exhibit strong specific binding to FA conjugates, thus supporting the idea that FA-based targeting methods can be applied to target both isoforms of the receptor. However, it is important to note that the FR- $\beta$  isoform was not internalized into tumor cells unlike FR- $\alpha$ . Therefore, FA-targeted delivery strategies that could target the receptors at the cell surface and still result in killing were investigated. Through collaboration with Dr. Julie Oliver, who specializes in the synthesis and use of nanoparticles, we sought to conjugate FA-BSA to gold nanoparticles (FA-BSA-Au<sub>18</sub> and BSA-Au<sub>18</sub>) to use as a potential targeting system. Importantly, the FA-BSA-Au<sub>18</sub> conjugates bound to FR- $\alpha$  on 4T1 cells while the BSA-Au<sub>18</sub> control conjugates did not (Fig. 21). The FA-BSA-Au<sub>18</sub> nanoparticles were found in clusters over the entire cell surface which was consistent with the previous data showing a distinct punctate FR- $\alpha$  staining pattern on 4T1 cells obtained through antibody labeling (Chapter 2, Figs. 9 and 10) and FA-BSA-FITC probe binding (Fig. 15). The FA-BSA-Au<sub>18</sub> conjugates also showed specific binding to the U937 cells (Fig. 22). However, in this case the nanoparticles were mostly bound to flattened areas of the membrane that were localized to discrete areas of the cell. This finding is consistent with the polarized staining pattern observed when using antibody labeling of FR- $\beta$  (Chapter 2, Figs. 9 and 10).

Overall, these data support the targeting of both FR- $\alpha$  and FR- $\beta$  receptors using FA-nanoparticle conjugates. Previous collaborative studies with Dr. Oliver demonstrated specific targeting of FR- $\alpha$  using an indirect antibody-nanoparticle-based system in 4T1 cells. Furthermore, using this strategy with gold-coated magnetite nanoparticles successfully killed 4T1 tumor cells by induction of hyperthermia at the cell-surface level<sup>178</sup>. Therefore, the aim of

the current studies was to develop a FA-nanoparticle conjugate that could deliver this hyperthermia-mediated therapy to both isoforms of the folate receptor in a single step. These current findings using FA-BSA-Au<sub>18</sub> nanoparticles as a model validated our premise that hyperthermia-mediated targeting through magnetic FA-nanoparticle conjugates (e.g., FA-BSA gold coated-magnetite) could be a potential targeting therapy to eliminate both FR- $\alpha$ - and FR- $\beta$ -expressing cells.

FR- $\alpha$  has been widely used as a targeting system to deliver drugs to epithelial tumor cells; however, concerns such as drug toxicity and non-specific tissue damage has resulted in only partial success of this therapeutic strategy. One contributing issue to the lack of success is that a detailed endocytic mechanism associated with this receptor isoform has not been described. A better understanding of FR- $\alpha$  function could provide valuable insights for devising alternative therapies to target this receptor. Therefore, we sought to better characterize the FR- $\alpha$  internalization pathway by comparing it to other standard endocytic receptor pathways in 4T1 tumor cells. Comparisons with the clathrin-receptor pathway marker transferrin indicated that FR- $\alpha$  is not associated with clathrin-mediated endocytosis as there was no co-localization between the FA-BSA-TRITC probe and the Tfn-FITC conjugate at any time points (Fig. 23). In addition, the FA-BSA-TRITC probe did not co-localize with the dextran-FITC conjugate (Fig. 24), thus demonstrating that the FR- $\alpha$  internalization pathway is also distinct from pinocytosis. These data taken together strongly indicate that FR- $\alpha$ -mediated internalization of bound ligand occurs through a non-typical mechanism or an endocytic pathway that needs further investigation.

One possible alternative internalization mechanism that has been suggested for FR is lipid rafts, although this has not been substantiated<sup>87</sup>. Hence, the association of FR to membrane lipid

rafts was investigated by determining their sensitivity to depletion of cholesterol, a major constituent of lipid rafts. Results showed that depleting cell membrane cholesterol with M $\beta$ CD treatment eliminated FA-BSA-TRITC probe binding in the 4T1 cells at both early and later time points (Fig. 25). In the case of the U937 cells, there was a tendency towards reduced probe binding, but these data did not reach statistical significance. Thus, overall, these results demonstrated that both FR- $\alpha$ , and to some degree FR- $\beta$  activity, was strongly affected by the absence of membrane cholesterol, thus indicating their dependence on lipid rafts. However, to confirm that these effects were induced due to cholesterol depletion and not from other indirect effects of M $\beta$ CD, the effects of cholesterol depletion on clathrin-mediated endocytosis and pinocytosis were examined (Fig. 26 and 27). Our results showed that transferrin endocytosis and pinocytosis of dextran were largely unaffected by cholesterol depletion. While there was a decrease in transferrin endocytosis at 120 minutes, this could be attributed to cellular stress or membrane damage from long-term cholesterol-deficient conditions. Collectively, the data show a dependency of both FR isoforms on membrane cholesterol compared to that of the other typical internalization pathways. Since cholesterol is a major component of lipid rafts it is most likely that lipid rafts play an important role in regulating FR ligand binding and trafficking in cells. Thus, these studies provide novel insights into trafficking mechanisms associated with FR endocytosis, which could be manipulated for potential receptor targeting.

## FIGURES AND LEGENDS

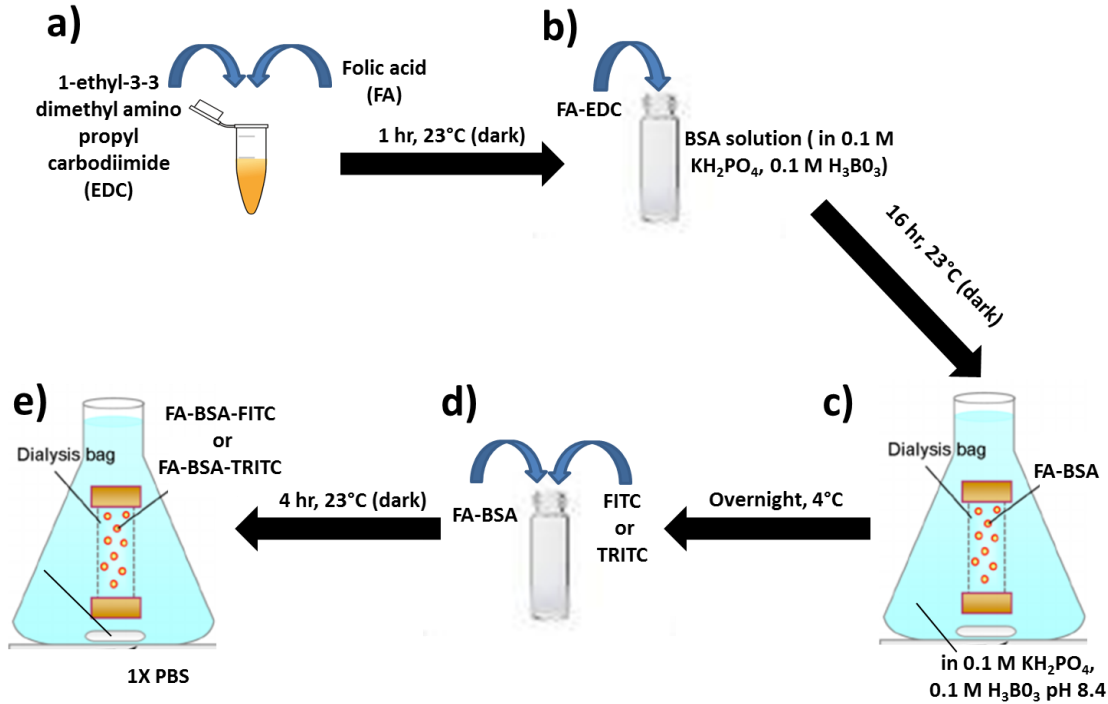


**Figure 13. Synthesis of folic acid-conjugated fluorescent probes.**

To specifically target folate receptors, folic acid (FA) was activated by the protein linker, EDC, to generate FA-EDC (a). FA-EDC was next coupled to bovine serum albumin (BSA), a protein carrier, to generate FA-BSA (b). Any unconjugated molecules were removed by dialyzing the product against sodium bicarbonate buffer overnight (c). Fluorescein isothiocyanate (FITC) or tetramethyl rhodamine (TRITC) was then attached to FA-BSA to generate FA-BSA-FITC and FA-BSA-TRITC, respectively (d), allowing visualization of the probe following dialysis of the product against PBS (e).

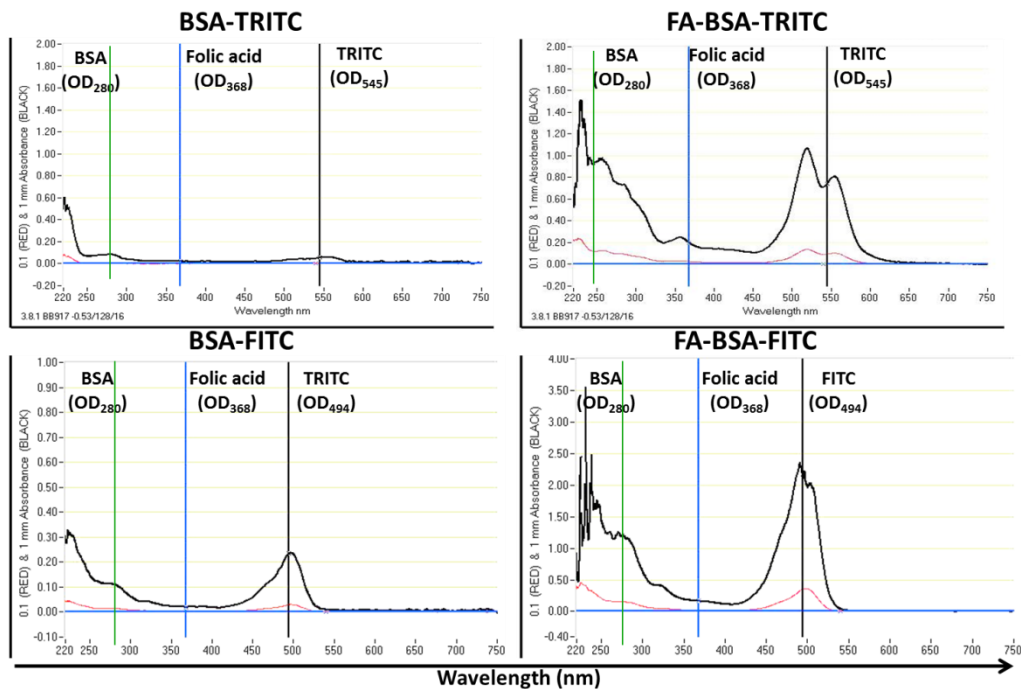
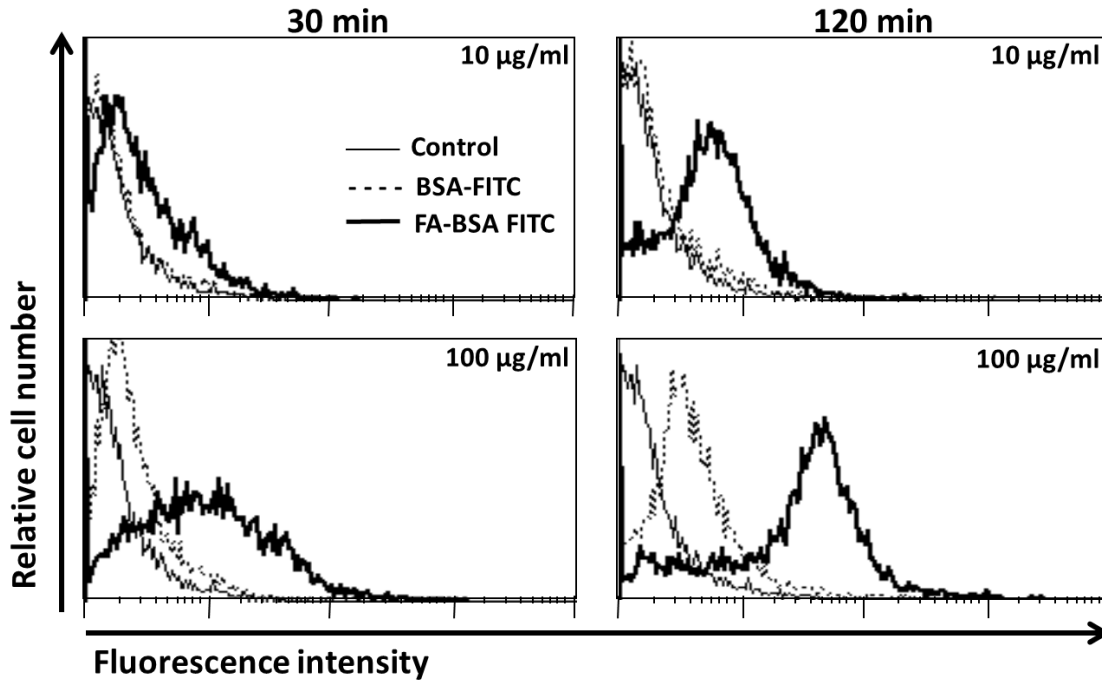


**Figure 14. UV-Vis analysis of the BSA-FITC, BSA-TRITC, FA-BSA-FITC and FA-BSA-TRITC probes**

The BSA-TRITC (left) and FA-BSA-TRITC (right) probes represented in the upper panel were quantified by measuring the absorbances of BSA, FA and TRITC using UV-Vis spectroscopy. The BSA-FITC (left) and FA-BSA-FITC (right) probes represented in the lower panel were quantified similarly. The concentrations of the probes were calculated using Beer-Lambert Law after using a correction factor for the TRITC or FITC dyes.

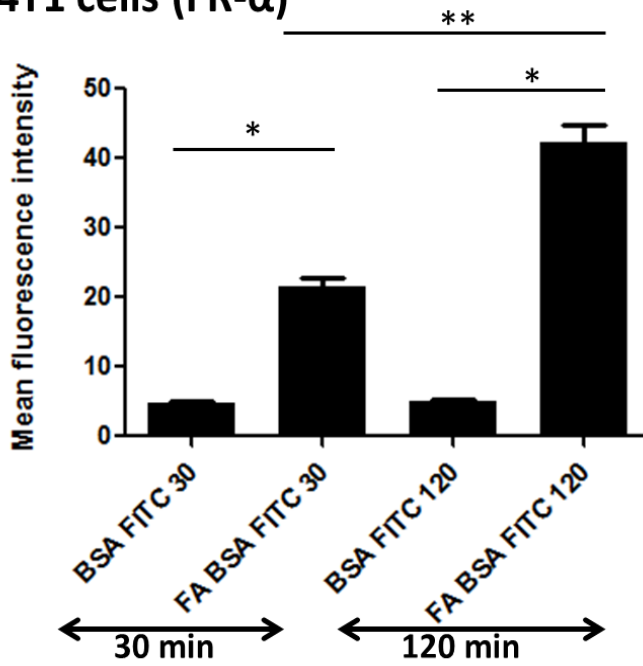


**A**

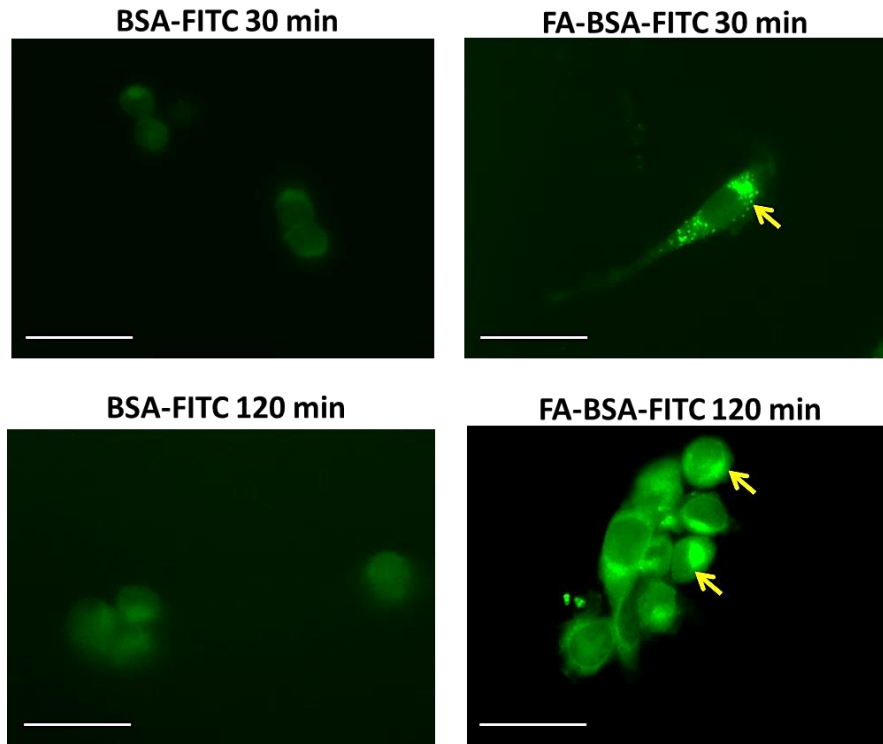


**B**

**4T1 cells (FR- $\alpha$ )**

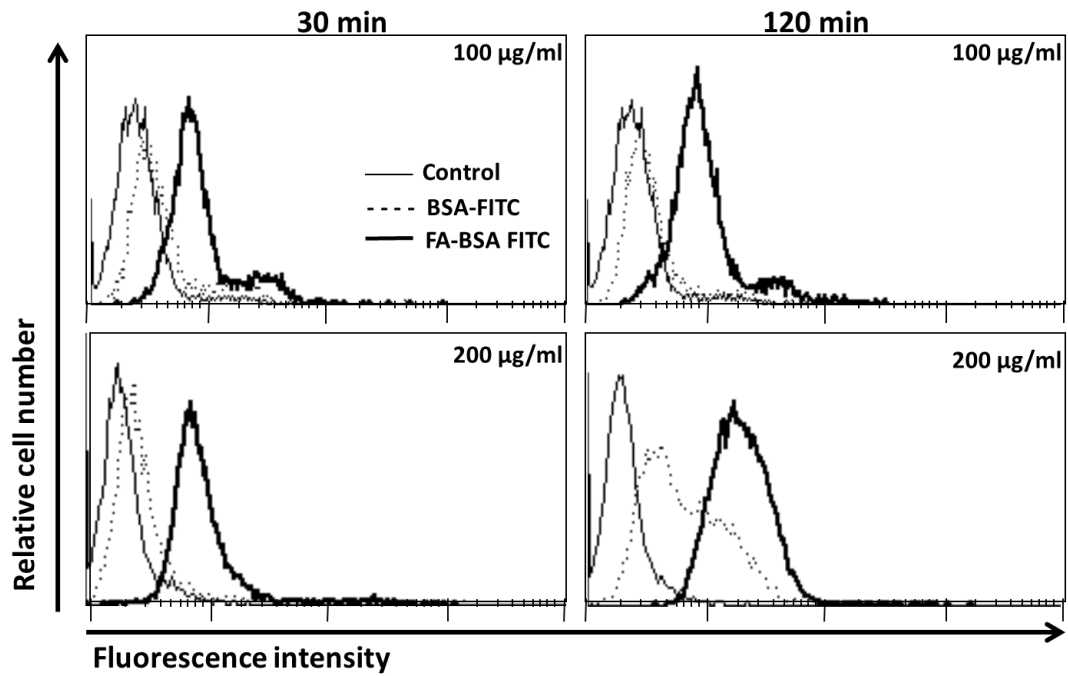
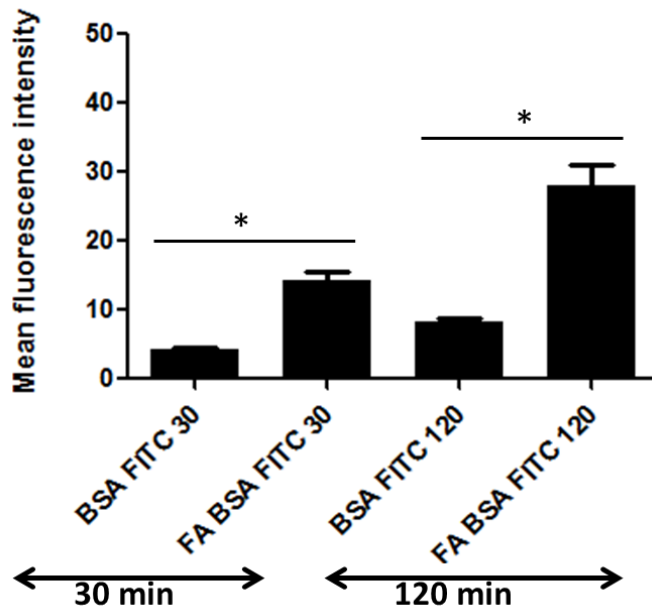


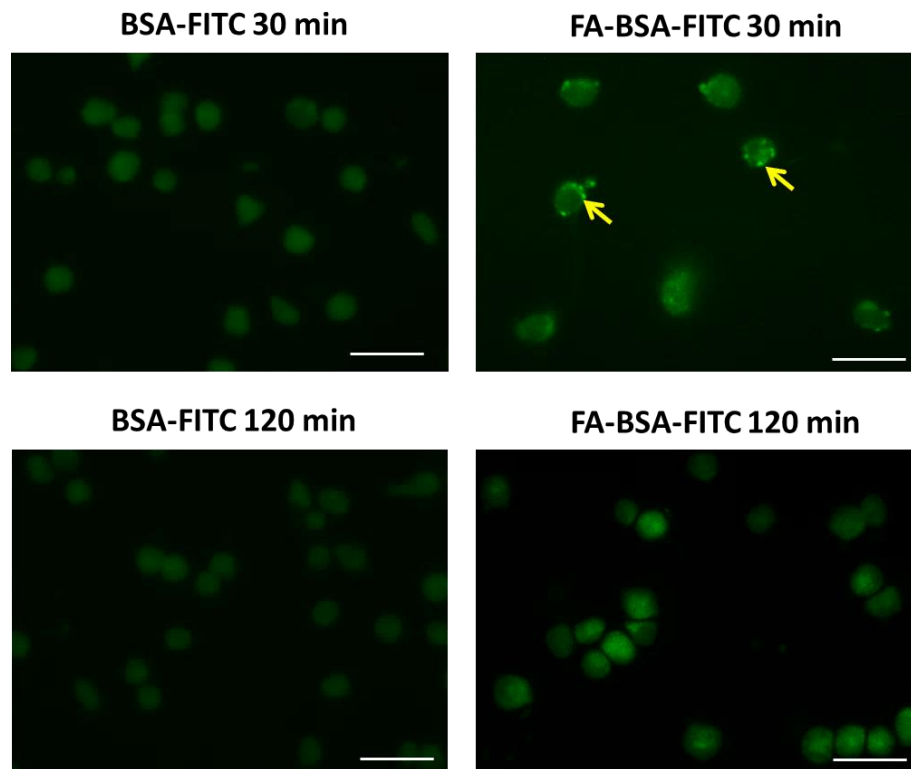
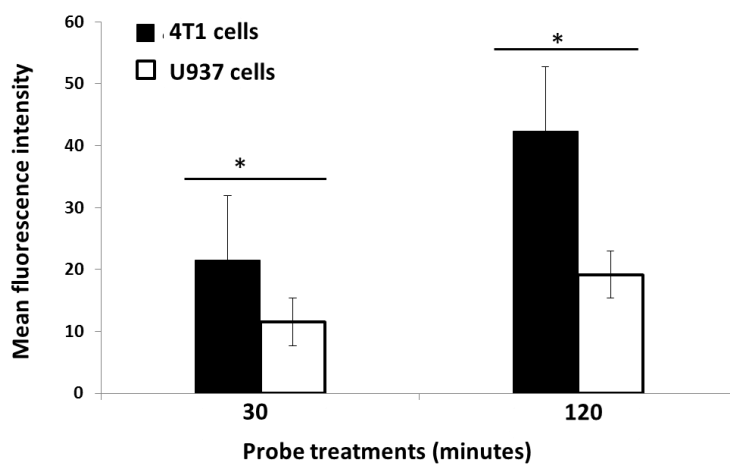
C



**Figure 15. FA-BSA-FITC probe showed specific binding to FR- $\alpha$  in 4T1 cells.**

4T1 cells were treated with the FA-BSA-FITC probe or BSA-FITC control for 30 or 120 minutes. A) Cells were treated with 10 or 100  $\mu\text{g}/\text{ml}$  of the conjugates and analyzed by flow cytometry. Histogram plots are representative of a minimum of 5 independent experiments. B) Summary data of the flow cytometry experiments represent the means  $\pm$  SEM of results. \*Difference in means between groups were significant,  $p < 0.05$ , \*\* $p < 0.05$ . C) 4T1 cells were grown on coverslips and treated with 1  $\mu\text{g}/\text{ml}$  of the FA-BSA-FITC or BSA-FITC probe and analyzed with fluorescence microscopy. Digital images were acquired at a constant exposure and pseudocolored using the MetaVue<sup>TM</sup> software. Scale bars are 2.5  $\mu\text{m}$ . Images are representative of 4 independent experiments.

**A****B****U937 cells (FR- $\beta$ )**

**C****D**

**Figure 16. FA-BSA-FITC probe showed specific binding to FR- $\beta$  in U937 cells.**

U937 cells were treated with the FA-BSA-FITC probe or BSA-FITC control for 30 or 120 minutes. A) Cells were treated with 100 or 200  $\mu\text{g}/\text{ml}$  of the conjugates and analyzed by flow

cytometry. Histogram plots are representative of a minimum of 5 independent experiments. B) Summary data of the flow cytometric experiments represent the Means  $\pm$  SEM of results. \*Difference in means between groups were significant,  $p < 0.05$ . C) U937 cells were treated with 100  $\mu\text{g/ml}$  of the FA-BSA-FITC probe or BSA-FITC control and analyzed with fluorescence microscopy. Digital images were acquired at a constant exposure and pseudocolored using MetaVue™ software. Scale bars = 0.5  $\mu\text{m}$ . Images are representative of 4 independent experiments. D) The mean fluorescence intensity of the FA-BSA-FITC probe (100  $\mu\text{g/ml}$ ) binding ability by the 4T1 cells was compared with that of the U937 cells and presented as means  $\pm$  SEM from 3-5 independent experiments. \*Differences in sample means were significant  $p < 0.05$ .

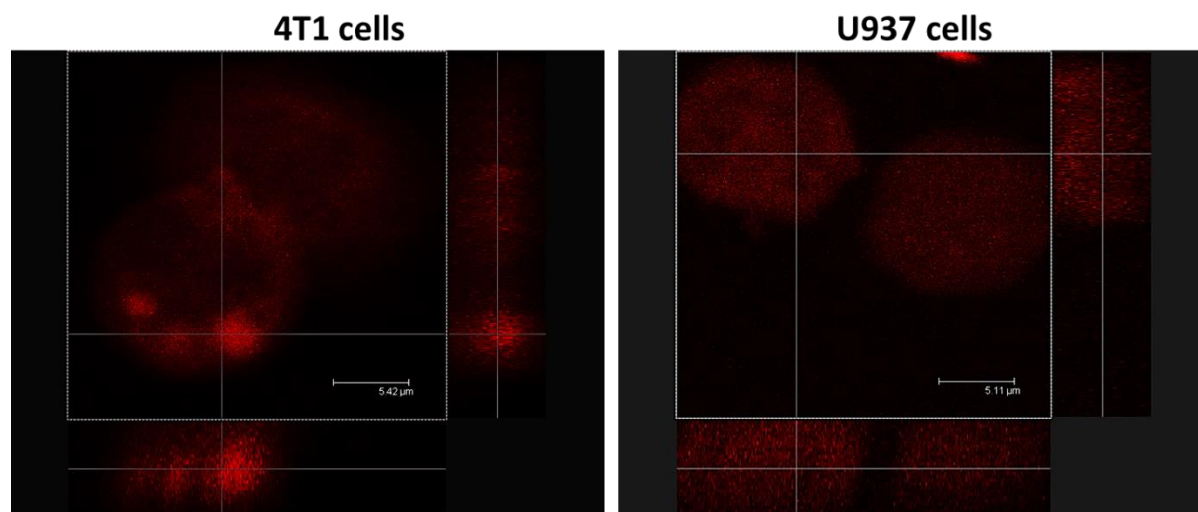


**Figure 17. Comparing FR- $\alpha$  and FR- $\beta$  internalization by high-resolution confocal microscopy**

4T1 and U937 cells were treated with FA-BSA-TRITC probe for 120 minutes and analyzed on a Leica Microsystems™ TCS SP2 confocal laser-scanning microscope. Images were acquired using a 40x objective and pseudocolored using the Leica confocal software. Images are representative of 3 independent experiments.

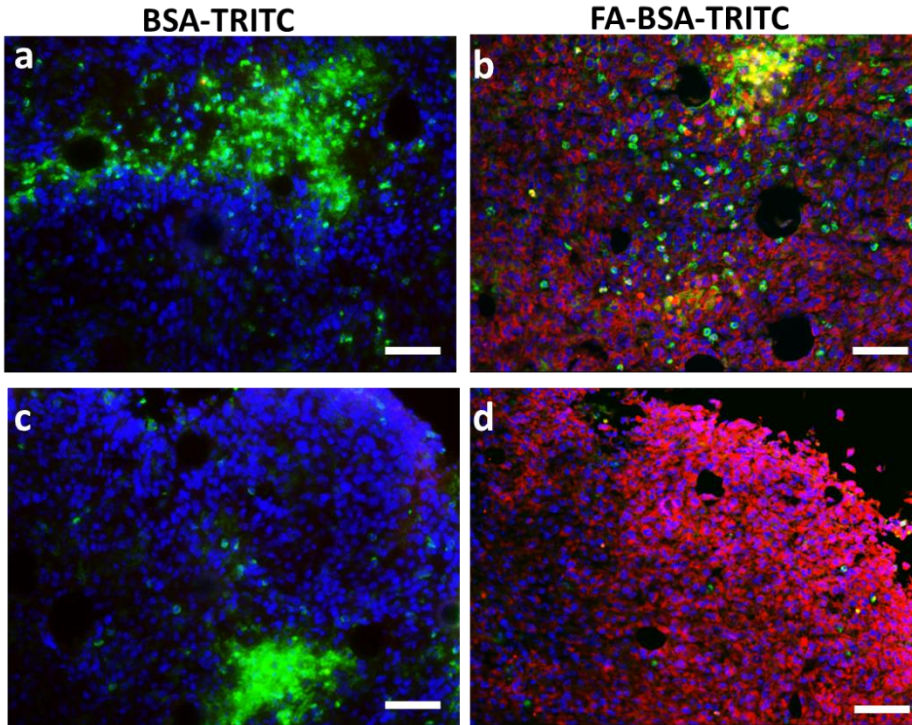


**Figure 18. The FA-BSA-TRITC probe showed strong staining on tumor sections harvested from 4-week 4T1 tumor-bearing mice.**

Tumors were harvested from advanced stage (4-week) 4T1 tumor-bearing BALB/c mice. Cryosections were immunolabeled against the myeloid cell marker CD11b. Sections were also treated with either the FA-BSA-TRITC probe or BSA-TRITC control (100  $\mu\text{g/ml}$ ) for 1 hour at room temperature. Sections were counterstained with DAPI to label cell nuclei (blue). The sections were mounted and analyzed with fluorescence microscopy. Digital monochromatic images were acquired at a constant exposure, and pseudocolored and overlaid using MetaVue™ software. Representative images show the difference in staining when treated with the BSA-TRITC or FA-BSA-TRITC probe (red). CD11b<sup>+</sup> cells (green) are predominantly myeloid-derived suppressor cells (MDSCs) present in clusters and as individual cells found in some areas of the tumor. Images are representative of 3 independent experiments. Scale bar = 100  $\mu\text{m}$ .

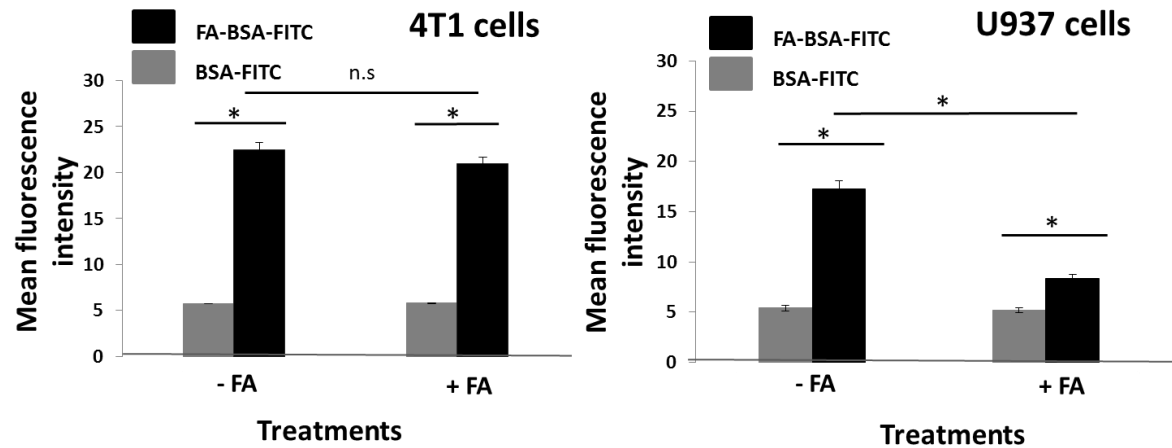
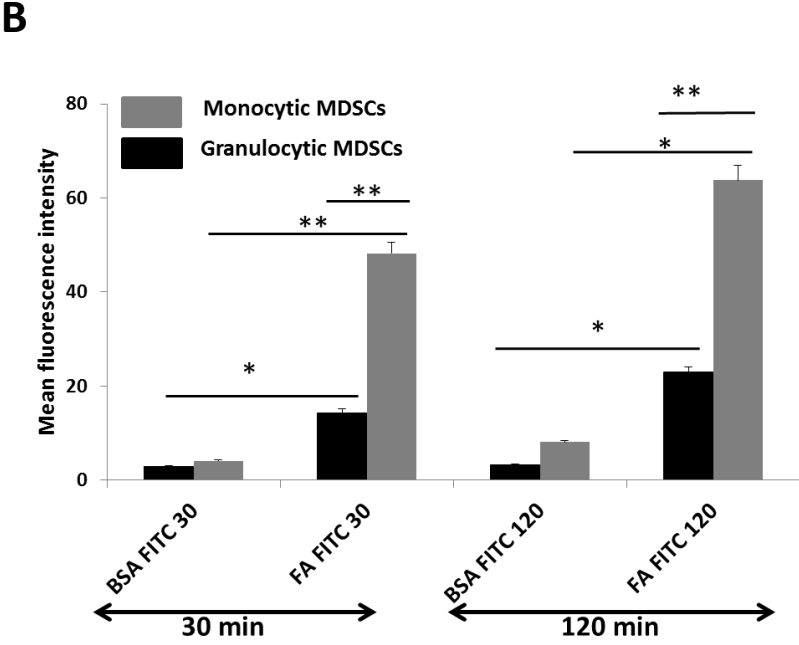
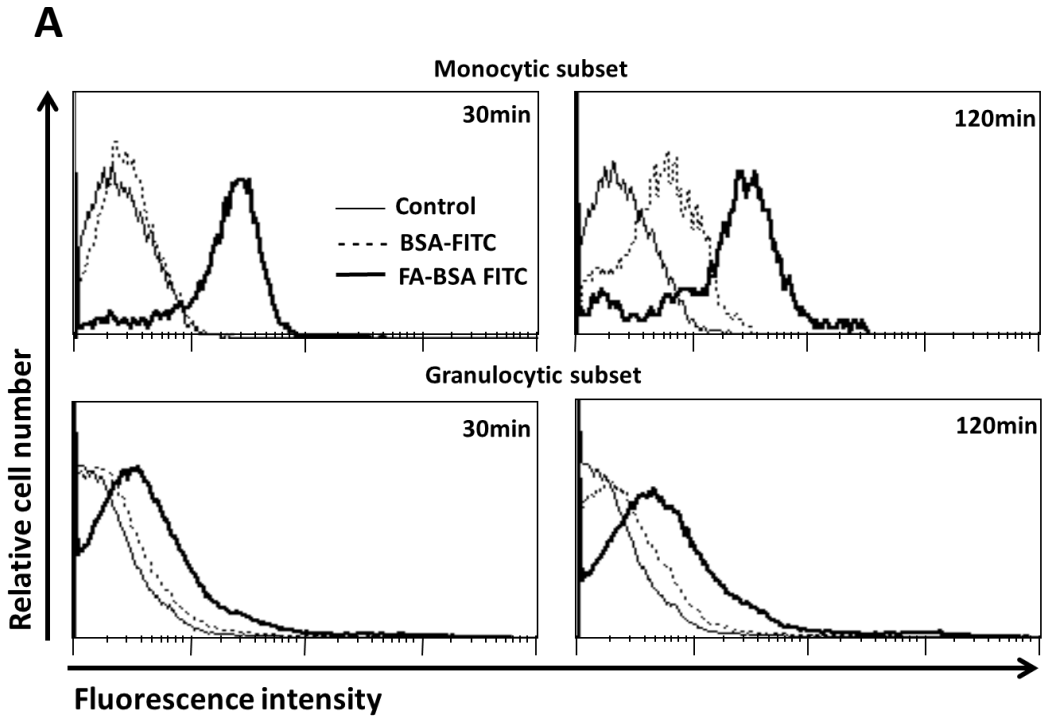


**Figure 19. Free folic acid did not compete with the FA-BSA-FITC probe for binding to the FR- $\alpha$  isoform.**

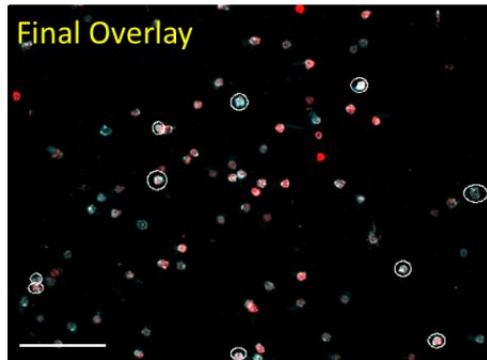
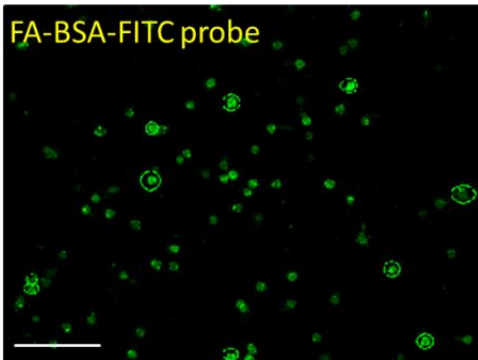
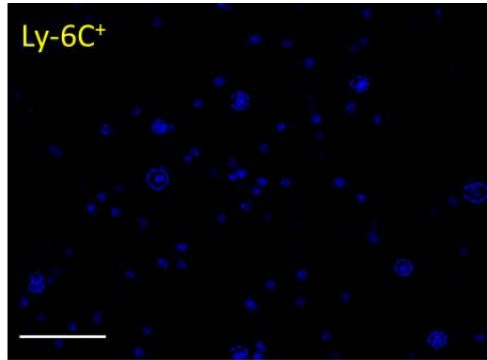
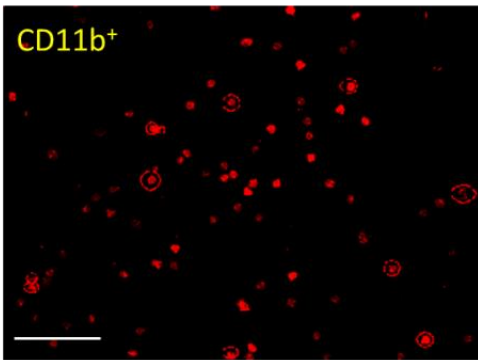
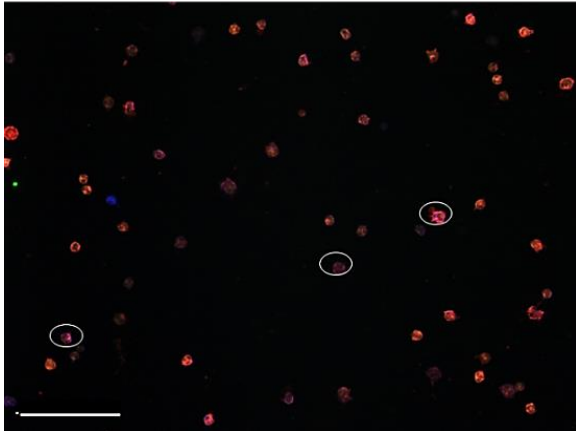
4T1 and U937 cells were treated with 2.2  $\mu$ M free FA for 10 minutes at 37°C followed by treatment with the FA-BSA-FITC probe or the BSA-FITC control at a concentration of 100  $\mu$ g/ml for 30 minutes at 37°C. Cells were then washed in PBS and fixed in 1.5% formaldehyde. Cells that were incubated with the probe in the absence of free FA were used as controls. The fluorescence intensity of the cells was quantified using flow cytometry. Data represent the mean  $\pm$  SEM results from 5 independent experiments. \*Differences in means between groups were significant,  $p < 0.05$ . n.s = non-significant.





C

BSA-FITC



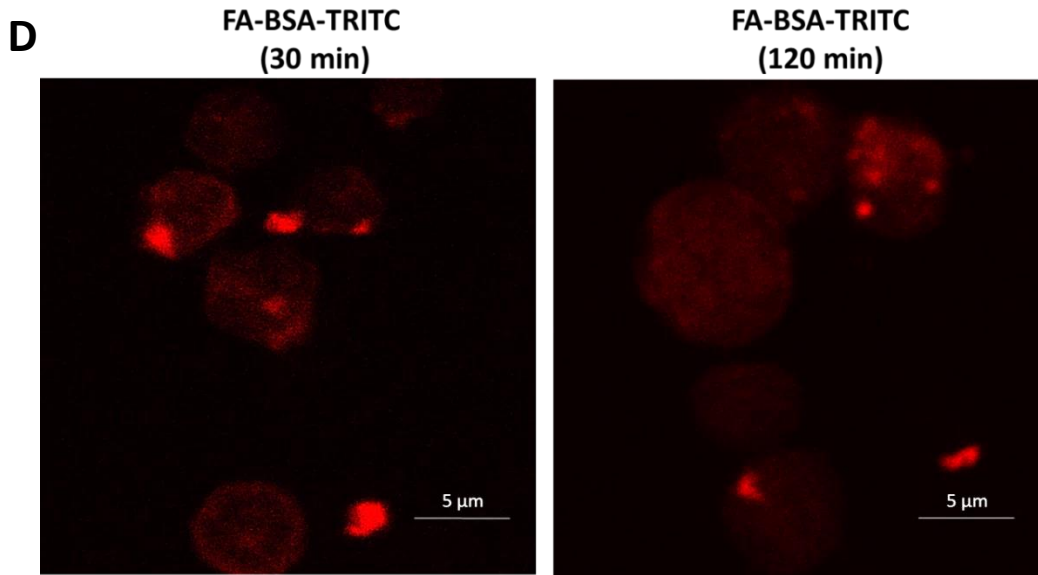


**Figure 20**

**Figure 20. The FA-BSA-FITC probe showed specific binding to FR- $\beta$  receptors on myeloid-derived suppressor cells (MDSCs).**

Bulk MDSCs were harvested from the spleens of advanced stage 4T1 tumor-bearing mice and were treated with the FA-BSA-FITC probe or BSA-FITC control for 30 or 120 minutes. A) Spleen cells were labeled with fluorochrome-conjugated antibodies against CD11b, Ly-6C and Ly-6G and treated with 100  $\mu$ g/ml of the probe and analyzed by flow cytometry. Individual subsets of MDSCs were gated and the mean fluorescence intensity of probe staining was quantified. Histogram plots are representative of a minimum of 5 independent experiments. B) Summary data of the flow cytometry experiments represent mean  $\pm$  SEM of a minimum of 5 independent experiments. \*Difference in means between groups were significant,  $p < 0.05$ ; \*\* $p < 0.005$ . C) Spleen cells were treated with 100  $\mu$ g/ml of the BSA-FITC (upper panel) or the FA-BSA-FITC probe (lower panels) for 30 minutes and immunolabeled with fluorochrome-conjugated antibodies against a granulocyte marker (CD11b), and MDSC markers (Ly-6G and

Ly-6C), and then analyzed by fluorescence microscopy. Images compare the binding specificity between the FA-targeted *vs* the untargeted probe. The circled cells on the FA-BSA-TRITC treated sample indicates the monocytic MDSCs binding the probe. D) Internalization of the FA-BSA-TRITC probe was also determined using confocal laser-scanning microscopy. Spleen cells were treated with 200  $\mu\text{g/ml}$  of the FA-BSA-TRITC probe for 30 (left) and 120 minutes (right) followed by labeling with CD11b, Ly-6G and Ly-6C to identify MDSCs. All digital images were acquired at a constant exposure using a 40x objective and pseudocolored using the MetaVue™ or Leica™ confocal software. Scale bars = 50  $\mu\text{m}$  (c) or 5  $\mu\text{m}$  (d). Images are representative of 3-4 independent experiments.

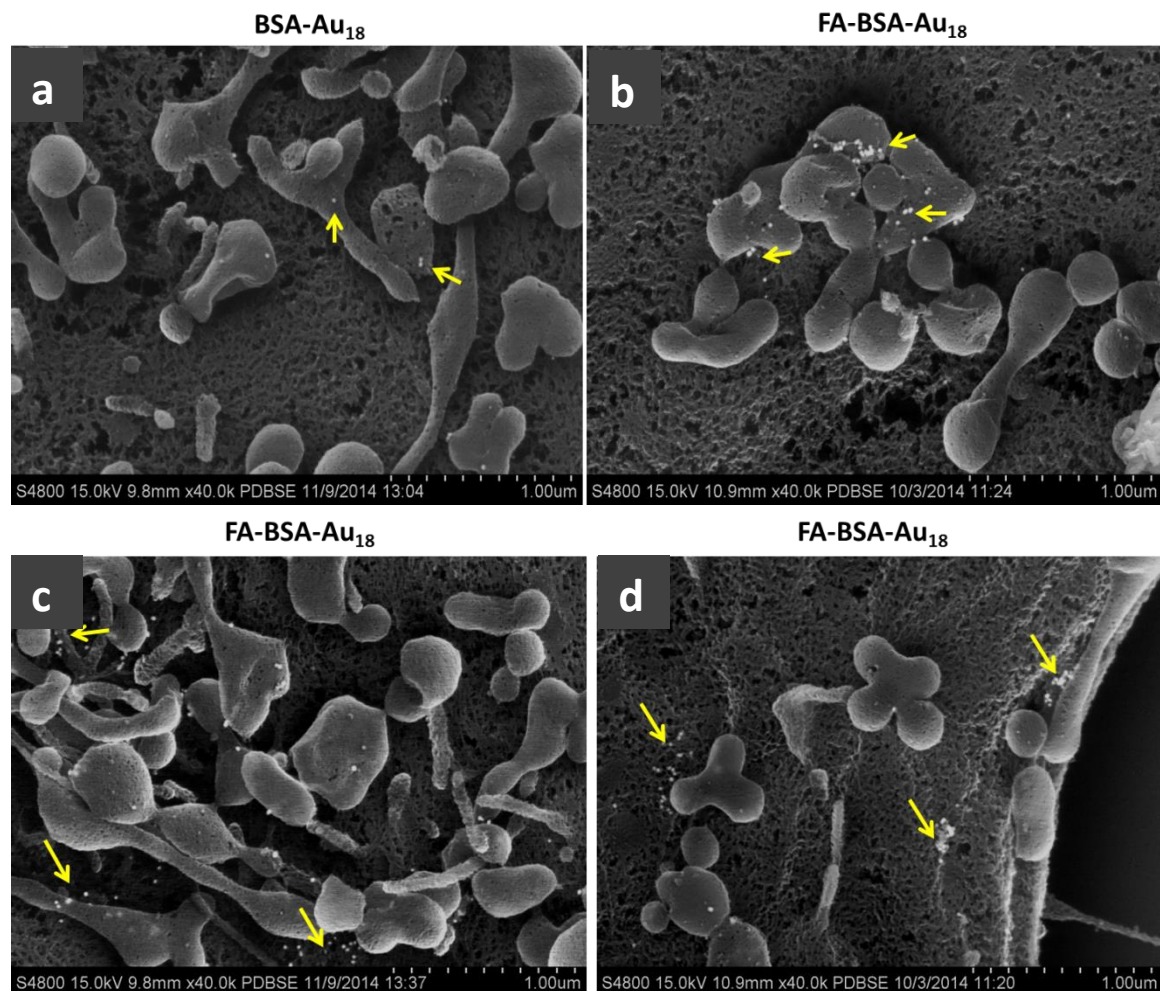
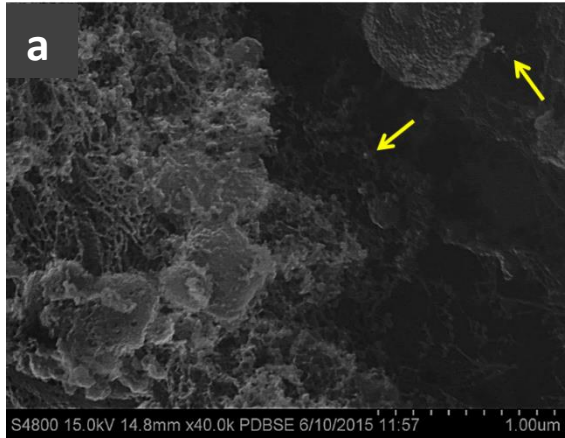


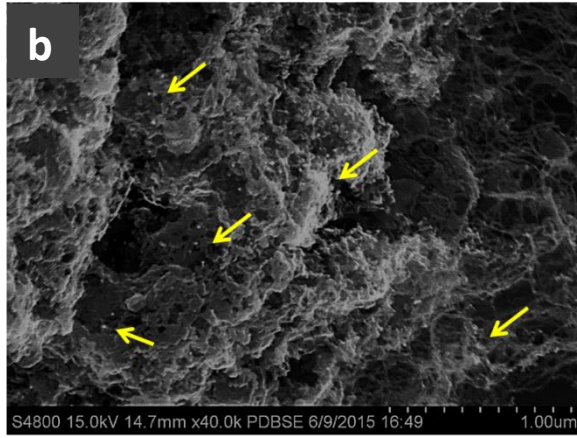
**Figure 21. The FA-BSA-Au<sub>18</sub> conjugates showed specific binding to FR- $\alpha$  receptors on the 4T1 cells.**

4T1 cells were grown on coverslips and treated with either BSA-Au<sub>18</sub> (a) or FA-BSA-Au<sub>18</sub> (b-d) conjugates for 1 hour at 37°C. Cells were fixed in 1.5% glutaraldehyde, post-fixed in OsO<sub>4</sub>, and prepared for SEM analysis. High-magnification back scattered electron images were acquired at a constant voltage and current setting. Images are representative of 3 independent experiments. The arrows point to nanoparticles that are bound on the cell surface.

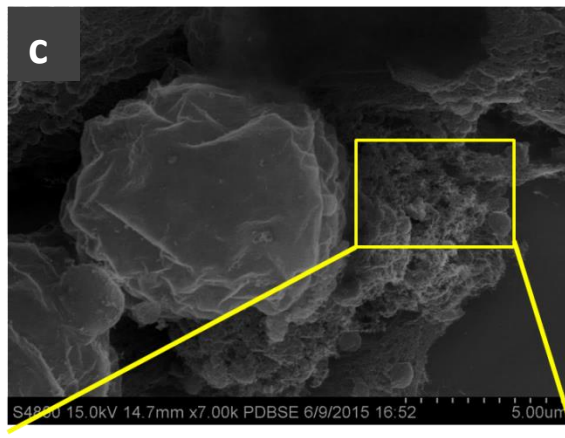
BSA-Au<sub>18</sub>



FA-BSA-Au<sub>18</sub>



FA-BSA-Au<sub>18</sub>



FA-BSA-Au<sub>18</sub>

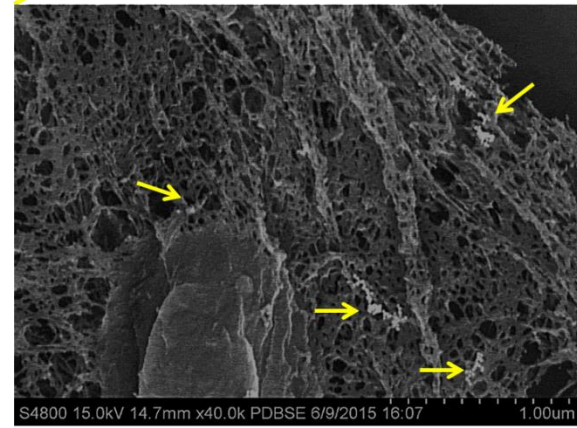
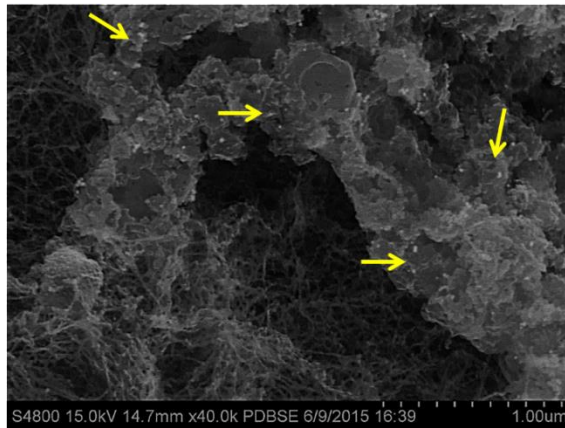
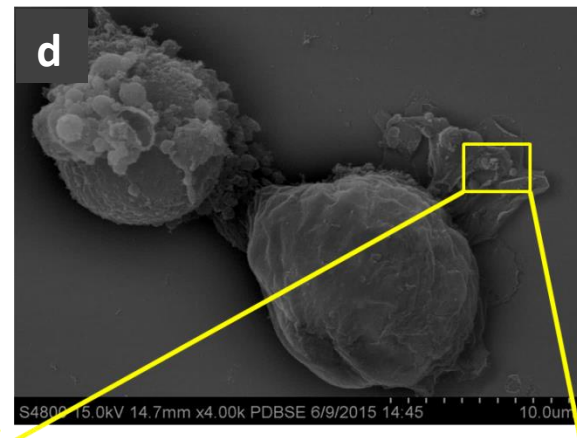


**Figure 22. The FA-BSA-Au<sub>18</sub> conjugates were localized to spread areas of the membrane of U937 cells.**

U937 cells were grown in suspension cultures and treated with either BSA-Au<sub>18</sub> or FA-BSA-Au<sub>18</sub> conjugates for 1 hour at 37°C. Cells were fixed in 1.5% glutaraldehyde and post-fixed in OsO<sub>4</sub>. Cells were washed and a drop of the cell suspension was then allowed to adhere to poly-L-lysine coated coverslips. Samples were prepared for electron microscopy and imaged on a scanning electron microscope. High-magnification back scattered electron images were acquired at a constant voltage and current setting. Images show comparison between BSA-Au<sub>18</sub> (a) and FA-BSA-Au<sub>18</sub> (b) conjugates. (c-d) Examples of membrane areas of the cell where most FA-BSA-Au<sub>18</sub> nanoparticles were bound. Images are representative of 3 independent experiments. The arrows point to the nanoparticles that were bound on the cell surface.

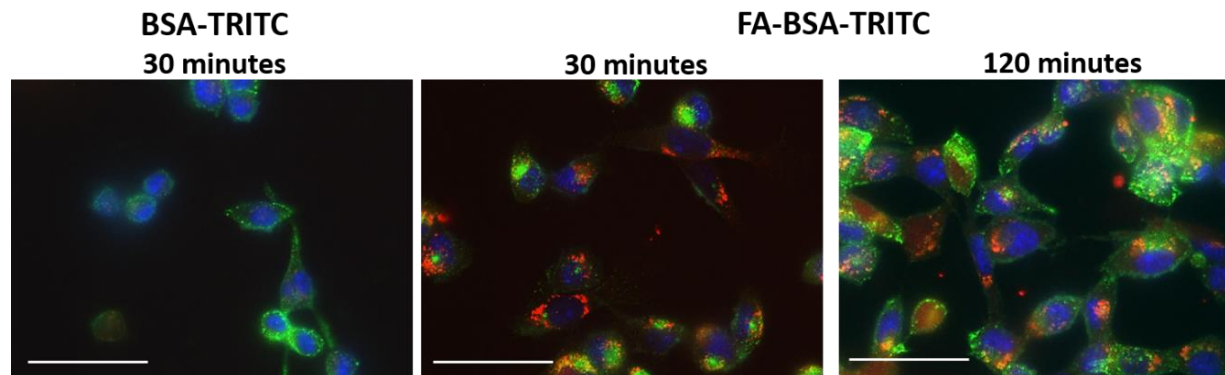


**Figure 23. Comparing FR- $\alpha$  and transferrin receptor internalization pathways**

4T1 cells were incubated with a transferrin-FITC conjugate (20  $\mu\text{g/ml}$ ) and the FA-BSA-TRITC probe or BSA-TRITC control at a concentration of 1  $\mu\text{g/ml}$  for 30 and 120 minutes at 37°C. Cells were washed with PBS, fixed in 1.5% formaldehyde and labeled with DAPI for nuclear staining. Cells were washed again, mounted with ProLong<sup>®</sup> Gold and analyzed by fluorescence microscopy. Digital monochromatic images were acquired at a constant exposure and pseudocolored and overlaid using MetaVue<sup>™</sup> software. Overlays include BSA-TRITC or FA-BSA-TRITC probe (red), transferrin-FITC (green) and DAPI (blue). Scale bars = 2.5  $\mu\text{m}$ . Images are representative of 3-5 independent experiments.



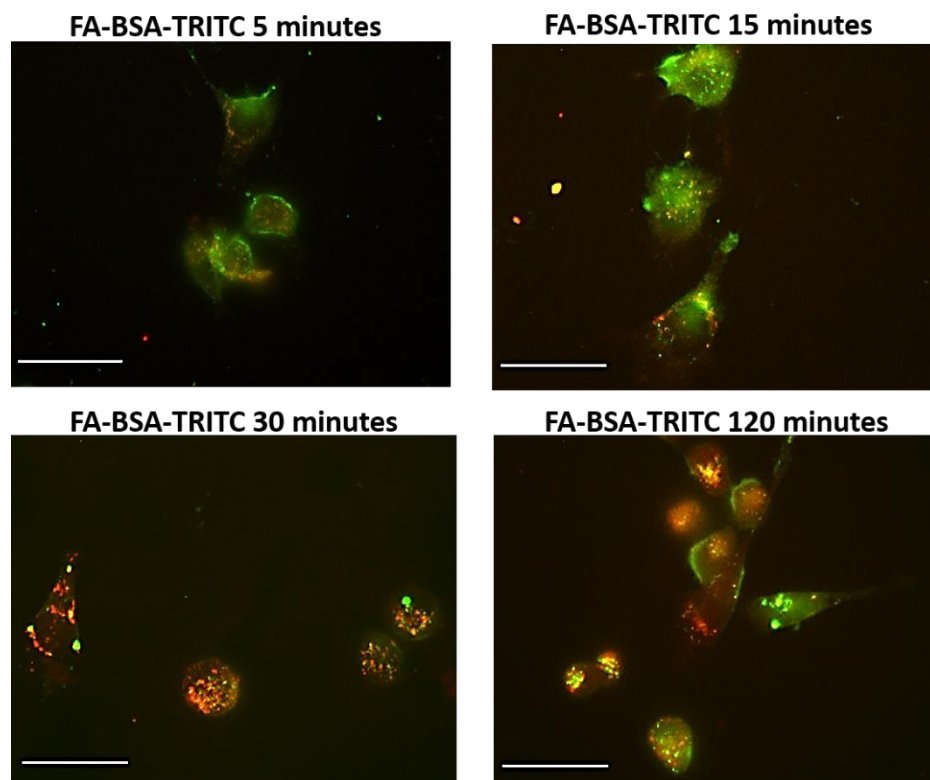


**Figure 24. Comparing FR- $\alpha$  internalization with dextran pinocytosis.**

4T1 cells were incubated with dextran-FITC conjugate (50  $\mu\text{g/ml}$ ) and the BSA-TRITC or FA-BSA-TRITC probe at a concentration of 1  $\mu\text{g/ml}$  for 5, 15, 30 and 120 minutes at 37°C. Cells were washed with PBS, fixed in 1.5% formaldehyde, and mounted with ProLong<sup>®</sup> Gold. Cells were analyzed by fluorescence microscopy. Digital monochromatic images were acquired at a constant exposure and pseudocolored and overlaid using MetaVue<sup>™</sup> software. Overlays include FA-BSA-TRITC (red) and dextran-FITC (green) across various time points ranging from 5, 15, 30 and 120 minutes. Scale bars = 2.5  $\mu\text{m}$ . Images are representative of 3 independent experiments.

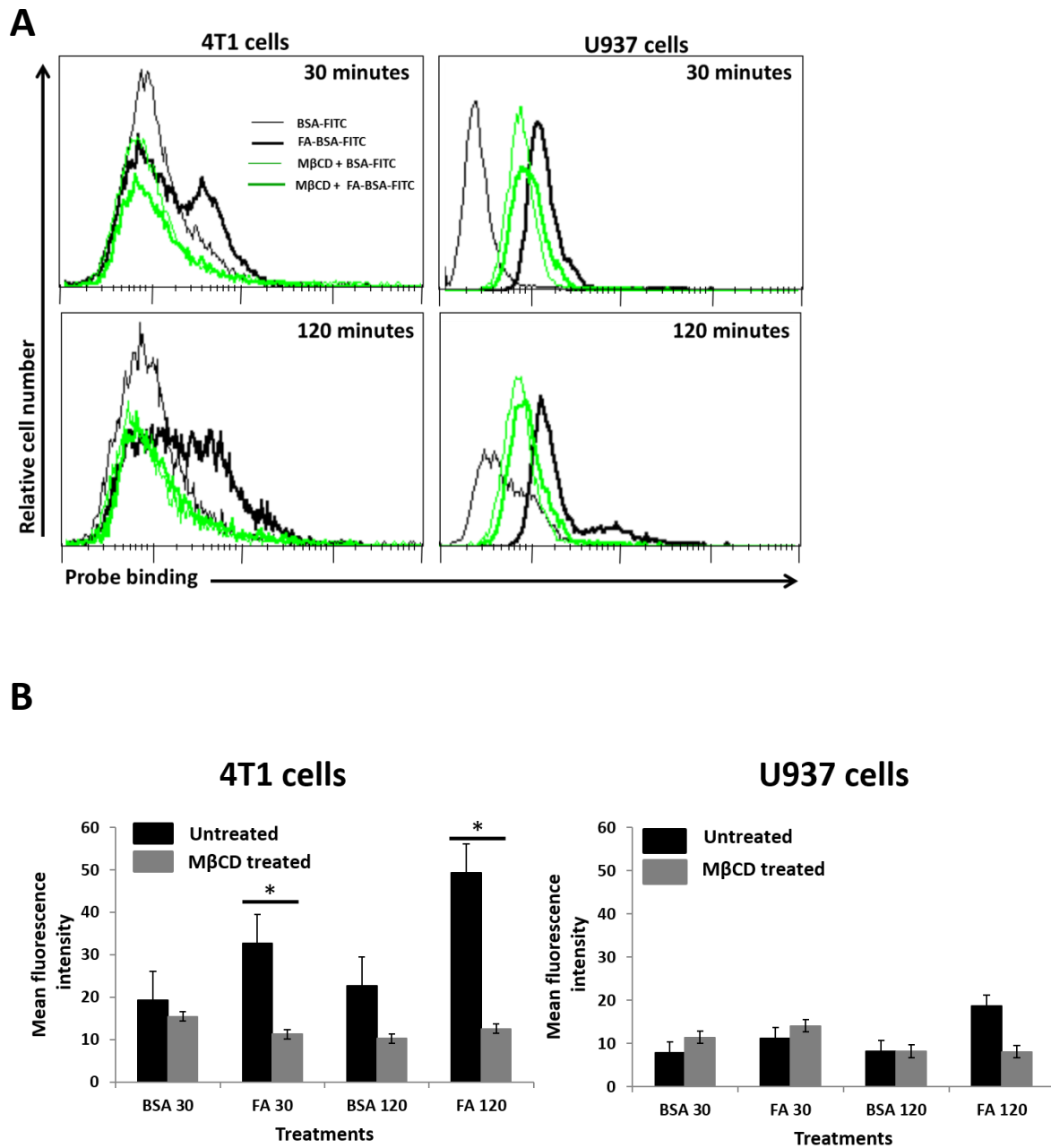
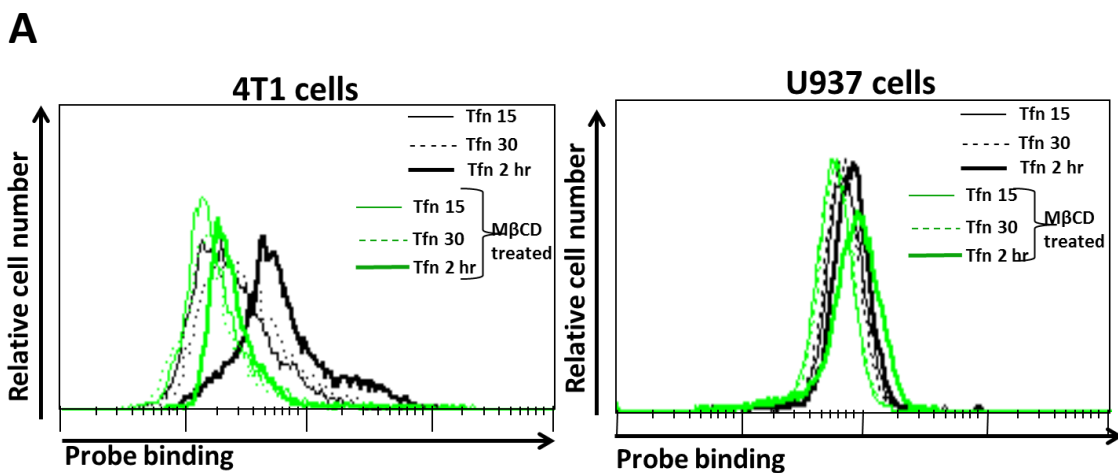


**Figure 25. FR- $\alpha$  activity was inhibited by cholesterol depletion.**

4T1 and U937 cells were incubated with M $\beta$ CD at a concentration of 5mM for 1 h at 37°C. All cells were washed with PBS and incubated with the BSA-FITC or FA-BSA-FITC probe at a concentration of 100  $\mu$ g/ml for 30 or 120 minutes at 37°C. Cells were washed with PBS, fixed in 1.5% formaldehyde and analyzed by flow cytometry. A) Histogram plots are representative of a

minimum of 3 independent experiments and indicate the difference in FR- $\alpha$  binding activity in 4T1 cells (left) and FR- $\beta$  binding activity in the U937 cells (right) after treatment with the probe under intact or cholesterol-depleted conditions. B) The summary data of the flow cytometric experiments of FR- $\alpha$  (left) and FR- $\beta$  (right) receptor activity in 4T1 cells and U937 cells, respectively, is graphed. Data represent the mean  $\pm$  SEM from 3 independent experiments. \*Difference in means between groups were significant,  $p < 0.05$ .



**B**

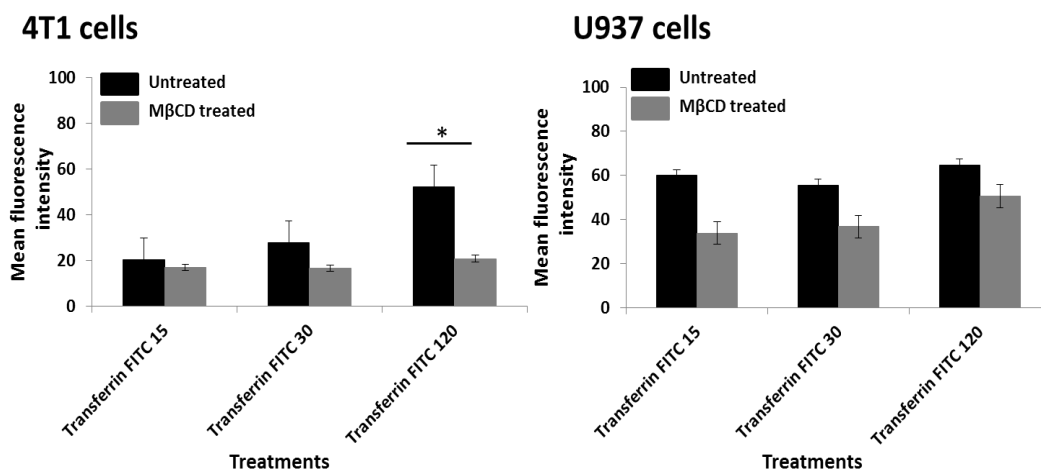


**Figure 26. Transferrin-mediated endocytosis was largely unaffected by cholesterol depletion in both 4T1 and U937 cells.**

4T1 and U937 cells were incubated MβCD at a concentration of 5mM for 1 h at 37°C. Cells were washed with PBS and incubated with transferrin-FITC conjugate at 20 μg/ml for 15, 30 or 120 minutes at 37°C. Cells were washed with PBS, fixed in 1.5% formaldehyde and analyzed by flow cytometry. A) Histogram plots are representative of a minimum of 3 independent experiments and indicate the difference in transferrin binding activity in 4T1 cells (left) and

U937 cells (right) after treatment with the transferrin-FITC conjugate under intact or cholesterol-depleted conditions. B) The summary data of the flow cytometry experiments of transferrin binding in 4T1 (left) and U937 (right) cells is graphed. Data represent the mean  $\pm$  SEM from 3 independent experiments. \*Difference in means between groups were significant,  $p < 0.05$ .

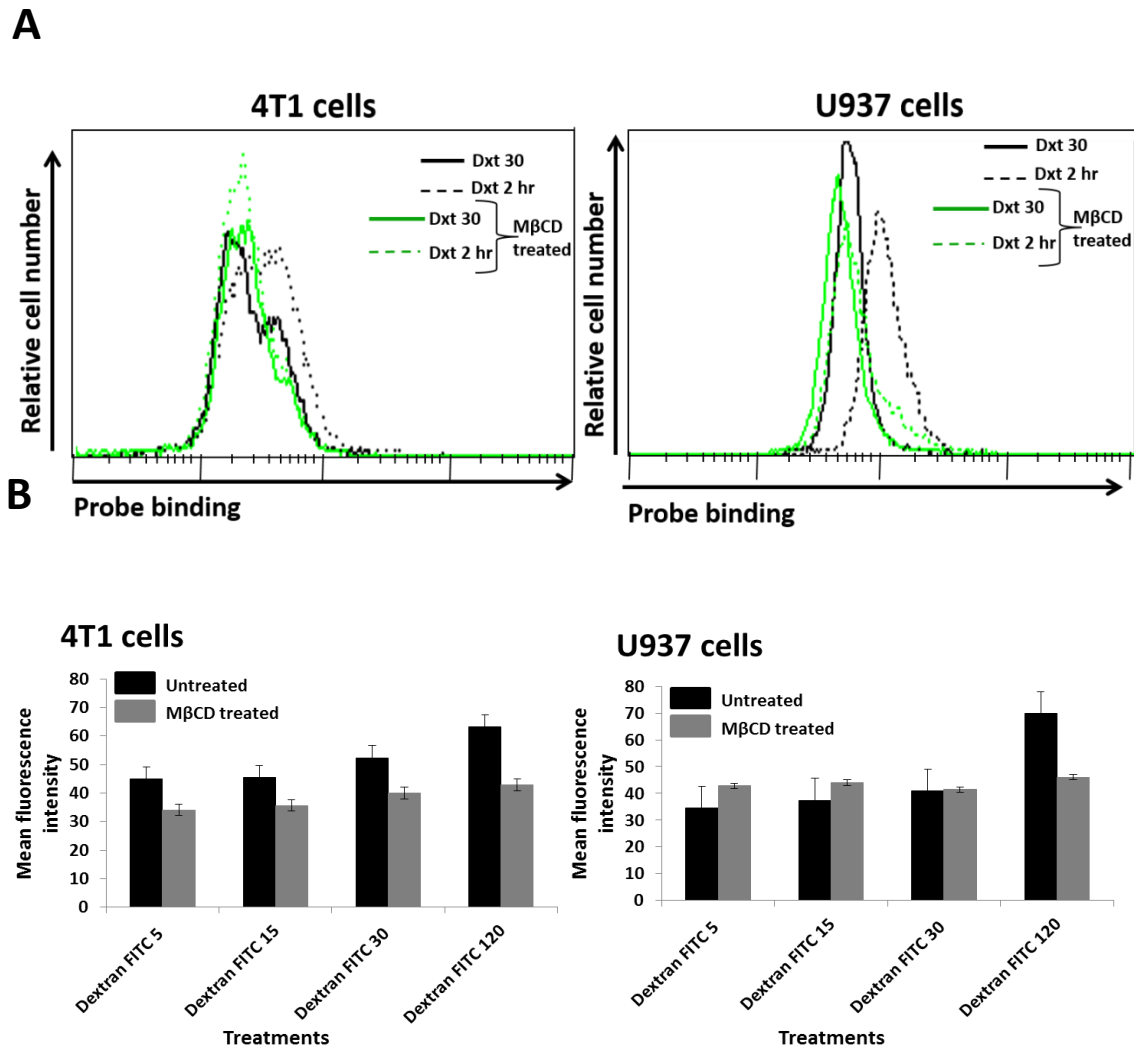


**Figure 27. Pinocytosis in 4T1 and U937 cells was unaffected by cholesterol depletion.**

4T1 and U937 cells were incubated with M $\beta$ CD at a concentration of 5mM for 1 h at 37°C. Cells were washed with PBS and incubated with dextran-FITC conjugate at 50  $\mu$ g/ml for 30 or 120 minutes at 37°C. Cells were washed with PBS, fixed in 1.5% formaldehyde and analyzed by flow cytometry. A) Histogram plots are representative of a minimum of 3 independent experiments and indicate the difference in dextran binding activity or pinocytosis in 4T1 cells (left) and U937 cells (right) after treatment with the dextran-FITC conjugate under intact or cholesterol-depleted conditions. B) Summary data of the flow cytometry experiments of dextran

binding in 4T1 (left) and U937 (right) cells. Data represent the mean  $\pm$  SEM from 3 independent experiments.

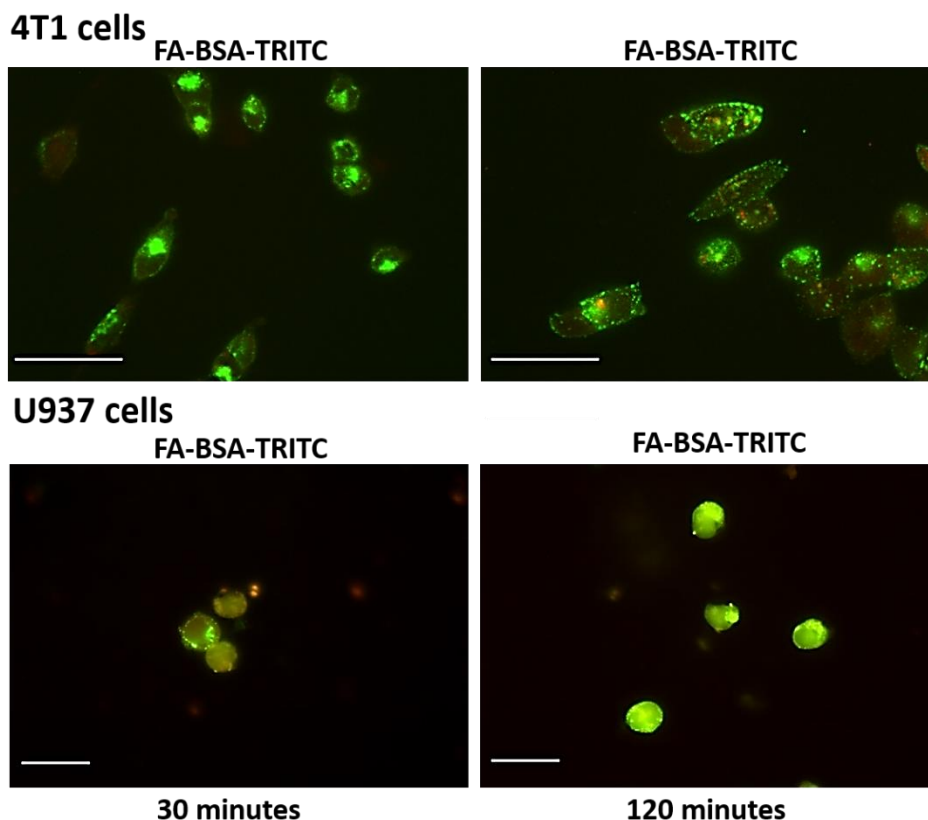


**Figure 28. Cholesterol depletion inhibited FA-BSA-TRITC probe binding and internalization without affecting transferrin receptor activity in 4T1 and U937 cells.**

4T1 and U937 cells were incubated with M $\beta$ CD at a concentration of 5mM for 1 h at 37°C followed by treatment with transferrin-FITC (20  $\mu$ g/ml) and the FA-BSA-TRITC probe at a concentration of 1  $\mu$ g/ml (4T1 cells) and 100  $\mu$ g/ml (U937 cells) for 30 or 120 minutes at 37°C. Cells were washed with PBS, fixed in 1.5% formaldehyde, mounted with ProLong<sup>®</sup> Gold and analyzed with fluorescence microscopy. Digital monochromatic images were acquired at a constant exposure and pseudocolored and overlaid using MetaVue<sup>™</sup> software. Overlays include BSA-TRITC or FA-BSA-TRITC (red) and transferrin-FITC (green). Scale bars for 4T1 and U937 cells are 2.5  $\mu$ m and 0.5  $\mu$ m, respectively. Images are representative of a minimum of 3 independent experiments.



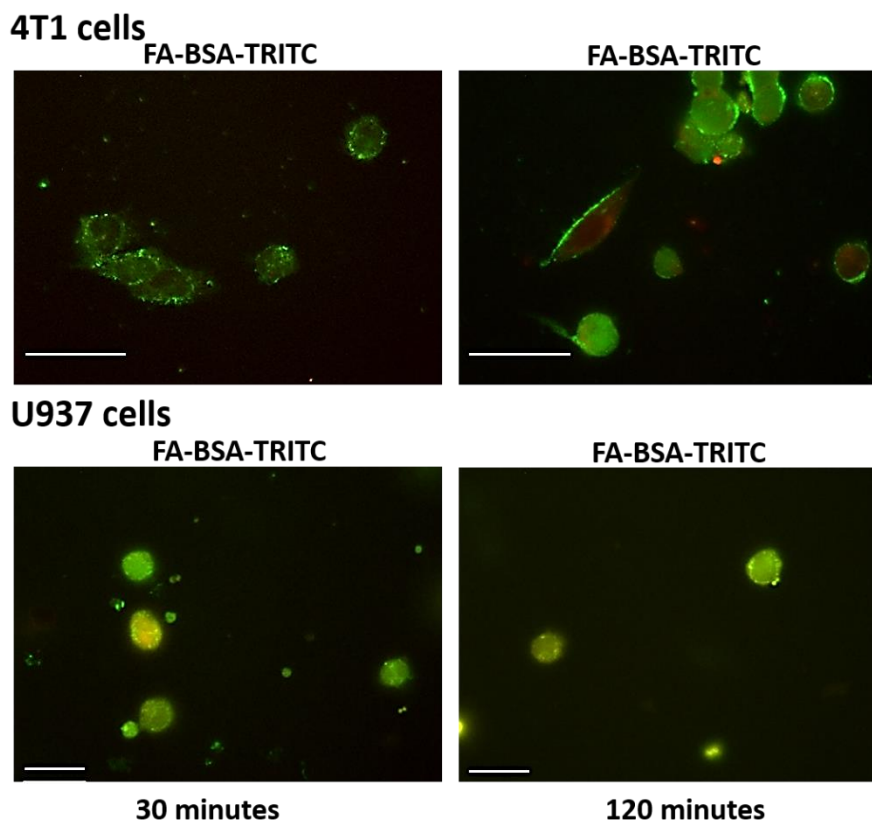


**Figure 29. Cholesterol depletion inhibited FA-BSA-TRITC probe binding and internalization but pinocytosis activity remained unaffected in 4T1 and U937 cells.**

4T1 and U937 cells were incubated with M $\beta$ CD at a concentration of 5mM for 1 h at 37°C followed by treatment with dextran-FITC (50  $\mu$ g/ml) and the FA-BSA-TRITC probe at a concentration of 1  $\mu$ g/ml (4T1 cells) and 100  $\mu$ g/ml (U937 cells) for 30 or 120 minutes at 37°C. Cells were washed with PBS, fixed in 1.5% formaldehyde, mounted with ProLong<sup>®</sup> Gold and analyzed with fluorescence microscopy. Digital monochromatic images were acquired at a constant exposure and pseudocolored and overlaid using MetaVue<sup>™</sup> software. Overlays include BSA-TRITC or FA-BSA-TRITC (red) and dextran-FITC (green). Scale bars for 4T1 and U937 cells are 2.5  $\mu$ m and 0.5  $\mu$ m, respectively. Images are representative of a minimum of 3 independent experiments.

## **CHAPTER 4**

DETERMINING THE POTENTIAL OF A NOVEL HISTONE DEACETYLASE INHIBITOR  
(HDACi) AS AN ANTI-CANCER AGENT

## ABSTRACT

An evolving field of cancer therapy is the use of drugs and small molecules that can mediate anti-tumor effects by altering gene expression in cells. Histone deacetylase (HDAC) inhibitors are one such category of small molecule inhibitors that exhibit abilities to regulate transcription in cancer cells, thus making them potential therapeutic molecules in cancer therapy. Tumor cells have been shown to have elevated HDAC levels, which skews the balance between histone acetyl transferase (HAT) and HDAC activities, thus inducing abnormal gene regulation in the cell. Treatment with HDAC inhibitors block HDAC functions by chelating the zinc ion in the HDAC enzyme, which reverses the repression of key tumor suppressor genes in cancer cells and restores the balance between the histone enzymes, enabling the normal cellular processes to occur. Some HDAC inhibitors such as Vorinostat and Romidepsin are approved by the FDA and are currently in use for the treatment of T cell lymphomas. However, major concerns associated with HDAC inhibitors are their lack of HDAC class specificity and acute toxicity to normal cells. Hence, there is a large demand for identification of novel inhibitors that would show improved selectivity to HDAC classes and be able to mediate anti-tumor activity with minimal damage to normal cells. Recently, Dr. Mahmum Hossain developed a panel of novel HDAC inhibitors based on the scaffolds of FK228 (Romidepsin) and SAHA (Vorinostat), which were designed to increase their solubility in aqueous solution and decrease systemic toxicity while maintaining their anti-tumor activity. As part of a collaboration, one of these novel synthesized compounds, that showed high HDAC class I specificity, compound 5 (Cpd5), was subjected to biologic testing to determine its intracellular inhibitory activity of HDAC *in vitro* and its *in vivo* pharmacokinetics.

*In vitro* studies showed that Cpd5 had strong anti-proliferative activity ( $IC_{50}$ ~300 nM) against a panel of human tumor cell lines. Results were comparable, albeit less effective, to the parent compound, FK228 ( $IC_{50}$ ~1 nM). Cpd5 also exhibited much lower levels of systemic toxicity (MTD > 200 mg/kg body weight) compared to FK228 (MTD = 3.25 mg/kg body weight) when tested in mice. In addition, 4T1 tumor-bearing mice treated with Cpd5 showed significant inhibition in the rate of tumor growth compared to DMSO-treated mice. Quantification of histone acetylation showed that Cpd 5-treated tumor cells exhibited dose-dependent increases in levels of acetylated H3 histones compared to control-treated cells. Liver microsomal assays and mass spectrometry analyses revealed that Cpd5 was metabolically stable and possessed desirable pharmacologic characteristics, including a relatively long half-life in tumor tissue. Therefore, Cpd5 exhibits characteristics supporting its continued development into a new anti-cancer therapeutic agent.

## INTRODUCTION

Acetylation regulates many cellular functions such as protein-protein interactions, DNA recognition and protein stability, and might act as a signaling mechanism that is similar to phosphorylation<sup>303</sup>. Histone acetylation and deacetylation in eukaryotic cells are maintained by histone acetyltransferases (HATs) and histone deacetylases (HDACs). These enzymes are responsible for modifications of chromatin structure and regulation of transcription<sup>303,306</sup>. HATs mediate their activity by adding acetyl groups to histone proteins, which leads to an increased negative charge and thus reduced binding to the DNA backbone, resulting in an open chromatin structure that induces activation of transcription factors. In contrast, HDACs catalyze the removal of the acetyl groups on lysine residues located on the NH<sub>2</sub> terminal tails of core histones, which leads to gene repression by chromatin condensation. As a result, inhibition of HDAC activity can result in a general hyperacetylation of histones, followed by the transcriptional activation of certain genes through relaxation of the DNA conformation. These post-translational modifications are essential for the regulation of many cellular processes<sup>307,327</sup>, and this balance between the HATs and the HDACs maintains homeostasis in the cell<sup>306</sup>.

There are 18 known human histone deacetylases, which are grouped into four classes based on their size, number of catalytic sites, subcellular localization, and sequence identity to yeast counterparts. Class I (HDACs 1-3 and 8), II (HDACs 4-7, 9, and 10), and IV (HDAC 11) enzymes are the 11 Zn<sup>2+</sup>-dependent histone deacetylase enzymes<sup>406</sup>. Class III proteins called sirtuins (SIRT 1-7) are defined by their dependency on the coenzyme and electron transporter NAD<sup>+</sup><sup>327</sup>. The class I HDACs are predominantly located in the nucleus, while the class II HDACs are located in the nucleus and cytoplasm. It has been found that Zn<sup>2+</sup>-dependent isozymes, especially class I and class II HDACs, are closely related to tumorigenesis<sup>309,310,344</sup>.

Therefore, in the past 10 years, over 490 clinical trials of more than 20 HDAC inhibitor candidates have been initiated as single agents or in combination with other chemotherapy drugs, culminating in the approval of two antitumor drugs, Vorinostat (SAHA) and Romidepsin (FK228) for the treatment of cutaneous T-cell lymphoma. Vorinostat is a pan-inhibitor that interacts with all HDAC classes while Romidepsin preferentially inhibits Class I<sup>407,408</sup>. FK228 is a particularly potent inhibitor that mediates its inhibitory activity through a reduced disulfide bond in its structure that directly interacts with the enzyme's active zinc, thus making it inactive.

HDACs are not only regulators of mitosis, cell differentiation, apoptosis, and chromatin organization but are also involved in the regulation of metabolism, learning, memory, and immune response<sup>409</sup>. Modification of epigenetics by selectively inhibiting specific isoforms of histones has emerged as a promising avenue toward disease therapy<sup>291,293,310</sup>. In particular, selective inhibition of HDACs by small molecules often leads to a cascade of chromatin remodeling, tumor suppressor gene reactivation, apoptosis, and regression of cancer<sup>290,382</sup>. HDAC1 and HDAC2 are 95% similar in terms of binding pocket and size of the protein. Therefore, HDAC1 and HDAC2-selective inhibitors are of great interest as potential anticancer agents expected to exhibit few side effects<sup>382,387,410</sup>.

In collaboration with Dr. Mahmud Hossain (Department of Chemistry, University of Wisconsin-Milwaukee), a novel compound was synthesized based on the scaffold of the FDA-approved HDAC inhibitor FK228. The compound, also known as Cpd5, was subjected to both *in vitro* and *in vivo* analysis to assess its potential as an anti-cancer agent. Anti-proliferative activity of Cpd5 was determined by performing MTT [3-(4,5-dimethylthiazol-2-yl)-2,5-Diphenyltetrazolium Bromide] assays against a panel of human prostate, breast, renal and ovarian tumor cell lines. Cpd 5 exhibited potent dose-dependent anti-proliferative activity in the

sub-micromolar range. Specifically, the IC<sub>50</sub> of Cpd5 was ~200-fold higher compared to FK228 but it was ~5-fold lower than SAHA. Analysis of the effects of Cpd5 on the histone acetylation levels in tumor cells revealed that Cpd5 induced a dose-dependent increase in the expression of acetylated H3 histones. Cpd5 was also injected into healthy BALB/c mice at escalating doses to determine the maximum tolerated dose (MTD) by the animals. Mice treated with Cpd5 exhibited a MTD >200 mg/kg body weight while the MTD of FK228 was only 3.25 mg/kg, thus indicating a dramatically lower systemic toxicity to Cpd5 *in vivo*. 4T1 tumor-bearing BALB/c mice were also injected with Cpd5 (25 mg/kg, i.p) to determine effects on tumor growth. Cpd5 was found to significantly inhibit the rate of tumor growth compared to SAHA or DMSO (vehicle)-treated mice. Metabolic studies performed with human and mouse liver microsomes demonstrated that Cpd5 was stable (~2 hours) in the samples. Pharmacokinetic studies were performed on healthy mice by injecting them with Cpd5 (10 mg/kg, i.p) followed by harvesting of blood, brain and tumors at various time points to determine drug availability in the samples over time. Mass spectrometric analysis indicated that Cpd5 was available in the system for as long as 2 hours, demonstrating a low clearance rate, desirable for a potential drug.

These preliminary data provide important evidence regarding the potential of Cpd5 as a novel anti-cancer agent. These results are promising because the compound exhibited strong inhibitory properties against several tumor cell lines but had minimal side effects *in vivo*. Based on these findings, histone acetylation levels induced in the cells correlated with the biologic activity of Cpd5 (i.e., modulation of histone activity) and not from random side effects. In addition, the low clearance rate and long half-life makes it even more attractive as a potential drug or therapeutic agent. Collectively, these studies help to identify the *in vitro* and *in vivo* activity profile of Cpd5, and thus highlight its potential use as a cancer therapeutic.

## MATERIALS AND METHODS

### Cell lines and reagents

A panel of human cell lines that included a prostate cancer line (DU145), cervical cancer line (HeLa), renal cancer line (RXF 393) and colon cancer line (HCT-116) were all purchased from ATCC (Manassas, VA). A 4T1 murine mammary carcinoma epithelial cell line was also purchased from ATCC. All human cell lines were cultured in DMEM medium (Life Technologies, Grand Island, NY), supplemented with 10% fetal bovine serum (Atlanta Biologicals, Flowery Branch, GA), 100 U/ml penicillin, 100 µg/ml streptomycin and 2 mM L-glutamine (all from ThermoFisher Scientific). Cell counts and viability were determined using a hemacytometer following appropriate dilution in trypan blue exclusion dye. The 4T1 cells were grown in RPMI 1640 media that was supplemented as above along with addition of 55 µM 2-mercaptoethanol (Life Technologies, Grand Island, NY) and maintained as described in Chapter 2, “Materials & Methods”.

Cpd5 was synthesized and purified by high-performance liquid chromatography (HPLC) in Dr. Hossain’s Lab (Department of Chemistry, University of Wisconsin-Milwaukee), as described<sup>411</sup>. The FDA-approved drugs, vorinostat (SAHA) and romidepsin (FK228), were purchased commercially (Selleckchem, Houston, TX) and used as positive controls for comparison purposes. Dimethylsulfoxide (DMSO, ThermoFisher) was used to dissolve the drugs and served as vehicle controls for all experiments.

[3-(4,5-dimethylthiazol-2-yl)-2,5-diphenyltetrazolium bromide] or MTT (Sigma Aldrich) was used as a colorimetric reagent to determine cell proliferation. Live cells actively convert MTT



into a purple insoluble formazan product, while dead cells do not, and this change can be measured spectrophotometrically after being dissolved in DMSO.

## **Animals**

Wild type BALB/c mice and C57BL/6J (B6) mice were originally purchased from the Jackson Laboratories (Bar Harbor, ME) housed and bred in a specific pathogen-free facility at the University of Wisconsin-Milwaukee, and screened regularly for pathogens. All procedures were approved by the Animal Care and Use Committee of the University of Wisconsin-Milwaukee. For tumor induction,  $1 \times 10^4$  4T1 cells in 50  $\mu$ l supplement-free RPMI 1640 medium were injected subcutaneously into the mammary fat pad of 8-12-week-old wild-type BALB/c female mice.

## **Determining anti-proliferative activity of Cpd5 by MTT**

The anti-proliferative effect of Cpd5 was tested on the DU145, HeLa, HCT-116 and RXF-393 cells using the MTT colorimetric assay. Briefly, 200  $\mu$ l of cell suspension ( $7 \times 10^4$  cells/ml) was dispensed into 96-well, flat-bottomed microplates (Nunc, Denmark) and incubated for 24 hours at 37°C and 5% CO<sub>2</sub>. After 24 hours, Cpd5 was added at various concentrations (1  $\mu$ M, 100 nM, 10 nM and 1 nM) and incubated for another 48 hours. Cells were then washed twice with PBS followed by incubation with 200  $\mu$ l of MTT solution (250  $\mu$ g/mL) for 4 hours. The formazan crystals were solubilized by the addition of 200  $\mu$ l of DMSO and by rotating the plate on a shaker for 10 minutes. Absorbance was determined at 570 nm with a reference wavelength of 690 nm using a microtiter plate reader (Infinite M200 Pro TECAN). All treatments were done in triplicate and control cells received fresh medium or 0.01% DMSO concentration equivalent to that in the treatment groups. The anti-proliferative effect of Cpd5 was expressed as the relative viability (% control). Relative viability = (experimental absorbance - background absorbance) /

(absorbance of DMSO-treated controls-background absorbance)  $\times$  100. Results were used to calculate the inhibitory concentration of the compound that led to 50% of control values (IC<sub>50</sub>).

### **Histone acetylation**

DU145 cells were seeded at a density of  $7 \times 10^4$  cells/ml into 24-well flat-bottomed multiwell plates and incubated for 24 hours at 37°C and 5% CO<sub>2</sub>. Cpd5 or FK228 was added at varying concentrations (1  $\mu$ M, 100 nM and 10 nM) to the wells and incubated for 24 hours. DMSO (0.01% ) was also included as a vehicle control while wells with untreated cells were included as negative controls. After 24 hours, cells were treated with 4% paraformaldehyde for 10 minutes followed by treatment with Tris-buffered saline, 0.1% Tween 20 (TBS-T), and 1% BSA for 1 hour at 4°C. Cells were next treated with a rabbit polyclonal anti-acetyl histone H3 (Lys K9/K14) antibody (Cell Signaling Technology) at a 1:2000 dilution and incubated overnight at 4°C. The primary antibody was washed off with TBS-T and 1% BSA solution followed by incubation with an Alexa Fluor<sup>®</sup> 488-conjugated goat anti-rabbit IgG antibody (Jackson ImmunoResearch, West Grove, PA) at a 1:500 dilution in TBS-T and 1% BSA for 1 hour at 4°C. The cell membranes were stained with Cell tracker<sup>™</sup> Red CMTPX (Molecular Probes) at a final concentration of 1  $\mu$ M for 30 minutes followed by the addition of Hoechst 33342 Nuclear Stain (Enzo Life Sciences) for 15 minutes. Cells were washed again, mounted with Prolong<sup>®</sup> Gold, and visualized using a Nikon inverted epifluorescence microscope. Images were acquired at a constant exposure setting, pseudocolored and overlaid using Metavue<sup>®</sup> software (Universal Imaging Corporation, Downingtown, PA).

### **Determining a maximum tolerated dose (MTD)**

To determine the MTD *in vivo*, each animal was initially weighed using a digital scale and injected with Cpd5, SAHA, FK228 or DMSO intraperitoneally (i.p), and mortality was monitored over two weeks. One mouse was given a single i.p injection of 200 mg/kg body weight, a second mouse received a dose of 100 mg/kg and a third mouse received a single dose of 50 mg/kg. The mice were observed and weighed every other day for a period of 2 weeks. They were euthanized if they lost more than 20% of their body weight or if there were other signs of overt toxicity. If none of the mice survived with the first three doses, the next three dose levels (25 mg/kg, 12.5 mg/kg and 6.25 mg/kg) were tested in a similar manner. This process was repeated until a tolerated dose was found, and the MTD value was determined. Each treatment was performed with three animals/group receiving the same dose of drug or vehicle (DMSO).

### **Tumor growth inhibition studies**

To determine the effects of Cpd5 on tumor growth, BALB/c mice were first injected with 4T1 cells ( $1 \times 10^4$  cells in 50  $\mu$ l) in supplement-free RPMI medium subcutaneously into the mammary fat pad. After 7 days, the animals were injected i.p. with 25 mg/kg body weight of Cpd5, SAHA or DMSO (vehicle) every other day. Injections were continued for 30 days and tumor growth was monitored by caliper measurements of the major (L, length; mm) and minor (W, width; mm) axes and tumor volume (V, volume;  $\text{mm}^3$ ) was calculated by the formula:  $V = (L \times W^2) / 2$ .

### **Human and murine liver microsomal assay**

To determine the metabolic stability of Cpd5, microsomal assays were performed in collaboration with Dr. Arnold, Department of Chemistry, University of Wisconsin-Milwaukee. Microsomes (0.5 mg/ml) were pre-incubated with a 2  $\mu$ M test compound for 5 minutes at 37°C

in 0.1 M phosphate buffer, pH 7.4. Specifically, Cpd5 was dissolved in DMSO to achieve a concentration of 1 mM. Verapamil at a concentration of 5  $\mu$ M in acetonitrile was used as an internal standard for the assay. The microsomal assay mixture (MAM) was prepared by combining 0.5 M potassium phosphate buffer (pH 7.4) with the co-factors NADPH A and NADPH B (Corning Incorporated, Corning, NY), and with Cpd5. The MAM was sonicated for 5 minutes on ice followed by incubation with human or murine liver microsomes at a concentration of 20 mg/ml (BD Gentest, San Jose, CA) for 10, 20, 30, 40, 50 and 60 minutes at 37°C. Samples incubated with only the MAM and no microsomes served as the control. The reactions were stopped by adding an equal volume of acetonitrile containing 5  $\mu$ M verapamil (internal standard). Samples were centrifuged at 5,000 x g for 5 minutes and 100  $\mu$ l of supernatant was transferred to Spin-X<sup>®</sup> HPLC filter tubes (Corning Incorporated). Samples were again centrifuged at 6,500 x g for 5 minutes and 5  $\mu$ L of the supernatant was then diluted in 500  $\mu$ l of LCMS grade methanol (ThermoFisher Scientific, Waltham, MA) and analyzed using a LCMS-8040 Triple Quadrupole Liquid Chromatograph Mass Spectrometer (LC-MS/MS, Shimadzu) to determine the intrinsic clearance of Cpd5 *in vitro*. The peak area ratio was calculated using the formula: peak area ratio = peak area of test compound (Cpd5) / peak area ratio of internal standard (verapamil). The percentage of compound remaining after time (T) was calculated using the formula: (peak area ratio at particular time T / peak area ratio at zero time point) x 100. All metabolic parameters are represented as mean  $\pm$  SD obtained through three assays that were run simultaneously in two independent experiments.

### **Pharmacokinetic Assay**

In order to determine the *in vivo* biodistribution of Cpd5, blood, brains and tumors were harvested from healthy B6 mice following a single i.p. injection of the Cpd5 (10 mg/kg) in

DMSO. Blood (200  $\mu$ l) was collected from animals at 5, 15, 30, 60, 90 and 120 minutes following injection. The blood was collected in 1.5 ml heparinized tubes and kept at  $-20^{\circ}\text{C}$  until analysis. Animals were euthanized at the 60- and 120-minute time-points and the brains were harvested from two of the mice. In addition, 4T1 tumor-bearing BALB/c mice at an advanced (4-weeks) stage were also injected with Cpd5 as described above. Animals were euthanized at 30 and 120 minutes and tumors were harvested. The brains and the tumors were transferred to 1.5 ml tubes followed by addition of 300  $\mu$ l acetonitrile and then homogenized using a mechanical homogenizer. The tissues were then centrifuged at 6,500 x g for 3 minutes. The supernatant was transferred to Spin-X<sup>®</sup> Centrifuge filter tubes and centrifuged at 6,500 x g for 5 minutes. Blood (200  $\mu$ l) was collected in 1.5 ml heparinized tubes and mixed with 200  $\mu$ l methanol and 100  $\mu$ l acetonitrile. Samples were centrifuged at 6,500 x g for 6 minutes. The supernatants from all samples were collected and analyzed on a LCMS-8040 Triple Quadrupole Liquid Chromatograph Mass Spectrometer (LC-MS/MS). Each time point represented three animals.

### **Statistical Analyses**

Data are presented as mean  $\pm$  SEM unless stated otherwise. Significant differences between sample means were determined using a Student's *t* test with  $p < 0.05$  being considered significant. Data between various treatment groups were analyzed using one-way ANOVA and then compared by Bonferroni multiple comparison tests using GraphPad Prism software, Version 3.00 (San Diego, CA, USA). Microsomal stability of Cpd5 was calculated by linear regression plots using GraphPad Prism software. Pharmacokinetic studies depicting availability of Cpd5 was determined by linear regression plots using Microsoft Excel. The in vivo tumor growth data was first analyzed by 2-way ANOVA and when significance was detected, the data were analyzed by

one-way ANOVA and compared by Bonferroni multiple comparison tests using GraphPad Prism software

## RESULTS

### **Cpd5 showed strong anti-proliferative activities against human tumor cell lines**

The *in vitro* anti-proliferative activity of Cpd5 was evaluated at different concentrations against a panel of human tumor cell lines that included a prostate tumor (DU-145), cervical tumor (HeLa), renal tumor (RXF 393) and colon tumor (HCT-116). SAHA and FK228 were used as positive controls to compare to the anti-proliferative activities of the novel Cpd5, while DMSO was used as the vehicle control. After 48 hours of drug treatment, cell proliferation was measured using an MTT assay and the percent cell survival was determined relative to that of the vehicle control. In comparison to the vehicle, Cpd5 induced a significant ( $p < 0.05$ ) inhibition in cell proliferation of all cell lines tested at 10 and 1  $\mu\text{M}$  (Fig. 30). Treatment of cell lines with SAHA resulted in nearly identical results. By contrast, FK228 exhibited detectable anti-proliferative activity even at 0.01  $\mu\text{M}$  and thus demonstrated the most potent anti-tumor effects of the HDACis. From the above data,  $\text{IC}_{50}$  values were calculated (Table I). The average  $\text{IC}_{50}$  value for Cpd5 was 0.475  $\mu\text{M}$  across all cell lines, which was  $\sim 190$ -fold higher than that of FK228 ( $\text{IC}_{50} = 0.0025 \mu\text{M}$ ). However, Cpd5 was  $\sim 5$ -fold more potent than SAHA ( $\text{IC}_{50} = 2.5 \mu\text{M}$ ). Thus, overall Cpd5 exhibited very potent *in vitro* anti-proliferative properties against a range of tumors.

### **Cpd5 treatment led to an increase in histone acetylation levels in DU-145 cells**

The above results showed that Cpd5 retained strong anti-proliferative activity *in vitro*. However, since HDAC inhibitors can affect a number of non-histone targets<sup>356</sup>, it was possible that the anti-proliferative effects were not due to changes in histone acetylation. Therefore, it was important to determine whether Cpd5 was able to induce changes in the acetylation levels of

histones in the treated cells. To examine this, the DU-145 cells were treated with Cpd5 and the acetylation levels of H3 histone proteins were determined by epifluorescence microscopy. Control-treated cells showed a low basal level of H3 acetylation that was detectable in a small percentage of the population (Fig. 31A). In contrast, Cpd5-treated cells exhibited intense staining of acetylated H3 that increased with increasing concentration (Fig. 31B). As expected, FK228 treatment resulted in very high levels of histone acetylation in virtually all cells (Fig. 31C). With increasing concentrations of FK228, the staining approached saturation and thus looked similar at both the 100 nM and the 1  $\mu$ M concentrations. Therefore, the acetylation levels of H3 in Cpd5-treated cells was comparatively lower than that for the FK228-treated cells, which was consistent with the anti-proliferative activity of the two compounds *in vitro*.

### **Cpd5 was metabolically stable**

The liver contains several drug-metabolizing enzymes and thus liver microsomes are useful in *in vitro* models for determining hepatic clearance. An indication of the potential *in vivo* activity of a compound or drug can be estimated by determining its rate of metabolism in the body. Hence, the microsomal assay analysis was chosen to determine the intrinsic clearance of Cpd5. Both human and murine microsomes were used for determining the metabolism of Cpd5. The percent peak area ratio when plotted over time generated a linear slope that remained mostly constant over time, thus indicating that Cpd5 remained in its original state after 60 minutes (Fig. 32). The graphs represent linear regression plots obtained from two independent experiments labeled as Experiment 1 (left) and Experiment 2 (right) following incubation with A) human or B) murine microsomes.

All metabolic parameters associated with Cpd5 were determined through these linear regression plots and are summarized in Table II. The half-life of Cpd5 was found to be  $391 \pm$



114 minutes when assayed with human microsomes in the first experiment and this was consistent in the second experiment ( $471 \pm 162$  minutes). In murine microsomes, Cpd5 exhibited a half-life of  $1,514 \pm 2,057$  min and  $666 \pm 500$  min in experiments 1 and 2, respectively. The intrinsic clearance obtained from the two experiments from the human microsomal assay was 0.147 and 0.177  $\mu\text{l}/\text{min}/\text{mg}$ , respectively. On the other hand, the murine microsomal assay yielded a clearance of 0.04577  $\mu\text{l}/\text{min}/\text{mg}$  and 0.103  $\mu\text{l}/\text{min}/\text{mg}$  in experiments 1 and 2, respectively. Both sets of data from the human and murine microsomal assays seemed to fit well into the “low clearance” category of drug standardization, thus indicating that Cpd5 was not readily eliminated by liver enzymes. The percentage of compound remaining after 60 minutes of treatment with human microsomes was  $88 \pm 0.36\%$  and  $90.3 \pm 0.36\%$  from experiments 1 and 2, respectively. The murine microsomes also showed similar values of  $94.1 \pm 0.47\%$  and  $89 \pm 0.51\%$ . Overall, it was evident that about 88-95% of Cpd5 was still found to be available in the samples after 60 minutes, thus indicating the stable nature of the compound.

### **Cpd5 was detectable *in vivo* for at least 2 hours**

To determine the pharmacokinetic parameters of Cpd5, mice were injected i.p. with 10 mg/kg Cpd5 and blood was sampled over a 2-hour time-period. Results demonstrated that Cpd5 remained detectable in the blood for at least 2 hours after the injection (Fig. 33). In addition, Cpd5 was also found in the brain and tumor after 2 hours (data not shown). These *in vivo* data, together with the previous *in vitro* microsomal assay data, showed that Cpd5 was metabolically stable and available *in vivo* for an extended period of time.

### **Cpd5 exhibited a high maximum tolerated dose (MTD) in mice**

The MTD for the HDAC inhibitors was determined by injecting wild type BALB/c mice with increasing doses of Cpd5, SAHA, and FK228, and monitoring morbidity and mortality over a two-week period (Table III). Results indicated that the mice remained healthy even at a dose of 200 mg Cpd5/kg body weight. SAHA also showed a MTD of >200 mg/kg while FK228 showed a MTD of only 3.25 mg/kg, which was at least 50 times lower than that for Cpd5. These results demonstrate that Cpd5 had much lower levels of systemic toxicity than the FDA-approved FK228 parent compound.

### **Cpd5 inhibited tumor growth in animals**

To determine effects of Cpd5 on tumor growth in mice, 4T1 cells were injected into BALB/c mice and tumors were allowed to grow for 7 days. The mice were randomized into three groups and received i.p. injections of Cpd5 (25 mg/kg), SAHA (25 mg/kg) or an equivalent volume of DMSO every other day for 30 days. Preliminary results showed that mice treated with Cpd5 exerted significant (by ~40-45%,  $p < 0.05$ ) inhibition in the rate of tumor growth from day 24 to 30 compared to the SAHA- and DMSO-treated animals (Fig. 34). This reduction in tumor growth was detectable after ~2 weeks of treatment and was maintained until the end of the experiment. Therefore, Cpd5 was able to slow the rate of tumor growth in mice.

## DISCUSSION

Chromatin modulation via modification of histone enzymes is crucial in regulating major cellular process such as gene transcription and DNA repair<sup>299</sup>. However, recent studies have implicated epigenetic aberrations in the initiation and progression of human cancer<sup>291,309,333</sup>. Epigenetics is responsible for mediating gene regulation via post-translational modifications of several protein complexes associated with the DNA. One such modification is the acetylation and deacetylation of histones, regulated by HATs and HDACs that work in coordination to maintain a proper balance in the cell. However, during cancer this balance is altered and this results in overexpression of deacetylated histones<sup>296</sup>. HDAC inhibitors are small molecules that can inhibit deacetylase activity, thus restoring the balance of histone acetylation in the cells and mediating several effects such as cellular differentiation, expression of tumor suppressor genes, apoptosis and anti-angiogenic activity<sup>352,369</sup>. Hence, there has been an expanding interest in developing these molecules as potential anti-cancer agents.

In order to qualify as a potential anti-cancer agent it is necessary that the naturally occurring or synthesized compound exhibit strong anti-proliferative activities but with minimal non-tumor toxicity. In addition, based on reports that suggest HDAC inhibitor-mediated effects varied with the type of tumor cell line<sup>290</sup>, it was first important to determine the *in vitro* effects of Cpd5 against a panel of major human tumor cell lines (Fig. 30). For this purpose, we chose several types of tumor lines (prostate, renal, cervical and colon cancer) and compared the activity of Cpd5 to that of SAHA and FK228, the two drugs currently approved by the FDA. Cpd5 showed consistent growth inhibitory concentrations (IC<sub>50</sub>) against all tested tumor lines with a stronger anti-proliferative activity than SAHA (Table I). Although Cpd5 demonstrated ~190-fold lower anti-proliferative activity than that of the parent compound FK228, its IC<sub>50</sub> concentrations were

still in the nM range. Therefore, overall Cpd5 was found to be more potent than SAHA but less potent than FK228.

A HDAC inhibitor is anticipated to mediate anti-cancer effects *in vitro* and *in vivo* via modifying the histone acetylation levels. Specifically, the inhibitor is responsible for blocking the functions of the overexpressed HDACs in tumor cells to restore the balance between the HATs and HDACs<sup>306</sup>. Therefore, experiments were performed to determine if Cpd5-mediated, anti-proliferative effects in tumor cells correlated with the acetylation levels of histones. The results clearly showed that Cpd5-treated DU-145 cells showed increased acetylated levels of H3 histone compared to control cells (Fig. 31). In addition, the intensity of histone acetylation in the cells increased with increases in Cpd5 concentrations. Thus, the *in vitro* and *in vivo* effects induced by Cpd5 can most likely be attributed to changes in the histone acetylation levels.

For a compound to qualify as a potential therapeutic agent, it must demonstrate favorable pharmacokinetic characteristics that include low metabolism, long half-life and appropriate biodistribution. Our results demonstrate that Cpd5 was metabolically stable for at least two hours in microsomal preparations, with 80-90% of the compound remaining in the samples (Fig. 32, Table II). Cpd5 had a low intrinsic clearance rate and thus fit into the “low clearance” category of drug standardization. In addition, Cpd5 was also found to be available in the blood, tumor and brain even after 2 hours (Fig. 33, and data not shown), which further supports its low clearance rate and stable nature. Overall, Cpd5, due to its potent anti-proliferative effects, stable nature and low clearance demonstrates a good potential to qualify as an anti-cancer drug.

Before analyzing the anti-tumor activity of the drug *in vivo*, it was first necessary to determine if Cpd5 led to any overt toxicity in the animals. FK228 turned out to be very toxic for the animals and exhibited a MTD of only 3.25 mg/kg body weight. In contrast, both SAHA and Cpd5 had MTDs of > 200 mg/kg (Table III). Thus, it was evident that Cpd5 exhibited much lower levels of systemic toxicity than the parent compound FK228. This high level of systemic toxicity of FK228 correlates with its potent anti-proliferative activity *in vitro* but severely limits the dose that can be safely given to patients. Importantly, while both SAHA and Cpd5 were equally tolerated *in vivo*, Cpd5 was significantly more potent than SAHA in inhibiting cellular proliferation. Consistent with this finding, Cpd5 treatment in 4T1 tumor-bearing mice resulted in a significant reduction in the tumor growth rate compared to SAHA-treated animals (Fig. 34). Unfortunately, no regression of the tumor was observed with this Cpd5 treatment, and thus other doses or treatment regimens need to be tested. As with the majority of cancer treatments, it is unlikely that a single treatment with any HDAC inhibitor will be successful but rather these agents will be used as adjuncts to other established treatments. Taken together, these data identify the potential of Cpd5 as a promising and novel HDAC inhibitor for the treatment of cancer.

## FIGURES AND LEGENDS

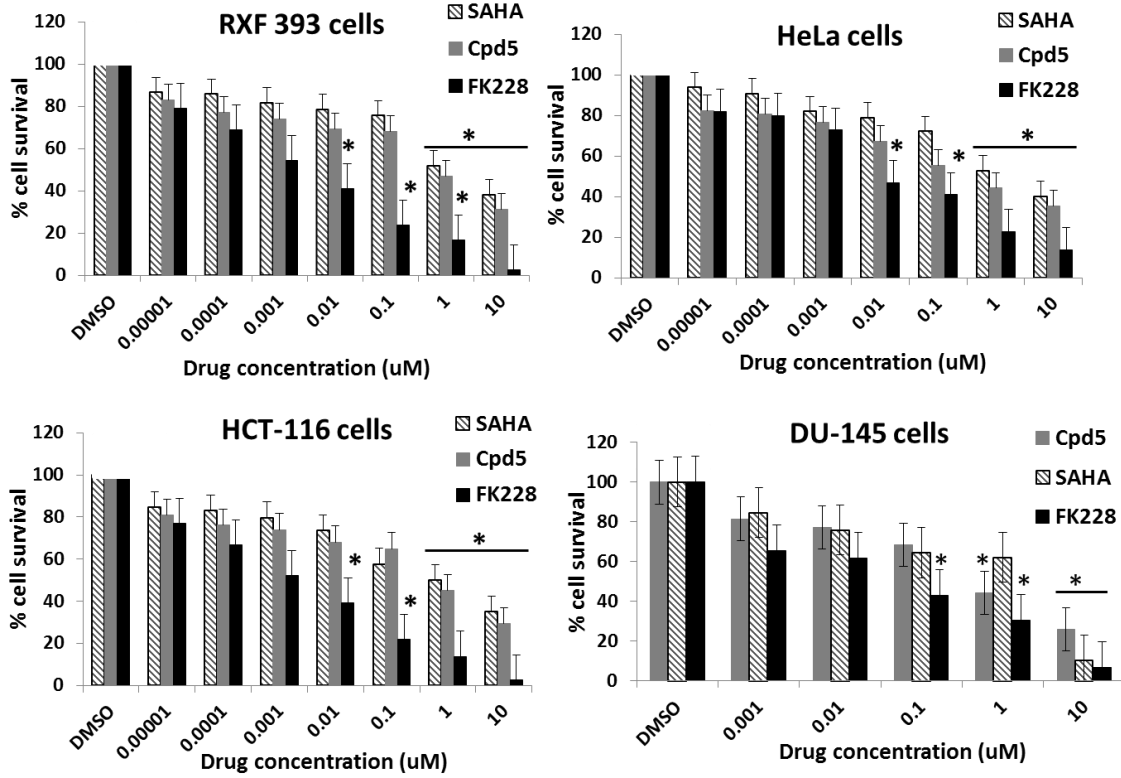


**Figure 30. *In vitro* anti-proliferative effects of Cpd5, SAHA and FK228 against a panel of human tumor cell lines.**

Four different human tumor cell lines (RXF 393, HeLa, HCT-116 and DU-145) were treated with Cpd5, FK228 or SAHA at varying concentrations for 48 hours. Cell proliferation was analyzed using an MTT assay. DMSO-treated wells served as vehicle controls and were used to calculate percent survival of the cells post drug treatment. Treatments were done in triplicate and presented as the mean  $\pm$  SEM. Statistical significance was determined using two-way ANOVA.

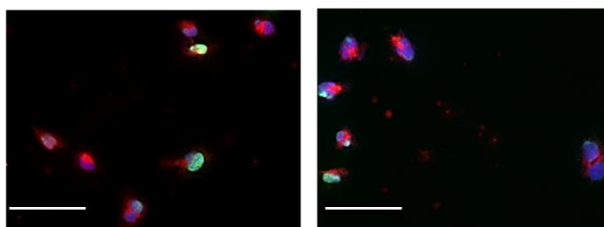
\*Differences between drug-treated and DMSO-treated cells were significant,  $p < 0.05$ .

<b>Compound (IC<sub>50</sub> in μM)</b>	<b>Cervical HeLa</b>	<b>Renal RXF 393</b>	<b>Prostate DU-145</b>	<b>Colon HCT-116</b>
<b>FK228</b>	0.00125	0.00122	0.0063	0.0012
<b>SAHA</b>	2.8	2.5	2	2.7
<b>Cpd5</b>	0.4	0.5	0.6	0.4

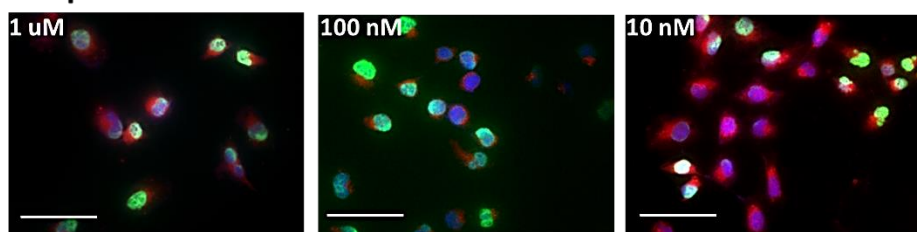
**Table I. Growth inhibitory concentration (IC<sub>50</sub>) of Cpd5, SAHA and FK228 against human tumor cell lines.**

Cells from human tumor cell lines (HeLa, RXF 393, DU-145 and HCT-116) were treated with Cpd5, FK228 or SAHA for 48 hours and proliferation was determined using an MTT assay as shown in Fig. 30. Values represent IC<sub>50</sub> of the test compounds that were calculated from the average of triplicate wells using GraphPad Prism software.

### A. DMSO (Control)



### B. Cpd5



### C. FK228

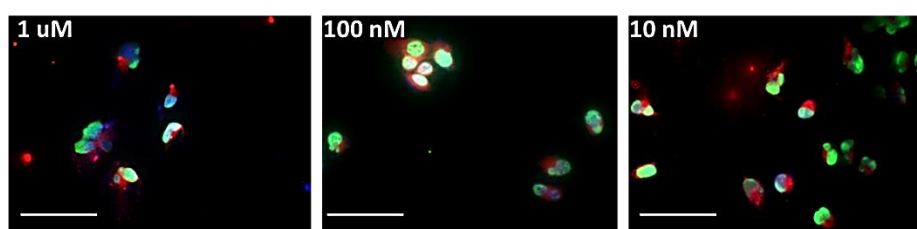


**Figure 31. Immunofluorescence staining of acetylated histones in DU-145 cells.**

DU-145 cells were grown overnight on coverslips and then incubated with DMSO (control) or the indicated concentrations of Cpd5 or FK228 for 24 hours at 37°C. Cells were then fixed with 4% paraformaldehyde, permeabilized and labeled with a purified rabbit polyclonal anti-acetyl histone H3 (Lys K9/K14) antibody which was detected using an Alexa Fluor<sup>®</sup> 488-conjugated goat-anti rabbit IgG antibody (Green). The cell membranes were stained with Cell Tracker<sup>™</sup> Red CMTPX (Red) followed by the addition of Hoechst 33342 Nuclear Stain (Blue). Cells were mounted with Prolong<sup>®</sup> Gold and visualized with an epifluorescence microscope. Images were acquired at a constant exposure setting, and pseudocolored and overlaid using MetaVue<sup>™</sup> software. Representative images are of cells showing the varying intensities of histone



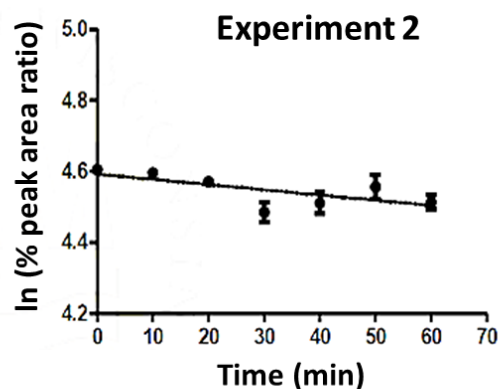
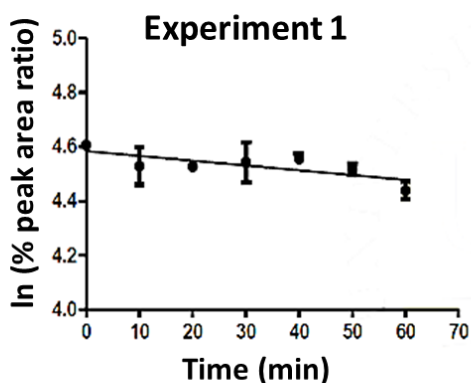
acetylation after treatment with A) DMSO (control), B) Cpd5 and C) FK228. Data are representative of a minimum of 3 independent experiments. Scale bars = 2.5  $\mu$ m.

<b>Metabolic parameters</b>	<b>Human microsomes</b>		<b>Murine microsomes</b>	
	<b>Experiment 1</b>	<b>Experiment 2</b>	<b>Experiment 1</b>	<b>Experiment 2</b>
<b>Half-life (min)</b>	391 $\pm$ 114	471 $\pm$ 162	1514 $\pm$ 2057	666 $\pm$ 500
<b>Intrinsic clearance (<math>\mu</math>l/min/mg)</b>	0.177	0.147	0.04577	0.103
<b>remaining at 60 min (%)</b>	88 $\pm$ 0.36	90.3 $\pm$ 0.36	94.1 $\pm$ 0.47	89 $\pm$ 0.51

**Table II. Metabolic activity of Cpd5 determined by human and murine microsomal assays.**

Human and murine liver microsomes were used to determine parameters associated with Cpd5 metabolism in the liver. Data were obtained from two independent experiments. Linear regression plots were constructed using GraphPad Prism and were used to calculate metabolic parameters (half-life, intrinsic clearance and percent availability) of Cpd5 over time. The data represents the mean  $\pm$  SD from three assays that were run simultaneously for both experiment 1 and experiment 2.

## A. Human



## B. Murine

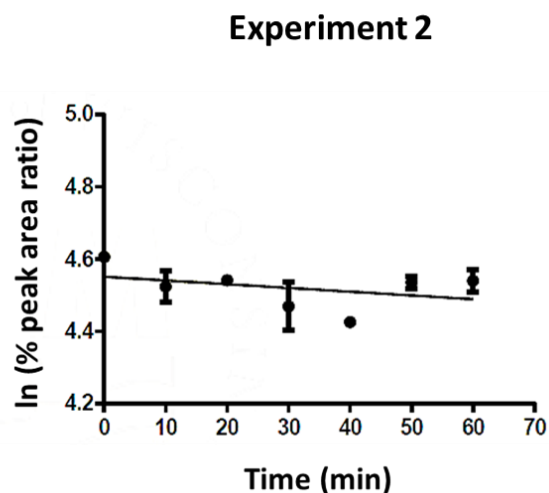
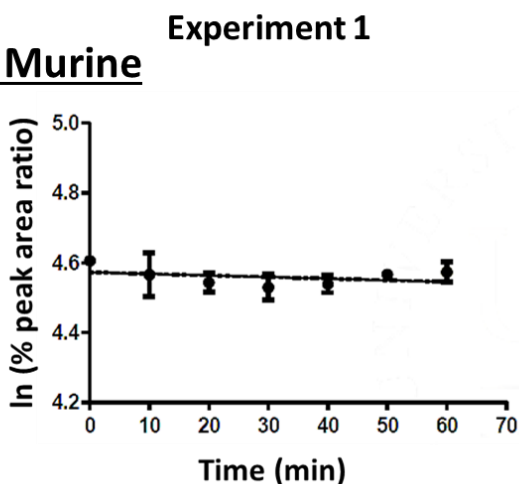


**Figure 32. Human and murine microsomal analysis depicting Cpd5 stability over time.**

The microsomal assay mixture (MAM) was prepared by mixing Cpd5 (1 mM) with the co-factors, NADPH A and B. The mixture was then incubated with the microsomes (20 mg/ml) at 37°C for 10, 20, 30, 40, 50 and 60 min. Verapamil (5  $\mu$ M) was included in the assay to serve as an internal standard. At the end of every time point, the samples were analyzed using a LCMS-8040 Triple Quadrupole Liquid Chromatograph Mass Spectrophotometer (LC-MS/MS). The disappearance of Cpd5 was monitored over a period of 60 minutes. Data are representative of 3 independent assays showing the stability of Cpd5 in form of linear regression plots after

treatment with A) human and B) murine microsomes. The peak area ratio was calculated using Microsoft Excel using the formula: Peak area ratio = Peak area of test compound (Cpd5) / peak area ratio of internal standard (Verapamil). These values were then used to generate linear regression plots using GraphPad Prism.

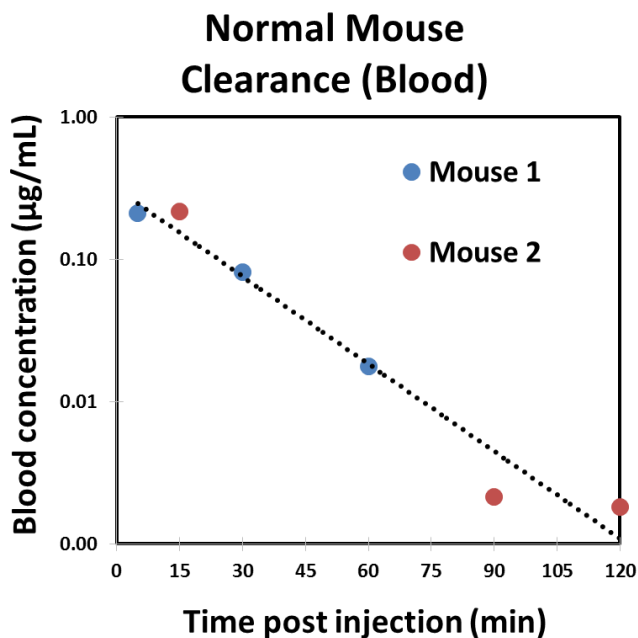


**Figure 33. Pharmacokinetic study depicting availability of Cpd5 in normal mouse blood.**

Normal mice were injected with Cpd5 (i.p.) and followed by collection of heparinized blood at various time points (5, 15, 30, 60, 90 and 120 minutes). Samples were centrifuged and the supernatants collected and analyzed on a LC-MS/MS. Concentration of Cpd5 in blood over time was determined by linear regression analysis using Microsoft Excel.

<b>Compound</b>	<b>MTD (mg/kg, i.p)</b>
<b>SAHA</b>	>200
<b>FK228</b>	3.125
<b>Cpd5</b>	>200

**Table III. Comparing systemic toxicity levels of Cpd5, FK228 and SAHA *in vivo*.**

Female BALB/c mice were injected with varying doses (200, 100, 50, 25, 12.5, 6.25 and 3.25 mg/kg) of Cpd 5, FK228, SAHA or DMSO (vehicle, not shown) intraperitoneally. The mice were observed and weighed every other day for a period of 2 weeks. This process was repeated until a tolerated dose was found, and the MTD value was determined. Each treatment was done with three animals/group receiving the same dose of drug or vehicle.

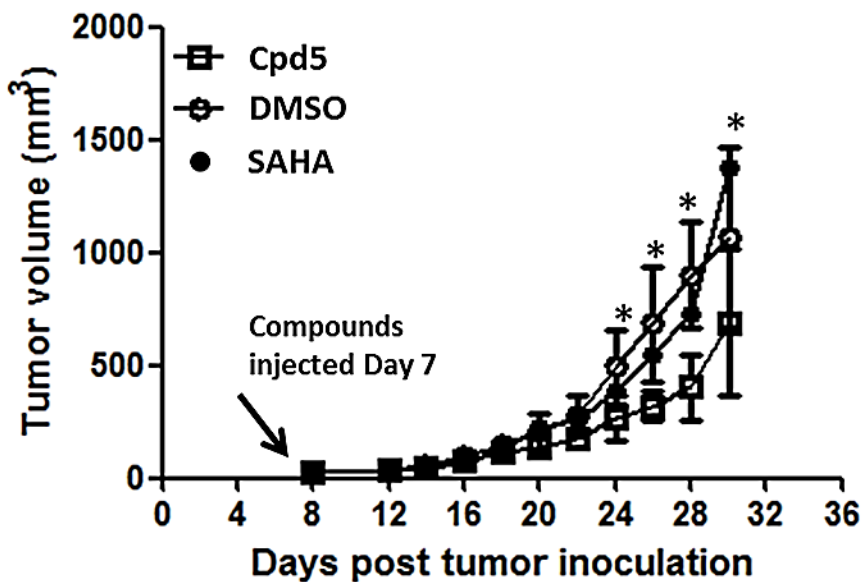


**Figure 34. Cpd5-mediated tumor growth inhibition in 4T1 tumor-bearing mice.**

Female BALB/c mice were injected with 4T1 cells subcutaneously into the mammary fat pad. After 7 days, mice were treated i.p. with Cpd5 (25 mg/kg), SAHA (25 mg/kg) or DMSO every other day for 30 days. Tumors were measured on treatment days and their volumes were determined as described in “Materials and Methods”. Data represents average tumor volume  $\pm$  SD of two independent experiments with one mouse per treatment. \*Significance between the various treatment groups was determined by two-way ANOVA and Bonferroni multiple comparison tests,  $p < 0.05$ .

**CHAPTER 5**

**CONCLUSIONS**

## CONCLUSIONS

Folate receptors are overexpressed on epithelial and myeloid carcinomas with most normal cells having negligible expression. In normal cells that do express FR, it is limited to the apical surface. These features have encouraged many studies utilizing FR to target tumor cells. To date, most of these studies involved drug delivery using FR-targeted nanocarriers and liposomes to the cells of interest. However, drug toxicity and non-specific targeting have been major issues that have resulted in only limited success of such anti-tumor therapies. There are multiple isoforms of FR among which the  $\alpha$  and  $\beta$  are membrane-associated and detectable in cells and tissues, thereby facilitating their study. However, most of the previous studies have focused solely on FR- $\alpha$  while ignoring FR- $\beta$ . Importantly, FR- $\beta$  is reported to be overexpressed on myeloid leukemias and thus is a potential target to treat these malignancies, which can be more challenging to treat than epithelial tumors. Herein, the role of FR- $\beta$  as a potential target was investigated and functional characteristics of both the FR- $\alpha$  and FR- $\beta$  isoforms were characterized.

One important observation from this study was that the FR- $\alpha$  and FR- $\beta$  exhibited differential functional characteristics. First, lineage-specific expression of FR- $\alpha$  and FR- $\beta$  was confirmed in the model 4T1 epithelial tumor cell line and the U937 myelomonocytic leukemia cell line, respectively. FR- $\alpha$  was overexpressed on the 4T1 cells and FR- $\beta$  on the U937 cells; however, as expected, the normal epithelial and myeloid cells did not exhibit FR- $\alpha$  and FR- $\beta$  expression, respectively. In addition, overexpression of the FR- $\alpha$  isoform was maintained *in vivo*, which is of relevance for designing targeting therapies utilizing this receptor.

Interestingly, antibody labeling studies showed that FR- $\alpha$  and FR- $\beta$  exhibited differential membrane staining patterns on the 4T1 and U937 cells, respectively. The FR- $\alpha$  appeared very

distinct and mostly in clusters on the 4T1 cells, while the FR- $\beta$  was localized to one end of the U937 cells. At this time it is not known what functional effect(s) this has on the receptors.

While it is well established that both FR isoforms exhibit relatively high affinity for folic acid, functional differences between these receptors are yet to be elucidated<sup>36</sup>. The findings from the present studies show that the activity profiles of the isoforms were very different from each other. The FR- $\alpha$  isoform was internalized into 4T1 cells within 5 minutes in response to folic acid, which was consistent with previous studies using other cell lines<sup>75</sup>. However, the FR- $\beta$  isoform was not internalized into the U937 cells following ligand binding. Further characterization of the isoform activities utilizing folic acid-fluorochrome conjugates such as FA-BSA-FITC and FA-BSA-TRITC was then performed. Specifically, the receptors were tracked intracellularly in response to folic acid conjugates vs unconjugated controls (BSA-FITC or BSA-TRITC). Results showed that the FA-BSA-FITC or FA-BSA-TRITC probes had strong binding to the tumor cells while the controls did not. This clearly indicated that both FR- $\alpha$  and FR- $\beta$  expressed on the 4T1 and U937 tumor cells exhibited specific binding ability for the folic acid conjugated probes. However, the FR- $\beta$  on the U937 cells did not internalize the folic acid-conjugated probes, unlike the internalization of FR- $\alpha$  observed in the 4T1 cells. Therefore, the results of the probe-mediated studies demonstrated that both FR isoforms could still be targeted utilizing folic acid-based strategies despite exhibiting differences in internalization.

These studies were expanded to determine the role of FR- $\beta$  in an *in vivo* cell model, thereby adding more relevance to the current research. For these studies, MDSCs were chosen due to their relevance to cancer. Specifically, MDSCs increase during inflammatory conditions such as cancer and suppress the immune system of the host. Our laboratory has previously demonstrated that MDSCs express FR- $\beta$ ; therefore, determining whether FR- $\beta$  could be used as a potential



target to eliminate MDSCs was logical. Although MDSCs can be identified with specific markers, similarities in expression of these with other normal cell populations such as neutrophils<sup>187</sup> and monocytes are a primary concern. Hence, our studies not only provide novel insights into using FR- $\beta$  as an additional MDSC marker but also as a potential target to eliminate MDSCs. Demonstration of specific binding of the folic acid-conjugated probes to both subsets of MDSCs showed that FR- $\beta$  expressed on MDSCs was functional for mediating folic acid binding. Importantly, the monocytic subset showed higher binding efficiency of the folic acid conjugates than the granulocytic subset, which could be beneficial, as the monocytic subset is reportedly more active and has higher suppressive activities. These findings support the idea that folic acid-dependent FR- $\beta$  targeting could be extended to eliminate MDSCs, thereby making this qualify as a potentially novel immunotherapeutic.

Based on the findings that the FR- $\beta$  isoform cannot internalize, a potential FR targeting mechanism that could lyse cells while remaining on the cell surface was investigated. Previous collaborative studies demonstrated that 4T1 tumor cells could be eliminated via antibody-conjugated gold-coated magnetite nanoparticles, through a technique known as hyperthermia<sup>178</sup>. Hence, the potential of this technique in using folic acid-nanoparticle conjugates was tested. However, before these studies could be attempted, the technique was first modeled using colloidal gold nanoparticles. FA-BSA-Au<sub>18</sub> and BSA-Au<sub>18</sub> (control) conjugates were generated and the FA-targeted conjugates were shown to bind specifically to both FR- $\alpha$  and FR- $\beta$ . These studies provide the foundation for future studies using FR-targeted magnetite nanoparticle conjugates for hyperthermia-mediated cell killing. Importantly, this technique could have an advantage over drug-dependent cell targeting, as the former does not suffer from systemic drug toxicity, non-specific tissue damage, or development of drug resistance.

The FR- $\alpha$  isoform internalizes into cells but the details associated with receptor trafficking mechanisms remain largely unknown. Interestingly, FR- $\alpha$  did not internalize via a clathrin-mediated endocytic pathway or by pinocytosis. Of interest is a report suggesting the possible role of lipid rafts in mediating FR endocytosis in cells<sup>88</sup>. Lipid rafts are lipid microdomains on the cell membrane that have high deposits of cholesterol and sphingolipids and could be involved in regulating the localization of the folate receptors on the cell surface. In addition, it is suggested that cholesterol anchors receptors and is considered to be a key player in triggering endocytosis. However, details of any such mechanism(s) are unknown. Therefore, the role of cholesterol in mediating FR- $\alpha$  and FR- $\beta$  activities was examined in the cells. Results of cholesterol depletion showed that probe binding through both FR- $\alpha$  and FR- $\beta$  was inhibited. However, it was the FR- $\alpha$  isoform that showed higher sensitivity to membrane cholesterol depletion than FR- $\beta$ . Furthermore, the internalization of FR- $\alpha$  was significantly inhibited in the absence of membrane cholesterol, thus indicating a possible crucial role for cholesterol in FR endocytosis (Fig. 35). Interestingly, the overall degree of cholesterol sensitivity of FR-mediated binding and endocytosis was much higher compared to the relative insensitivity of other trafficking pathways. These studies increase the overall understanding of FR trafficking in tumor cells, which could then be exploited for therapeutic studies. Other than drug delivery and hyperthermia-mediated receptor targeting, proteins associated with the FR-trafficking pathways could also serve as potential targets.

So far in this study, the folate receptor isoforms have been characterized and their potential use for targeting epithelial and myeloid malignancies demonstrated. In addition to this, the latter studies sought to determine the potential of therapeutics in exploiting tumor cell activity at the nuclear level. In collaboration with Dr. Hossain (Department of Chemistry, UW-Milwaukee), the

effectiveness of novel HDAC inhibitors in modifying histone activity in cells with potential for anti-tumor effects were studied. Many investigators have attempted to define a role for HDACs and HDAC inhibitors in cancer therapy. Previous reports have indicated that aberrant recruitment and overexpression of HDACs can lead to the suppression of tumor-suppressor genes, which may promote tumor onset and progression. Therefore, this has made HDACs attractive candidate targets for anti-cancer therapies. To date, many natural and synthetic compounds have been identified that are able to inhibit Class I and II HDACs. However, major concerns involve non-specific class activity and broad toxicity of HDAC inhibitors. Overt toxicity is not surprising given that HDACs not only modulate histone proteins but also several non-histone substrates. Although the mechanism(s) of their action is still not completely elucidated, much effort is being put into discovering novel compounds that exhibit higher HDAC class specificity and lower toxicity. Despite a tremendous amount of work and a large number of clinical trials, there are presently only two HDAC inhibitors, FK228 (romidepsin) and SAHA (vorinostat) that are FDA-approved for the treatment of cancer. Based on the scaffolds of these two compounds, the Hossain lab synthesized a panel of novel compounds that are being tested for their potential as novel HDAC inhibitors. One of the most effective compounds (Cpd5) was selected for detailed analyses in this thesis. Compared to FK228 (the parent compound), Cpd5 exhibited lower anti-proliferative activity against a panel of human tumor cell lines, and had markedly lower toxic effects in animals. In addition, Cpd5 showed increased acetylation of histones, had desirable pharmacokinetic properties, and was able to slow tumor growth in animals. These findings validated the further pursuit of developing Cpd5 into a therapeutic drug for cancer treatment.

In conclusion, these studies provide a better understanding of the folate receptor isoforms to be used to target epithelial and myeloid malignancies. We have characterized FR- $\alpha$  and FR- $\beta$ ,

and identified their differential activity, which would be relevant in devising therapeutic strategies. In addition, investigation of FR-trafficking pathways has highlighted receptor mechanisms that could be further studied to identify more molecular targets. The role of epigenetics in cancer therapy was also studied utilizing a novel HDAC inhibitor, and its prospects as a potential anticancer agent were investigated. Based on these findings, it is proposed that future development of Cpd5 as a therapeutic could involve FR targeting (Fig. 36). In this way, HDAC inhibitor-mediated effects would be targeted to the cells of interest, thus leaving healthy cells unharmed. These studies therefore, address a major concern of non-specific targeting in cancer therapy and provide new insights into future therapeutic strategies with improved selectivity.

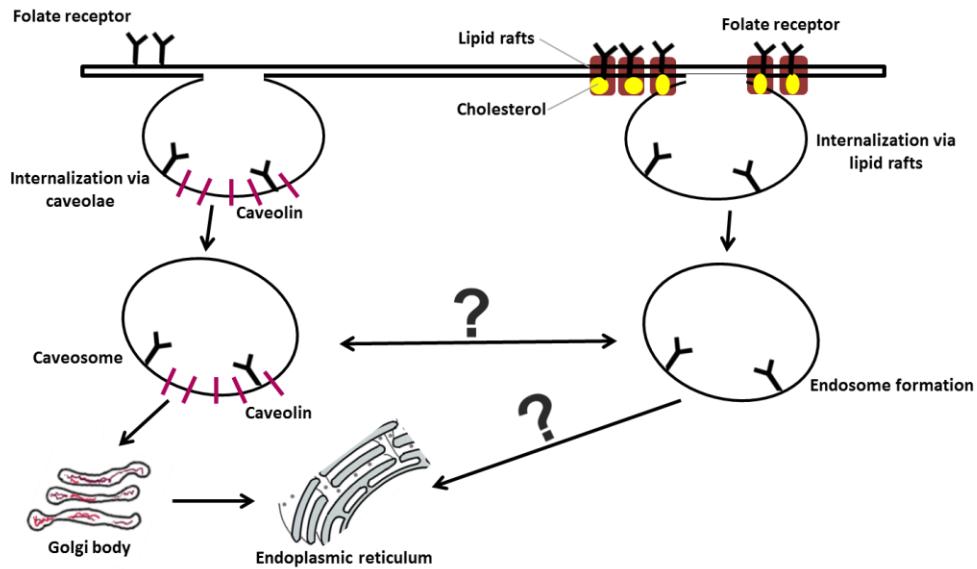


**Figure 35. FR- $\alpha$  (and to a lesser extent FR- $\beta$ ) exhibited sensitivity to membrane cholesterol depletion and is internalized via non-clathrin coated pathways.**

Model shown depicts two potential pathways through which FR internalization may occur. FR can internalize via a caveolae-mediated pathway through the formation of endosomal vesicles also known caveosomes, which is reported to be regulated by the protein, caveolin. It is also likely that FR can internalize via lipid-rafts that are made up of high deposits of cholesterol and sphingolipids with the cholesterol playing a potential role in mediating FR binding and endocytosis. However, the molecular mechanisms of the two pathways are not completely elucidated and hence interactions between lipid-raft-mediated endosomes and caveosomes need to be investigated.

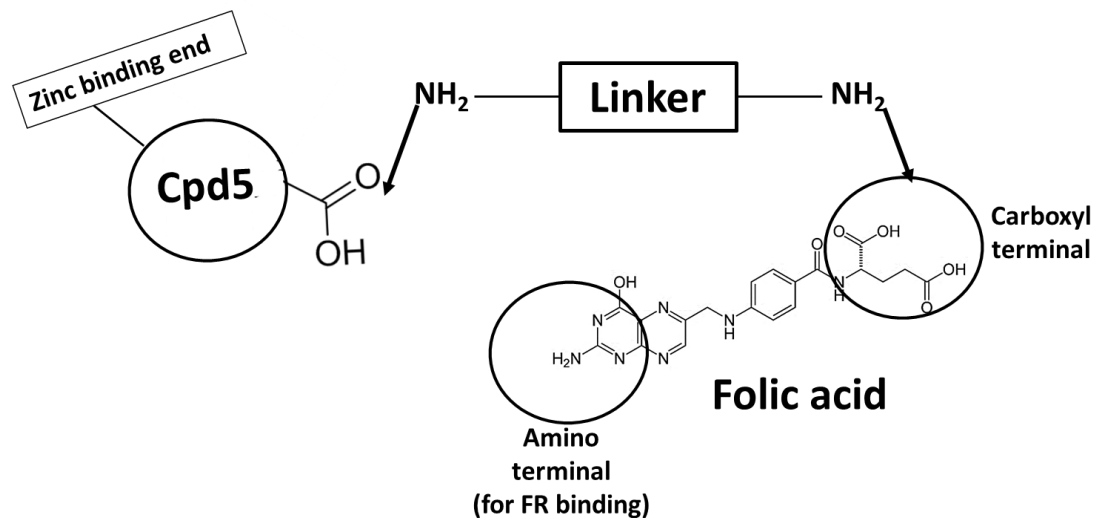


**Figure 36. Cpd5 conjugation to folic acid to induce selective targeting in tumor cells.**

HDAC inhibitors have been used as chemotherapeutic agents but their non-specific nature leads to adverse effects on non-target cells. Therefore, targeting HDAC inhibitors directly to tumors could help improve their therapeutic efficiency. One possible targeting mechanism would involve conjugating Cpd5 to the carboxyl terminus of folic acid. Importantly, a linker (e.g., EDC) that allows the amino terminus of folic acid to bind to FRs expressed on tumor cells is required. In this way, the HDAC inhibitor would only enter FR<sup>+</sup> cells (tumor cells), thereby preventing non-specific effects of HDAC inhibitors on normal cells.

## REFERENCES

- (1) Clifton, G. T.; Sears, A. K.; Clive, K. S.; Holmes, J. P.; Mittendorf, E. a.; Ioannides, C. G.; Ponniah, S.; Peoples, G. E. Folate receptor  $\alpha$ : A storied past and promising future in immunotherapy. *Hum. Vaccin.* **2011**, *7* (2), 183–190.
- (2) Lu, Y.; Low, P. S. Folate-mediated delivery of macromolecular anticancer therapeutic agents. *Adv. Drug Deliv. Rev.* **2012**, *64* (SUPPL.), 342–352.
- (3) Yamada, A.; Taniguchi, Y.; Kawano, K.; Honda, T.; Hattori, Y.; Maitani, Y. Design of folate-linked liposomal doxorubicin to its antitumor effect in mice. *Clin. Cancer Res.* **2008**, *14* (24), 8161–8168.
- (4) Campbell, I. G.; Jones, T. a; Foulkes, W. D.; Trowsdale, J. Folate binding protein is a marker for ovarian cancer. *Cancer Res* **1991**, *51* (19), 5329–5338.
- (5) Section, E. Cooperative Interaction of Immobilized Folate Binding Protein with. *Society* **1984**, No. 16, 1723–1726.
- (6) Antony, A. C. Folate receptors. *Annu. Rev. Nutr.* **1996**, *16*, 501–521.
- (7) Ross, J. F.; Chaudhuri, P. K.; Ratnam, M. Differential regulation of folate receptor isoforms in normal and malignant tissues in vivo and in established cell lines. Physiologic and clinical implications. *Cancer* **1994**, *73* (9), 2432–2443.
- (8) Wang, H.; Zheng, X.; Behm, F. G.; Ratnam, M. Differentiation-independent retinoid induction of folate receptor type  $\beta$ , a potential tumor target in myeloid leukemia. *Blood* **2000**, *96* (10).
- (9) Shen, F.; Ross, J. F.; Wang, X.; Ratnam, M. Identification of a novel folate receptor, a truncated receptor, and receptor type beta in hematopoietic cells: cDNA cloning, expression, immunoreactivity, and tissue specificity. *Biochemistry* **1994**, *33* (5), 1209–1215.
- (10) Elnakat, H.; Ratnam, M. Distribution, functionality and gene regulation of folate receptor isoforms: Implications in targeted therapy. *Advanced Drug Delivery Reviews.* **2004**, *56* (8), 1067–1084.
- (11) Lacey, S. W.; Sanders, J. M.; Rothberg, K. G.; Anderson, R. G.; Kamen, B. A. Complementary DNA for the folate binding protein correctly predicts anchoring to the membrane by glycosyl-phosphatidylinositol. *J. Clin. Invest.* **1989**, *84* (2), 715–720.
- (12) Sadasivan, E.; Rothenberg, S. P. The complete amino acid sequence of a human folate binding protein from KB cells determined from the cDNA. *J. Biol. Chem.* **1989**, *264* (10), 5806–5811.
- (13) Elwood, P. C. Molecular cloning and characterization of the human folate-binding protein cDNA from placenta and malignant tissue culture (KB) cells. *J. Biol. Chem.* **1989**, *264* (25), 14893–14901.
- (14) Parker, N.; Turk, M. J.; Westrick, E.; Lewis, J. D.; Low, P. S.; Leamon, C. P. Folate receptor expression in carcinomas and normal tissues determined by a quantitative

radioligand binding assay. *Anal. Biochem.* **2005**, 338 (2), 284–293.

- (15) Ratnam, M.; Marquardt, H.; Duhring, J. L.; Freisheim, J. H. Homologous membrane folate binding proteins in human placenta: cloning and sequence of a cDNA. *Biochemistry* **1989**, 28 (20), 8249–8254.
- (16) Shen, F.; Wu, M.; Ross, J. F.; Miller, D.; Ratnam, M. Folate receptor type gamma is primarily a secretory protein due to lack of an efficient signal for glycosylphosphatidylinositol modification: protein characterization and cell type specificity. *Biochemistry* **1995**, 34 (16), 5660–5665.
- (17) Spiegelstein, O.; Eudy, J. D.; Finnell, R. H. Identification of two putative novel folate receptor genes in humans and mouse. *Gene* **2000**, 258 (1–2), 117–125.
- (18) Monaco, H. L. Crystal structure of chicken riboflavin-binding protein. *EMBO J.* **1997**, 16 (7), 1475–1483.
- (19) Bernstein, S. L.; Guo, Y.; Peterson, K.; Wistow, G.; Miller, N.; MacGregor, D.; Avshalumov, M.; Rice, M.; Sacco, R.; Chong, J.; et al. Expressed sequence tag analysis of adult human optic nerve for NEIBank: Identification of cell type and tissue markers. *BMC Neurosci.* **2009**, 10 (1), 121.
- (20) Srinivasarao, M.; Galliford, C. V.; Low, P. S. Principles in the design of ligand-targeted cancer therapeutics and imaging agents. *Nat. Rev. Drug Discov.* **2015**, 14 (3), 203–219.
- (21) Antony, a C. Folate Receptors. *Annu. Rev. Nutr.* **1996**, 16 (1), 501–521.
- (22) Weitman, S. D.; Lark, R. H.; Coney, L. R.; Fort, D. W.; Frasca, V.; Zurawski, V. R.; Kamen, B. a. Distribution of the Folate Receptor GP38 in Normal and Malignant Cell Lines and Tissues Distribution of the Folate Receptor GP38 in Normal and Malignant Cell Lines and. **1992**, 3396–3401.
- (23) Anand, J. Folate-targeted gene delivery to cancers. **1999**.
- (24) Matherly, L. H.; Goldman, D. I. Membrane transport of folates. *Vitam. Horm.* **2003**, 66, 403–456.
- (25) Salazar, M. D.; Ratnam, M. The folate receptor: what does it promise in tissue-targeted therapeutics? *Cancer Metastasis Rev.* **2007**, 26 (1), 141–152.
- (26) O’Shannessy, D. J.; Somers, E. B.; Maltzman, J.; Smale, R.; Fu, Y.-S. Folate receptor alpha (FRA) expression in breast cancer: identification of a new molecular subtype and association with triple negative disease. *Springerplus* **2012**, 1, 22.
- (27) Toffoli, G.; Cernigoi, C.; Russo, A.; Gallo, A.; Bagnoli, M.; Boiocchi, M. Overexpression of folate binding protein in ovarian cancers. *Int. J. Cancer* **1997**, 74 (2), 193–198.
- (28) Senol, S.; Ceyran, A. B.; Aydin, A.; Zemheri, E.; Ozkanli, S.; Kösemetin, D.; Sehitoglu, I.; Akalin, I. Folate receptor  $\alpha$  expression and significance in endometrioid endometrium carcinoma and endometrial hyperplasia. *Int. J. Clin. Exp. Pathol.* **2015**, 8 (5), 5633–5641.
- (29) Cagle, P. T.; Zhai, Q. J.; Murphy, L.; Low, P. S. Folate receptor in adenocarcinoma and squamous cell carcinoma of the lung: potential target for folate-linked therapeutic agents. *Arch. Pathol. Lab. Med.* **2013**, 137 (2), 241–244.



- (30) Wu, M.; Gunning, W.; Ratnam, M. Expression of folate receptor type alpha in relation to cell type, malignancy, and differentiation in ovary, uterus, and cervix. *Cancer Epidemiol. Biomarkers Prev.* **1999**, *8* (9), 775–782.
- (31) Weitman, S. D.; Frazier, K. M.; Kamen, B. A. The folate receptor in central nervous system malignancies of childhood. *J. Neurooncol.* **1994**, *21* (2), 107–112.
- (32) Toffoli, G.; Russo, A.; Gallo, A.; Cernigoi, C.; Miotti, S.; Sorio, R.; Tumolo, S.; Boiocchi, M. Expression of folate binding protein as a prognostic factor for response to platinum-containing chemotherapy and survival in human ovarian cancer. *Int. J. cancer* **1998**, *79* (2), 121–126.
- (33) Horiuchi, K.; Mishima, K.; Ohsawa, M.; Sugimura, M.; Aozasa, K. Prognostic factors for well-differentiated squamous cell carcinoma in the oral cavity with emphasis on immunohistochemical evaluation. *J. Surg. Oncol.* **1993**, *53* (2), 92–96.
- (34) Ramamoorthy, K.; Potala, S.; Verma, R. S. Insilco analysis of functionally important residues in folate receptors. *Bioinformation* **2007**, *2* (4), 157.
- (35) Chen, C.; Ke, J.; Zhou, X. E.; Yi, W.; Brunzelle, J. S.; Li, J.; Yong, E.-L.; Xu, H. E.; Melcher, K. Structural basis for molecular recognition of folic acid by folate receptors. *Nature* **2013**, *500* (7463), 486–489.
- (36) Shen, F.; Wang, H.; Zheng, X.; Ratnam, M. Expression levels of functional folate receptors alpha and beta are related to the number of N-glycosylated sites. *Biochem. J.* **1997**, *327* ( Pt 3), 759–764.
- (37) Wibowo, A. S.; Singh, M.; Reeder, K. M.; Carter, J. J.; Kovach, A. R.; Meng, W.; Ratnam, M.; Zhang, F.; Dann, C. E. Structures of human folate receptors reveal biological trafficking states and diversity in folate and antifolate recognition. *Proc. Natl. Acad. Sci. U. S. A.* **2013**, *110* (38), 15180–15188.
- (38) Wang, X.; Shen, F.; Freisheim, J. H.; Gentry, L. E.; Ratnam, M. Differential stereospecificities and affinities of folate receptor isoforms for folate compounds and antifolates. *Biochem. Pharmacol.* **1992**, *44* (9), 1898–1901.
- (39) Maziarz, K. M.; Monaco, H. L.; Shen, F.; Ratnam, M. Complete mapping of divergent amino acids responsible for differential ligand binding of folate receptors alpha and beta. *J. Biol. Chem.* **1999**, *274* (16), 11086–11091.
- (40) Rijnboutt, S.; Jansen, G.; Posthuma, G.; Hynes, J. B.; Schornagel, J. H.; Strous, G. J. Endocytosis of GPI-linked membrane folate receptor-alpha. *J. Cell Biol.* **1996**, *132* (1–2), 35–47.
- (41) Kane, M. A.; Waxman, S. Role of folate binding proteins in folate metabolism. *Lab. Invest.* **1989**, *60* (6), 737–746.
- (42) Kamen, B. a.; Smith, A. K. A review of folate receptor alpha cycling and 5-methyltetrahydrofolate accumulation with an emphasis on cell models in vitro. *Advanced Drug Delivery Reviews.* **2004**, *56* (8), 1085–1097.
- (43) Ross, J. F.; Wang, H.; Behm, F. G.; Mathew, P.; Wu, M.; Booth, R.; Ratnam, M. Folate receptor type beta is a neutrophilic lineage marker and is differentially expressed in myeloid leukemia. *Cancer* **1999**, *85* (2), 348–357.

- (44) Wang, H.; Zheng, X.; Behm, F. G.; Ratnam, M. Differentiation-independent retinoid induction of folate receptor type beta, a potential tumor target in myeloid leukemia. *Blood* **2000**, *96* (10), 3529–3536.
- (45) Ross, J. F.; Wang, H.; Behm, F. G.; Mathew, P.; Wu, M.; Booth, R.; Ratnam, M. Folate receptor type beta is a neutrophilic lineage marker and is differentially expressed in myeloid leukemia. *Cancer* **1999**, *85* (2), 348–357.
- (46) Reddy, J. a; Haneline, L. S.; Srour, E. F.; Antony, a C.; Clapp, D. W.; Low, P. S. Expression and functional characterization of the beta-isoform of the folate receptor on CD34(+) cells. *Blood* **1999**, *93* (11), 3940–3948.
- (47) Pan, X. Q.; Zheng, X.; Shi, G.; Wang, H.; Ratnam, M.; Lee, R. J. Strategy for the treatment of acute myelogenous leukemia based on folate receptor beta-targeted liposomal doxorubicin combined with receptor induction using all-trans retinoic acid. *Blood* **2002**, *100* (2), 594–602.
- (48) Nakashima-Matsushita, N.; Homma, T.; Yu, S.; Matsuda, T.; Sunahara, N.; Nakamura, T.; Tsukano, M.; Ratnam, M.; Matsuyama, T. Selective expression of folate receptor ?? and its possible role in methotrexate transport in synovial macrophages from patients with rheumatoid arthritis. *Arthritis Rheum.* **1999**, *42* (8), 1609–1616.
- (49) Gent, Y. Y.; Weijers, K.; Molthoff, C. F.; Windhorst, A. D.; Huisman, M. C.; Smith, D. E.; Kularatne, S. a; Jansen, G.; Low, P. S.; Lammertsma, A. a; et al. Evaluation of the novel folate receptor ligand [18F]fluoro-PEG-folate for macrophage targeting in a rat model of arthritis. *Arthritis Res. Ther.* **2013**, *15* (2), R37.
- (50) Feng, Y.; Shen, J.; Streaker, E. D.; Lockwood, M.; Zhu, Z.; Low, P. S.; Dimitrov, D. S. A folate receptor beta-specific human monoclonal antibody recognizes activated macrophage of rheumatoid patients and mediates antibody-dependent cell-mediated cytotoxicity. *Arthritis Res. Ther.* **2011**, *13* (2), R59.
- (51) Turk, M. J.; Breur, G. J.; Widmer, W. R.; Paulos, C. M.; Xu, L. C.; Grote, L. A.; Low, P. S. Folate-targeted imaging of activated macrophages in rats with adjuvant-induced arthritis. *Arthritis Rheum.* **2002**, *46* (7), 1947–1955.
- (52) Brigle, K. E.; Spinella, M. J.; Westin, E. H.; Goldman, I. D. Increased expression and characterization of two distinct folate binding proteins in murine erythroleukemia cells. *Biochem. Pharmacol.* **1994**, *47* (2), 337–345.
- (53) Westerhof, G. R.; Schornagel, J. H.; Kathmann, I.; Jackman, A. L.; Rosowsky, A.; Forsch, R. A.; Hynes, J. B.; Boyle, F. T.; Peters, G. J.; Pinedo, H. M. Carrier- and receptor-mediated transport of folate antagonists targeting folate-dependent enzymes: correlates of molecular-structure and biological activity. *Mol. Pharmacol.* **1995**, *48* (3), 459–471.
- (54) Kaufman, Y.; Drori, S.; Cole, P. D.; Kamen, B. A.; Sirota, J.; Ifergan, I.; Arush, M. W. Ben; Elhasid, R.; Sahar, D.; Kaspers, G. J. L.; et al. Reduced folate carrier mutations are not the mechanism underlying methotrexate resistance in childhood acute lymphoblastic leukemia. *Cancer* **2004**, *100* (4), 773–782.
- (55) Matherly, L. H.; Hou, Z. Structure and function of the reduced folate carrier a paradigm of a major facilitator superfamily mammalian nutrient transporter. *Vitam. Horm.* **2008**, *79*, 145–184.

- (56) Kane, M. a.; Portillo, R. M.; Elwood, P. C.; Antony, a. C.; Kolhouse, J. F. The influence of extracellular folate concentration on methotrexate uptake by human KB cells. Partial characterization of a membrane-associated methotrexate binding protein. *J. Biol. Chem.* **1986**, *261* (1), 44–49.
- (57) Mauritz, R.; Peters, G. J.; Kathmann, I.; Teshale, H.; Noordhuis, P.; Comijn, E. M.; Pinedo, H. M.; Jansen, G. Dynamics of antifolate transport via the reduced folate carrier and the membrane folate receptor in murine leukaemia cells in vitro and in vivo. *Cancer Chemother. Pharmacol.* **2008**, *62* (6), 937–948.
- (58) Kelemen, L. E. The role of folate receptor?? in cancer development, progression and treatment: Cause, consequence or innocent bystander? *Int. J. Cancer* **2006**, *119* (2), 243–250.
- (59) Spinella, M. J.; Brigle, K. E.; Sierra, E. E.; Goldman, I. D. Distinguishing between Folate Receptor- mediated Transport and Reduced Folate Carrier-mediated Transport in L1210 Leukemia Cells. *J. Biol. Chem.* **1995**, *270* (14), 7842–7849.
- (60) Sabharanjak, S.; Mayor, S. Folate receptor endocytosis and trafficking. *Adv. Drug Deliv. Rev.* **2004**, *56* (8), 1099–1109.
- (61) Zhu, W. Y.; Alliegro, M. A.; Melera, P. W. The rate of folate receptor alpha (FR??) synthesis in folate depleted CHL cells is regulated by a translational mechanism sensitive to media folate levels, while stable overexpression of its mRNA is mediated by gene amplification and an increase in transc. *J. Cell. Biochem.* **2001**, *81* (2), 205–219.
- (62) Antony, A.; Tang, Y.-S.; Khan, R. A.; Biju, M. P.; Xiao, X.; Li, Q.-J.; Sun, X.-L.; Jayaram, H. N.; Stabler, S. P. Translational upregulation of folate receptors is mediated by homocysteine via RNA-heterogeneous nuclear ribonucleoprotein E1 interactions. *J. Clin. Invest.* **2004**, *113* (2), 285–301.
- (63) Zhao, R.; Goldman, I. D. Resistance to antifolates. *Oncogene* **2003**, *22* (47), 7431–7457.
- (64) Jhaveri, M. S.; Wagner, C.; Trepel, J. B. Impact of extracellular folate levels on global gene expression. *Mol. Pharmacol.* **2001**, *60* (6), 1288–1295.
- (65) Salbaum, J. M.; Finnell, R. H.; Kappen, C. Regulation of folate receptor 1 gene expression in the visceral endoderm. *Birth Defects Res. Part A - Clin. Mol. Teratol.* **2009**, *85* (4), 303–313.
- (66) Brzezińska, A.; Wińska, P.; Balińska, M. Cellular aspects of folate and antifolate membrane transport. *Acta Biochim. Pol.* **2000**, *47* (3), 735–749.
- (67) Chen, C.; Ke, J.; Zhou, X. E.; Yi, W.; Brunzelle, J. S.; Li, J.; Yong, E.-L.; Xu, H. E.; Melcher, K. Structural basis for molecular recognition of folic acid by folate receptors. *Nature* **2013**, *500* (7463), 486–489.
- (68) Kamen, B. A.; Capdevila, A. Receptor-mediated folate accumulation is regulated by the cellular folate content. *Proc. Natl. Acad. Sci. U. S. A.* **1986**, *83* (16), 5983–5987.
- (69) Antony, A. C.; Kane, M. A.; Portillo, R. M.; Elwood, P. C.; Kolhouse, J. F. Studies of the

role of a particulate folate-binding protein in the uptake of 5-methyltetrahydrofolate by cultured human KB cells. *J. Biol. Chem.* **1985**, *260* (28), 14911–14917.

- (70) Leamon, C. P.; Low, P. S. Delivery of macromolecules into living cells: a method that exploits folate receptor endocytosis. *Proc. Natl. Acad. Sci. U. S. A.* **1991**, *88* (13), 5572–5576.
- (71) Zwicke, G. L.; Mansoori, G. A.; Jeffery, C. J. Targeting of Cancer Nanotherapeutics. *Nano Rev.* **2012**, *1*, 1–11.
- (72) Müller, C.; Schibli, R. Folic acid conjugates for nuclear imaging of folate receptor-positive cancer. *J. Nucl. Med.* **2011**, *52* (1), 1–4.
- (73) Turek, J. J.; Leamon, C. P.; Low, P. S. Endocytosis of folate-protein conjugates: ultrastructural localization in KB cells. *J. Cell Sci.* **1993**, *106* ( Pt 1), 423–430.
- (74) Hilgenbrink, A. R.; Low, P. S. Folate receptor-mediated drug targeting: From therapeutics to diagnostics. *J. Pharm. Sci.* **2005**, *94* (10), 2135–2146.
- (75) Paulos, C. M.; Reddy, J. a; Leamon, C. P.; Turk, M. J.; Low, P. S. Ligand binding and kinetics of folate receptor recycling in vivo: impact on receptor-mediated drug delivery. *Mol. Pharmacol.* **2004**, *66* (6), 1406–1414.
- (76) Rijnboutt, S.; Jansen, G.; Posthuma, G.; Hynes, J. B.; Schornagel, J. H.; Strous, G. J. Endocytosis of GPI-linked membrane folate receptor-alpha. *J. Cell Biol.* **1996**, *132* (1–2), 35–47.
- (77) Lee, R. J.; Wang, S.; Low, P. S. Measurement of endosome pH following folate receptor-mediated endocytosis. *Biochim. Biophys. Acta* **1996**, *1312* (3), 237–242.
- (78) Wileman, T.; Harding, C.; Stahl, P. Receptor-mediated endocytosis. *Biochem. J.* **1985**, *232* (1).
- (79) Zhao, X.; Li, H.; Lee, R. J. Targeted drug delivery via folate receptors. *Expert Opin. Drug Deliv.* **2008**, *5* (3), 309–319.
- (80) Yang, J.; Chen, H.; Vlahov, I. R.; Cheng, J.-X.; Low, P. S. Characterization of the pH of folate receptor-containing endosomes and the rate of hydrolysis of internalized acid-labile folate-drug conjugates. *J. Pharmacol. Exp. Ther.* **2007**, *321* (2), 462–468.
- (81) Rothberg, K. G.; Ying, Y.; Kolhouse, J. F.; Kamen, B. A.; Anderson, R. G. W. The glycopospholipid-linked folate receptor internalizes folate without entering the clathrin-coated pit endocytic pathway. *J. Cell Biol.* **1990**, *110* (3), 637–649.
- (82) Mayor, S.; Rothberg, K. G.; Maxfield, F. R. Sequestration of GPI-anchored proteins in caveolae triggered by cross-linking. *Science* **1994**, *264* (5167), 1948–1951.
- (83) Anderson, R. G.; Kamen, B. A.; Rothberg, K. G.; Lacey, S. W. Potocytosis: sequestration and transport of small molecules by caveolae. *Science* **1992**, *255* (5043), 410–411.
- (84) Lakhan, S. E.; Sabharanjak, S.; De, A.; Bessler, M.; Mason, P.; Hillmen, P.; Miyata, T.; Yamada, N.; Takeda, J.; Luzzatto, L. Endocytosis of glycosylphosphatidylinositol-anchored proteins. *J. Biomed. Sci.* **2009**, *16* (1), 93.
- (85) Pelkmans, L.; Helenius, A. Endocytosis via caveolae. *Traffic* **2002**, *3* (5), 311–320.

- (86) Lakhan, S. E.; Sabharanjak, S.; De, A. Endocytosis of glycosylphosphatidylinositol-anchored proteins. *J. Biomed. Sci.* **2009**, *16*, 93.
- (87) Varma, R.; Mayor, S. GPI-anchored proteins are organized in submicron domains at the cell surface. *Nature* **1998**, *394* (6695), 798–801.
- (88) Laude, A. J.; Prior, I. A. Plasma membrane microdomains: organization, function and trafficking. *Mol. Membr. Biol.* **2004**, *21* (3), 193–205.
- (89) Chang, W. J.; Rothberg, K. G.; Kamen, B. A.; Anderson, R. G. Lowering the cholesterol content of MA104 cells inhibits receptor-mediated transport of folate. *J. Cell Biol.* **1992**, *118* (1), 63–69.
- (90) Mayor, S.; Sabharanjak, S.; Maxfield, F. R. Cholesterol-dependent retention of GPI-anchored proteins in endosomes. *EMBO J.* **1998**, *17* (16), 4626–4638.
- (91) Simons, K.; Sampaio, J. L. Membrane organization and lipid rafts. *Cold Spring Harb. Perspect. Biol.* **2011**, *3* (10), a004697.
- (92) Nichols, B. J.; Kenworthy, A. K.; Polishchuk, R. S.; Lodge, R.; Roberts, T. H.; Hirschberg, K.; Phair, R. D.; Lippincott-Schwartz, J. Rapid cycling of lipid raft markers between the cell surface and Golgi complex. *J. Cell Biol.* **2001**, *153* (3), 529–541.
- (93) Nichols, B. Endocytosis of lipid-anchored proteins: excluding GEECs from the crowd. *J. Cell Biol.* **2009**, *186* (4), 457–459.
- (94) Xu, S.; Olenyuk, B. Z.; Okamoto, C. T.; Hamm-Alvarez, S. F. Targeting receptor-mediated endocytotic pathways with nanoparticles: rationale and advances. *Adv. Drug Deliv. Rev.* **2013**, *65* (1), 121–138.
- (95) Sabharanjak, S.; Mayor, S. Folate receptor endocytosis and trafficking. *Adv. Drug Deliv. Rev.* **2004**, *56* (8), 1099–1109.
- (96) Low, P. S.; Antony, A. C. Folate receptor-targeted drugs for cancer and inflammatory diseases. *Advanced Drug Delivery Reviews.* **2004**, *56* (8), 1055–1058.
- (97) Bareford, L. M.; Swaan, P. W. Endocytic mechanisms for targeted drug delivery. *Adv. Drug Deliv. Rev.* **2007**, *59* (8), 748–758.
- (98) Leamon, C. P.; Low, P. S. Cytotoxicity of momordin-folate conjugates in cultured human cells. *J. Biol. Chem.* **1992**, *267* (35), 24966–24971.
- (99) Leamon, C. P.; Pastan, I.; Low, P. S. Cytotoxicity of folate-*Pseudomonas* exotoxin conjugates toward tumor cells. Contribution of translocation domain. *J. Biol. Chem.* **1993**, *268* (33), 24847–24854.
- (100) Atkinson, S. F.; Bettinger, T.; Seymour, L. W.; Behr, J. P.; Ward, C. M. Conjugation of folate via gelonin carbohydrate residues retains ribosomal-inactivating properties of the toxin and permits targeting to folate receptor positive cells. *J. Biol. Chem.* **2001**, *276* (30), 27930–27935.
- (101) Lee, R. J.; Philip, S. Delivery of Liposomes into Cultured KB cells via folate. *J. Biol. Chem.* **1994**, *269* (5), 3198–3204.
- (102) Lee, R. J.; Low, P. S. Folate-mediated tumor cell targeting of liposome-entrapped

- doxorubicin in vitro. *Biochim. Biophys. Acta - Biomembr.* **1995**, 1233 (2), 134–144.
- (103) Goren, D.; Horowitz, A. T.; Tzemach, D.; Tarshish, M.; Zalipsky, S.; Gabizon, A. Nuclear delivery of doxorubicin via folate-targeted liposomes with bypass of multidrug-resistance efflux pump. *Clin. Cancer Res.* **2000**, 6 (5), 1949–1957.
- (104) Xu, L.; Pirolo, K. F.; Chang, E. H. Tumor-targeted p53-gene therapy enhances the efficacy of conventional chemo/radiotherapy. *J. Control. Release* **2001**, 74 (1–3), 115–128.
- (105) Douglas, J. T.; Rogers, B. E.; Rosenfeld, M. E.; Michael, S. I.; Feng, M.; Curiel, D. T. Targeted gene delivery by tropism-modified adenoviral vectors. *Nat. Biotechnol.* **1996**, 14 (11), 1574–1578.
- (106) Stella, B.; Arpicco, S.; Peracchia, M. T.; Desmaële, D.; Hoebeke, J.; Renoir, M.; D'Angelo, J.; Cattel, L.; Couvreur, P. Design of folic acid-conjugated nanoparticles for drug targeting. *J. Pharm. Sci.* **2000**, 89 (11), 1452–1464.
- (107) Říhová, B. Receptor-mediated targeted drug or toxin delivery. *Adv. Drug Deliv. Rev.* **1998**, 29 (3), 273–289.
- (108) Kataoka, K.; Harada, A.; Nagasaki, Y. Block copolymer micelles for drug delivery: design, characterization and biological significance. *Adv. Drug Deliv. Rev.* **2001**, 47 (1), 113–131.
- (109) Lu, J. Y.; Lowe, D. A.; Kennedy, M. D.; Low, P. S. Folate-targeted enzyme prodrug cancer therapy utilizing penicillin-V amidase and a doxorubicin prodrug. *J. Drug Target.* **1999**, 7 (1), 43–53.
- (110) Kranz, D. M.; Patrick, T. A.; Brigle, K. E.; Spinella, M. J.; Roy, E. J. Conjugates of folate and anti-T-cell-receptor antibodies specifically target folate-receptor-positive tumor cells for lysis. *Proc. Natl. Acad. Sci. U. S. A.* **1995**, 92 (20), 9057–9061.
- (111) Lu, Y.; Low, P. S. Folate targeting of haptens to cancer cell surfaces mediates immunotherapy of syngeneic murine tumors. *Cancer Immunol. Immunother.* **2002**, 51 (3), 153–162.
- (112) Leamon, C. P.; Low, P. S. Selective targeting of malignant cells with cytotoxin-folate conjugates. *J. Drug Target.* **1994**, 2 (2), 101–112.
- (113) Hwang, J.; Fitzgerald, D. J.; Adhya, S.; Pastan, I. Functional domains of pseudomonas exotoxin identified by deletion analysis of the gene expressed in E. coli. *Cell* **1987**, 48 (1), 129–136.
- (114) Lin, C.; Sunkara, G.; Cannon, J. B.; Ranade, V. Recent advances in prodrugs as drug delivery systems. *Am. J. Ther.* **2012**, 19 (1), 33–43.
- (115) Han, H. K.; Amidon, G. L. Targeted prodrug design to optimize drug delivery. *AAPS PharmSci* **2000**, 2 (1), E6.
- (116) Ladino, C. A.; Chari, R. V.; Bourret, L. A.; Kedersha, N. L.; Goldmacher, V. S. Folate-maytansinoids: target-selective drugs of low molecular weight. *Int. J. Cancer* **1997**, 73 (6), 859–864.
- (117) Steinberg, G.; Borch, R. F. Synthesis and evaluation of pteronic acid-conjugated nitroheterocyclic phosphoramidates as folate receptor-targeted alkylating agents. *J. Med.*

- Chem.* **2001**, *44* (1), 69–73.
- (118) Paranjpe, P. V.; Chen, Y.; Kholodovych, V.; Welsh, W.; Stein, S.; Sinko, P. J. Tumor-targeted bioconjugate based delivery of camptothecin: design, synthesis and in vitro evaluation. *J. Control. Release* **2004**, *100* (2), 275–292.
- (119) Leamon, C. P.; Reddy, J. A. Folate-targeted chemotherapy. *Adv. Drug Deliv. Rev.* **2004**, *56* (8), 1127–1141.
- (120) Reddy, J. A.; Westrick, E.; Vlahov, I.; Howard, S. J.; Santhapuram, H. K.; Leamon, C. P. Folate receptor specific anti-tumor activity of folate-mitomycin conjugates. *Cancer Chemother. Pharmacol.* **2006**, *58* (2), 229–236.
- (121) Leamon, C. P.; Reddy, J. A.; Vlahov, I. R.; Vetzal, M.; Parker, N.; Nicoson, J. S.; Xu, L.-C.; Westrick, E. Synthesis and biological evaluation of EC72: a new folate-targeted chemotherapeutic. *Bioconjug. Chem.* **2002**, *13* (4), 803–811.
- (122) Bae, Y. H.; Park, K. Targeted drug delivery to tumors: myths, reality and possibility. *J. Control. Release* **2011**, *153* (3), 198–205.
- (123) Hamann, P. R.; Hinman, L. M.; Hollander, I.; Beyer, C. F.; Lindh, D.; Holcomb, R.; Hallett, W.; Tsou, H.-R.; Upešlacis, J.; Shochat, D.; et al. Gemtuzumab ozogamicin, a potent and selective anti-CD33 antibody-calicheamicin conjugate for treatment of acute myeloid leukemia. *Bioconjug. Chem.* **2002**, *13* (1), 47–58.
- (124) Neville, D. M.; Srinivasachar, K.; Stone, R.; Scharff, J. Enhancement of immunotoxin efficacy by acid-cleavable cross-linking agents utilizing diphtheria toxin and toxin mutants. *J. Biol. Chem.* **1989**, *264* (25), 14653–14661.
- (125) Davis, M. E.; Chen, Z. (Georgia); Shin, D. M. Nanoparticle therapeutics: an emerging treatment modality for cancer. *Nat. Rev. Drug Discov.* **2008**, *7* (9), 771–782.
- (126) Sinha, R.; Kim, G. J.; Nie, S.; Shin, D. M. Nanotechnology in cancer therapeutics: bioconjugated nanoparticles for drug delivery. *Mol. Cancer Ther.* **2006**, *5* (8), 1909–1917.
- (127) Mousa, S. A.; Bharali, D. J. Nanotechnology-based detection and targeted therapy in cancer: nano-bio paradigms and applications. *Cancers (Basel)*. **2011**, *3* (3), 2888–2903.
- (128) Torchilin, V. P. Passive and active drug targeting: drug delivery to tumors as an example. *Handb. Exp. Pharmacol.* **2010**, No. 197, 3–53.
- (129) Greish, K. Enhanced permeability and retention (EPR) effect for anticancer nanomedicine drug targeting. *Methods Mol. Biol.* **2010**, *624*, 25–37.
- (130) Haley, B.; Frenkel, E. Nanoparticles for drug delivery in cancer treatment. *Urol. Oncol.* **2008**, *26* (1), 57–64.
- (131) Byrne, J. D.; Betancourt, T.; Brannon-Peppas, L. Active targeting schemes for nanoparticle systems in cancer therapeutics. *Adv. Drug Deliv. Rev.* **2008**, *60* (15), 1615–1626.
- (132) Modi, S.; Prakash Jain, J.; Domb, A. J.; Kumar, N. Exploiting EPR in polymer drug conjugate delivery for tumor targeting. *Curr. Pharm. Des.* **2006**, *12* (36), 4785–4796.
- (133) Liu, Y.; Wang, W.; Yang, J.; Zhou, C.; Sun, J. pH-sensitive polymeric micelles triggered drug release for extracellular and intracellular drug targeting delivery. *Asian J. Pharm. Sci.* **2013**, *8* (3), 159–167.

- (134) Cho, K.; Wang, X.; Nie, S.; Chen, Z. G.; Shin, D. M. Therapeutic nanoparticles for drug delivery in cancer. *Clin. Cancer Res.* **2008**, *14* (5), 1310–1316.
- (135) Palumbo, C.; Bei, R.; Procopio, A.; Modesti, A. Molecular targets and targeted therapies for malignant mesothelioma. *Curr. Med. Chem.* **2008**, *15* (9), 855–867.
- (136) Zwicke, G. L.; Mansoori, G. A.; Jeffery, C. J. Utilizing the folate receptor for active targeting of cancer nanotherapeutics. *Nano Rev.* **2012**, *3*.
- (137) Ahmed, M.; Narain, R. Carbohydrate-based materials for targeted delivery of drugs and genes to the liver. *Nanomedicine (Lond)*. **2015**, *10* (14), 2263–2288.
- (138) Schrama, D.; Reisfeld, R. A.; Becker, J. C. Antibody targeted drugs as cancer therapeutics. *Nat. Rev. Drug Discov.* **2006**, *5* (2), 147–159.
- (139) Deonarain, M. P.; Kousparou, C. A.; Epenetos, A. A. Antibodies targeting cancer stem cells: a new paradigm in immunotherapy? *MAbs* **2009**, *1* (1), 12–25.
- (140) Richter, M.; Zhang, H. Receptor-targeted cancer therapy. *DNA Cell Biol.* **2005**, *24* (5), 271–282.
- (141) Zhu, Y.; Choi, S. H.; Shah, K. Multifunctional receptor-targeting antibodies for cancer therapy. *Lancet. Oncol.* **2015**, *16* (15), e543-54.
- (142) Qian, Z. M.; Li, H.; Sun, H.; Ho, K. Targeted drug delivery via the transferrin receptor-mediated endocytosis pathway. *Pharmacol. Rev.* **2002**, *54* (4), 561–587.
- (143) Kedar, U.; Phutane, P.; Shidhaye, S.; Kadam, V. Advances in polymeric micelles for drug delivery and tumor targeting. *Nanomedicine Nanotechnology, Biol. Med.* **2010**, *6* (6), 714–729.
- (144) Nasongkla, N.; Bey, E.; Ren, J.; Ai, H.; Khemtong, C.; Setti Guthi, J.; Chin, S.; Sherry, A. D.; Boothman, D. A.; Gao, J. Multifunctional polymeric micelles as cancer-Targeted, MRI-ultrasensitive drug delivery systems. *Nano Lett.* **2006**, *6* (11), 2427–2430.
- (145) Cheng, Y.; Zhao, L.; Li, Y.; Xu, T. Design of biocompatible dendrimers for cancer diagnosis and therapy: current status and future perspectives. *Chem. Soc. Rev.* **2011**, *40* (5), 2673–2703.
- (146) Baker, J. R. Dendrimer-based nanoparticles for cancer therapy. *Hematology Am. Soc. Hematol. Educ. Program* **2009**, 708–719.
- (147) Elhissi, A. M. A.; Ahmed, W.; Hassan, I. U.; Dhanak, V. R.; D'Emanuele, A.; Elhissi, A. M. A.; Ahmed, W.; Hassan, I. U.; Dhanak, V. R.; D'Emanuele, A. Carbon nanotubes in cancer therapy and drug delivery. *J. Drug Deliv.* **2012**, *2012*, 837327.
- (148) Çağdaş, M.; Sezer, A. D.; Bucak, S. Liposomes as Potential Drug Carrier Systems for Drug Delivery. *Application of Nanotechnology in Drug Delivery*; **2014**.
- (149) Slepishkin, V. A.; Simões, S.; Dazin, P.; Newman, M. S.; Guo, L. S.; Pedroso de Lima, M. C.; Düzgüneş, N. Sterically stabilized pH-sensitive liposomes. Intracellular delivery of aqueous contents and prolonged circulation in vivo. *J. Biol. Chem.* **1997**, *272* (4), 2382–2388.
- (150) Lee, R. J.; Wang, S.; Turk, M. J.; Low, P. S. The effects of pH and intraliposomal buffer strength on the rate of liposome content release and intracellular drug delivery. *Biosci. Rep.* **1998**, *18* (2), 69–78.



- (151) Reddy, J. A.; Dean, D.; Kennedy, M. D.; Low, P. S. Optimization of folate-conjugated liposomal vectors for folate receptor-mediated gene therapy. *J. Pharm. Sci.* **1999**, *88* (11), 1112–1118.
- (152) Litzinger, D. C.; Huang, L. Phosphatidylethanolamine liposomes: drug delivery, gene transfer and immunodiagnostic applications. *Biochim. Biophys. Acta* **1992**, *1113* (2), 201–227.
- (153) Yildiz, I.; Shukla, S.; Steinmetz, N. F. Applications of viral nanoparticles in medicine. *Curr. Opin. Biotechnol.* **2011**, *22* (6), 901–908.
- (154) Steinmetz, N. F. Viral nanoparticles as platforms for next-generation therapeutics and imaging devices. *Nanomedicine* **2010**, *6* (5), 634–641.
- (155) Zhang, W.; Zhang, Z.; Zhang, Y. The application of carbon nanotubes in target drug delivery systems for cancer therapies. *Nanoscale Res. Lett.* **2011**, *6* (1), 555.
- (156) Yi, C.; Qi, S.; Zhang, D.; Yang, M. Covalent conjugation of multi-walled carbon nanotubes with proteins. *Methods Mol. Biol.* **2010**, *625*, 9–17.
- (157) Karchemski, F.; Zucker, D.; Regev, O. Carbon nanotubes-liposomes conjugate as a platform for drug delivery into cells. *J. Control. Release* **2012**, *160* (2), 339–345.
- (158) Chen, Y.; Star, A.; Vidal, S. Sweet carbon nanostructures: carbohydrate conjugates with carbon nanotubes and graphene and their applications. *Chem. Soc. Rev.* **2013**, *42* (11), 4532–4542.
- (159) Yin, M.; Wang, M.; Miao, F.; Ji, Y.; Tian, Z.; Shen, H.; Jia, N. Water-dispersible multiwalled carbon nanotube/iron oxide hybrids as contrast agents for cellular magnetic resonance imaging. *Carbon N. Y.* **2012**, *50* (6), 2162–2170.
- (160) Wang, X.; Qian, X.; Beitler, J. J.; Chen, Z. G.; Khuri, F. R.; Lewis, M. M.; Shin, H. J. C.; Nie, S.; Shin, D. M. Detection of circulating tumor cells in human peripheral blood using surface-enhanced Raman scattering nanoparticles. *Cancer Res.* **2011**, *71* (5), 1526–1532.
- (161) Liu, S.; Jia, B.; Qiao, R.; Yang, Z.; Yu, Z.; Liu, Z.; Liu, K.; Shi, J.; Ouyang, H.; Wang, F. A novel type of dual-modality molecular probe for MR and nuclear imaging of tumor: preparation, characterization and in vivo application. *Mol. Pharm.* **2009**, *6* (4), 1074–1082.
- (162) Connor, E. E.; Mwamuka, J.; Gole, A.; Murphy, C. J.; Wyatt, M. D. Gold Nanoparticles are taken up by human cells but do not cause acute cytotoxicity. *Small* **2005**, *1* (3), 325–327.
- (163) Male, K. B.; Lachance, B.; Hrapovic, S.; Sunahara, G.; Luong, J. H. T. Assessment of cytotoxicity of quantum dots and gold nanoparticles using cell-based impedance spectroscopy. *Anal. Chem.* **2008**, *80* (14), 5487–5493.
- (164) Cherukuri, P.; Glazer, E. S.; Curley, S. A. Targeted hyperthermia using metal nanoparticles. *Adv. Drug Deliv. Rev.* **2010**, *62* (3), 339–345.
- (165) Deatsch, A. E.; Evans, B. A. Heating efficiency in magnetic nanoparticle hyperthermia. *J. Magn. Magn. Mater.* **2014**, *354*, 163–172.
- (166) Bañobre-López, M.; Teijeiro, A.; Rivas, J. Magnetic nanoparticle-based hyperthermia for

cancer treatment. *Reports Pract. Oncol. Radiother.* **2013**, *18* (6), 397–400.

- (167) Silva, A. C.; Oliveira, T. R.; Mamani, J. B.; Malheiros, S. M. F.; Malavolta, L.; Pavon, L. F.; Sibov, T. T.; Amaro, E.; Tannús, A.; Vidoto, E. L. G.; et al. Application of hyperthermia induced by superparamagnetic iron oxide nanoparticles in glioma treatment. *Int. J. Nanomedicine.* **2011**, *6*, 591–603.
- (168) Luo, S.; Wang, L. F.; Ding, W. J.; Wang, H.; Zhou, J. M.; Jinn, H. K.; Su, S. F.; Ouyang, W. W. Clinical trials of magnetic induction hyperthermia for treatment of tumours. *OA Cancer.* **2014**, *2* (1), 2.
- (169) Johannsen, M.; Thiesen, B.; Wust, P.; Jordan, A. Magnetic nanoparticle hyperthermia for prostate cancer. *Int. J. Hyperthermia* **2010**, *26* (8), 790–795.
- (170) Johannsen, M.; Gneveckow, U.; Taymoorian, K.; Thiesen, B.; Waldöfner, N.; Scholz, R.; Jung, K.; Jordan, A.; Wust, P.; Loening, S. A. Morbidity and quality of life during thermotherapy using magnetic nanoparticles in locally recurrent prostate cancer: results of a prospective phase I trial. *Int. J. Hyperthermia* **2007**, *23* (3), 315–323.
- (171) Surapaneni, M. S.; Das, S. K.; Das, N. G. Designing Paclitaxel drug delivery systems aimed at improved patient outcomes: current status and challenges. *ISRN Pharmacol.* **2012**, *2012*, 623139.
- (172) Ma, P.; Mumper, R. J. Paclitaxel nano-delivery systems: A comprehensive review. *J. Nanomed. Nanotechnol.* **2013**, *4* (2), 1000164.
- (173) Xiao, Y.; Hong, H.; Matson, V. Z.; Javadi, A.; Xu, W.; Yang, Y.; Zhang, Y.; Engle, J. T. W.; Nickles, R. J.; Cai, W. Gold nanorods conjugated with doxorubicin and cRGD for combined anti-cancer drug delivery and PET imaging. *Theranostics* **2012**, *2* (8), 757–768.
- (174) Aryal, S.; Grailer, J. J.; Pilla, S.; Steeber, D. A.; Gong, S. Doxorubicin conjugated gold nanoparticles as water-soluble and pH-responsive anticancer drug nanocarriers. *J. Mater. Chem.* **2009**, *19* (42), 7879.
- (175) Elbially, N. S.; Fathy, M. M.; Khalil, W. M. Doxorubicin loaded magnetic gold nanoparticles for in vivo targeted drug delivery. *Int. J. Pharm.* **2015**, *490* (1–2), 190–199.
- (176) Khalvati, B.; Sheikhsaran, F.; Sharifzadeh, S.; Kalantari, T.; Behzad Behbahani, A.; Jamshidzadeh, A.; Dehshahri, A. Delivery of plasmid encoding interleukin-12 gene into hepatocytes by conjugated polyethylenimine-based nanoparticles. *Artif. cells, Nanomed. Biotechnol.* **2016**, 1–9.
- (177) Friedman, A. D.; Claypool, S. E.; Liu, R. The smart targeting of nanoparticles. *Curr. Pharm. Des.* **2013**, *19* (35), 6315–6329.
- (178) Krystofiak, E. S.; Matson, V. Z.; Steeber, D. A.; Oliver, J. A. Elimination of tumor cells using folate receptor targeting by antibody-conjugated, gold-coated magnetite nanoparticles in a murine breast cancer model. *J. Nanomater.* **2012**, *2012*, 1–9.
- (179) Steichen, S. D.; Caldorera-Moore, M.; Peppas, N. A. A review of current nanoparticle and targeting moieties for the delivery of cancer therapeutics. *Eur. J. Pharm. Sci.* **2013**, *48* (3), 416–427.

- (180) Zhi, L.; Toh, B.; Abastado, J. J. Myeloid Derived Suppressor Cells: Subsets, Expansion, and Role in Cancer Progression. *Cdn.Intechopen.Com* **2011**, 1–26.
- (181) Hanahan, D.; Weinberg, R. A. Hallmarks of cancer: the next generation. *Cell* **2011**, *144* (5), 646–674.
- (182) Pashov, A.; Monzavi-Karbassi, B.; Kieber-Emmons, T. Immune surveillance and immunotherapy: lessons from carbohydrate mimotopes. *Vaccine* **2009**, *27* (25–26), 3405–3415.
- (183) Yu, H.; Kortylewski, M.; Pardoll, D. Crosstalk between cancer and immune cells: role of STAT3 in the tumour microenvironment. *Nat. Rev. Immunol.* **2007**, *7* (1), 41–51
- (184) Parish, C. R. Cancer immunotherapy: The past, the present and the future. *Immunol. Cell Biol.* **2003**, *81* (2), 106–113.
- (185) Murdoch, C.; Muthana, M.; Coffelt, S. B.; Lewis, C. E. The role of myeloid cells in the promotion of tumour angiogenesis. *Nat. Rev. Cancer* **2008**, *8* (8), 618–631.
- (186) Pillay, J.; Tak, T.; Kamp, V. M.; Koenderman, L. Immune suppression by neutrophils and granulocytic myeloid-derived suppressor cells: Similarities and differences. *Cell. Mol. Life Sci.* **2013**, *70* (20), 3813–3827.
- (187) Montero, A. J.; Diaz-Montero, C. M.; Kyriakopoulos, C. E.; Bronte, V.; Mandruzzato, S. Myeloid-derived suppressor cells in cancer patients. *J. Immunother.* **2012**, *35* (2), 107–115.
- (188) Gabilovich, D. I.; Nagaraj, S. Myeloid-derived suppressor cells as regulators of the immune system. *Nat. Rev. Immunol.* **2009**, *9* (3), 162–174.
- (189) Nagaraj, S.; Gupta, K.; Pisarev, V.; Kinarsky, L.; Sherman, S.; Kang, L.; Herber, D. L.; Schneck, J.; Gabilovich, D. I. Altered recognition of antigen is a mechanism of CD8+ T cell tolerance in cancer. *Nat. Med.* **2007**, *13* (7), 828–835.
- (190) Lee, D. W.; Barrett, D. M.; Mackall, C.; Orentas, R.; Grupp, S. A. The Future Is Now: Chimeric Antigen Receptors as New Targeted Therapies for Childhood Cancer. *Clin. Cancer Res.* **2012**, *18* (10), 2780–2790.
- (191) Park, J. H.; Geyer, M. B.; Brentjens, R. J. CD19-targeted CAR T-cell therapeutics for hematologic malignancies: interpreting clinical outcomes to date. *Blood* **2016**, *127* (26).
- (192) Ugel, S.; De Sanctis, F.; Mandruzzato, S.; Bronte, V.; Mantovani, A.; Allavena, P.; Sica, A.; Balkwill, F.; Mangerich, A.; Dedon, P. Tumor-induced myeloid deviation: when myeloid-derived suppressor cells meet tumor-associated macrophages. *J. Clin. Invest.* **2015**, *125* (9), 3365–3376.
- (193) Talmadge, J. E.; Gabilovich, D. I. History of myeloid-derived suppressor cells. *Nat. Rev. Cancer* **2013**, *13* (10), 739–752.
- (194) Greten, T. F.; Manns, M. P.; Korangy, F. Myeloid derived suppressor cells in human diseases. *Int. Immunopharmacol.* **2011**, *11* (7), 802–807.
- (195) Wesolowski, R.; Markowitz, J.; Carson, W. E. Myeloid derived suppressor cells – a new therapeutic target in the treatment of cancer. *J. Immunother. Cancer* **2013**, *1* (1), 10.

- (196) Mundy-Bosse, B. L.; Young, G. S.; Bauer, T.; Binkley, E.; Bloomston, M.; Bill, M. A.; Bekaii-Saab, T.; Carson, W. E.; Lesinski, G. B. Distinct myeloid suppressor cell subsets correlate with plasma IL-6 and IL-10 and reduced interferon-alpha signaling in CD4 + T cells from patients with GI malignancy. *Cancer Immunol. Immunother.* **2011**, *60* (9), 1269–1279.
- (197) Youn, J.-I.; Nagaraj, S.; Collazo, M.; Gabrilovich, D. I. Subsets of myeloid-derived suppressor cells in tumor-bearing mice. *J. Immunol.* **2008**, *181* (8), 5791–5802.
- (198) Ostrand-Rosenberg, S.; Sinha, P. Myeloid-derived suppressor cells: linking inflammation and cancer. *J. Immunol.* **2009**, *182* (8), 4499–4506.
- (199) Lechner, M. G.; Liebertz, D. J.; Epstein, A. L. Characterization of cytokine-induced myeloid-derived suppressor cells from normal human peripheral blood mononuclear cells. *J. Immunol.* **2010**, *185* (4), 2273–2284.
- (200) Radoja, S.; Rao, T. D.; Hillman, D.; Frey, A. B. Mice bearing late-stage tumors have normal functional systemic T cell responses in vitro and in vivo. *J. Immunol.* **2000**, *164* (5), 2619–2628.
- (201) Haverkamp, J. M.; Crist, S. A.; Elzey, B. D.; Cimen, C.; Ratliff, T. L. In vivo suppressive function of myeloid-derived suppressor cells is limited to the inflammatory site. *Eur. J. Immunol.* **2011**, *41* (3), 749–759.
- (202) Marigo, I.; Dolcetti, L.; Serafini, P.; Zanovello, P.; Bronte, V. Tumor-induced tolerance and immune suppression by myeloid derived suppressor cells. *Immunol. Rev.* **2008**, *222*, 162–179.
- (203) Fujimura, T.; Mahnke, K.; Enk, A. H. Myeloid derived suppressor cells and their role in tolerance induction in cancer. *J. Dermatol. Sci.* **2010**, *59* (1), 1–6.
- (204) Watanabe, S.; Deguchi, K.; Zheng, R.; Tamai, H.; Wang, L.-X.; Cohen, P. A.; Shu, S. Tumor-induced CD11b+Gr-1+ myeloid cells suppress T cell sensitization in tumor-draining lymph nodes. *J. Immunol.* **2008**, *181* (5), 3291–3300.
- (205) Sawanobori, Y.; Ueha, S.; Kurachi, M.; Shimaoka, T.; Talmadge, J. E.; Abe, J.; Shono, Y.; Kitabatake, M.; Kakimi, K.; Mukaida, N. Chemokine-mediated rapid turnover of myeloid-derived suppressor cells in tumor-bearing mice. *Blood* **2008**, *111* (12), 5457–5466.
- (206) Umansky, V.; Sevko, A. Tumor microenvironment and myeloid-derived suppressor cells. *Cancer Microenviron.* **2013**, *6* (2), 169–177.
- (207) Jatiani, S. S.; Baker, S. J.; Silverman, L. R.; Reddy, E. P. Jak/STAT pathways in cytokine signaling and myeloproliferative disorders: approaches for targeted therapies. *Genes Cancer* **2010**, *1* (10), 979–993.
- (208) Wilcox, R. A. Cancer-associated myeloproliferation: old association, new therapeutic target. *Mayo Clin. Proc.* **2010**, *85* (7), 656–663.
- (209) Lee, K. H.; Wang, E.; Nielsen, M. B.; Wunderlich, J.; Migueles, S.; Connors, M.;

- Steinberg, S. M.; Rosenberg, S. A.; Marincola, F. M. Increased vaccine-specific T cell frequency after peptide-based vaccination correlates with increased susceptibility to in vitro stimulation but does not lead to tumor regression. *J. Immunol.* **1999**, *163* (11), 6292–6300.
- (210) Yu, H.; Pardoll, D.; Jove, R. STATs in cancer inflammation and immunity: a leading role for STAT3. *Nat. Rev. Cancer* **2009**, *9* (11), 798–809.
- (211) Kujawski, M.; Kortylewski, M.; Lee, H.; Herrmann, A.; Kay, H.; Yu, H. Stat3 mediates myeloid cell-dependent tumor angiogenesis in mice. *J. Clin. Invest.* **2008**, *118* (10), 3367–3377.
- (212) Ray, A.; Chakraborty, K.; Ray, P. Immunosuppressive MDSCs induced by TLR signaling during infection and role in resolution of inflammation. *Front. Cell. Infect. Microbiol.* **2013**, *3*, 52.
- (213) Lechner, M. G.; Liebertz, D. J.; Epstein, A. L. Characterization of cytokine-induced myeloid-derived suppressor cells from normal human peripheral blood mononuclear cells. *J. Immunol.* **2010**, *185* (4), 2273–2284.
- (214) Trikha, P.; Carson, W. E.; III. Signaling pathways involved in MDSC regulation. *Biochim. Biophys. Acta* **2014**, *1846* (1), 55–65.
- (215) Vasquez-Dunddel, D.; Pan, F. STAT3 regulates arginase-I in myeloid-derived suppressor cells from cancer patients. *J. Clin. Invest.* **2013**, *123* (4)
- (216) Ostrand-Rosenberg, S. Myeloid-derived suppressor cells: More mechanisms for inhibiting antitumor immunity. *Cancer Immunol. Immunother.* **2010**, *59* (10), 1593–1600.
- (217) Gruner, A.; Li, Z.; Zhao, Z.; Zhu, X.; Ren, Q.; Nie, F.; Gao, J.; Gao, X.; Yang, T.; Zhou, W.; et al. Differences in iNOS and arginase expression and activity in the macrophages of rats are responsible for the resistance against *T. gondii* infection. *PLoS One* **2012**, *7* (4), e35834.
- (218) Youn, J.-I.; Gabrilovich, D. I. The biology of myeloid-derived suppressor cells: the blessing and the curse of morphological and functional heterogeneity. *Eur. J. Immunol.* **2010**, *40* (11), 2969–2975.
- (219) Kusmartsev, S.; Gabrilovich, D. I. Immature myeloid cells and cancer-associated immune suppression. *Cancer Immunol. Immunother.* **2002**, *51* (6), 293–298.
- (220) Bronte, V.; Brandau, S.; Chen, S.-H.; Colombo, M. P.; Frey, A. B.; Greten, T. F.; Mandruzzato, S.; Murray, P. J.; Ochoa, A.; Ostrand-Rosenberg, S. Recommendations for myeloid-derived suppressor cell nomenclature and characterization standards. *Nat. Commun.* **2016**, *7*, 12150.
- (221) Damuzzo, V.; Pinton, L.; Desantis, G.; Solito, S.; Marigo, I.; Bronte, V.; Mandruzzato, S. Complexity and challenges in defining myeloid-derived suppressor cells. *Cytom. Part B Clin. Cytom.* **2015**, *88* (2), 77–91.
- (222) Matsumura, T.; Kobayashi, K.; Ato, M. Myeloid-derived Suppressor Cells ( MDSCs ) and their related Cell Subpopulations.
- (223) Talmadge, J. E.; Gabrilovich, D. I. History of myeloid-derived suppressor cells. *Nat. Rev. Cancer* **2013**, *13* (10), 739–752.

- (224) Flörcken, A.; Takvorian, A.; Singh, A.; Gerhardt, A.; Ostendorf, B. N.; Dörken, B.; Pezzutto, A.; Westermann, J. Myeloid-derived suppressor cells in human peripheral blood: Optimized quantification in healthy donors and patients with metastatic renal cell carcinoma. *Immunol. Lett.* **2015**, *168* (2), 260–267.
- (225) Almand, B.; Clark, J. I.; Nikitina, E.; van Beynen, J.; English, N. R.; Knight, S. C.; Carbone, D. P.; Gabrilovich, D. I. Increased production of immature myeloid cells in cancer patients: a mechanism of immunosuppression in cancer. *J. Immunol.* **2001**, *166* (1), 678–689.
- (226) Lechner, M. G.; Megiel, C.; Russell, S. M.; Bingham, B.; Arger, N.; Woo, T.; Epstein, A. L. Functional characterization of human Cd33+ and Cd11b+ myeloid-derived suppressor cell subsets induced from peripheral blood mononuclear cells co-cultured with a diverse set of human tumor cell lines. *J. Transl. Med.* **2011**, *9*, 90.
- (227) Manjili, M. H. Phenotypic plasticity of MDSC in cancers. *Immunol. Invest.* **2012**, *41* (6–7), 711–721.
- (228) Kusmartsev, S.; Gabrilovich, D. I. Effect of tumor-derived cytokines and growth factors on differentiation and immune suppressive features of myeloid cells in cancer. *Cancer Metastasis Rev.* **2006**, *25* (3), 323–331.
- (229) Giallongo, C.; Parrinello, N.; Tibullo, D.; La Cava, P.; Romano, A.; Chiarenza, A.; Barbagallo, I.; Palumbo, G. a.; Stagno, F.; Vigneri, P. Myeloid-derived suppressor cells (MDSCs) are increased and exert immunosuppressive activity together with polymorphonuclear leukocytes (PMNs) in chronic myeloid leukemia patients. *PLoS One* **2014**, *9* (7).
- (230) Ma, C.; Kapanadze, T.; Gamrekelashvili, J.; Manns, M. P.; Korangy, F.; Greten, T. F. Anti-Gr-1 antibody depletion fails to eliminate hepatic myeloid-derived suppressor cells in tumor-bearing mice. *J. Leukoc. Biol.* **2012**, *92* (6), 1199–1206.
- (231) Ribechini, E.; Leenen, P. J. M.; Lutz, M. B. Gr-1 antibody induces STAT signaling, macrophage marker expression and abrogation of myeloid-derived suppressor cell activity in BM cells. *Eur. J. Immunol.* **2009**, *39* (12), 3538–3551.
- (232) Gong, D.; Shi, W.; Yi, S.; Chen, H.; Groffen, J.; Heisterkamp, N.; Blobel, G.; Schiemann, W.; Lodish, H.; Iseki, S. TGF $\beta$  signaling plays a critical role in promoting alternative macrophage activation. *BMC Immunol.* **2012**, *13* (1), 31.
- (233) Zhou, X.; Spittau, B.; Krieglstein, K. TGF $\beta$  signalling plays an important role in IL4-induced alternative activation of microglia. *J. Neuroinflammation* **2012**, *9*, 210.
- (234) Dufait, I.; Schwarze, J. K.; Liechtenstein, T.; Leonard, W.; Jiang, H.; Escors, D.; De Ridder, M.; Breckpot, K. Ex vivo generation of myeloid-derived suppressor cells that model the tumor immunosuppressive environment in colorectal cancer. *Oncotarget* **2015**, *6* (14), 12369–12382.
- (235) Goenka, S.; Kaplan, M. H. Transcriptional regulation by STAT6. *Immunol. Res.* **2011**, *50* (1), 87–96.
- (236) Kusmartsev, S.; Gabrilovich, D. I. STAT1 signaling regulates tumor-associated macrophage-mediated T cell deletion. *J. Immunol.* **2005**, *174* (8), 4880–4891.

- (237) Sinha, P.; Parker, K. H.; Horn, L.; Ostrand-Rosenberg, S. Tumor-induced myeloid-derived suppressor cell function is independent of IFN- $\gamma$  and IL-4R $\alpha$ . *Eur. J. Immunol.* **2012**, *42* (8), 2052–2059.
- (238) Alderton, W. K.; Alderton, W. K.; Cooper, C. E.; Cooper, C. E.; Knowles, R. G.; Knowles, R. G. Nitric oxide synthases: structure, function and inhibition. *Biochem. J.* **2001**, *357* (Pt 3), 593–615.
- (239) Raber, P.; Ochoa, A. C.; Rodríguez, P. C. Metabolism of L-Arginine by myeloid-derived suppressor cells in cancer: Mechanisms of T cell suppression and therapeutic perspectives. *Immunol. Invest.* **2012**, *41* (6–7), 614–634
- (240) Rodriguez, P. C.; Zea, A. H.; Culotta, K. S.; Zabaleta, J.; Ochoa, J. B.; Ochoa, A. C. Regulation of T cell receptor CD3zeta chain expression by L-arginine. *J. Biol. Chem.* **2002**, *277* (24), 21123–21129.
- (241) Heltemes-Harris, L. M.; Willette, M. J. L.; Vang, K. B.; Farrar, M. A. The role of STAT5 in the development, function, and transformation of B and T lymphocytes. *Ann. N. Y. Acad. Sci.* **2011**, *1217* (1), 18–31.
- (242) Lin, J. X.; Li, P.; Liu, D.; Jin, H. T.; He, J.; Rasheed, M. A. U.; Rochman, Y.; Wang, L.; Cui, K.; Liu, C. Critical Role of STAT5 transcription factor tetramerization for cytokine responses and normal immune function. *Immunity* **2012**, *36* (4), 586–599.
- (243) Yu, H. R.; Kuo, H. C.; Huang, L. T.; Chen, C. C.; Tain, Y. L.; Sheen, J. M.; Tiao, M. M.; Huang, H. C.; Yang, K. D.; Ou, C. Y.; et al. L-Arginine modulates neonatal lymphocyte proliferation through an interleukin-2 independent pathway. *Immunology* **2014**, *143* (2), 184–192.
- (244) Niedbala, W.; Cai, B.; Liew, F. Y. Role of nitric oxide in the regulation of T cell functions. *Ann. Rheum. Dis.* **2006**, *65* (Suppl 3), iii37-iii40.
- (245) Hesse, M.; Modolell, M.; La Flamme, A. C.; Schito, M.; Fuentes, J. M.; Cheever, A. W.; Pearce, E. J.; Wynn, T. A. Differential regulation of nitric oxide synthase-2 and arginase-1 by type 1/type 2 cytokines in vivo: Granulomatous pathology is shaped by the pattern of L-Arginine metabolism. *J. Immunol.* **2001**, *167* (11), 6533–6544.
- (246) Weiss, J. M.; Ridnour, L. a; Back, T.; Hussain, S. P.; He, P.; Maciag, A. E.; Keefer, L. K.; Murphy, W. J.; Harris, C. C.; Wink, D. Macrophage-dependent nitric oxide expression regulates tumor cell detachment and metastasis after IL-2/anti-CD40 immunotherapy. *J. Exp. Med.* **2010**, *207* (11), 2455–2467.
- (247) Nathan, C.; Xie, Q. W. Regulation of biosynthesis of nitric oxide. *Journal of Biolog. Chem.* **1994**, *269* (19), 13725–13728.
- (248) Sullivan, L. B.; Chandel, N. S. Mitochondrial reactive oxygen species and cancer. *Cancer Metab.* **2014**, *2* (1), 17.
- (249) Liou, G.-Y.; Storz, P. Reactive oxygen species in cancer. *Free Radic. Res.* **2010**, *44* (5), 479–496.

- (250) Corzo, C. A.; Cotter, M. J.; Cheng, P.; Cheng, F.; Kusmartsev, S.; Sotomayor, E.; Padhya, T.; McCaffrey, T. V; McCaffrey, J. C.; Gabrilovich, D. I. Mechanism regulating reactive oxygen species in tumor-induced myeloid-derived suppressor cells. *J. Immunol.* **2009**, *182* (9), 5693–5701.
- (251) Jayaraman, P.; Parkh, F.; Lopez-Rivera, E.; Hailemichael, Y.; Clark, A.; Ma, G.; Cannan, D.; Ramacher, M.; Kato, M.; Overwijk, W. W. Tumor-expressed iNOS controls induction of functional myeloid derived suppressor cells (MDSC) through modulation of VEGF release. *J. Immunol.* **2008**, *141* (4), 520–529.
- (252) Simon, H. U.; Haj-Yehia, A; Levi-Schaffer, F. Role of reactive oxygen species (ROS) in apoptosis induction. *Apoptosis* **2000**, *5* (5), 415–418.
- (253) Hildeman, D. A.; Mitchell, T.; Teague, T. K.; Henson, P.; Day, B. J.; Kappler, J.; Marrack, P. C. Reactive oxygen species regulate activation-induced T cell apoptosis. *Immunity* **1999**, *10* (6), 735–744.
- (254) Bogdan, C. Nitric oxide and the immune response. *Nat. Immunol.* **2001**, *2* (10), 907–916.
- (255) Fukumura, D.; Kashiwagi, S.; Jain, R. K. The role of nitric oxide in tumour progression. *Nat. Rev. Cancer* **2006**, *6* (7), 521–534.
- (256) Giulivi, C. Characterization and function of mitochondrial nitric-oxide synthase. *Free Radic. Biol. Med.* **2003**, 397–408.
- (257) Groves, J. T.; Wang, C. C. Nitric oxide synthase: models and mechanisms. *Curr. Opin. Chem. Biol.* **2000**, *4*, 687–695 DOI:.
- (258) Wheeler, M. L.; Defranco, A. L. Prolonged production of reactive oxygen species in response to B cell receptor stimulation promotes B cell activation and proliferation. *J. Immunol.* **2012**, *189* (9), 4405–4416.
- (259) Kusmartsev, S.; Nefedova, Y.; Yoder, D.; Gabrilovich, D. I. Antigen-specific inhibition of CD8+ T cell response by immature myeloid cells in cancer is mediated by reactive oxygen species. *J. Immunol.* **2004**, *172*, 989–999.
- (260) Alvarez, B.; Radi, R. Peroxynitrite reactivity with amino acids and proteins. *Amino Acids.* **2003**, *25* (3-4), 295–311.
- (261) Pacher, P.; Beckman, J. S.; Liaudet, L. Nitric oxide and peroxynitrite in health and disease. *Physiol. Rev.* **2007**, *87* (1), 315–424.
- (262) Chen, L.; Flies, D. B. Molecular mechanisms of T cell co-stimulation and co-inhibition. *Nat. Rev. Immunol.* **2013**, *13*, 227–242.
- (263) Cooke, C.-L. M.; Davidge, S. T. Peroxynitrite increases iNOS through NF- $\kappa$ B and decreases prostacyclin synthase in endothelial cells. *Am. J. Physiol. Cell Physiol.* **2002**, *282* (2), 395–402.
- (264) Virág, L.; Szabó, É.; Gergely, P.; Szabó, C. Peroxynitrite-induced cytotoxicity: Mechanism and opportunities for intervention. *Toxicol. Lett.* **2003**, *140–141*.
- (265) Gabrilovich, D. I.; Ostrand-Rosenberg, S.; Bronte, V. Coordinated regulation of myeloid cells by tumours. *Nat. Rev. Immunol.* **2012**, *12* (4), 253–268.
- (266) Monu, N. R.; Frey, A. B. Myeloid-derived suppressor cells and anti-tumor T cells: a complex relationship. *Immunol. Invest.* **2012**, *41* (6–7), 595–613.



- (267) Kusmartsev, S.; Nefedova, Y.; Yoder, D.; Gabrilovich, D. I. Antigen-specific inhibition of CD8+ T cell response by immature myeloid cells in cancer is mediated by reactive oxygen species. *J. Immunol.* **2004**, *172* (2), 989–999.
- (268) Guernonprez, L.; Ducrocq, C.; Gaudry-Talarmain, Y. M. Inhibition of acetylcholine synthesis and tyrosine nitration induced by peroxynitrite are differentially prevented by antioxidants. *Mol. Pharmacol.* **2001**, *60* (4), 838–846.
- (269) Bierie, B.; Moses, H. L. Transforming growth factor beta (TGF-beta) and inflammation in cancer. *Cytokine Growth Factor Rev.* **2010**, *21* (1), 49–59.
- (270) Lechner, M. G.; Liebertz, D. J.; Epstein, A. L. Characterization of cytokine-induced myeloid-derived suppressor cells from normal human peripheral blood mononuclear cells. *J. Immunol.* **2010**, *185* (4), 2273–2284.
- (271) Fichtner-Feigl, S.; Strober, W.; Kawakami, K.; Puri, R. K.; Kitani, A. IL-13 signaling through the IL-13 $\alpha$ 2 receptor is involved in induction of TGF- $\beta$ 1 production and fibrosis. *Nat. Med.* **2006**, *12* (1), 99–106.
- (272) Yang, L.; Pang, Y.; Moses, H. L. TGF- $\beta$  and immune cells: an important regulatory axis in the tumor microenvironment and progression. *Trends in Immunology.* 2010, *31* (6), 220–227.
- (273) Pickup, M.; Novitskiy, S.; Moses, H. L. The roles of TGF $\beta$  in the tumour microenvironment. *Nat. Rev. Cancer* **2013**, *13* (11), 788–799.
- (274) Hanson, E. M.; Clements, V. K.; Sinha, P.; Ilkovitch, D.; Ostrand-Rosenberg, S. Myeloid-derived suppressor cells down-regulate L-selectin expression on CD4+ and CD8+ T cells. *J. Immunol.* **2009**, *183* (2), 937–944.
- (275) Jones, N.; Agrawal, D.; Elrefaei, M.; Hanson, A.; Novitsky, V.; Wong, J. T.; Cao, H. Evaluation of antigen-specific responses using in vitro enriched T cells. *J. Immunol. Methods* **2003**, *274* (1–2), 139–147.
- (276) Schlecker, E.; Stojanovic, A.; Eisen, C.; Quack, C.; Falk, C. S.; Umansky, V.; Cerwenka, A. Tumor-Infiltrating monocytic myeloid-derived suppressor cells mediate CCR5-dependent recruitment of regulatory T cells favoring tumor growth. *J. Immunol.* **2012**, *189* (12), 5602–5611.
- (277) Centuori, S. M.; Trad, M.; LaCasse, C. J.; Alizadeh, D.; Larmonier, C. B.; Hanke, N. T.; Kartchner, J.; Janikashvili, N.; Bonnotte, B.; Larmonier, N. Myeloid-derived suppressor cells from tumor-bearing mice impair TGF- $\beta$ -induced differentiation of CD4<sup>+</sup>CD25<sup>+</sup>FoxP3<sup>+</sup> Tregs from CD4<sup>+</sup>CD25<sup>-</sup>FoxP3<sup>-</sup> T cells. *J. leukoc. biol.* **2012**, 987–997.
- (278) Fujimura, T.; Kambayashi, Y.; Aiba, S. Crosstalk between regulatory T cells (Tregs) and myeloid derived suppressor cells (MDSCs) during melanoma growth. *Oncoimmunology* **2012**, *1* (8), 1433–1434.
- (279) Huang, B.; Pan, P. Y.; Li, Q.; Sato, A. I.; Levy, D. E.; Bromberg, J.; Divino, C. M.; Chen, S. H. Gr-1+CD115+ immature myeloid suppressor cells mediate the development of tumor-induced T regulatory cells and T-cell anergy in tumor-bearing host. *Cancer Res.* **2006**, *66* (2), 1123–1131.
- (280) Serafini, P.; Mgebhoff, S.; Noonan, K.; Borrello, I. Myeloid-derived suppressor cells

promote cross-tolerance in B-cell lymphoma by expanding regulatory T cells. *Cancer Res.* **2008**, *68* (13), 5439–5449

- (281) Pan, P. Y.; Ma, G.; Weber, K. J.; Ozao-Choy, J.; Wang, G.; Yin, B.; Divino, C. M.; Chen, S. H. Immune stimulatory receptor CD40 is required for T-cell suppression and T regulatory cell activation mediated by myeloid-derived suppressor cells in cancer. *Cancer Res.* **2010**, *70* (1), 99–108.
- (282) Li, H.; Han, Y.; Guo, Q.; Zhang, M.; Cao, X. Cancer-expanded myeloid-derived suppressor cells induce anergy of NK cells through membrane-bound TGF-beta 1. *J. Immunol.* **2009**, *182* (1), 240–249.
- (283) Sinha, P.; Clements, V. K.; Bunt, S. K.; Albelda, S. M.; Ostrand-Rosenberg, S. Cross-talk between myeloid-derived suppressor cells and macrophages subverts tumor immunity toward a type 2 response. *J. Immunol.* **2007**, *179* (2), 977–983.
- (284) Schmid, M. C.; Varner, J. A. Myeloid cells in the tumor microenvironment: modulation of tumor angiogenesis and tumor inflammation. *J. Oncol.* **2010**, 26.
- (285) Murdoch, C.; Muthana, M.; Coffelt, S. B.; Lewis, C. E. The role of myeloid cells in the promotion of tumour angiogenesis. *Nat. Rev. Cancer* **2008**, *8* (8), 618–631.
- (286) Ostrand-Rosenberg, S.; Sinha, P.; Beury, D. W.; Clements, V. K. Cross-talk between myeloid-derived suppressor cells (MDSC), macrophages, and dendritic cells enhances tumor-induced immune suppression. *Semi Cancer Biol.* **2012**, 275–281.
- (287) Yang, L.; DeBusk, L. M.; Fukuda, K.; Fingleton, B.; Green-Jarvis, B.; Shyr, Y.; Matrisian, L. M.; Carbone, D. P.; Lin, P. C. Expansion of myeloid immune suppressor Gr<sup>+</sup>CD11b<sup>+</sup> cells in tumor-bearing host directly promotes tumor angiogenesis. *Cancer Cell* **2004**, *6* (4), 409–421.
- (288) Keskinov, A. A.; Shurin, M. R. Myeloid regulatory cells in tumor spreading and metastasis. *Immunobiology.* **2014**.
- (289) Hiratsuka, S.; Nakamura, K.; Iwai, S.; Murakami, M.; Itoh, T.; Kijima, H.; Shipley, J. M.; Senior, R. M.; Shibuya, M. MMP9 induction by vascular endothelial growth factor receptor-1 is involved in lung-specific metastasis. *Cancer Cell* **2002**, *2* (4), 289–300.
- (290) Pan, L. N.; Lu, J.; Huang, B. HDAC inhibitors: a potential new category of anti-tumor agents. *Cell. Mol. Immunol.* **2007**, *4* (5), 337–343.
- (291) Smith, L. T.; Otterson, G. A.; Plass, C. Unraveling the epigenetic code of cancer for therapy. *Trends Genet.* **2007**, *23* (9), 449–456.
- (292) Mählknecht, U.; Hoelzer, D. Histone acetylation modifiers in the pathogenesis of malignant disease. *Mol. Med.* **2000**, *6* (8), 623–644.
- (293) Jaenisch, R.; Bird, A. Epigenetic regulation of gene expression: how the genome integrates intrinsic and environmental signals. *Nat. Genet.* **2003**, *33* Suppl, 245–254.
- (294) Kornberg, R. D.; Lorch, Y. Twenty-five years of the nucleosome, fundamental particle of the eukaryote chromosome. *Cell* **1999**, *98* (3), 285–294.
- (295) Luger, K. Dynamic nucleosomes. *Chromosome Research.* **2006**, *14* (1), 5–16.

- (296) Kim, D. H.; Kim, M.; Kwon, H. J. Histone deacetylase in carcinogenesis and its inhibitors as anti-cancer agents. *J. Biochem. Mol. Biol.* **2003**, *36* (1), 110.
- (297) Tessarz, P.; Kouzarides, T. Histone core modifications regulating nucleosome structure and dynamics. *Nat. Rev. Mol. Cell Biol.* **2014**, *15* (11), 703–708.
- (298) Grunstein, M. Histone acetylation in chromatin structure and transcription. *Nature* **1997**, *389* (6649), 349–352.
- (299) Bannister, A. J.; Kouzarides, T. Regulation of chromatin by histone modifications. *Cell Res.* **2011**, *21* (3), 381–395.
- (300) Clayton, A. L.; Hazzalin, C. A.; Mahadevan, L. C. Enhanced Histone Acetylation and Transcription: A Dynamic Perspective. *Molecular Cell.* **2006**, *23* (3), 289–296.
- (301) Venkatesh, S.; Workman, J. L. Histone exchange, chromatin structure and the regulation of transcription. *Nat. Rev. Mol. Cell Biol.* **2015**, *16* (3), 178–189.
- (302) Gräff, J.; Tsai, L.-H. Histone acetylation: molecular mnemonics on the chromatin. *Nat. Rev. Neurosci.* **2013**, *14* (2), 97–111.
- (303) Kuo, M. H.; Allis, C. D. Roles of histone acetyltransferases and deacetylases in gene regulation. *BioEssays.* **1998**, *20* (8), 615–626.
- (304) Legube, G.; Trouche, D. Regulating histone acetyltransferases and deacetylases. *EMBO Rep.* **2003**, *4* (10), 944–947.
- (305) Marks, P. A.; Miller, T.; Richon, V. M. Histone deacetylases. *Curr Opin Pharmacol.* **2003**, *3* (4), 344–351.
- (306) Simone, C.; Peserico, A. Physical and functional HAT/HDAC interplay regulates protein acetylation balance. *J Biomed and Biotechnol.* **2011**, 2011
- (307) Icardi, L.; De Bosscher, K.; Tavernier, J. The HAT/HDAC interplay: Multilevel control of STAT signaling. *Cytokine and Growth Factor Rev.* **2012**, *23* (6), 283–291.
- (308) Toussiro, E.; Abbas, W.; Khan, K. A.; Tissot, M.; Jeudy, A.; Baud, L.; Bertolini, E.; Wendling, D.; Herbein, G. Imbalance between HAT and HDAC activities in the PBMCs of patients with ankylosing spondylitis or rheumatoid arthritis and influence of HDAC inhibitors on TNF alpha production. *PLoS One* **2013**, *8* (8).
- (309) Miremedi, A.; Oestergaard, M. Z.; Pharoah, P. D. P.; Caldas, C. Cancer genetics of epigenetic genes. *HumMol Gen.* **2007**, 16.
- (310) Lin, H. Y.; Chen, C. S.; Lin, S. P.; Weng, J. R.; Chen, C. S. Targeting histone deacetylase in cancer therapy. *Med Res Rev.* **2006**, *26* (4), 397–413.
- (311) Gray, S. G.; Ekström, T. J. The human histone deacetylase family. *Exp. Cell Res.* **2001**, *262* (2), 75–83.
- (312) Gregoretti, I. V.; Lee, Y. M.; Goodson, H. V. Molecular evolution of the histone deacetylase family: Functional implications of phylogenetic analysis. *J. Mol. Biol.* **2004**, *338* (1), 17–31.
- (313) Hu, E.; Chen, Z.; Fredrickson, T.; Zhu, Y.; Kirkpatrick, R.; Zhang, G. F.; Johanson, K.; Sung, C. M.; Liu, R.; Winkler, J. Cloning and characterization of a novel human class I histone deacetylase that functions as a transcription repressor. *J. Biol. Chem.* **2000**, 275

- (20), 15254–15264.
- (314) Verdin, E.; Dequiedt, F.; Kasler, H. G. Class II histone deacetylases: Versatile regulators. *Trends in Genetics*. **2003**, 19 (5), 286–293.
- (315) Fischle, W.; Kiermer, V.; Dequiedt, F.; Verdin, E. The emerging role of class II histone deacetylases. *Biochem. Cell. Biol.* **2001**, 79 (3), 337–348.
- (316) Yang, X.-J.; Grégoire, S. Class II histone deacetylases: from sequence to function, regulation, and clinical implication. *Mol. Cell. Biol.* **2005**, 25 (8), 2873–2884.
- (317) de Ruijter, A. J. M.; van Gennip, A. H.; Caron, H. N.; Kemp, S.; van Kuilenburg, A. B. P. Histone deacetylases (HDACs): characterization of the classical HDAC family. *Biochem. J.* **2003**, 370 (Pt 3), 737–749.
- (318) North, B. J.; Verdin, E. Sirtuins: Sir2-related NAD-dependent protein deacetylases. *Genome Biol.* **2004**, 5 (5), 224.
- (319) Luo, R. X.; Postigo, A. A.; Dean, D. C.; Adams, P. .; Kaelin, W. .; Alevizopoulos, A.; Dusserre, Y.; Tsai-Pflugelder, M.; Weid, T. Von der; Wahli, W. Rb interacts with histone deacetylase to repress transcription. *Cell* **1998**, 92 (4), 463–473.
- (320) Guenther, M. G.; Barak, O.; Lazar, M. A. The SMRT and N-CoR corepressors are activating cofactors for histone deacetylase 3. *Mol. Cell. Biol.* **2001**, 21 (18), 6091–6101.
- (321) Martin, M.; Kettmann, R.; Dequiedt, F. Class IIa histone deacetylases: regulating the regulators. *Oncogene* **2007**, 26 (37), 5450–5467 D.
- (322) Parra, M. Class IIa HDACs - New insights into their functions in physiology and pathology. *FEBS J.* **2015**, 282 (9), 1736–1744.
- (323) Bertos, N. R.; Wang, A. H.; Yang, X. J. Class II histone deacetylases: structure, function, and regulation. *Biochem. Cell Biol.* **2001**, 79 (3), 243–252.
- (324) Jones, P.; Altamura, S.; De Francesco, R.; Gallinari, P.; Lahm, A.; Neddermann, P.; Rowley, M.; Serafini, S.; Steinkühler, C. Probing the elusive catalytic activity of vertebrate class IIa histone deacetylases. *Bioorganic Med. Chem. Lett.* **2008**, 18 (6), 1814–1819.
- (325) Tong, J. J.; Liu, J.; Bertos, N. R.; Yang, X.-J. Identification of HDAC10, a novel class II human histone deacetylase containing a leucine-rich domain. *Nucleic Acids Res.* **2002**, 30 (5), 1114–1123.
- (326) Zhao, Z.; Xu, H.; Gong, W. Histone deacetylase 6 (HDAC6) is an independent deacetylase for alpha-tubulin. *Protein Pept. Lett.* **2010**, 17 (5), 555–558.
- (327) Dai, Y.; Faller, D. V. Transcription regulation by class III histone deacetylases (HDACs)-Sirtuins. *Transl. Oncogenomics* **2008**, 3, 53–65.
- (328) Liu, T.; Liu, P. Y.; Marshall, G. M. The critical role of the class III histone deacetylase SIRT1 in cancer. *Cancer Res.* **2009**, 69 (5), 1702–1705.
- (329) Gao, L.; Cueto, M. A.; Asselbergs, F.; Atadja, P. Cloning and functional characterization of HDAC11, a novel member of the human histone deacetylase family. *J. Biol. Chem.* **2002**, 277 (28), 25748–25755.

- (330) Ropero, S.; Esteller, M. The role of histone deacetylases (HDACs) in human cancer. *Molecular Oncology*. **2007**, 1 (1), 19–25.
- (331) Singh, B. N.; Zhang, G.; Hwa, Y. L.; Li, J.; Dowdy, S. C.; Jiang, S.-W. Nonhistone protein acetylation as cancer therapy targets. *Expert Rev. Anticancer Ther.* **2010**, 10 (6), 935–954.
- (332) Das, C.; Kundu, T. Transcriptional regulation by the acetylation of nonhistone proteins in humans – A new target for therapeutics. *IUBMB Life (International Union Biochem. Mol. Biol. Life)* **2005**, 57 (3), 137–149.
- (333) Tycko, B. Epigenetic gene silencing in cancer. *J. Clin. Invest.* **2000**, 105 (4), 401–407.
- (334) Jones, R. G.; Thompson, C. B. Tumor suppressors and cell metabolism: a recipe for cancer growth. *Genes Dev.* **2009**, 23 (5), 537–548.
- (335) Christensen, D. P.; Dahllöf, M.; Lundh, M.; Rasmussen, D. N.; Nielsen, M. D.; Billestrup, N.; Grunnet, L. G.; Mandrup-Poulsen, T. Histone deacetylase (HDAC) inhibition as a novel treatment for diabetes mellitus. *Mol. Med.* **2011**, 17 (5–6), 378–390.
- (336) Krock, B. L.; Skuli, N.; Simon, M. C. Hypoxia-induced angiogenesis: good and evil. *Genes Cancer* **2011**, 2 (12), 1117–1133.
- (337) Marks, P. A.; Xu, W. S. S.; Dokmanovic, M.; Dokmanovic, M.; Clarke, C.; Marks. Histone deacetylase inhibitors: Potential in cancer therapy. *Expert Opin. Investig. Drugs* **2009**, 107 (4), 600–608.
- (338) Dokmanovic, M.; Marks, P. A. Prospects: Histone deacetylase inhibitors. *J. Cell. Biochem.* **2005**, 96 (2), 293–304.
- (339) Marks, P. A.; Richon, V. M.; Breslow, R.; Rifkind, R. a. Histone deacetylase inhibitors as new cancer drugs. *Curr. Opin. Oncol.* **2001**, 13, 477–483.
- (340) Osada, H.; Tatematsu, Y.; Saito, H.; Yatabe, Y.; Mitsudomi, T.; Takahashi, T. Reduced expression of class II histone deacetylase genes is associated with poor prognosis in lung cancer patients. *Int. J. Cancer* **2004**, 112 (1), 26–32.
- (341) Falkenberg, K. J.; Johnstone, R. W. Histone deacetylases and their inhibitors in cancer, neurological diseases and immune disorders. *Nat. Rev. Drug Discov.* **2014**, 13 (9), 673–691.
- (342) Johnstone, R. W. Histone-deacetylase inhibitors: novel drugs for the treatment of cancer. *Nat. Rev. Drug Discov.* **2002**, 1 (4), 287–299.
- (343) Xu, W. S.; Parmigiani, R. B.; Marks, P. A. Histone deacetylase inhibitors: molecular mechanisms of action. *Oncogene* **2007**, 26 (37), 5541–5552.
- (344) Lane, A. A.; Chabner, B. A. Histone deacetylase inhibitors in cancer therapy. *J. Clin. Oncol.* **2009**, 27 (32), 5459–5468.
- (345) Rosato, R. R.; Grant, S. Histone deacetylase inhibitors: insights into mechanisms of lethality. *Expert Opin. Ther. Targets* **2005**, 9 (4), 809–824.
- (346) Bolden, J. E.; Peart, M. J.; Johnstone, R. W. Anticancer activities of histone deacetylase inhibitors. *Nat. Rev. Drug Discov.* **2006**, 5 (9), 769–784.
- (347) Ververis, K.; Hiong, A.; Karagiannis, T. C.; Licciardi, P. V. Histone deacetylase inhibitors

- (HDACIS): Multitargeted anticancer agents. *Biologics: Targets and Therapy*. **2013**, 7 (1), 47–60.
- (348) Liu, T.; Kuljaca, S.; Tee, A.; Marshall, G. M. Histone deacetylase inhibitors: Multifunctional anticancer agents. *Cancer Treatment Reviews*. **2006**, 32 (3), 157–165.
- (349) Caron, C.; Boyault, C.; Khochbin, S. Regulatory cross-talk between lysine acetylation and ubiquitination: Role in control of protein stability. *BioEssays*. **2005**, 27 (4), 408–415.
- (350) Matus, D. Q.; Lohmer, L. L.; Kelley, L. C.; Schindler, A. J.; Kohrman, A. Q.; Barkoulas, M.; Zhang, W.; Chi, Q.; Sherwood, D. R. Invasive cell fate requires G1 cell-cycle arrest and histone deacetylase-mediated changes in gene expression. *Dev. Cell* **2015**, 35 (2), 162–174.
- (351) Zhang, J.; Zhong, Q. Histone deacetylase inhibitors and cell death. *Cell and Mol Life Sciences*, **2014**, 71 (20), 3885–3901.
- (352) Walkinshaw, D. R.; Yang, X. J. Histone deacetylase inhibitors as novel anticancer therapeutics. *Curr. Oncol.* **2008**, 15 (5), 237–243.
- (353) Alvarez, A. A.; Field, M.; Bushnev, S.; Longo, M. S.; Sugaya, K. The effects of histone deacetylase inhibitors on glioblastoma-derived stem cells. *J. Mol. Neurosci.* **2014**, 55 (1), 7–20.
- (354) Kong, D.; Ahmad, A.; Bao, B.; Li, Y.; Banerjee, S.; Sarkar, F. H. Histone deacetylase inhibitors induce epithelial-to-mesenchymal transition in prostate cancer cells. *PLoS One* **2012**, 7 (9) e45045.
- (355) Marks, P. A.; Richon, V. M.; Rifkind, R. A. Histone deacetylase inhibitors: inducers of differentiation or apoptosis of transformed cells. *J. Natl. Cancer Inst.* **2000**, 92 (15), 1210.
- (356) Ocker, M. Deacetylase inhibitors - focus on non-histone targets and effects. *World J. Biol. Chem.* **2010**, 1 (5), 55–61.
- (357) Bolden, J. E.; Shi, W.; Jankowski, K.; Kan, C.-Y.; Cluse, L.; Martin, B. P.; MacKenzie, K. L.; Smyth, G. K.; Johnstone, R. W. HDAC inhibitors induce tumor-cell-selective pro-apoptotic transcriptional responses. *Cell Death Dis.* **2013**, 4 (2), e519.
- (358) Matthews, G. M.; Newbold, A.; Johnstone, R. W. Intrinsic and extrinsic apoptotic pathway signaling as determinants of histone deacetylase inhibitor antitumor activity. *Adv. Cancer Res.* **2012**, 116, 165–197.
- (359) Stevens, F. E.; Beamish, H.; Warren, R.; Gabrielli, B. Histone deacetylase inhibitors induce mitotic slippage. *Oncogene* **2008**, 27 (10), 1345–1354.
- (360) Gammoh, N.; Lam, D.; Puente, C.; Ganley, I.; Marks, P. A.; Jiang, X. Role of autophagy in histone deacetylase inhibitor-induced apoptotic and nonapoptotic cell death. *Proc. Natl. Acad. Sci. U. S. A.* **2012**, 109 (17), 6561–6565.
- (361) Zhang, J.; Ng, S.; Wang, J.; Zhou, J.; Tan, S. H.; Yang, N.; Lin, Q.; Xia, D.; Shen, H. M. Histone deacetylase inhibitors induce autophagy through FOXO1-dependent pathways. *Autophagy* **2015**, 11 (4), 629–642.
- (362) Ariffin, J. K.; das Gupta, K.; Kapetanovic, R.; Iyer, A.; Reid, R. C.; Fairlie, D. P.; Sweet, M. J. Histone deacetylase inhibitors promote mitochondrial reactive oxygen species

production and bacterial clearance by human macrophages. *Antimicrob. Agents Chemother.* **2016**, *60* (3), 1521–1529.

- (363) Rosato, R. R.; Almenara, J. A.; Maggio, S. C.; Coe, S.; Atadja, P.; Dent, P.; Grant, S. Role of histone deacetylase inhibitor-induced reactive oxygen species and DNA damage in LAQ-824/fludarabine antileukemic interactions. *Mol. Cancer Ther.* **2008**, *7* (10), 3285–3297.
- (364) Ellis, L.; Hammers, H.; Pili, R. Targeting tumor angiogenesis with histone deacetylase inhibitors. *Cancer Letters.* **2009**, *280* (2), 145–153.
- (365) Weis, S. M.; Cheresch, D. A. Tumor angiogenesis: molecular pathways and therapeutic targets. *Nat. Med.* **2011**, *17* (11), 1359–1370.
- (366) Kato, H.; Tamamizu-Kato, S.; Shibasaki, F. Histone deacetylase 7 associates with hypoxia-inducible factor 1alpha and increases transcriptional activity. *J. Biol. Chem.* **2004**, *279* (40), 41966–41974.
- (367) Wang, S.; Li, X.; Parra, M.; Verdin, E.; Bassel-Duby, R.; Olson, E. N. Control of endothelial cell proliferation and migration by VEGF signaling to histone deacetylase 7. *Proc. Natl. Acad. Sci. U. S. A.* **2008**, *105* (22), 7738–7743.
- (368) Marchion, D.; Münster, P. Development of histone deacetylase inhibitors for cancer treatment. *Expert Rev. Anticancer Ther.* **2007**, *7* (4), 583–598.
- (369) Dokmanovic, M.; Clarke, C.; Marks, P. A. Histone deacetylase inhibitors: overview and perspectives. *Mol. Cancer Res.* **2007**, *5* (10), 981–989.
- (370) Bantscheff, M.; Hopf, C.; Savitski, M. M.; Dittmann, A.; Grandi, P.; Michon, A. M.; Schlegl, J.; Abraham, Y.; Becher, I.; Bergamini, G.; et al. Chemoproteomics profiling of HDAC inhibitors reveals selective targeting of HDAC complexes. *Nat. Biotechnol.* **2011**, *29* (3), 255–265.
- (371) Bertrand, P. Inside HDAC with HDAC inhibitors. *Euro J Med Chem.* **2010**, *45* (6), 2095–2116.
- (372) Yoshida, M.; Kijima, M.; Akita, M.; Beppu, T. Potent and specific inhibition of mammalian histone deacetylase both in vivo and in vitro by trichostatin A. *J. Biol. Chem.* **1990**, *265* (2891009148), 17174–9.
- (373) Marks, P. A.; Breslow, R. Dimethyl sulfoxide to vorinostat: development of this histone deacetylase inhibitor as an anticancer drug. *Nat. Biotechnol.* **2007**, *25* (1), 84–90.
- (374) Duvic, M.; Talpur, R.; Ni, X.; Zhang, C.; Hazarika, P.; Kelly, C.; Chiao, J. H.; Reilly, J. F.; Ricker, J. L.; Richon, V. M. Phase 2 trial of oral vorinostat (suberoylanilide hydroxamic acid, SAHA) for refractory cutaneous T-cell lymphoma (CTCL). *Blood* **2007**, *109* (1), 31–39.
- (375) Furlan, A.; Monzani, V.; Reznikov, L. L.; Leoni, F.; Fossati, G.; Modena, D.; Mascagni, P.; Dinarello, C. A. Pharmacokinetics, safety and inducible cytokine responses during a phase 1 trial of the oral histone deacetylase inhibitor ITF2357 (givinostat). *Mol. Med.*

- 2011**, *17* (5–6), 353–362.
- (376) Galli, M.; Salmoiraghi, S.; Golay, J.; Gozzini, A.; Crippa, C.; Pescosta, N.; Rambaldi, A. A phase II multiple dose clinical trial of histone deacetylase inhibitor ITF2357 in patients with relapsed or progressive multiple myeloma. *Ann. Hematol.* **2010**, *89* (2), 185–190.
- (377) Andreu-Vieyra, C. C. V; Berenson, J. J. R. The potential of panobinostat as a treatment option in patients with relapsed and refractory multiple myeloma. *Ther. Adv. Hematol.* **2014**, *5* (6), 197–210
- (378) Morabito, F.; Voso, M. T.; Hohaus, S.; Gentile, M.; Vigna, E.; Recchia, A. G.; Iovino, L.; Benedetti, E.; Lo-Coco, F.; Galimberti, S. Panobinostat for the treatment of acute myelogenous leukemia. *Expert Opin. Investig. Drugs* **2016**, *25* (9), 1117–31.
- (379) Prince, H. M.; Bishton, M. J.; Johnstone, R. W. Panobinostat (LBH589): a potent pan-deacetylase inhibitor with promising activity against hematologic and solid tumors. *Future Oncol.* **2009**, *5* (5), 601–612.
- (380) Shao, W.; Growney, J. D.; Feng, Y.; O'Connor, G.; Pu, M.; Zhu, W.; Yao, Y. M.; Kwon, P.; Fawell, S.; Atadja, P. Activity of deacetylase inhibitor panobinostat (LBH589) in cutaneous T-cell lymphoma models: Defining molecular mechanisms of resistance. *Int. J. Cancer* **2010**, *127* (9), 2199–2208.
- (381) Jain, S.; Zain, J. Romidepsin in the treatment of cutaneous T-cell lymphoma. *J. Blood Med.* **2011**, *2*, 37–47.
- (382) Khan, O.; La Thangue, N. B. HDAC inhibitors in cancer biology: emerging mechanisms and clinical applications. *Immunol. Cell Biol.* **2012**, *90* (1), 85–94.
- (383) Campas-Moya, C. Romidepsin for the treatment of cutaneous T-cell lymphoma. *Drugs Today (Barc)*. **2009**, *45* (11), 787–795.
- (384) Finnin, M. S, Donigian, J. R, Pavletich, N. P. Structure of the histone deacetylase SIRT2. *Nat. Struct. Biol.* **2001**, *8* (7), 621–625.
- (385) Vanommeslaeghe, K.; Van Alsenoy, C.; De Proft, F.; Martins, J. C.; Tourwé, D.; Geerlings, P. Ab initio study of the binding of Trichostatin A (TSA) in the active site of histone deacetylase like protein (HDLP). *Org. Biomol. Chem.* **2003**, *1* (16), 2951–2957.
- (386) Chen, P. C.; Patil, V.; Guerrant, W.; Green, P.; Oyelere, A. K. Synthesis and structure-activity relationship of histone deacetylase (HDAC) inhibitors with triazole-linked cap group. *Bioorganic Med. Chem.* **2008**, *16* (9), 4839–4853.
- (387) Finnin, M. S.; Donigian, J. R.; Cohen, A; Richon, V. M.; Rifkind, R. A; Marks, P. A; Breslow, R.; Pavletich, N. P. Structures of a histone deacetylase homologue bound to the TSA and SAHA inhibitors. *Nature* **1999**, *401* (6749), 188–193.
- (388) Vannini, A.; Volpari, C.; Gallinari, P.; Jones, P.; Mattu, M.; Carfi, A.; De Francesco, R.; Steinkühler, C.; Di Marco, S.; Blander, G. Substrate binding to histone deacetylases as shown by the crystal structure of the HDAC8–substrate complex. *EMBO Rep.* **2007**, *8* (9), 879–884.
- (389) O'Shannessy, D. J.; Somers, E. B.; Maltzman, J.; Smale, R.; Fu, Y.-S. Folate receptor alpha (FRA) expression in breast cancer: identification of a new molecular subtype and



- association with triple negative disease. *Springerplus* **2012**, *1* (1), 22.
- (390) Puig-Kröger, A.; Sierra-Filardi, E.; Domínguez-Soto, A.; Samaniego, R.; Corcuera, M. T.; Gómez-Aguado, F.; Ratnam, M.; Sánchez-Mateos, P.; Corbí, A. L. Folate receptor  $\beta$  is expressed by tumor-associated macrophages and constitutes a marker for M2 anti-inflammatory/regulatory macrophages. *Cancer Res.* **2009**, *69* (24), 9395–9403.
- (391) Khalil, I. A.; Kogure, K.; Akita, H.; Harashima, H. Uptake pathways and subsequent intracellular trafficking in nonviral gene delivery. *Pharmacol. Rev.* **2006**, *58* (1), 32–45.
- (392) Srinivasarao, M.; Galliford, C. V.; Low, P. S. Principles in the design of ligand-targeted cancer therapeutics and imaging agents. *Nat. Rev. Drug Discov.* **2015**, *14* (3), 203–219.
- (393) Holm, J.; Hansen, S. I.; Høier-Madsen, M.; Bostad, L. High-affinity folate binding in human choroid plexus. Characterization of radioligand binding, immunoreactivity, molecular heterogeneity and hydrophobic domain of the binding protein. *Biochem. J.* **1991**, No. Pt 1, 267–271.
- (394) Yuan, Y.; Nymoen, D. A.; Dong, H. P.; Bjørang, O.; Shih, I. M.; Low, P. S.; Trope, C. G.; Davidson, B. Expression of the folate receptor genes FOLR1 and FOLR3 differentiates ovarian carcinoma from breast carcinoma and malignant mesothelioma in serous effusions. *Hum. Pathol.* **2009**, *40* (10), 1453–1460.
- (395) Doucette, M. M.; Stevens, V. L. Folate receptor function is regulated in response to different cellular growth rates in cultured mammalian cells. *J. Nutr.* **2001**, *131* (11), 2819–2825.
- (396) Pulaski, B. a; Ostrand-Rosenberg, S. Mouse 4T1 breast tumor model. *Curr. Protoc. Immunol.* **2001**, Chapter 20, Unit 20.2.
- (397) Hilgenbrink, A. R.; Low, P. S. *J Pharm Sci*, **2005**, *94* (10), 2135-2146.
- (398) Stephenson, S. M.; Low, P. S.; Lee, R. J. Folate receptor-mediated targeting of liposomal drugs to cancer cells. *Methods Enzymol.* **2004**, *387*, 33–50.
- (399) Matson, V. Migration of myeloid-derived suppressor cells to tumor and tumor-draining lymph node in a murine model of breast cancer, University of Wisconsin-Milwaukee, **2014**.
- (400) Bareford, L. M.; Swaan, P. W. Endocytic mechanisms for targeted drug delivery. *Adv. Drug Deliv. Rev.* **2007**, *59* (8), 748–758.
- (401) Steeber, D. A.; Green, N. E.; Sato, S.; Tedder, T. F. Lymphocyte migration in L-selectin-deficient mice. Altered subset migration and aging of the immune system. *J. Immunol.* **1996**, *157* (3), 1096–1106.
- (402) Leamon, C. P.; Low, P. S. Delivery of macromolecules into living cells: a method that exploits folate receptor endocytosis. *Proc. Natl. Acad. Sci. U. S. A.* **1991**, *88* (13), 5572–5576.
- (403) Lu, Y.; Klein, P. J.; Westrick, E.; Xu, L.-C.; Santhapuram, H. K. R.; Bloomfield, A.; Howard, S. J.; Vlahov, I. R.; Ellis, P. R.; Low, P. S. Strategy to prevent drug-related hypersensitivity in folate-targeted hapten immunotherapy of cancer. *AAPS J.* **2009**, *11* (3), 628–638.
- (404) Qu, X.; Yang, C.; Zhang, J.; Ding, N.; Lu, Y.; Huang, L.; Xiang, G. In vitro evaluation of

- a folate-bovine serum albumin-doxorubicin conjugate. *J. Drug Target.* **2010**, *18* (5), 351–361.
- (405) Bergenfelz, C.; Larsson, A. M.; Von Stedingk, K.; Gruvberger-Saal, S.; Aaltonen, K.; Jansson, S.; Jernström, H.; Janols, H.; Wullt, M.; Bredberg, A.; et al. Systemic monocytic-MDSCs are generated from monocytes and correlate with disease progression in breast cancer patients. *PLoS One* **2015**, *10* (5).
- (406) de Ruijter, A. J. M.; van Gennip, A. H.; Caron, H. N.; Kemp, S.; van Kuilenburg, A. B. P. Histone deacetylases (HDACs): characterization of the classical HDAC family. *Biochem. J.* **2003**, *370* (Pt 3), 737–749.
- (407) Bertino, E. M.; Otterson, G. A. Romidepsin: a novel histone deacetylase inhibitor for cancer. *Expert Opin. Investig. Drugs* **2011**, *20*, 1151–1158.
- (408) Richon, V. M. Cancer biology: mechanism of antitumour action of vorinostat (suberoylanilide hydroxamic acid), a novel histone deacetylase inhibitor. *Br. J. Cancer* **2006**, *95*, S2–S6.
- (409) Joshi, P.; Greco, T. M.; Guise, A. J.; Luo, Y.; Yu, F.; Nesvizhskii, A. I.; Cristea, I. M. The functional interactome landscape of the human histone deacetylase family. *Mol. Syst. Biol.* **2013**, *9* (672), 672.
- (410) Bots, M.; Verbrugge, I.; Martin, B. P.; Salmon, J. M.; Ghisi, M.; Baker, A.; Stanley, K.; Shortt, J.; Ossenkoppele, G. J.; Zuber, J. Differentiation therapy for the treatment of t(8;21) acute myeloid leukemia using histone deacetylase inhibitors. *Blood* **2014**, *123* (9), 1341–1352.
- (411) Ulicki, J.S.; Wang, C.; Biswas, S.; Liu, X.; Matson, V.; Spindler, B.D.; Murphy, D.J.; Tang, W.; Steeber, D.A.; Hossain, M.M.; Cheng, Y. Design, synthesis and biological evaluation of small, potent histone deacetylase (HDAC) inhibitors which reveal a selectivity profile for HDAC1 and HDAC2: Based on the scaffolds of FK228 and thailandepsins A and B. *J. Med. Chem.*

## Sreya Biswas

University of Wisconsin-Milwaukee  
3209 N Maryland Avenue, Milwaukee, WI-53211  
[biswas@uwm.edu](mailto:biswas@uwm.edu); [sreyabiswas88@yahoo.co.in](mailto:sreyabiswas88@yahoo.co.in)

### EDUCATION -----

- Ph.D. in Biological Sciences, Research Area in Molecular Biology, 2016  
University of Wisconsin-Milwaukee, Milwaukee, WI, United States  
Dissertation: Characterization of folate receptor isoforms  $\alpha$  and  $\beta$  for targeting of epithelial and myeloid cells  
Advisor: Douglas Steeber, Ph.D.
- B.Tech in Biotechnology, 2010  
West Bengal University of Technology, West Bengal, India

### RESEARCH -----

#### INTERESTS

Basic and applied research in the field of Immunology and Cancer Biology

- Tumor targeting in both in-vitro and in-vivo systems
- Immunotherapeutics
- Drug discovery

#### GRADUATE RESEARCH

My research is focused on targeting the folate receptor (FR) subtypes FR- $\alpha$  and FR- $\beta$ , expressed on epithelial and myeloid cell lines, respectively, for use in cancer treatment. Previously it has been shown that FR- $\alpha$  can be an effective targeting strategy and therefore this receptor has been well studied. However, at present very little is known about the beta form, including whether it would also be a useful target. FR- $\beta$  has been found to be expressed by myeloid derived suppressor cells (MDSC) which function to inhibit the anti-tumor response of cancer patients. Hence targeting and eliminating these cells could be an important anti-tumor therapy. I studied the role of FR- $\alpha$  and FR- $\beta$  on a murine breast cancer model (4T1) and on a myelo-monocytic

tumor model (U937), respectively, to characterize them and determine the potential of using folic acid-based techniques to selectively target them.

## **PUBLICATIONS -----**

- X. Liu, **Sreya Biswas**, M.G. Berg, C. M. Antapli, F. Wang, M.C Tang, G. Tang, L. Zhang, G. Dreyfuss, and Y. Cheng., *Genomics-Guided Discovery of Thailanstatins A, B and C as Potent Pre-mRNA Splicing Inhibitors and Antiproliferative Agents from Burkholderia thailandensis MSMB43*; Journal of Natural Products., 2013, 76 (4) 685-693
- X. Liu, **Sreya Biswas**, G. Tang and Y. Cheng., *Isolation and Characterization of Spliceostatin B, a New Analogue of FR901464, from Pseudomonas sp. No. 2663*; Journal of Antibiotics, 2013, 66, 555–558
- X. Liu, H. Zhu, **Sreya Biswas** and Y. Cheng., *Improved production of cytotoxic thailanstatins A and D through metabolic engineering of Burkholderia thailandensis MSMB43 and pilot scale fermentation*; Synthetic and Systems Biotechnology, 2016, 1 (1) 34-38
- J. S. Ulicki, C. Wang, **Sreya Biswas**, X. Li, V. Matson, B.D. Spindler, D.J. Murphy, W. Tang, D. A. Steeber, M.M Hossain and Y. Cheng., *Design, Synthesis and Biological Evaluation of Small, Potent Histone Deacetylase (HDAC) Inhibitors which Reveal a Selectivity Profile for HDAC1 and HDAC2: Based on the Scaffolds of FK228 and Thailandepsins A and B.*, Journal of Medicinal Chemistry (manuscript for submission)
- **Sreya Biswas**; D. A. Steeber., *Characterizing folate receptor beta (FR- $\beta$ ) to determine its potential in targeting myeloid cells*; (manuscript in preparation)

## **CONFERENCES AND SYMPOSIA -----**

### ATTENDED

- Autumn Immunology Conference 2015, Chicago Marriott Downtown, November 2015
- 8<sup>th</sup> Annual Center for Human Immunology Symposium (CHI), Blood Research Institute, Milwaukee, Wisconsin, September 2014
- 7<sup>th</sup> Annual Center for Human Immunology Symposium (CHI), Blood Research Institute, Milwaukee, Wisconsin, September 2013

- Science and Research Integrity Professional Development Seminar Series, University of Wisconsin, Milwaukee, 2011: Responsible Conduct of Research

## TALKS

Biological Sciences Colloquium, UW-Milwaukee, 2015: Characterization of FR- $\alpha$  and FR- $\beta$  isoforms for targeting of epithelial and myeloid cells

## TEACHING EXPERIENCE -----

University of Wisconsin-Milwaukee, Milwaukee, WI, United States

2011-2013: Teaching Assistant

- Anatomy and Physiology II Laboratory, BIO SCI 203
- Elements of Biology Laboratory, BIO SCI 102

2013-2014: Teaching Coordinator, Elements of Biology, BIO SCI 102

2014-2015: Teaching Assistant

- Anatomy and Physiology II Laboratory, BIO SCI 203
- Elements of Biology Laboratory, BIO SCI 102

2015-2016: Teaching Assistant

- Elements of Biology, BIO SCI 102
- Laboratory for Immunological Techniques, BIO SCI 402

## RESEARCH MENTORING -----

2012-2016: Research Supervisor

- Department of Biological Sciences
  - Jessye Hale, undergraduate
  - Amy Donahue, undergraduate
  - Navi Lehal, undergraduate
  - Ian Clavel, undergraduate
  - Cammy Truong, graduate student
  - Joseph Skurski, graduate student
  - Jacob Parrott, graduate student
  - Ari Stone, undergraduate

- Jessica Mai-Sher Yang, undergraduate
- Leah Uecker, undergraduate
- Xiangyang Liu, post-doctoral fellow
  
- Department of Chemistry
  - Shamshul Arefin Ahmed, graduate student
  - Ahila Na

## **AWARDS** -----

2014-2015: Ruth Walker Graduate Grant-in-Aid Award for Outstanding Achievement  
Joseph B. Baier Award for Excellence in Immunology Research

2013: Ruth Walker Graduate Grant-in-Aid Award for Outstanding Achievement

2011-2015: UW-Milwaukee, Chancellor's Award

## **SERVICE** -----

2014-2015: Graduate Organization of Biological Sciences, UW-Milwaukee

- Secretary
- Mentor for new graduate students

2014: Graduate Student Representative, Biological Sciences Graduate Program Open House, University of Wisconsin-Milwaukee

2012- Mentor for new graduate students

2006-2010: Departmental Representative, Department of Biotechnology, Haldia Institute of Technology, India